Photograph: A picture formed by the action of light on a base material coated with a sensitized solution that is chemically treated to fix the image points at the desired density.

Photographic interpretation: The art and science of examining photographic images for the purpose of identifying objects and judging their significance.

Pixel: A picture element having both spatial and spectral properties. The spatial variable defines the apparent size of the resolution cell (i.e., the area on the ground represented by the data values), and the spectral variable defines the intensity of the spectral response for that cell in a particular band.

Point operations: Operations that modify the brightness values of each pixel in an image data set independent of surrounding pixel values.

Polygon-based GIS: A geographic information system (GIS) based on standard Cartesian coordinate digitization techniques. Sometimes called a vector-based GIS.

Preprocessing: Application of digital image processing techniques to the raw remote sensor data prior to visual or further machine-assisted image analysis.

Principal components analysis: A statistical form of data compression.

Radiant flux: The time rate or flow of radiant energy on to, off of, or through a surface.

Radiant temperature: Concentration of the radiant flux from a material. Radiant temperature is the product of the kinetic temperature multiplied by the emissivity to the one-fourth power.

Radiometer: An instrument for quantitatively measuring the intensity of EMR in some band of wavelengths of any part of the EM spectrum. Usually used with a modifier, such as an IR radiometer or a microwave radiometer.

Radiometric correction: Correcting gain and offset variations in MSS data. Procedure calibrates and corrects the radiation data provided by the sensor detectors.

Radiometric resolution: The sensitivity of a detector to differences in signal strength as it records the radiant flux reflected or emitted from the terrain.

Rectification: The process by which the geometry of an image area is made planimetric.

Reflectance: The ratio of the radiant energy reflected by a body to that incident on it.

Registration: The process of geometrically aligning two or more sets of image data such that resolution cells for a single ground area can be digitally or visually superimposed.

Remote sensing: The measurement or acquisition of information of some property of an object or phenomenon by a recording device that is not in physical contact with the object or phenomenon under study.

Resolution or resolving power: The measure of the ability of an optical system to distinguish between signals that are spatially near or spectrally similar.

Roll: Rotation of an aircraft about the longitudinal axis causing a wing-up or wing-down attitude.

Sampling rate: The temporal, spatial, or spectral rate at which measurements are taken.

Satellite: An object in orbit around a celestial body.

Scale: The ratio of a distance on an image or map to its corresponding distance on the ground.

Scanner: Any device that uses a scanning device to produce an image.

Scattering: The process by which small particles suspended in a medium of a different index of refraction diffuse a portion of the incident radiation in all directions.

Sensor: Any device that gathers energy, EMR or other, converts it into a signal, and presents it in a form suitable for obtaining information about the environment.

Pictometry EX2002 (Part 5 of 13)
Roofr v. Pictometry
IPR2023-00436

OFEK07064

Sidelap: The extent of lateral overlap between images acquired on adjacent flight lines.

Signal-to-noise ratio: The ratio of the level of the information-bearing signal power to the level of the noise power.

Signature analysis techniques: Techniques that use the variation in the spectral reflectance or emittance of objects as a method of identifying the objects.

Signature extension: The use of statistics obtained from one geographical area to classify data from similar areas some distance away; includes consideration of changes in atmosphere, and other geographical and temporal conditions that can cause differences in signal level for single classes of interest. *See also* Spectral signature.

Smoothing: The averaging of densities in adjacent areas to produce more gradual transitions.

Software: The computer programs that drive the hardware components of a data processing system; includes system monitoring programs, programming language processors, data-handling utilities, and data analysis programs.

Spatial filter: An image transformation used to enhance certain spatial characteristics of an image.

Spatial frequency: The number of changes in brightness value per unit distance for any particular part of an image.

Spatial resolution: The ability of an entire remote sensor system, including lens, antennas, display, exposure, processing, and other factors, to render a sharply defined image. Also, a measure of the smallest angular or linear separation between two objects that can be resolved by the sensor.

Spectral band: An interval in the electromagnetic spectrum defined by two wavelengths or frequencies.

Spectral classes: Those classes that are inherent in the remote sensor data and must be identified and then labeled by the analyst. Often encountered in unsupervised classification of remote sensor data.

Spectral reflectance: The reflectance of electromagnetic energy at specified wavelength intervals.

Spectral regions: Conveniently designated ranges of wavelengths subdividing the electromagnetic spectrum; for example, the visible region, X-ray region, infrared region, middle-infrared region.

Spectral resolution: The dimension and number of specific wavelength intervals in the electromagnetic spectrum to which a sensor is sensitive.

Spectral response: The response of a material as a function of wavelength to incident electromagnetic energy, particularly in terms of the measurable energy reflected from and emitted by the material.

Spectral signature: Term referring to the spectral characteristic of an object in a scene, which infers that each object reflects radiation in a unique and identifiable manner. *See also* Spectral response.

Supervised classification: A computer-implemented process through which each measurement vector is assigned to a class according to a specified decision rule, where the possible classes have been defined on the basis of representative training samples of known identity.

System: Structured organization of people, theory, methods, and equipment to carry out an assigned set of tasks.

Table digitizer: Equipment used to digitize the x,y geographic coordinates of map information.

Temporal resolution: How often a given sensor obtains imagery of a particular area.

OFEK07065

Texture: The frequency of change and arrangement of tones in an image.

Tone: Each distinguishable shade of gray from white to black on an image.

Training: The process of informing an image processor which sites to analyze for spectral properties as a prerequisite to supervised classification.

Training sites: Recognizable areas on an image with distinct (spectral) properties useful for identifying other similar areas.

Transmittance: The ratio of the radiant energy transmitted through a body to that incident upon it.

User friendly: Jargon for equipment or a technique that is easy to use.

Vignetting: A gradual reduction in density of parts of a photographic image caused by the stopping of some of the rays entering the lens.

Visible wavelengths: The radiation range in which the human eye is sensitive, approximately 0.4 to 0.7 μm.

Wavelength: Wavelength = velocity/frequency. In general, the mean distance between maxima (or minima) of a roughly periodic pattern. Specifically, the least distance between particles moving in the same phase of oscillation in a wave disturbance. Optical and infrared wavelengths are measured in nanometers, micrometers, and angstroms.

Yaw: Rotation of an aircraft about its vertical axis, causing the longitudinal axis to deviate from the flight line.

Zenith: The point in the celestial sphere that is exactly overhead; opposed to nadir.

OFEK07066

Index

analog-to-digital conversion (A to D), 1, 13
ancillary data, 23, 214, 269
anniversary dates, 235
atmospheric, 3, 20–22, 96–97
  absorption, 97–98
  scattering, 96–97

band, 12,63
biophysical variables, 2–4, 42, 254
  color, 2–3, 20–22
  planimetric (x,y) location, 2–3, 11–12
  soil moisture content, 2–3, 20–22, 34
  temperature, 2, 20–22, 34, 42, 122–123
  texture or surface roughness, 2–3
  topographic/bathymetric (z) elevation, 2, 34, 254
  vegetation biomass, 2–3, 20–22, 34, 160–161, 254
  vegetation chlorophyll absorption, 2–3, 20–22, 34, 159, 183–185, 261
  vegetation moisture content, 2–3, 20–22, 34–35
bit, 5, 58
bit-mapped, 60
brightness map, 73–81
brightness value (BV), 12, 63, 69, 73, 139
byte, 58

calibration, 23
cathode-ray-tube (CRT), 12, 74, 83
change detection, 234–253
  algorithms, 236–251
    change vector analysis, 251
    classification comparisons, 245–246
    image differencing, 237–241
    image ratioing, 241–245
    preprocessing, 246–251
  considerations, 234–236, 251–252
charge coupled device (CCD), 17, 37
class intervals, 74–77, 122
classification:
  accuracy assessment, 225–229
    overall, 225–226
    site-specific, 226–229
  incorporating ancillary data, 222–225
    contextual techniques, 6, 224–225
    layered classification techniques, 224
    supervised relaxation labeling techniques, 224
  supervised, 178–214
    algorithms, 206–214
      maximum likelihood, 212–214
      minimum distance to means, 209–211
      parallelepiped, 206–209

OFEK07067

classification (*continued*)
classification scheme (system), 179–186
Michigan Land Use, 180, 183
Standard Land Use Coding Manual, 180–181
U.S. Fish and Wildlife Wetland, 180, 183–185
U.S. Geological Survey Land Use/Cover, 179–183, 186–187
feature selection, 157, 189–206
graphic methods, 192–198
n-dimensional parallelepipeds, 194–198, 250
radiometric interpretive legend, 192, 194
spectral plots, 192–193
statistical methods, 198–206
divergence, 199–201
bhattacharyya distance, 201
training site selection, 120, 186–189, 226
signature extension problem, 188
measurement vectors, 188–189
unsupervised, 178, 215–222
classes,
information, 179, 215
spectral, 179, 215
Pass #1: cluster building, 215–219
information required, 215–216
iterations, 216–219
Pass #2: assignment of pixels to clusters, 219–222
cluster labeling, 219–222
minimum distance classification, 209–211, 219
clustering (see classification), 178, 215–222
collateral material, 6, 7
computer compatible tape (CCT), 11, 47, 73
contingency table, 212, 228
contrast, 124
convergence of evidence, 7
convolution mask (kernel), 138–139
coordinate transform coefficients, 104, 110–115, 196

data acquisition, 11–49
densitometer approach, 11–19
linear photodiode digitization, 17
optical-mechanical scanning, 12
video digitization, 16
data already in a digital format, 19–49
in situ, 1
data dimensionality, 151, 189
data formats, 45–48
band interleaved by line, 47
band interleaved by pixel, 47
band sequential, 45–47
run-length encoding, 47
data rate, 30, 37
densitometer, 12
density, 12
dichotomous key, 240
digital elevation models, 115, 224
digital image processing, 6
considerations, 8, 9
functions, 51–53
mainframe, 50–53
microcomputer, 50–55
minicomputer, 50–55
procedures, 6, 7
systems, 50–62, Appendix B
digital-to-analog converter (DAC), 82, 84, 87–88
display alternatives, 73–93
black and white hard-copy, 74–82
crossed-line shading, 79–82, 213, 237
line printer, 74–77
line plotter, 77–79
video image, 74, 82–93
black and white, 82–84
color, 85–89
color composites, 89–91
video to hard-copy, 91–92
color camera, 92
film writer, 15, 16, 92
ink jet, 92

Earth Observation Satellite (EOSAT) Company, 8
Earth Resource Observation System (EROS), 25
Earth Resource Technology Satellite (ERTS), 24

OFEK07068

electromagnetic radiation (EMR), 1–2
elements of image interpretation, 6–7
errors:
  commission, 198–199, 212, 228, 244
  external, 94
  internal, 94
  omission, 198–199, 212, 228, 234, 244
expert systems, 6

filters, 138
filter wheel, 13, 15
fourier analysis, 138
frame grabber, 16

Gaussian, 127, 129
geographic data types, 255–257
geographic information systems (GIS), 9, 51–53, 254–271
  components, 255–256
  data encoding, 255–262
    grid (raster), 258–262, 264
    polygon (vector), 255–258, 262, 264
  data management, 262–263
    layers (overlays), 261–263
  data manipulation, 263–267
  data output, 267–269
geometric distortions, 16, 102
  systematic & nonsystematic, 102
glossary, 366
green vegetation index, 162–165
ground control point (GCP), 102

hardware, 51–52, 92, Appendix B
histogram, 69–72, 97–101
hybrid variables, 2
hypothesis testing, 7

image analysis, 7, 9
image enhancement, 117–176
  contrast enhancement, 124–135
    linear, 125–129
      min-max contrast stretch, 127–128
      percentage, 127–130
      piecewise, 129, 131
    nonlinear, 129–135
      histogram equalization, 129–133
      histogram hyperbolization, 134
      logarithmic, 134–135
image enhancement (*continued*)
  density slicing, 74, 85–87, 120
  edge enhancement, 144–151
    linear, 144–149
      compass gradient masks, 145–146
      laplacian, 147–148
      running difference, 144
    nonlinear, 149–151
      Kirsch, 150
      Roberts, 150
      Sobel, 149
  magnification, 119–120
  pan, 120
  principal components analysis, 64, 151–158, 166, 246
  ratioing, 135–138, 244
  reduction, 117–118
  roaming, 120
  spatial filtering, 138–144
    low frequency, 139–141, 246
    high frequency, 141–143, 246
  texture transformations, 6, 169–173, 246–247
    first order statistics, 169–170
    fourier texture measures, 172
    second-order statistics, 170–172
  transects, 120–124
  vegetation Indices, 157–168
    ELAI, 168
    greeness above bare soil, 168
    image differencing, 161
    normalized difference index, 160
    perpendicular vegetation indices, 167–168
    tasseled cap transformation, 161–166
    transformed vegetation index, 160
image preprocessing, 23, 94–116
  geometric correction, 23, 102–115
    rectification, 103, 235
      intensity interpolation, 105–107
      spatial interpolation, 104–105
    registration, 103, 235
  radiometric correction, 23, 95–102
    adjustments, 97–101
    atmospheric effects, 96–102
    detector response error, 95–96
  restoration, 94

OFEK07069

image processing system characteristics, 51–52, 55–61
arithmetic coprocessor, 57
batch or interactive, 56
central processing unit (CPU), 55, 84, 88
color resolution, 59–61
compilers, 58
display resolution, 59
image processor, 60, 82, 84, 88, 120
look-up tables, 83–89
mass storage, 58
operating systems, 58
random access memory (RAM), 57, 58
image understanding, 56
information classes, 179
information extraction, 23
thematic, 177–233
instantaneous-field-of-view (IFOV), 4, 28, 30–31, 37, 44, 186

kernel size, 139
optimum, 145

land use (cover) mapping, 3, 20–22, 177–233
line dropout, 95
line start problem, 96
local operations, 117

manual (visual) image analysis, 6–9, 23, 169
map, 225
assumed true (ground truth), 225–227
remote sensing derived, 225–229
map projections, 23, 103, 108
conformal, 108
Universal Transverse Mercator (UTM), 108–109, 236
equivalent, 108
measurement vector, 64, 156, 188–189, 214
mean, 64, 189, 206, 209, 220–222
microdensitometer, 12–16
flatbed, 12–13
rotating drum, 14–16
model, 1, 3, 7, 255, 269
multispectral, 13, 177–178
classification, 177–233

off-nadir viewing, 39
optimum index factor, 90–91, 136

pattern recognition, 7
photodiode, 17–19
photographs, 11
picture element, 12
pixel, 12, 44, 63, 179
point operations, 117

radiance, 137
rectification, 103
reflectance, 35, 120, 137, 159, 167
registration, 103
remote sensing, 1
remote sensing systems, 11, 20–23
aerial photography, 16, 21, 31, 183, 238–239
aircraft multispectral scanner (MSS), 8, 21, 41–45, 183
Heat Capacity Mapping Mission (HCMM), 21
Landsat multispectral scanner (MSS), 20, 24–30, 236
Landsat return beam vidicon (RBV), 20, 25
Landsat thematic mapper (TM), 8, 20, 28, 30–36, 180–181, 236
NHAP aerial photography, 16, 183
NOAA AVHRR/2, 20, 160–161
NOAA Coastal Zone Color Scanner (CZCS), 21
NOAA SMS/GOES, 21
Shuttle Space Imaging Radar (SIR A-B), 21
SPOT High-Resolution Visible (HRV), 23, 36–41
Thermal infrared multispectral scanner (TIMS), 22, 42
resampling, 106–107
nearest-neighbor, 106
bilinear interpolation, 107
cubic convolution, 107
resolution, 4
radiometric, 5, 20, 30, 37
spatial, 4, 20, 30, 37, 44, 186–188
spectral, 5, 20, 30, 34, 37, 43
temporal, 5, 20, 30, 37–40

OFEK07070

RGB, 84–87
root mean square error, 105

software, 51–53, 61
  SENSOR image processing programs, 61, Appendix A
    BRIGHTNESS MAP, 81–82, 211, 309–322
    CLASSIFY, 211, 355–363
    CREATE STATS, 323
    DIVERGENCE, 201, 346–354
    format of the files, 273
    HISTOGRAM, 69–70, 299–308
    LANDREAD, 47, 277–284
    limitations, 273
    PIPED, 197, 337–345
    PRINTSTATS, 333–336
    STATISTICS, 68, 292–298
    TMREAD, 47, 285–291
    TRAINING, 188, 324–332
soil brightness index, 162–165
spatial dependency matrices, 170–172
spectral classes, 179
spectral reflectance curve (signatures), 35, 159, 188, 42
spectral signature extension, 188
statistics, 63–72
  accuracy assessment, 225–229
  classification, 64, 206–222
  correlation, 66–69, 151
  feature selection, 64, 157, 198–206
  principal components, 64, 151–157
  regression, 98, 101, 109–115
  univariate, 64–65, 68
  variance-covariance, 64–67, 153, 190–192
stereoscopic viewing, 7, 38
  SPOT base-height ratios, 38
striping, 95
sun synchronous orbit, 26

training sites, 7, 120, 177

U.S. Geological Survey 7.5′ and 15′ quadrangles, 108–110

vegetation indices, 157–169
vidicon camera, 14
vignetting, 16

wavelength, 3, 35, 159

zooming, 119–120

OFEK07071

INTRODUCTORY Digital Image Processing

JOHN R. JENSEN

John R. Jensen

Other books of interest...

INTRODUCTORY CARTOGRAPHY
John Campbell

COMPUTER-ASSISTED CARTOGRAPHY: Principles and Practices
Mark S. Monmonier

ISBN 0-13-500828-X

OFEK07072

PRACTICAL PHOTOGRAMMETRIC CONTROL BY KINEMATIC GPS

Commander Lewis A. Lapine

NOAA Nautical Charting Division

Commander Lewis Lapine is chief of the Photogrammetry Branch of the Nautical Charting Division, National Ocean Service, National Oceanic and Atmospheric Administration, Rockville, Maryland 20852, USA.

This article describes kinematic techniques based on the global positioning system and used in the establishment of photogrammetric control at the Ohio Transportation Research Center in support of a GPS/photogrammetry experiment. The equipment, techniques, processing, and precision are discussed in detail with emphasis on using the techniques for establishing photogrammetric control for mapping projects.

The global positioning system has been widely used for geodetic control during the past several years. Now, GPS geodetic surveying is fast becoming an efficient and economical method for establishing survey control for large-scale mapping projects. Usually, the control is established in a relative mode among several fixed receivers, located over known or unknown monumented points, with the observations collected during a time span that often exceeds one hour. The strength of the solution in part depends on the changing geometry of the satellites' positions in relation to receivers on the ground. This article describes kinematic procedures that can obtain the same high degree of precision in several minutes. The procedure allows the establishment of more stations with fewer receivers over an equivalent time span. The strength of the solution depends on maintaining signal phase lock between satellites and individual GPS receivers. The solution is improved by revisiting each station several times during the observing period.

THE STATIC TECHNIQUE

The static differential method transforms the observed electronic signals from a group of GPS satellites into pseudorange and phase information.

Pseudorange is the time delay between transmission and reception of the satellite signal. The term *pseudorange* implies that the range (distance) between the receiver and satellite is not exact but contaminated by clock errors in both satellite and receiver clocks and by atmosphere-induced signal delays. The range between the satellite and ground receiver is computed by multiplying the time delay by the speed of light.

The phase information comes from an electronic counter within the receiver that adds or subtracts whole and partial wavelengths (cycles) of the carrier signal as they arrive at the antenna. Each wavelength is approximately 19 centimeters. The phase information, like the pseudorange, is a measure of the range between the receiver and satellite. The range can be computed by multiplying the cycle count by 19 centimeters. The total number of whole, or integer, cycles between the receiver and satellite is not known when the receiver is first turned on but is computed during postprocessing. The receiver counts the change in number of cycles. As the satellite range increases relative to the receiver, the number of integer cycles will increase. Conversely, as the range decreases, the number of integer cycles will also decrease.

The length of time required for data collection for the static mode of GPS observations depends on the desired positional precision and geometric strength of the satellite configuration. The continual change in satellite geometry enables the computation of the integer number of the carrier signal wavelengths or cycles between the various satellites and terrestrial receivers. The determination of the integer number of wavelengths is possible so long as the signals are not overly contaminated by atmospheric effects that generally restrict ground station separation to less than 60 kilometers.

THE KINEMATIC DIFFERENCE

Kinematic differential techniques are similar to static techniques with the exception that occupation time at a particular site can be reduced to as little as 90 seconds. This technique requires a minimum of two receivers. One static receiver is positioned over a known geodetic control point. A second receiver is installed on a vehicle and transported between the static point and other survey points, which form a traverse loop back to the static receiver station. In the kinematic technique, the a priori knowledge of the integer number of wavelengths is obtained through a technique known as an antenna swap, which will be described in detail later.

Kinematic differential techniques require that simultaneous phase lock be maintained by both receivers on a minimum of the same four satellites throughout the traverse loop. To satisfy this requirement two conditions must be met. First, the receivers selected for the work must be designed to track the phase signal while in motion. Second, no obstructions can block the path between the satellites and the receivers. The requirement to maintain phase lock on the same four satellites will become easier to satisfy as the GPS constellation fills out and more satellites are visible over the horizon at a given time. Receivers are already available with sufficient channels for the simultaneous reception of the increased number of satellite signals.

Assuming that more than four satellites are being tracked by the receivers, any com-

OFEK07584

bination of a minimum of the same four satellites is sufficient for a solution even if some of the other satellites become blocked for short periods of time during transit. The solution for the base line components is dependent on solving for four unknown quantities: the receiver X, Y, and Z position components and time. Thus, a solution of four or more observation equations containing four unknowns is necessary. The cycle gain or loss from the blocked satellites can then be determined from the computed base line components. That is, a geodetic inverse computation can be used to compute the distance between the receiver and blocked satellite at the time of blockage. The integer number of cycles can then be obtained by dividing the distance by 19 centimeters.

If only four satellites are available, their geometry must be sufficiently strong only during the period of time when the mobile receiver is collecting data at one of the traverse points. The satellite signals only need to be strong enough to avoid loss of signal lock, because the signals are not being used for positioning while in the transit mode. Strong geometry implies that, at the very least, a unique solution exists for the unknown parameters of position and time, which would not be the case if, for instance, two of the four satellites were at nearly the same range and azimuth.

The phase information, which can be converted into distance information (number of cycles times wavelength) for both static and kinematic techniques, is postprocessed by a double differencing technique to obtain the base line vector components. Double differencing maximizes the base line precision by minimizing the effects of clock errors, orbit uncertainties, and other sources of error. The errors are eliminated from the solution because their magnitude and sign are nearly equal. When these errors are arithmetically subtracted during the double differencing, they cancel each other out.

Unfortunately, differencing also causes a loss of signal. The signal is the portion of the information that contributes to the accuracy of the base line components. Therefore, a practical limit to the number of differencing levels is usually reached at the double-difference level.

PURPOSE OF SURVEY

If this discussion and terminology discourage the reader from undertaking GPS surveys without the assistance of outside expertise, do not despair; help is on the way. GPS manufacturers have begun to recognize the importance of simplified operating procedures, user-friendly computer software, and open communications with their users. To prove this point, the remainder of this article will demonstrate a successful application of GPS surveying using both static and kinematic differential techniques by personnel who were not very well versed with the technology or terminology at the start of the project.

The purpose of the project was to establish a system of high-quality three-dimensional geodetic control points on the World Geodetic System 1984 datum. These control points will serve as a reference frame for ground and airborne kinematic GPS photogrammetry experiments to be conducted by the National Oceanic and Atmospheric Administration (NOAA), the Ohio Department of Transportation (ODOT), and the Ohio State University (OSU). The entire survey might have been performed using established static GPS techniques. However, time and equipment constraints dictated the need for a more efficient technique to maximize the number of targeted ground control points for the ensuing photogrammetric surveys.

Time and equipment constraints dictated the need to use a technique more efficient than established static GPS techniques.

LOCATION OF SURVEY

The site selected for the network is the Transportation Research Center (TRC) at Marysville, Ohio. Built by the state of Ohio in 1972, the facility is designed for transportation research studies. The TRC was recently turned over to the Honda Motor Corporation, but the Ohio State University still manages it.

The site offers many advantages for the project. The physical layout of the TRC is compatible with the need for continuous exposures of the horizon to provide adequate satellite visibility. The facility already has a high-quality network of photo-control points ideally suited for kinematic GPS applications, both by ground vehicles and aircraft. The TRC is secure enough to leave valuable equipment unattended for several hours, is not congested by traffic, and contains an on-site runway for aircraft operations. The survey area is located entirely inside the boundaries of the TRC.

The major feature within the facility is a 7-mile, high-speed oval test track with four lanes, as shown in Figure 1. The track has parallel 2-mile straightaways with 1.5-mile, steeply banked, 180-degree turns. The existing paneled system of points, although not all positioned, was established by the OSU Department of Geodetic Science and Surveying for in-flight aerial camera calibration.

The existing points were easily recovered with the aid of their badly weathered panels. Because the network is designed with camera calibration in mind, the reestablishment of the same points on a world datum would also suit the needs of future projects. The majority of the panels (25 stations) exist along the inside edge of the high-speed track on a blacktopped low-speed lane. The centers of the photo targets are marked by spikes. A service road, which runs down the central portion of the oval, contains 10 additional targeted points.

These points, as well as approximately 15 other new points, form the framework for the ground vehicle kinematic survey. The target locations are generally free of any obstructions to the horizon above 20 degrees elevation. A single overpass prevents a complete

OFEK07585

Reference System. The operations began with observation of static GPS base lines from the Union County Airport (MARYPORT1986) to three survey monuments within the TRC. Station MARYPORT1986 is a National Geodetic Survey (NGS) GPS station determined on the North American Datum 1983. The TRC monuments are three-dimensional marks connected to a local datum within the TRC. The static survey, composed of three independently measured base lines, has a misclosure of 3 millimeters over a length of 36 kilometers (0.1 ppm). The shortest leg of the traverse checked an electronic distance measurement from the terrestrial survey of 5 millimeters over a length of 3 kilometers (6 ppm).

All comparisons to a terrestrial survey refer to horizontal and vertical control surveys performed in 1983 by personnel from the OSU Department of Geodetic Science and Surveying and the ODOT Bureau of Aerial Engineering. The primary stations for the terrestrial survey are three-dimensionally stable sleeved-rod marks similar to NGS design. Although the documented procedures did not follow strict Federal Geodetic Control Committee specifications, the adjusted horizontal control coordinates yielded an average standard error after adjustment of 4 millimeters in planimetry.

The vertical control survey was accomplished by single-run three-wire leveling ties made to all primary stations. The secondary stations are the photo targets. The centers of the photo targets are marked by spikes driven into asphalt. A more complete description of the terrestrial survey is contained in a draft report (D.C. Merchant, "Aerial Photo Test at the Transportation Research Center of Ohio," Ohio State University Department of Geodetic Science and Surveying, 1983).

During kinematic operations, at least one receiver was operating on one of the TRC static base line stations. Both static and mobile receivers collected information synchronized to GPS time on the same 15-second time interval from the same four or five satellites. Simultaneous data collection was necessary for the relative double differencing reduction of data.

To maximize the efficiency of the operation, we used a static sampling time span of 90 seconds by the mobile receiver that yielded seven 15-second epochs of data. A shorter sampling interval may be adequate, but a longer sampling interval or longer epoch (i.e., a 30-second rate) would be inefficient and should only be used in open traverse (no position check) type operations, where additional observations may ensure more confidence in the final results.

Once the initial kinematic GPS traverses were computed, the results showed that an excellent and consistent agreement existed with the terrestrial survey. The comparisons were based on computed distances and angles obtained from the corresponding coordinate systems. (See Tables 1 and 2.) The number of observations listed in Tables 1 and 2 reflect the total number of 15-second epochs used to compute the mean observations. The samples were collected during the various traverses. The kinematic survey was expanded to include all required photo targets. Closures of several millimeters obviated the need for any adjustment. Repeat observations were combined by a weighted mean based on the number of observations.

Ground Vehicle Kinematic Equipment. The survey was conducted using three five-channel GPS receivers. The receivers were of the single L1 frequency phase comparison type. Data were sampled at a 15-second epoch rate and recorded on portable computers. Sufficient satellite coverage was generally limited to a three- or four-hour period each day during this survey.

A specially equipped NGS field truck was used to transport the kinematic GPS receiver and antenna. The truck used shock-mounted racks for the receiver and an antenna mount. The antenna was mounted on top of a rigid pole attached to the vehicle by a support mechanism with three degrees of freedom. The mount allowed the antenna to be transported and placed vertically over the survey mark without being detached from the vehicle. The unique feature of the mount was that the pole could be made vertical over the mark despite the tilt of the vehicle. The antenna was always supported at the same height above the mark.

The Antenna Swap Procedure. Prior to the start of all kinematic surveying, an "antenna swap" was performed between the mobile receiver and the static receiver. The receivers lacked any significant electronic or hardware differences. The base station or static receiver simply did not move.

An antenna swap enables the quick and sure determination of integer cycles between

Table 1: Comparison of distances from GPS and terrestrial surveys (GPS distances minus terrestrial distances)

Station numbers	Number of observations	Difference (meters)
202–203	219	+0.0079
203–204	282	−0.0143
204–205	339	+0.0005
205–206	334	+0.0063
206–207	273	+0.0063
501–502	291	−0.0085
502–503	214	−0.0026
503–504	203	−0.0036
504–505	305	+0.0087
505–506	479	−0.0059
506–507	437	+0.0043
511–512	262	−0.0023
512–513	362	+0.0065
513–514	447	−0.0094
521–522	339	−0.0125
522–523	415	−0.0085
523–524	468	+0.0111
524–525	386	−0.0094
525–526	348	−0.0029
526–527	319	+0.0083
527–528	335	+0.0030
220–221	197	−0.0019
221–222	128	−0.0087
222–223	110	+0.0133
223–224	89	−0.0058
224–225	117	+0.0001
225–226	148	−0.0062
226–227	148	−0.0038
227–228	134	+0.0115
N = 29	Mean difference = −0.0014	Standard deviation = 0.0076

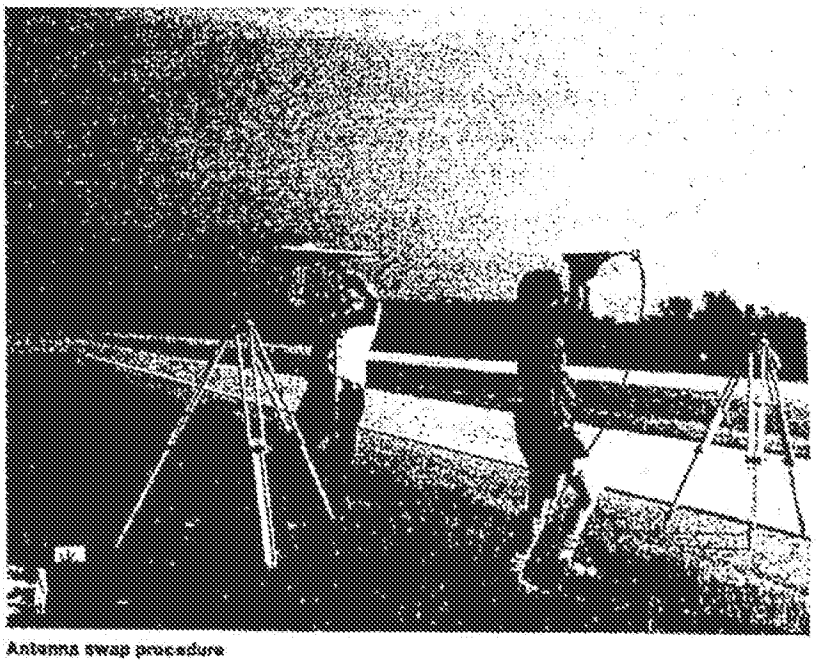
OFEK07586

the base station location and the satellites being monitored at the time. To perform an antenna swap, one simply exchanges the position of the base station antenna with the kinematic antenna. In one particular case, when the static receiver was located at TRC 3, the kinematic antenna was initially set up over T&C 14. The distance between those two points was 4.0633 meters as measured by tape in 1983, 4.065 meters as measured by this survey crew in 1988, and 4.066 meters as measured by the antenna swap!

A full antenna swap procedure normally involves one minute in the normal antenna positions, followed by one minute in the swapped positions, followed by another minute in the normal positions. In each position, the antennas are oriented to magnetic north to avoid possible eccentricity due to antenna phase center ambiguity. Users are cautioned not to proceed until a complete antenna swap has been performed free of cycle slips.

Throughout the antenna swap process, careful attention was paid to the computer displays to ensure the continuity of data recordings. Personnel moving the antennas were careful to keep their heads below the antenna ground plane and to avoid any large tilts to the antenna. Upon completion of the swap, the kinematic antenna was installed on the vehicle.

Another antenna swap was performed each time the kinematic receiver completed the traverse loop. In fact, antenna swaps are only required if there has been a change in satellites or cycle slips since the last antenna swap. Integers for each satellite must be obtained only once during the survey if no cycle slips occur.



Antenna swap procedure

Cycle Slips. The occurrence of cycle slips by the receiver used in the experiment can be detected if the continuous epoch count display on the computer is reset to zero. In such situations, the satellite signal has been momentarily interrupted — for example, the signal was blocked from reaching the antenna by some physical obstruction (a head, tree, building, or severe meteorological phenomen such as lightning).

Because a cycle is only 19 centimeters i length, many cycles can be lost in a fractic of a second due to the speed at which the sa ellite travels and the changing position of th kinematic receiver. Cycle slips can cause m nor inconveniences in processing or majc problems, such as a total loss of the tra verse. The greatest source of cycle slips en countered during this survey were tree along the service road. Survey operation were normally conducted only when all sat ellites were at an elevation of at least 25 de grees above the horizon.

The Kinematic Traverses. Three kinematic trav erses were performed. In each case, the bas or home station for the traverse was TRC 7 or TRC 8. A traverse, in this case, only re fers to the route of the kinematic survey. Each station along the route was actually po sitioned by a three-dimensional vector from the base station.

The receivers did not require a maximum speed limit below which they needed to be transported. Speeds up to 35 miles per hour were recorded in the high-speed turns during the TRC survey. The most important effort is to avoid tilting the truck during transit in a way that would cause satellite blockage by the antenna ground plane or objects above the horizon. Therefore, the high-bank portion of the turns on the test track were avoided as much as possible, as were steeply

Table 2: Angular differences between GPS and terrestrial surveys (GPS angles minus terrestrial angles)

Station numbers		Difference (arc seconds)
202,203,204		−11.55
203,204,205		−06.22
204,205,206		+03.54
205,206,207		+03.49
501,502,503		−00.20
502,503,504		+04.73
503,504,505		+06.91
504,505,506		+01.92
505,506,507		−00.53
511,512,513		+04.94
512,513,514		−00.79
521,522,523		−01.43
522,523,524		+00.42
523,524,525		−05.12
524,525,526		+04.40
525,526,527		−04.01
526,527,528		+02.71
N = 16	Mean difference = 1.11	Standard deviation = 3.3

OFEK07587

sloped shoulders along the edge of the track.

The first traverse covered all marks on the service road. This survey was used to work out the details for kinematic operations. The second traverse connected 18 high-altitude targets on the high-speed track and covered that entire 7-mile circuit. The third traverse connected the low-altitude targets on one side of the high-speed track to several of the high-altitude targets on the same side of the track and to two targets on the service road. Several of the targets were positioned from different base stations as a check on the consistency of the base network. Each traverse route was surveyed at least twice during a single session and repeated on different days.

The average elapsed time from when the antenna became static at one point until it was again static on the next point was three minutes. Upon arriving at each point, the truck was stopped and the engine switched off. The driver and front-seat passenger left the vehicle, plumbed the antenna over the mark, and then aligned it to magnetic north. Once the antenna was motionless, the driver informed the recorder, who waited for the next 15-second satellite epoch to record the displayed UTC (Universal Time Coordinated) time of the epoch.

Kinematic procedures allow the establishment of more stations with fewer receivers during an equivalent time span.

The person recording the time remained in the back jumpseat of the vehicle monitoring the data collection throughout the kinematic portion of the survey. Ninety seconds were added to the beginning time and, when this new time was displayed by the computer, the antenna was returned to the transport position on the truck. The beginning and ending times denote that portion of time when the antenna remains motionless on the survey marker. In all, seven 15-second epochs were recorded in the static mode. With certain simple modifications to the antenna rack, the operation could easily be handled by two people, a driver–antenna tender and a recorder. The recorder never has to leave the vehicle.

COMPUTATIONS

All GPS data, both static and kinematic, were reduced using postprocessing software designed by the receiver manufacturer. Routines for converting three-dimensional Cartesian coordinates to geodetic latitude, longitude, and ellipsoidal height and space inverse solutions were taken from *NOAA Technical Memorandum NOS NOS 13* (T. Vincenty and B.R. Bowring, National Geodetic Survey, Rockville, Maryland, 1978) and *Geometric Geodesy* (R.H. Rapp, Volume 1, Ohio State University, Department of Geodetic Science and Surveying, Columbus, Ohio, 1974). Several customized routines were written by the author for comparison purposes. Kinematic processing techniques are usually germane to the software being used and will not be discussed.

RESULTS

Because the terrestrial survey was computed on a plane elevated 330 meters above sea level, it was not possible to make a coordinate-by-coordinate comparison with the GPS coordinates. The results of the kinematic survey were, therefore, compared with the terrestrial work in two ways. First, the horizontal chord distances between adjacent targets were computed from the GPS three-dimensional coordinates and compared with plane distances computed from the adjusted "plane coordinates" from the terrestrial survey. The three-dimensional horizontal chord distances were determined from GPS vectors by correcting the space vector between adjacent targets for the elevation difference between the two marks. The average difference in distance was −1.0 millimeter with a standard deviation from the mean of 8 millimeters for 29 comparisons, as shown in Table 1.

The second comparison was made between horizontal angles computed from the GPS coordinates and the "plane angles" computed from the adjusted terrestrial control. The average difference was 1.1 arc seconds with a standard deviation from the mean of 3.3 seconds for 16 comparisons, as shown in Table 2.

The requirement to redefine the existing local control datum fit well with Federal Aviation Administration airport survey projects conducted by NOAA that require implementing ground vehicle kinematic GPS applications. Future research will combine aerotriangulation using ground control and kinematic positioning by GPS of the camera exposure stations to perform a simultaneous calibration of the entire airborne photogrammetric system. This type of research also fits well within NOAA's need for GPS-controlled photogrammetric mapping in areas of sparse geodetic control. In this case, little or no ground control will be needed for aerotriangulation. Knowledge of the exposure station positions alone will enable the transformation of photo coordinates into the object space.

ACKNOWLEDGMENT

This article is based in part on a paper presented at the American Society of Photogrammetry and Remote Sensing–American Congress on Surveying and Mapping fall convention held in Cleveland, Ohio, September 17–20, 1989. The author is extremely grateful to the ODOT, Bureau of Aerial Engineering, for their support throughout the survey operations, which caused many interruptions to normal duties. Thanks to Professor Clyde Goad whose boundless energy and devotion to teaching kindled my interest in kinematics. I am also indebted to the TRC personnel who went along with an operation that stretched the limits of the operating guidelines for the high-speed track. Finally, thanks to GRH, a great surveyor and friend, who did not want to be officially recognized for his contributions. No product endorsement is intended or implied by NOAA. ■

For product information, turn to page 65 and see Manufacturers.

AIRBORNE KINEMATIC GPS POSITIONING FOR PHOTOGRAMMETRY THE DETERMINATION OF THE CAMERA EXPOSURE STATION

Lewis A. Lapine, Ph.D.
Chief, National Geodetic Survey
Silver Spring, MD 20910

ABSTRACT

Kinematic GPS positioning of airborne platforms coupled with aerial photogrammetry has become an operational reality within NOAA. Real time GPS positioning is utilized for navigation, while post processed carrier phase differencing is employed for exposure station locations. Since it is not presently practical for the exposure station event to control the GPS collection, the antenna phase center position at the time of exposure must be computed by interpolating the aircraft trajectory after the appropriate timing biases have been added to the observed exposure time. This paper will discuss present and future methods for determining the position of the exposure station event.

INTRODUCTION

Kinematic GPS positioning of airborne platforms coupled with aerial photogrammetry has become an operational reality within NOAA (Lapine 1990). Real time GPS positioning is utilized for navigation, while post processed carrier phase differencing is employed for exposure station locations. Nearly every NOAA aerial mapping project employs some combination of airborne GPS and ground control for the aerotriangulation process. In every case, the requirement for ground control has been reduced. Operational efficiency has increased as the need for expensive and labor intensive ground control has diminished. This technology is rapidly maturing such that it will become the most commercially viable approach for aerial mapping. Commercialization will be heavily dependent on instrumentation, capitalization costs and processing efforts, all of which are now in the favor of the technology. Instrumentation is available as a result of other GPS and photogrammetric applications. Capitalization costs have decreased as a result of the increased market share of GPS in the surveying and mapping fields. Post processing software has been improved by the manufacturers, academia and federal sector (Mader 1992) to the point where user friendly software is efficient and readily available. Since it is not presently possible to sample the GPS signal at the instant of exposure, some form of interpolation of the GPS positional information is required. The ultimate goal is to select a sampling rate and interpolation model which yield exposure station accuracy commensurate with the final mapping product while at the same time minimizing post processing effort.

OFEK07723

RELATIONSHIP OF THE GPS ANTENNA PHASE CENTER TO EXPOSURE STATION

The GPS receiver collects the carrier phase and pseudo-range information pertaining to the trajectory of the aircraft throughout the photo mission. The raw data is post processed into trajectory information consisting of GPS time-tagged geocentric positions for the GPS antenna phase center. This position is correlated to the camera exposure station through time and orientation of the spatial offsets between two origins, earth center and photo center. Exposures rarely coincide with the times at which the antenna positions are recorded. Therefore, the antenna position at the time of exposure must be computed by interpolation. The camera exposure station position can then be determined using an orthogonal three-dimensional transformation incorporating the spatial offsets between the entrance node of the lens system and GPS antenna phase center and a priori estimates for the elements of exterior orientation. These a priori estimates may be refined during aerotriangulation and more accurate exposure stations computed after each iteration of the aerotriangulation solution (Lucas 1989). The error of the individual component observations can be propagated during this process to yield a variance-covariance matrix for the camera exposure station.

INTERPOLATION ACCURACY AS A FUNCTION OF GPS SAMPLING RATE

Since it is not presently practical to control the GPS collection by the exposure event, the antenna phase center position at the time of exposure must be computed by interpolating the aircraft trajectory after the appropriate timing biases have been removed from the observed exposure time. The exposure station position accuracy is a function of the kinematic positioning accuracy (1 or 2 cm relative accuracy for most geodetic quality GPS receivers), sampling rate and interpolation model. GPS receiver manufactures have increased sampling rates in part to enhance the accuracy of interpolation. The inclination would be to sample the GPS receiver at as high a frequency as possible to minimize the time difference between GPS epochs and exposure times. This practice also increases the processing burden. A more practical solution would be to select a sampling rate and interpolation model which yield exposure station accuracy commensurate with the final mapping product while at the same time minimizing post processing effort. Operational experience gained by NOAA has demonstrated that a 1 hertz GPS sample is adequate for photo scales as large as 1:10,000 when using the interpolation model discussed in this paper. Higher sampling rates or more different interpolation models may be necessary for low altitude (larger scale) photography to accommodate aircraft trajectories influenced by short period turbulence. To this end, the following analysis of the interpolation process is presented.

The GPS signals are generally sampled on a nearly uniform time interval affected only by a very small (one usec/sec) (King and Durboraw 1988) drift in the receiver

OFEK07724

clock. The signals, subsequent to being post-processed generally have receiver clock drift removed and are time shifted so that all antenna positions are equally spaced in time. The interpolation becomes simplified since the data points are evenly spaced in time. As mentioned above, the length of the uniform interval (time between successive epochs of data) is governed by the GPS receiver hardware and may be the limiting factor for the accurate interpolation of the exposure station position from the aircraft trajectory. The interpolation precision is well correlated to the limit of positional resolution which can be expected from kinematic GPS (Lapine, 1991). Longer time intervals degrade the interpolation. The following example used GPS data collected at a 1-second rate and then thinned to 2-second and 5-second rates by removing the appropriate sample points. The thinned data sets were interpolated for the missing midpoint samples. The GPS data used for this test came from two data sets collected aboard the NOAA Citation II jet and one data set from the Texas Highway Department King Air Turbo-prop. Comparison of the interpolated positions with the observed positions indicate a standard deviation about the mean difference as great as 41 cm. The number of samples whose position difference was greater than 20 centimeters was recorded for each data set and reported in Table 1.

The Citation and King Air results are still commensurate with kinematic positioning expectations when thinned to 2 seconds. The sample standard deviations for the data thinned to 5 seconds for the King Air suggest a serious degradation in position. It is interesting to note that the magnitude of the standard deviations associated with the NOAA Citation are different from the Texas King Air. The population variances were tested and failed the equality test based on the F statistic (Hamilton 1964). The differences between the 2- and 5-second populations are most likely caused by the inability to model the aircraft trajectories over a time span greater than 2 seconds. The difference between the NOAA and Texas populations may result from the same inability to model the trajectories or may be caused by a larger signal-to-noise ratio in the receivers used for the tests (different manufactures). The trend indicates that sampling intervals greater than 1 second should be avoided if the full accuracy of kinematic GPS positioning is required. However, the good comparison between the data thinned to 2 seconds and observed positions does validate the ability of the interpolation process when sampling at 1 hertz.

An interesting alternative to the above timing situation would be to activate the camera shutter with the 1-second timing pulse generated by the GPS receiver. In this procedure one may be able to entirely eliminate the time difference between GPS fix information and exposure. Interpolation of the GPS navigation file would be eliminated except possibly for a constant time offset between the timing signal and the camera response to the signal. A short test conducted aboard the NOAA aircraft indicated that the time delay would be on the order of 0.1 second for the particular Wild RC-10 camera used in the test. The camera

OFEK07725

service manual states that the maximum time delay between rotating shutter blade opening and capping shutter delay is on the order of 0.070 second. The time delay depends on the shutter speed, position of the rotating shutter blades at the time the pulse was initiated, and the vacuum status. One major problem with this procedure would be the inability to accurately control overlap.

Table 1
Evaluation of 2- and 5-Second Sample Rates for GPS Phase Information During a Photo Mission

Aircraft Type	Sample Size	Sample Rate	% of sample > 20 cm	Mean/Std Dev of Sample (m) X,Y, and Z
King Air	2086	2 Sec	15	0.000/0.055 -0.001/0.122 0.001/0.114
King Air	1039	5 sec	58	-0.002/0.270 0.004/0.412 -0.007/0.409
Citation	1715	2 sec	4	0.000/0.031 0.000/0.063 -0.001/0.055
Citation	1503	2 sec	5	0.000/0.032 0.001/0.084 0.000/0.063
Citation	873	5 sec	33	0.000/0.292 -0.002/0.261 0.002/0.281
Citation	748	5 sec	34	0.001/0.286 0.000/0.274 -0.002/0.261

INTERPOLATION ALGORITHM

The objective of the interpolation is to compute, using a limited portion of the navigation file, a position for the antenna phase center at the time of exposure which is within a half epoch of the central time of the limited data set i.e., less than 0.5 second for a 1-Hertz sample.

The interpolation algorithm uses a second-order polynomial whose three coefficients are solved for by least squares method. The polynomial represents a curve which fits the aircraft trajectory over a 5-epoch period. A different curve is fit to each coordinate axis. The coefficients of this polynomial can be used to compute the aircraft position offset, velocity and acceleration in each coordinate direction.

OPEK07726

The following models are used for interpolating the antenna phase center coordinates:

$$X_1 = a_x + b_x t_1 + c_x t_1^2 \quad (1)$$
$$X_2 = a_x + b_x t_2 + c_x t_2^2 \quad (2)$$
$$\vdots \qquad \vdots \qquad \vdots \qquad \vdots$$
$$X_i = a_x + b_x t_i + c_x t_i^2 \quad (3)$$

where $t_i = time_i - time_3$; when $i = 1,2,\ldots 5$;
$time_3$ is the central time and

$t_1 \ldots t_5$ are the five consecutive time tags of GPS antenna phase center positional data

Similar equations could be written for the other two models:

$$Y = a_y + b_y t + c_y t^2 \quad (4)$$
$$Z = a_z + b_z t + c_z t^2 \quad (5)$$

The unknown parameters for each model can be related to distance, velocity and acceleration by differentiating the above equations as follows:

distance from origin = a_i (6)
velocity = $dX/dt = b + 2ct$, and (7)
acceleration = $dX^2/d^2t = 2c$ at t_3 . (8)

The observation equations are:

$$v_x = a_x + b_x t + c_x t^2 - X = 0 \quad (9)$$
$$v_y = a_y + b_y t + c_y t^2 - Y = 0 \quad (10)$$
$$v_z = a_z + b_z t + c_z t^2 - Z = 0 \quad (11)$$

The coefficient matrix elements for all three models are the partial derivatives of the model with respect to the unknowns. The coefficient matrix is the same for all three models, as follows:

$$A = \begin{bmatrix} -1 & -(t_1-t_3) & -(t_1-t_3)^2 \\ -1 & -(t_2-t_3) & -(t_2-t_3)^2 \\ -1 & -(t_3-t_3) & -(t_3-t_3)^2 \\ -1 & -(t_4-t_3) & -(t_4-t_3)^2 \\ -1 & -(t_5-t_3) & -(t_5-t_3)^2 \end{bmatrix} \quad (12)$$

From this point forward in the discussion, time differences will be denoted as simply "t" to simplify the expressions.

The observation vectors composed of the observed coordinate values for each GPS epoch are:

for X;	for Y;	for Z;
$-X_1$	$-Y_1$	$-Z_1$
$-X_2$	$-Y_2$	$-Z_2$
$-X_3$	$-Y_3$	$-Z_3$
$-X_4$	$-Y_4$	$-Z_4$
$-X_5$	$-Y_5$	$-Z_5$

(13)

OFEK07727

A least squares solution minimizing the function

$$PHI = V' \; P \; V \tag{14}$$

is used to solve for the unknown parameters (Uotila 1986). The P matrix is the scaled inverse of the variance-covariance matrix (Sigma I_b) for the observed quantities. The scaling is represented by $Sigma_0^2$, the variance of unit weight, which in this case has the value of 1. The solution for the unknown parameters begins with the normal equations noted as follows:

$$V_x = AK_x + X \tag{15}$$
$$V_y = AK_y + Y \tag{16}$$
$$V_z = AK_z + Z \tag{17}$$

where;

$$K_x = -(A'PA)^{-1}(A'PX) \tag{18}$$
$$K_y = -(A'PA)^{-1}(A'PY) \tag{19}$$
$$K_z = -(A'PA)^{-1}(A'PZ) \tag{20}$$

and the ' symbol represents the transpose matrix. For the moment consider the weight matrix P to be the Identity matrix I,

$$A'IA = \begin{bmatrix} 5 & 5t & 5t^2 \\ 5t & 5t^2 & 5t^3 \\ 5t^2 & 5t^3 & 5t^4 \end{bmatrix} \tag{21}$$

$$A'IX = \begin{bmatrix} x_1 + x_2 + x_3 + x_4 + x_5 \\ x_1t + x_2t + x_3t + x_4t + x_5t \\ x_1t^2 + x_2t^2 + x_3t^2 + x_4t^2 + x_5t^2 \end{bmatrix} \tag{22}$$

similar equations can be written for A'PY and A'PZ.

VARIANCE-COVARIANCE WEIGHT MATRIX FOR GPS OBSERVATIONS

The variance-covariance matrix, P, is used to weight the contribution of each observation considering the span of time between the central observation point and the camera exposure station. The assumption is made that the five observations are independent and, therefore, the co-variances between observations are zero. Several different choices for the variances were considered. The first choice was equal weights. This choice was not considered appropriate considering possible non-uniformity of the trajectory. A second choice was to compute the variances by giving more weight to the center value of the interpolation, a central weight scheme. The justification for this decision is based on the increasing difficulty to accurately model a trajectory as the distance between the central data point and its neighbors increases. This fact was confirmed in Table 1. The weight for the central value is, therefore, greatest with decreasing weights for the other data points as the time span from the data point to the central value increases. Several central weight systems were tried including the use of the Geometric Dilution of Precision

OFEK07728

(Spilker 1980), an estimate of GPS relative accuracy, obtained from the satellite geometry at the time of exposure. The final scheme weights the data points as a binomial expansion technique. The central variance was chosen to be 1.0 cm^2. The following formula for the variances of the weight matrix ($Sigma_{ob}$) follows:

$$\begin{bmatrix} 2^2*0.01\ m^2 & 0 & 0 & 0 & 0 \\ 0 & 2^1*0.01\ m^2 & 0 & 0 & 0 \\ 0 & 0 & 2^0*0.01\ m^2 & 0 & 0 \\ 0 & 0 & 0 & 2^1*0.01\ m^2 & 0 \\ 0 & 0 & 0 & 0 & 2^2*0.01\ m^2 \end{bmatrix} \quad (23)$$

or

$$\begin{bmatrix} 4\ cm^2 & 0 & 0 & 0 & 0 \\ 0 & 2\ cm^2 & 0 & 0 & 0 \\ 0 & 0 & 1\ cm^2 & 0 & 0 \\ 0 & 0 & 0 & 2\ cm^2 & 0 \\ 0 & 0 & 0 & 0 & 4\ cm^2 \end{bmatrix} \quad (24)$$

The time separation from the central observation is inversely proportional to the weight. No correlation was considered between observations. The P (weight) matrix is a diagonal matrix with the following elements when a 1 Hertz sample rate is used:

$$P_{11} = 1.0 / Sigma^2_1 = 1/(2^2 * 0.01\ m^2) \quad (25)$$
$$P_{22} = 1.0 / Sigma^2_2 = 1/(2^1 * 0.01\ m^2) \quad (26)$$
$$P_{33} = 1.0 / Sigma^2_3 = 1/(2^0 * 0.01\ m^2) \quad (27)$$
$$P_{44} = 1.0 / Sigma^2_4 = 1/(2^1 * 0.01\ m^2) \quad (28)$$
$$P_{55} = 1.0 / Sigma^2_5 = 1/(2^2 * 0.01\ m^2) \quad (29)$$

The <u>a priori</u> variance of unit weight is 1.0. The validity of this weight system can be proven using a Chi Square test of the <u>a posteriori</u> variance of unit weight against the <u>a priori</u> variance of unit weight. The test indicated equal variances in 43 of 45 selected interpolation tests. The validity must be tempered by the knowledge that the degrees of freedom for the test is only 2 (number of observations - number of unknowns, 5 - 3 = 2).

The interpolated values for the antenna phase center at the time of the exposure are expressed as follows:

$$X_{exp} = K_x(1) + K_x(2)*(time_{exp} - time_3) + K_x(3)*(time_{exp} - time_3)^{exp} \quad (30)$$

$$Y_{exp} = K_y(1) + K_y(2)*(time_{exp} - time_3) + K_y(3)*(time_{exp} - time_3)^{exp} \quad (31)$$

$$Z_{exp} = K_z(1) + K_z(2)*(time_{exp} - time_3) + K_z(3)*(time_{exp} - time_3)^{exp} \quad (32)$$

As a final note, the model used in this paper only approximates the actual trajectory of the aircraft. The mathematical modeling process acts as a filter, smoothing the aircraft trajectory using a second order polynomial. It would be interesting to examine the extent of smoothing

OFEK07729

which actually takes place. The model is validated by the results illustrated in Table 1. This same model was independently developed by James Lucas (Lucas 1989) and is currently used within the National Geodetic Survey.

ANTENNA PHASE CENTER TRANSFORMATION TO EXPOSURE STATION

The interpolated geocentric position of the antenna phase center at the exposure time can now be transformed through the previously determined system of spatial offsets to the position of the exposure station.

Errors introduced by the observed quantities and interpolation model can be propagated through the above system of interpolation equations if the variances for the unknown parameters and time can be estimated. The variance-covariance for the parameters is obtained from the inverse of the normal equation matrix scaled by the a posteriori variance of unit weight. The estimate for timing error is obtained empirically as follows:

1. Knowledge of the precision for the GPS time tags which are receiver dependent.

2. Knowledge of the uncertainty in timing delay between the camera and GPS which is GPS receiver and camera system dependent.

3. Knowledge about the uncertainty of shutter timing offset measurement at the midpoint of shutter opening which is camera dependent (Taylor 1964).

The first two error sources are insignificant considering the velocity of the aircraft and the stability of the receiver and timing clocks. The largest contributing factor is, therefore, the shutter timing offset. This error is currently estimated to be 0.0005 sec (Lucas 1989). This estimate will decrease in magnitude as camera manufacturers refine internal timing techniques associated with forward motion compensation requirements (Coker 1989). The error estimate for the GPS position is given as 2 cm in planimetry and 4 cm in elevation (Mader 1992) . These values have been accepted as true. Assuming that there is no correlation between the position, timing and unknown parameters, a combined variance-covariance matrix can be derived. The derivation can be found in the author's dissertation (Lapine 1991) and will not be developed at this time.

Several assumptions are made about the camera and aircraft attitudes and the resultant contribution to the error in the exposure station position:

a. The exposure station will be defined as the entrance node to the lens system of the camera.

b. Vertical photography is assumed a priori and refined during the aerotriangulation. The initial swing angle is estimated by the azimuth between two consecutive antenna positions and can be refined as improved knowledge is obtained from aerotriangulation.

OFEK07730

c. The pitch and drift angles are measured between the aircraft and the camera. The pitch and drift angles were zero when the spatial offsets were measured.

d. The variance-covariance matrix for the exposure station can be propagated through the various models using a priori estimates of the precision for the observations.

The antenna and camera coordinate systems are right-handed as are the three rotations about the camera axes. Three rotations and three translations are used in the transformation:

a. The antenna coordinates at the time of exposure are converted from WGS84 rectilinear to ellipsoidal latitude, longitude and elevation. The latitude (lat) and longitude (lon) are then used to rotate the WGS84 coordinates into an East, North, local vertical system.

b. The covariance matrix from the interpolation model error propagation is similarly transformed to obtain a covariance matrix in the local vertical system.

c. The spatial offset components between the camera and antenna are then rotated into the local coordinate system using the standard gimbal form. The rotation elements of Kappa and drift are combined into a single rotation. Rotational elements of Phi and pitch are also combined. No determination of roll was made during the flight, so Omega is treated independently.

It may be argued that the camera rotates about a set of mechanical gimbals whose rotational center may or may not be coincident with the exposure station. If there is any eccentricity between the gimbal rotational center and the exposure station, then the angles of exterior orientation can not be algebraically summed with the observed angles of pitch and swing. The eccentricity discussion will begin with the particular situation encountered in NOAA's application where pitch and swing angles are small (less than 2°).

By design of the RC-10 camera mount, the optical axis, about which swing is measured also coincides with the vertical axis of the mount, therefore swing and kappa angles can be combined without an eccentricity correction. Such is not the case for the pitch angle. The exposure station has a vertical separation of approximately 27 mm from the gimbal origin (the gimbal center is probably at the camera's center of gravity). The aircraft pitch relative to the camera mount was measured during actual flight conditions and is referenced to the gimbals. A maximum and generally constant pitch angle of 1.5° was measured and occurred at the lower limit of the Citation's operating speed. The consequences of not taking the eccentricity into account are as follows:

$$\text{Maximum pitch error} = 0.027\text{m} * \sin(1.5^{\circ}) = 0.0007\ \text{m}$$

OFEK07731

A displacement error of the exposure station of less than 1 mm in the direction of flight is introduced if the eccentricity correction is neglected. In the most general case, a camera mount consists of a double concentric two orthogonal axis gimbal. The mechanical design of the gimbals and the magnitude of the rotation angles may dictate a more thorough investigation of the effect of the eccentricity.

The gimbal form rotation matrix (Merchant 1988) is formed by the product of the three independent rotations of pitch roll and swing. The order of multiplication is important only in the general case mentioned above. The order of rotation for the specific case is not critical, considering, the design of the camera mount, magnitude of the angles (generally less than 2°), and the fact that the rotations are being treated in a purely analytical application.

The combined rotation matrix would transform survey coordinates to photo coordinates. Since the spatial offsets are measured in the photo system, the transpose of the combined matrix is required. The product of the transposed matrix times the spatial offset vector yields values for the spatial offsets in the survey system. The spatial offsets may now be algebraically added to the interpolated position of the antenna position at the time of exposure. The result is a set of GPS coordinates for the exposure station and the associated estimates for the position precision.

REFERENCES

American Society of Photogrammetry, (1980), Manual of Photogrammetry, Fourth Edition, Banta Publishing Company, New York, New York.

Coker, Clayton, and Clynch, James R., and Brock, Chris, (1989), "Calibration of the Exposure Status Signal from the Wild RC20 Aerial Camera," Technical Report, Applied Research Laboratories, The University of Texas, Austin, Texas.

Hamilton, Walter Clark, (1964), Statistics in Physical Science, The Ronald Press Company, New York, New York.

King, Michael and Durboraw, I. Newton III, (1988), "A Detailed Description of Signal Processing in Motorola's Eagle GPS Receiver," Unpublished Proprietary Report, Motorola Inc., Tempe, Arizona.

Lapine, Lewis A., (1990), "Practical Photogrammetric Control By Kinematic GPS," GPS World, Vol. 1, No. 3, pp. 44-49.

Lapine, Lewis A., (1991), Analytical Calibration of the Airborne Photogrammetric System Using A Priori Knowledge of the Exposure Station Obtained from Kinematic Global Positioning System Techniques, University Microfilms International, Dissertation Information Services, Ann Arbor, Michigan.

OPEK07732

Lucas, James R., (1989), "GPS-Assisted Phototriangulation Package (GAPP) User's Guide, Version 1.02," NOAA Technical Memorandum NOS CGS 2, Geodetic Information Center, NOAA, Rockville, Maryland.

Mader, Gerald L., (1992), "OMNI 3.22 Users Guide," National Geodetic Survey Manual.

Merchant, Dean C., (1988), Analytical Photogrammetry Theory and Practice, Fourth Edition, Parts I and II, Department of Geodetic Science, The Ohio State University, Columbus, Ohio.

Spilker, J. J., Jr., (1980), "GPS Signal Structure and Performance Characteristics," Global Positioning System, Volume 1, Papers published in "Navigation," The Institute of Navigation, Washington, D.C.

Taylor, Eugene A., (1964), "Calibration of the Coast and Geodetic Survey Satellite-Tracking System," Invited Papers, The International Society for Photogrammetry, Technical Commission V, Lisbon, Portugal, pp. 13-36.

Tudhope, Robert Lorne (1988), "Dynamic Aerial Camera Calibration Combining Highly Convergent and Vertical Photography," M.S. Thesis, Department of Geodetic Science and Surveying, The Ohio State University, Columbus, Ohio.

Uotila, U. A., (1986), Adjustment Computation Notes, Department of Geodetic Science, The Ohio State University, Columbus, Ohio.

OFEK07733

AIRBORNE VIDEO SYSTEM
USERS GUIDE

Written by
Dick Myhre, USDA Forest Service

Barry Russell and Carl Sumpter,
Management Assistance Corporation of America

December 1992

USDA Forest Service
Forest Pest Management
Methods Applications Group
3825 East Mulberry Street
Fort Collins, Colorado 80524
(303) 498-1778

Prepared and Edited by
Kori Webster, Mark Fitte, and Sue Emond,
Management Assistance Corporation of America

OPEK07773

Chapter 9

How to Use the Complx Video Caption Generator

9.1 Specifications and Description of the Complx Video Caption Generator 100

9.2 Overlaying LORAN C and GPS Information on Video Imagery 102

OFEK07774

9.1 Specifications and Description of the Compix Video Caption Generator

The Airborne Video System requires a video caption/timing interface system (Compix LP701) to correlate video imagery and location coordinates (see fig. 9.1). The Compix LP701 overlays navigation and location coordinates on the video imagery to aid in post-flight evaluation and processing of the video imagery. There are three display formats for the video caption data:

- BLACK—white text on black background
- CLEAR—white text with no background
- OFF—no text

You may use the timing function to correlate LORAN C positions or GPS positions and times to a specific video frame. The timing function increases post-processing speed and accuracy.

OFEK07775



Figure 9.1 Compix video caption generator

OFEK07776

9.2 Overlaying LORAN C and GPS Information on Video Imagery

LORAN C Receivers

The Compix LP701 interfaces with several aircraft LORAN C navigation receivers (see fig. 9.2a). The Compix LP701 overlays the following LORAN C data onto the video imagery:

- latitude and longitude, displayed in degrees, minutes, and decimal minutes
- track of the aircraft (true heading in degrees)
- date
- time (24-hr. military format), to the nearest second

See the Compix LP701 Operating Instructions for additional information on the various LORAN C receivers compatible with the Compix.

GPS Receivers

The Compix LP701 interfaces with the Trimble Pathfinder TANS, NavTrac, and TransPak II GPS navigation receivers (see fig. 9.2b).

The Compix LP701 overlays the following GPS data onto the video imagery:

- track of the aircraft (true heading in degrees)
- ground speed (knots/mph)
- altitude (mean sea level/height above ellipsoid)
- date
- latitude and longitude, displayed in degrees, minutes, and decimal minutes, or degrees, minutes, seconds, and decimal seconds

OFEK07777

- time (displayed in 24-hr., military format on the internal clock, or in GPS time on the receiver)

See the Compix LP701 Operating Instructions for information on how to set the display parameters.

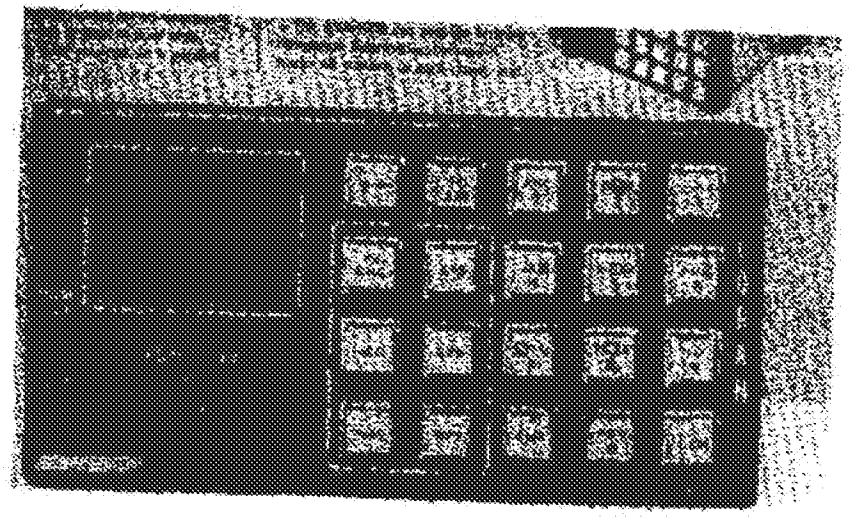


Figure 9.2a LORAN C receiver



Figure 9.2b GPS receiver

OFEK07778

AN AIRBORNE VIDEO SYSTEM DEVELOPED WITHIN FOREST PEST MANAGEMENT - STATUS AND ACTIVITIES

Richard J. Myhre
USDA Forest Service
Forest Pest Management/Method Application Group
3825 East Mulberry
Fort Collins, CO 80524

Bruce Silvey
USDA Forest Service
National Forests and Grassland in Texas
701 N. First Street
Lufkin, TX 75901

INTRODUCTION

Airborne videography is emerging as a remote sensing tool available to resource managers. Recent changes in this technology have made video a viable sensor for the acquisition of timely information for resource management applications.

It is important to understand the role videography can play in the pest management arena related to existing aerial survey technologies. Forest Pest Management (FPM) has the responsibility for the detection, evaluation, and control of insect and disease impacts upon the Nation's forest resources. Resource managers require estimates of the location and intensity of pest damage to plan and conduct suppression or salvage programs. Often, these estimates are obtained from aerial detection surveys conducted for the purpose of discovering pest outbreaks when they first appear or are in the developing stages, and to monitor changes.

Often these surveys are flown as part of an ongoing systematic monitoring plan. Historically, aerial detection surveys have been of two basic types: (1) visual sketchmapping surveys, and (2) aerial photography surveys.

Sketchmapping Surveys

Visual sketchmapping is the technique of delineating the area of pest-caused damage onto maps based on observations by a pest specialist flying in a small aircraft. Aerial sketchmapping has been the most efficient and economical method of detecting and appraising recognizable pest damage over large remote forest areas. Sketchmapping is highly subjective, however; the resulting data can be no more accurate than the competence of the sketchmapper and the conditions under which the data were obtained. No two sketchmappers will and can be expected to record the same pest outbreak in exactly the same way. For this reason, sketchmapping should be regarded more as an art than as an exact science (Klein et al. 1983).

When an outbreak is detected, its causal agent and host are identified, and its location is marked on the survey map. Sketchmap surveys are used to record current year defoliation and mortality, locate new infestation areas, detect new and potential pest problems for ground evaluation, stratify damage intensity for aerial photographic surveys, and provide records of pest outbreaks and their rate of spread. Although annual sketchmap surveys supply

OFEK07758

resource managers with current and useful information about the status of pests, more reliable remote sensing techniques could provide improved data on the location and extent of the pest damage.

Aerial Photographic Surveys

Aerial photography is another available survey tool for forest pest management. Color and color-infrared photography are valuable tools for assessing insect and disease activity on forest lands. Photography has been used to estimate current and/or total levels of damage and mortality from pests. Photos provide a historical record of pest activity and have been used to monitor the rate of spread and trends of a pest over time. Chemical, biological, and cultural treatment methods can be evaluated using aerial photography to determine the vegetation damage prevented.

Most aerial photography applications in pest management can be divided into two broad classes -- mapping photography and sampling photography. Mapping photography is generally used for mapping the total extent of a pest problem (delineating polygons of damage), or mapping a pest's vegetation type. This type of photography usually covers a large ground area and therefore enables the photointerpreter to observe various patterns, trends, and distribution of the pest activity. Sampling photography is generally used with some type of survey sampling design. This types of photography is used when it is not operationally feasible or cost effective to evaluate 100 percent of the area of concern. A sampling design utilizing aerial photos can be used to obtain an estimate of pest activity and the photo estimate can be strengthened by ground sampling. Since most sampling photography is acquired at larger photo scales, the interpreter can obtain more reliable data, such as tree counts, identifiable pest symptoms and tree species, etc. (Ryhre 1988).

The use of aerial photography as a detection method has certain advantages and is very useful, but it has some disadvantages and limitations. The primary advantages of photography are that a permanent image record is preserved for a point-in-time and that photography provides a source of detailed information. Through the use of photointerpretation techniques and equipment, aerial photos can provide more accurate information than sketchmapping methods. One of the main disadvantages of using photography over sketchmapping is the high cost and the amount of time required in processing film and prints, interpreting photos, and transferring information from photos to a map. This delay can severely impact suppression and control decisions.

BACKGROUND AND DEVELOPMENT OF AIRBORNE VIDEOGRAPHY

Interest in video technology was generated within Forest Pest Management (FPM) as a tool to enhance and supplement the existing sketchmapping survey techniques, or to fill gaps where aerial photography surveys are not being utilized due to cost. Video technology has been evaluated by the Methods Applications Group (MAG) of FPM for pest management applications.

In the mid-1980's improvements were made in image quality, affordability, and portability that made video equipment increasingly viable as a remote sensing tool. In 1986 a test was conducted to evaluate the operational feasibility of a color

OFEK07759

infrared (CIR) video camera for forest pest problems. The camera used in this test was a prototype CIR camera developed by the University of Minnesota, and is now marketed under the trade name Biovision®. The objective of this assessment was to determine if CIR video imagery obtained with an airborne video camera is capable of detecting aerially visible tree defoliation and mortality caused by forest insects. Two general conclusions were apparent from the examination of the video imagery, sketchmap data, and aerial photography. First, the degree of detail possible in mapping classes of defoliation from video is superior to that obtainable via the sketchmapping technique. Second, the positional accuracy of polygons (map locations) of insect damage appears to be greater when using video imagery (Ranson et al. 1988). The discouraging part of the test was the poor resolution of the CIR tube camera. However, enough positive results were obtained from this assessment that FPM/NAO decided to continue pursuing this technology.

In 1988, following the CIR video test previously discussed, NAO personnel evaluated the status of commercially available video technology that could be adopted for airborne use. Our intent was to eventually deploy video systems to multiple field locations, so we restricted our evaluation to commercially available "off-the-shelf" technology. The evaluation produced the following information:

1. New solid-state cameras using charged couple device (CCD) sensors are superior to tube cameras. Solid-state cameras are less prone to damage from vibration making them more suitable for aircraft operation.

2. Shuttered video cameras are available that produce higher quality imagery by reducing blur from image motion and vibration that arise in airborne operations.

3. A new recording system called Super-VHS (S-VHS) is now available. S-VHS has several advantages over VHS, including increased resolution (400 lines of horizontal resolution for S-VHS vs 240 lines for VHS), improved color quality, and, improved signal-to-noise ratio through increased band width.

Based on the new advancements in video, FPM/NAO personnel developed an airborne video package suitable for addressing forest pest management applications. This package consists of an airborne video image acquisition module and a video image processing module (Nyhro et al. 1990).

Video Image Acquisition System

The airborne video image acquisition system developed by FPM/NAO consists of a variety of components that have been consolidated into one package. Many of these components are commercially available from various vendors, while a few components essential to linking the system have been developed by NAO. The specially designed items include the video camera mount, electronic junction box, and specialized cabling. These components are now being custom-made commercially.

® Mention of commercial products is for convenience only and does not imply endorsement by USDA Forest Service.

OFEK07760

The airborne system has been developed and field tested using the equipment discussed later in this paper. Using equipment or components other than the specified items may result in malfunctions, loss of image quality, or problems with image processing techniques.

Video Image Processing System

Once video imagery has been successfully captured on tape, it can be used immediately in management applications. This use can be as simple as viewing the video tape on the monitor or using the imagery to do sketchmapping in the office. There are, however, more sophisticated tools for using video imagery. R&D has been using the Map and Image Processing System (MIPS), a product of MicroImages Inc. of Lincoln, Nebraska. MIPS runs in a DOS operating environment on any 80386 microcomputer with a math coprocessor. The software supports an array of peripheral devices including digitizers, plotters, color printers, scanners and optical disc drives.

MIPS offers the advantage of being able to capture video frames from tapes and convert them to a digital form. In R&D's case, the frames are captured as TARGA files, but other formats are supported. Once the frames are stored as digital images, they can be geometrically corrected to a map base and mosaiced. The software permits the user to annotate polygons of pest activity using a cursor on the screen. This digital data can be moved easily to a variety of geographic information systems for use and analysis with other data. There are a number of other image processing systems in the market place with similar capabilities (Pywell et al. 1992).

STATUS OF THE VIDEO IMAGE ACQUISITION SYSTEM

Airborne videography has undergone an ample amount of evaluation and testing to demonstrate this technology has definite applications to forest pest management activities. The video system is designed to be installed in small aircraft such as those used for the sketchmapping survey flights. This capability will allow more users to become operational with videography technology than they would with aerial photography technology (especially 9 by 9 inch format camera systems). The real advantage of implementing videography at the field unit level is the utility of a remote sensing tool in the hands of the local resource expertise that know the country and the problems.

Airborne System Components

The airborne video image acquisition system currently in use by FPM is comprised of the following components, each of which is essential to the operation of the system and the acquisition of video imagery:

Video Camera. The video camera includes three major features: (1) Super VHS (S-VHS) recording format, (2) solid-state chip sensor consisting of three charge-coupled devices (CCD) sensors responsive to red, green, and blue light, and (3) a variable, high-speed electronic shutter system for reducing image motion and blurring. Camera accessories include a zoom lens (15x) with remote control for zooming and exposure or illumination control, an electronic viewfinder, and a tripod-mount adapter to attach the camera to the camera mount.

OFEK07761

Camera Mount. The mount was designed to hold the camera in a vertical position over an aircraft camera hole; and handle corrections for tip and tilt, and drift rotation.

Video Recorder. A portable S-VHS recorder is used for recording both video imagery and audio notes during the mission flight.

Video Monitor. A color monitor is used while in-flight to observe what is being recorded and to adjust the camera for image quality.

Power Converter. The airborne video system requires 12 volts DC to operate. Most aircraft have 24-28vDC electrical power and require the use of a 24vDC to 12vDC power converter.

Caption Generator. The caption generator links the video camera, recorder, and an aircraft navigation system (a LOng Range Aid to Navigation (LORAN)) unit or a Global Positioning System (GPS) unit. The caption generator allows the user to overlay the date, time, latitude and longitude coordinates, and true heading of the aircraft onto the video frames when using LORAN. Altitude and GPS time may also be displayed when using GPS. The overlayed information helps the user locate and interpret the video imagery after the flight.

Electrical Junction Box. The junction box was designed to help connect all of the various cables and components of the airborne video system.

Cabling. The total system requires a number of cables and connectors to link the various components together. Most of the cables are commercially available and accompany the manufacturers components, while a few of the cables were specially designed.

Electronic Navigation Equipment. Although navigation systems are not actually a component of the video system, they are a very important linkage to the system, and play a key role in the overall airborne system operation. There are two types of electronic navigation systems that have been tested with this video system - LORAN-C, a groundbased radio navigation system; and GPS, a satellite radio navigation and positioning system. Navigation systems are linked to the caption generator through an RS-232 interface.

Together these components provide a compact and versatile image acquisition system. They fit easily into almost any small, single engine aircraft having a 6-inch or larger camera hole. As the system provides instant feedback on image coverage and quality, users can quickly become proficient in its use.

Video technology is rapidly changing; and new, emerging technologies will be a part of the future. In order to deliver an operational system, the status of NAG's 1991 developments reflect the system discussed here. NAG will continue to evaluate the status of new video technologies and when appropriate, upgrade the system and amend the User's Guide with supplement chapters/sections.

Technology Transfer Activities

In order to implement the airborne video technology at the field organization level, a technology transfer phase must occur between the technology development phase and the implementation/operational phase. Several technology transfer activities have been initiated

OFEK07762

in order to facilitate the operational use of the airborne video acquisition system.

Consolidated Procurement Package. To simplify the transfer and implementation of this technology, a consolidated procurement package was established for the video image acquisition system. The consolidated package ensures that the users of the video system have all the correct components, and that the system will function as it was designed and field tested.

Prior to the establishment of the consolidated procurement package, four systems were purchased with technical assistance from NAG. The Forest Service groups who first obtained the systems include (see Figure 1):

1. NE Area/FPM Field Office - St. Paul, MN
2. Region 8/Natl. Forests in Texas - Lufkin, TX
3. Region 8/ FPM Field Office - Alexandria, LA
4. Nationwide Forestry Applic. Program - Salt Lake City, UT

Under the procurement package established for fiscal year 1991, six systems were purchased and delivered to the following groups (see Figure 1):

5. Region 2/FPM - Denver, CO
6. Region 3/Kaibab N.F. - Williams, AZ
   and Region 3/FPM
7. Region 4/FPM Field Office - Boise, ID
8. NE Area/FPM Field Office - Durham, NH
9. NE Area/FPM Field Office - Morgantown, WV
10. FPM/NAG - Fort Collins, CO

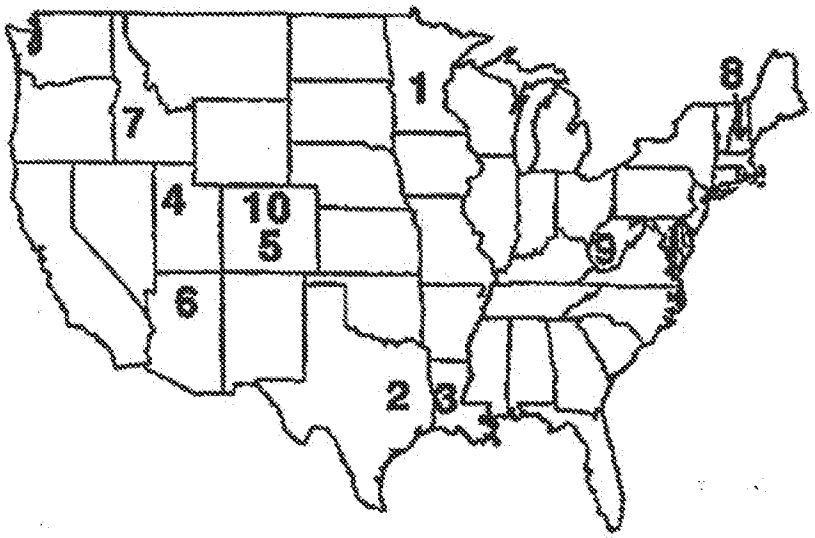


Figure 1. Locations of existing airborne video systems.

A second consolidated procurement package is being evaluated for 1992. A call letter has gone out from the Washington Office (Director of Forest Pest Management) to Forest Service units requesting information from them and their State cooperators to determine the level of interest for a second procurement package.

OFEK07763

Video User's Guide. In order to facilitate the operational use of the airborne video system by the users, a User's Guide was prepared. Although most of the components are accompanied by manufacturer's equipment manuals, most of the manufacturers do not address airborne use and applications. The first version (draft copy) of the Airborne Video System User's Guide was used in a recent training session and will be revised, based on user's comments, and a final version will be available in late summer 1992. The User's Guide is made up of 14 chapter dealing with the following subject material:

- Background of airborne videography.
- Components of the airborne video system.
- Assembly of the system (components and cabling).
- Description and operation of each component.
- Aircraft requirements.
- Aircraft installation procedures.
- How to plan a video mission.
- How to conduct airborne operations.

Video Training. A video training session was held in March 1992 for all the Forest Service units who purchased the systems under the procurement package. All trainees were given hands-on experience with the complete system. The draft version of the User's Guide was issued to each trainee and the contents of the guide were covered in the training session.

Plans for future training programs are being coordinated with the Nationwide Forestry Applications Program (NFAP) in Salt Lake City, Utah. Several training modules are being discussed, with NFAP providing the overall Forest Service training program for airborne videography and NAO providing training to FPM units.

OPERATIONAL USE OF AIRBORNE VIDEO

Several Forest Service groups have become operational with the airborne video technology. The accomplishments of one such group will be discussed in this paper and will highlight the implementation and applications of the video system. The National Forests and Grasslands in Texas (NFGT) entered into aerial video in January of 1991 with the purchase of the airborne video camera system developed by FPM. It was felt that a phase-in approach to aerial videography was the best approach to take for the NFGT, which would allow various units to be well along the learning curve with the airborne system before encountering the image processing system.

Implementation

The NFGT was able to exploit a ready resource of an aircraft through the Texas State Forest Service. The Texas Forest Service has a Cessna 207 aircraft that is equipped for aerial photography with a Zeiss Mapping camera system. This made the adaptation of the video system quite simple. There was no commercially made mounts available at this time so a video camera mount was constructed of 3/4 inch plywood, the camera was attached to this mount, and the video camera was then attached to the Zeiss camera mount. This allows the video camera/mount assembly to be quickly installed in the aircraft. The design is modular for easy installation since aircraft usage may alternate between aerial photography and aerial videography on a daily basis. A video crew, consisting of a

OFEK07764

videographer and navigator, can install the system in about twenty minutes and remove it in less time.

It seemed apparent to the NFGT that aerial videography was a valuable field tool and undertook its implementation accordingly. The Resource Computer Specialist (B. Silvey), who is responsible for the NFGT's aerial videography program, wrote a user's guide for NFGT personnel that covers installation of the equipment, mission planning, and in-flight video operations. A "ground school" was then conducted for the Forest with a video team from each district in attendance. It is felt that each unit will best be able to determine its own needs, and therefore, will best be able to plan and acquire their own imagery.

Implementation is being carried out in incremental steps. The Supervisor's Office acquired the camera system and the fully functional image processing system, which was purchased in May, 1991, as the first step. This allowed the NFGT to get the program started and begin acquiring imagery and learn the processes of image analysis. It was decided that the Resource Computer Specialist act as a technical support contact for the individual units as they move into full implementation. The second step was to place S-VHS player/recorders and high resolution monitors on each of the unit locations so that they could view their own imagery without making a special trip into the Supervisor's Office. A couple of units are preparing to make the final step toward the ultimate goal and are exploring funding to purchase the full image processing system.

Applications

The video system was perceived by the NFGT as a multi-disciplinary tool. It was funded as such, even though it was developed as a forest pest management tool. As the NFGT becomes further involved with aerial videography and its applications for resource management, they are validating that perception. Airborne videography is not a panacea but rather a valuable adjunct to the technologies already in place, and perhaps more importantly, compliments the new technologies on the horizon.

There have been many hours of video imagery gathered on the NFGT, and while a good deal of this imagery has dealt with forest pest problems, its use is not solely limited to that activity. Every unit in the NFGT has flown videography missions.

Traditionally, the NFGT obtains a high quality set of aerial photography covering all the NFGT lands in Texas about once every eight to ten years. Given the intensity with which these lands are managed and the status of natural occurrences (i.e. fire and forest pest activities) it has been apparent for a number of years that the photos lack currency. The problem with the photography cycle can be ameliorated by the use of aerial video.

The two Grasslands that are administered by the NFGT were totally flown with video to establish a baseline for two key issues in the Grasslands' management, namely brush invasion of grazing range and watershed erosion.

A recreation area was flown to aid the Landscape Architect and his staff in analyzing different proposals for the renovation of campgrounds. The proposed selections were imported from a CAD program and displayed over the video image. This allowed for a more

OFEK07765

accurate appraisal of each alternative and a chance to see if the impact of the proposed changes were in conflict with the actual status on the ground as shown by the video image.

NFOT administers a number of Wildernesses and Scenic Areas that require significant amounts of monitoring when insect populations seem to be on the increase or are at epidemic levels. In the past, NFOT has used light aircraft for the detection (sketchmapping) of Southern Pine Beetle (SPB) infestations and then sent people into the field to verify the locations and obtain certain infestation information. With the use of video, NFOT has modified this system. The approach is to fly the areas with the video camera system, capture the images from the tape to the computer, geo-reference these images, and then make calculations as necessary. These may include acreages, numbers of trees infested, and geo-position in reference to private lands and/or endangered species populations.

NFOT have a number of very good predictive models for the population growth of the SPB, however these models only estimate population numbers. They are currently gathering video images of infestations as they grow and are developing vectors showing the extent of the infestations. These vectors can then be overlayed creating an image that accurately portrays the growth dynamics of the infestation. They believe that once they have gathered this type of information on a number of infestations, they can begin to develop computer models that will more accurately predict infestation dynamics.

There are still other uses for the video technology that NFOT are anticipating. One of these is a system for the Forest Fire Dispatcher to be able to call up an image of any area under the NFOT administration, simply by pointing to an area on a computer stored map, to better aid fire crews in their access or their fire suppression tactics.

SUMMARY

Airborne videography has demonstrated its usefulness as an additional remote sensing tool for resource managers. The major advantages of video over the present sketchmapping methods are: (1) video tape provides a permanent record of conditions as they exist at the time of the survey, (2) video recording eliminates the subjective evaluation of the observer while in flight, (3) imagery provides improved positional accuracy of the data collected, and (4) video provides more accurate estimates of the areal extent (acreage) and severity of the pest damage. The major advantages of video over aerial photography are: (1) imagery is available to be viewed and analyzed the same day it is acquired, (2) video can be acquired under high overcast or broken cloud conditions where photography cannot be obtained, (3) the cost of video imagery is far less than conventional frame photography, and (4) the video operator can view "live" imagery on a monitor in the aircraft concurrent with acquisition making video less subject to error due to camera exposure adjusted interactively.

The technology is relatively inexpensive to acquire and use. Field-level personnel with little or no remote sensing background can be trained quickly to operate the equipment efficiently.

OPEK07766

Although the video developmental efforts at FPM/WAO have been centered around pest management activities, it is apparent that this technology has a wider range of applications and uses for other resource management disciplines. Almost as soon as these units became operational, field personnel began finding new applications for the systems. Video imagery has been acquired of other resource interest and in addition to the uses demonstrated by the National Forests and Grassland in Texas, video shows potential applications for post-fire evaluation (mapping burned areas), wetland mapping, riparian/stream habitat, storm damage assessment, and wildlife surveys.

In conclusion, the important point to be made here is that no one remote sensing system or method will meet all aerial survey needs and data requirements. Sketchmapping, aerial photography and videography each have their advantages and disadvantages. The resource manager or specialist must address the airborne technique to the survey design and the resulting information/data required.

REFERENCES

Klein, W.H., S. Tunnock, J.G.D. Ward, and J.A.E. Roof. 1983. Aerial Sketchmapping. In Forest Insect & Disease Survey Methods Manual, USDA Forest Service, Forest Pest Management/Methods Application Group, Fort Collins, CO, 15 p.

Ramsey, A.S., R.J. Myhre, S.M. Dewhurst, and D.E. Meisner. 1988. Assessment of a Color Infrared Aerial Video System for Forest Insect Detection and Evaluation. In Proceedings of Second Forest Service Remote Sensing Applications Conference, Slidell, LA, April 1988, pp. 242-252.

Myhre, R.J. 1988. Aerial Photography for Forest Pest Management. In Proceedings of Second Forest Service Remote Sensing Applications Conference, Slidell, LA, April 1988, pp. 153-162.

Myhre, R.J., L.A. Graham, and C.W. Sumpter. 1990. Airborne Video Technology. In Proceedings of Third Forest Service Remote Sensing Applications Conference, Tucson, AZ, April 1990, pp. 293-298.

Myhre, R.J., C.W. Sumpter, and L.A. Graham. 1991. Airborne Videography - A Potential Tool for Resource Managers. In Proceedings of Resource Technology 90 Symposium, Washington, D.C., November, 1990, pp. 590-594.

Pyssll, H.R., and R.J. Myhre. 1992. In Press. Monitoring Forest Health with Airborne Videography. Proceeding of IUFRO Conference, Canberra, Australia, January, 1992.

OFEK07767

AIRBORNE VIDEOGRAPHY - A POTENTIAL TOOL FOR RESOURCE MANAGERS

Richard J. Myhre
Carl W. Sumpter
USDA Forest Service
Forest Pest Management/Methods Application Group
3825 East Mulberry Street
Fort Collins, Colorado 80524

Lee A. Graham
University of Arizona
School of Renewable Natural Resources
Biological Sciences East
Tucson, Arizona 85721

ABSTRACT

Airborne videography is a potential remote sensing tool for resource managers. Recent changes in this technology have made video a viable sensor for the acquisition of timely information for resource management applications. Airborne video is presently being evaluated and a total system is being developed for use by forest pest managers in the USDA Forest Service. The package consists of two major modules - an airborne video image acquisition system and a video image processing system. This paper describes the image acquisition system, while the image processing system will be discussed by Lee A. Graham in a separate paper within this proceedings.

INTRODUCTION

Television or video (Latin word meaning "I see") has been in existence for many years. It was not until recent years that this technology moved into the remote sensing arena. In the early 1980's a variety of research and development efforts began to evaluate videography as a potential remote sensing tool for natural resource management. Over this time period a variety of airborne cameras have emerged; a few are commercially available and the rest are still in the research and development mode.

Interest in videography was generated within Forest Pest Management (FPM) of the USDA Forest Service as a potential tool to supplement and improve current forest pest surveys. Since insect and disease damage is one of the most serious causes of tree mortality and growth loss in North American forests, pest surveys play a major role in pest management activities.

Resource managers require estimates of the location and intensity of pest damage to plan and conduct suppression or salvage programs. Often, these estimates are obtained from aerial sketch map surveys conducted by federal and state pest specialists flying in small aircraft. Aerial sketch mapping has been the most efficient and economical method of detecting and appraising pest damage

OPEK07753

over large remote forest areas. Sketch mapping is highly subjective, however; the resulting data can be no more accurate than the competence of the sketch mapper and the conditions under which the data were obtained. No two sketch mappers will or can be expected to record the same pest outbreak in exactly the same way. For this reason, sketch mapping should be regarded more as an art than as an exact science (Klein et al., 1983).

Sketch map surveys are used to record current year defoliation and mortality, locate new infestation areas, detect new and potential pest problems for ground evaluations, stratify damage intensity for aerial photo surveys, and provide historical records of insect outbreaks and their rate of spread. Most of this work is done when insect activity and the resultant damage is at the peak of visible symptoms, usually judged by color change. Although annual sketch map surveys supply resource managers with current and useful information about the status of pests, more reliable techniques could provide improved data on the location and extent of the pest damage.

Because of improvement in image quality, affordability, and portability, video equipment has become increasingly viable as a remote sensing tool. Video imagery may be able to provide resource managers with better information for managing pest activities. A joint project with USDA Forest Service/Forest Pest Management and the University of Minnesota/Remote Sensing Laboratory was begun in 1986 to assess the operational feasibility of a color infrared (CIR) video camera for forest pest problems. The objective of this assessment was to determine if CIR video imagery obtained with an airborne video camera is capable of detecting aerially visible tree defoliation and mortality caused by forest insects. The assessment tests were conducted over areas containing mountain pine beetle mortality in Wyoming and forest tent caterpillar defoliation in Minnesota (Munson et al., 1988). Two general conclusions were apparent from the examination of the video imagery, sketch map data, and aerial photography. First, the degree of detail possible in mapping classes of defoliation from video is superior to that obtainable via the sketch mapping technique. Second, the positional accuracy of polygons (map locations) of insect damage appears to be greater when using video imagery. The discouraging part of the tests was the poor resolution of the color infrared tube camera. However, enough positive results were obtained from this assessment that the Methods Application Group (MAG) of Forest Pest Management decided to continue pursuing this technology.

STATUS OF VIDEOGRAPHY

Airborne video imagery is a tool for resource managers dealing with forest pest activities and problems. It provides a new mechanism for acquiring timely information to assess and evaluate the status of resources and for identifying and monitoring problem areas. This technology also shows promise for applications in other resource management domains. Airborne videography should not be viewed as replacement for aerial photography, but can be substituted for photography where the needs do not demand the quality and cost of photography. There are many resource activities where remote sensing and aerial photography data are not being used, primarily due to cost. These gaps could be filled by using airborne videography techniques.

OPEK07754

Advantages

Videography has many attributes that make it attractive as an additional remote sensing system. The advantages of airborne video over conventional aerial photography and camera systems are listed below:

1. Imagery is available immediately, making video particularly useful in applications requiring rapid turnaround time such as pest surveys and disaster assessment (i.e., fires, flooding, etc.).

2. The operator can view "live" imagery on a monitor in the aircraft concurrent with the acquisition, making video less subject to error than photography. The image display allows camera exposure settings to be adjusted interactively.

3. The audio track permits notation in flight.

4. Airborne video provides a straightforward pathway from the videotape to digital format for computerized image processing.

5. Video cameras and videotape are lower in cost relative to conventional aerial photography cameras and film.

6. Airborne video improves the success rate in acquiring the desired coverage at a given point in time (especially important where narrow biological windows are involved).

7. Video cameras have higher light sensitivity than film cameras.

8. Video is useful in foreign countries where aerial film and processing may be difficult to obtain.

New Advancements

Based on the CIR video test previously discussed, MAG conducted an evaluation to determine the status of commercially available video technology on the market that could be adopted for airborne use. This evaluation produced the following information:

1. New solid state cameras are superior to tube cameras for improving resolution. Solid state cameras use CCD (charge coupled device) chip sensors.

2. Shuttered video cameras are available that produce higher quality imagery plus reduce image motion/blur and vibration problems that may arise in airborne operations.

3. VHS recorders and tape will soon be supplemented by a new recording system called Super-VHS (S-VHS). S-VHS has several advantages over the present system, including increased resolution, improved color quality and improved signal-to-noise ratio through increased ban width.

OPEK07755

Based on the new advancements in video, FPM/MAG personnel began development of an airborne video package suitable for addressing forest pest management applications. This package consists of an airborne video acquisition module and a video image processing module (Myhre et al., 1990). This paper discusses the airborne video image acquisition system currently being developed by the MAG Remote Sensing Program.

AIRBORNE VIDEO IMAGE ACQUISITION SYSTEM

The airborne video image acquisition system being assembled by FPM/MAG consists of the following components:

Video Camera
The major features of the camera are (a) S-VHS format, (b) three charge coupled device (CCD) sensors responsive to red, green, and blue light, (c) high speed electronic shutter system for reducing image motion and blurring, and (d) remote-controlled zoom lens and exposure control.

Video Recorder
A portable S-VHS recorder unit is used for recording both audio and video data.

Camera Mount
A special camera mount is being designed to accommodate a video camera.

Video Monitor
A small monitor is used in-flight to observe what is being recorded and to adjust the camera for image quality.

Auxiliary Equipment
This includes cabling to link all components and the power converters and inverters needed to match equipment power demands to power sources (both aircraft and portable power supplies).

Caption Generator
This unit provides a linkage between the video camera/recorder and an aircraft navigation system. Through this linkage, positional information (latitude, longitude, aircraft track or bearing) can be recorded on video frames and in microcomputer text files.

Electronic Navigation Unit
A LORAN-C navigation system can provide positional data as well as time, date, and aircraft heading through an RS-232 interface to the caption generator.

The only components of the airborne system that are not commercially available are the video camera mount and a specially designed electrical junction box to simplify handling of the various cable connectors. Plans are being made to have these components commercially available. The Remote Sensing Program personnel are developing techniques to address video mission flight planning and airborne operations to ease use of the airborne video system.

OFEK07756

SUMMARY

A need for alternative imagery sources for detecting and evaluating forest pest insect damage has been recognized by the USDA Forest Service. FPM/MAG has responded by evaluating video technology and by developing an airborne video package that can be used by forest pest managers in the field. This package includes a data acquisition module, consisting of video camera, recorder, monitor, caption generator, and geographic positioning component and a video image processing module, providing methods for manual and computer-assisted interpretation of forest resources and pest damage from video data.

REFERENCES

Klein, W.H., S. Tunnock, J.G.D. Ward, and J.A.E. Knof. 1983. Aerial Sketchmapping. In Forest Insect & Disease Survey Methods Manual, USDA Forest Service, Forest Pest Management/Methods Application Group, Fort Collins, CO, 15 p.

Munson, A.S., R.J. Myhre, S.M. Dewhurst, and D.E. Meisner. 1988. Assessment of a Color Infrared Aerial Video System for Forest Insect Detection and Evaluation. In Proceedings of Second Forest Service Remote Sensing Applications Conference, Slidell, LA, April 1988, pp. 242-252.

Myhre, R.J., L.A. Graham, and C.W. Sumpter. In Press. Airborne Video Technology. In Proceedings of Third Forest Service Remote Sensing Conference, Tucson, AZ, April 1990.

PROCEEDINGS:

RESOURCE TECHNOLOGY 90

Second International Symposium on Advanced Technology in Natural Resource Management

Georgetown University Conference Center
Washington, D.C.
November 12 - 15, 1990

OFEK07757

Kidwell, K.B. (ed.). 1986. NOAA Polar Orbiter Data Users Guide. National Oceanic and Atmospheric Administration, National Climatic Data Center, Satellite Data Services Division, Washington D.C.

Logan, T.L. 1983. Regional forest biomass modelling from combined AVHRR and Landsat data. Presented at: CERMA Energy Resource Management Conference, San Francisco, CA, August 22-26, 1983. 16 p.

McKinley, R.A., E.P. Chine, and L.F. Werth. 1985. Operational fire fuels mapping with NOAA-AVHRR data. In: Proceedings, Pecora 10, Remote Sensing in Forest and Range Resource Management. American Society for Photogrammetry and Remote Sensing, Falls Church, VA. pp. 295-304.

NASA. 1987. ELAS, Earth Resources Laboratory Applications Software, Volumes I and II. National Aeronautics and Space Administration, National Space Technology Laboratories, Earth Resources Laboratory, NSTL, MS.

Philipson, W.R., and W.L. Teng. 1988. Operational Interpretation of AVHRR vegetation indices for world crop production. Photogrammetric Engineering and Remote Sensing, Vol. 54, No. 1, pp. 55-59.

Roller, N.E.G., and J.E. Colwell. 1986. Coarse-resolution satellite data for ecological surveys. BioScience, Vol. 36, No. 7, pp. 468-475.

Townshend, J.R.G., and C.J. Tucker. 1984. Objective assessment of Advanced Very High Resolution Radiometer data for land cover mapping. Int. J. Remote Sensing, Vol. 5, No. 2, pp. 497-504.

Tucker, C.J. 1979. Red and photographic infrared linear combinations for monitoring vegetation. Remote Sensing of Environment, Vol. 8, pp. 127-150.

Tucker, C.J., J.R.G. Townshend, and T.E. Goff. 1985. African land-cover classification using satellite data. Science, Vol. 227, No. 4685, pp. 369-375.

USGS. 1986. Requirements for the reception and processing of AVHRR data optimized for land science applications, Draft Proposal. U.S. Department of Interior, Geological Survey, EROS Data Center, Sioux Falls, SD. 13 p.

Ward, J.H., and M.E. Hook. 1963. Application of an hierarchical grouping procedure to a problem of grouping profiles. Educational and Psychological Measurement, Vol. 23, No. 1, pp. 69-81.

Werth, L.F., R.A. McKinley, and E.P. Chine. 1985. The use of wildland fire fuel maps produced with NOAA AVHRR scanner data. In: Proceedings, Pecora 10, Remote Sensing in Forest and Range Resource Management. American Society for Photogrammetry and Remote Sensing, Falls Church, VA. pp. 326-331.

AERIAL PHOTOGRAPHY FOR FOREST PEST MANAGEMENT

Richard J. Myhre
USDA Forest Service
Forest Pest Management/Methods Application Group
3825 East Mulberry
Fort Collins, Colorado 80524

ABSTRACT

Aerial photography has been used as a tool by resource managers to detect, map, and evaluate ongoing pest problems, as well as new and unusual problems as they arise. Operational methods currently being used and the selection of photo parameters (film type, photo scale, timing, etc.) are discussed. A nationwide aerial photography program was established in 1982 to support forest pest management activities. Three examples of the application of aerial photography to pest problems are highlighted. Two applications involve the use of sampling photography in survey designs in Vermont and Wisconsin. The other application covers the use of mapping photography for assessing prairie dog management in South Dakota.

INTRODUCTION

Insects and diseases pose a major problem to managers of National Forests and State and private lands throughout the United States. The total annual loss to forest timber resources from insects and diseases amounts to 2.4 billion cubic feet per year, as compared to 0.1 billion cubic feet of loss caused by wildfire (Ciesla 1983). Forest pests cause a wide variety of injury which includes: tree mortality, reduction in growth, deformity, decay, and reduced seed crops that affect future reforestation.

Aerial photography has been used to estimate current and/or total (overall) levels of damage and mortality from pests. Photos are a historical record of pest activity and have been used to monitor the rate of spread and trends of a pest over time. Chemical, biological, and cultural treatment methods can be evaluated with the use of aerial photography in terms of vegetation damage prevented. As the needs of resource managers arise, pest management and remote sensing specialists join forces to utilize aerial photography as a management tool to assess the problem. Selecting the optimum photo parameters (film type, photo scale, biological window/timing, etc.) to address the specific pest activity is critical to the information needs of the resource manager.

In 1982 a nationwide aerial photography program was established to provide technical assistance and support to USDA Forest Service pest management activities. The photo program was organized to be administered and operated by the Methods Application Group (MAG), a Washington, D.C. Office Forest Pest Management (FPM) detached unit located in Fort Collins, Colorado (Myhre 1984a, Myhre 1984b). The photo program was established to meet special FPM requirements that were previously difficult to fulfill or were not being met at all due to the following:

1. Timing of photo acquistion is critical for capturing insect

or disease damage symptoms at their peak (biological window).
2. Unusual requirements, i.e., sampling photography, locating established ground plots.
3. The need to respond quickly to unpredicted events (such as catastrophic insect and disease outbreaks) is difficult to acquire through commercial services due to time consuming contract procedures.
4. New situations often arise where aerial photography may be useful in assessing a pest related problem. Time and money can be lost by embarking on an operational photo mission when the photo parameters have yet to be proven successful. Control must be maintained when conducting a feasibility test for using aerial photography in a new application (Myhre 1982).
5. Provide technical assistance in photo mission planning and photo acquisition support.

The photo program utilizes a Forest Service Beechcraft Queen Air B-80* for all photo mission activities. The camera system is a Zeiss RMK 21/23 9-inch format mapping camera with a 210mm (8-1/4 inch) focal length lens. Visual navigation is performed with a Zeiss NT-1 navigation telescope which is also used to determine amount of drift for setting the camera for crab correction.

PHOTO PARAMETERS AND METHODS

In any photographic mission design, a variety of parameters/elements go together to make up a total mission package. Photographic parameters and methods must be given careful consideration as to the pest problem being evaluated and the resource data required to be extracted by photo interpretation.

Types of Photo Coverage

Most aerial photography applications in pest management can be divided into two broad classes - mapping photography and sampling photography. "Mapping photography" can be defined as a block of continuous photo coverage that, when assembled into a photo mosaic, could be termed a photo map. "Sampling photography" can be defined as photo coverage of a small area that is representative of a larger unit or type.

Mapping photography is generally used for mapping the total extent of a pest problem (delineating polygons of damage), or mapping a pest's vegetation host type. Mapping photography covers a larger ground area and therefore enables the photo interpreter to observe various patterns or trends and distribution of the pest activity.

Sampling photography is generally used in conjunction with some type of survey sampling design. This type of photography is used when it is not operationally feasible or cost effective to evaluate 100 percent of the area of concern. A sampling design utilizing aerial photography can be used to obtain an estimate of pest activity and the photo estimate strengthened by ground sampling. Since most sampling photography is acquired at larger photo scales, the interpreter can obtain more reliable data, such as tree counts, identifying pest symptoms, identifying tree species, etc.

*Mention of commercial products does not imply endorsement by the USDA Forest Service.

Aerial Film Types

Color and color infrared films are the two major film types used for pest detection and assessment. The application of a particular film to a given problem depends on the specific pest and host vegetation type being evaluated, need to separate species types, the difficulty in detecting vegetation stress, and the amount of atmospheric haze in a photo area.

Kodak Aerochrome Infrared (Type 2443) has been the most widely used of all film types, followed by Ektachrome EF (Type SO-397), and occasionally Aerocolor Negative film (Type 2445) when the user needs multi-copies of the photography. Color infrared is preferred for separating healthy vegetation from declining or stressed vegetation, separating conifers from hardwoods, and for haze penetration. Normal color film is usually preferred for species identification and for new/inexperienced photo interpreters.

Photo Scales

Most of the aerial photography acquired for pest management use can be grouped into the two broad categories of photo coverage types and a corresponding group of scales. Mapping or block area coverage has usually been acquired at scales of 1:16,000 to 1:24,000. The most common photo scales for sampling photography are 1:4,000 to 1:8,000.

There appears to be an increasing demand for the use of larger scales of photography among pest management users. The emphasis is on reducing ground/field data collection activities, and increasing the photo interpretation data collection. Photo interpreters are being asked to observe, identify, and record information such as pest symptoms within individual tree crowns, identify species, classify decline/stress trees, and count individual trees that are dying or dead.

Timing of Photo Acquisition

The timing of photo acquisition for insect and disease photography is extremely critical. The biological window for capturing insect and disease damage symptoms at their peak may be narrow (often as short as several weeks). If the photography is taken too early, not all of the damage will be imaged, and the resulting estimates will be conservative. If the photography is taken too late, damage could be masked by refoliation or prior year's damage. Timing can vary from year to year, depending on phenology and weather. Photo missions are often conducted after an examination of a small sample on the ground indicates that timing is optimum. This is the only way that sound, consistent data can be obtained when the biological window is narrow and critical. Timing requires close coordination between the aerial photographer and the local pest management staff.

Navigation Aids

Some form of navigation aid is required whether flying parallel flight lines, sampling points, or ground plots. A major portion of all pest management missions are flown using a combination of electronic (Loran-C) and visual (maps or photos) navigation aids.

The conventional (visual) aids are usually maps or existing (past) aerial photo coverage. The selection of maps or photo products for navigation aids depends on what products are available for the photo area and the mission design and requirements. Maps and photos should be of an appropriate scale for the type of mission being flown, and they should contain the type of information that is easily

1313

identifiable from the air.

Loran-C (Long Range Aid to Navigation) is used on all photo missions to different degrees, ranging from finding the photo area to navigating along flight lines to locating sampling points. The Loran navigational system increases the efficiency and reduces cost on aerial photo missions. Visual navigation aids are used to supplement the Loran system to fine-tune the locating of sampling points and ground plots. This is especially critical in areas of marginal Loran reception.

APPLICATIONS

Most of the applications of aerial photography fall into the two general categories of mapping and sampling photography (previously discussed). Occasionally there have been examples of combined mapping and sampling photography, such as a spruce-fir decline survey conducted in New Hampshire, New York, and Vermont in 1984 (Weiss et al. 1985). The sampling units were rectangular blocks, each 8,000 acres in size, requiring approximately 56 photos (with overlap and sidelap) to cover a sample block.

One of the major areas where aerial photos have been utilized in forest pest management has been the acquisition of sampling photography to support sampling survey designs. Many of these sampling surveys have been conducted in the Northeastern United States to evaluate declining hardwood and spruce-fir forests. Several different sampling approaches have been utilized in States such as Maine, New Hampshire, New York, Vermont, and Wisconsin. The surveys conducted in Vermont and Wisconsin will be highlighted as examples.

Pest problems may be in existance for some time and may not be recognized as a serious management problem until they become a threat to a natural resource. As new and unusual pest problems arise, aerial photography should be tested and evaluated for its application to specific problems. An example of this is the detection and evaluation of prairie dog activity on rangelands. The use of aerial photography to determine the effectiveness of prairie dog management and control activities will be discussed. This is also an example of a mapping photography application.

Vermont Survey

A Statewide hardwood tree health survey was conducted in 1985 and 1986 to determine the current health of Vermont hardwood forests and to establish a data base for future monitoring of the health status (Kelley and Eav 1987).

Survey objectives and design. The specific objectives of the survey were to: (1) determine the area of hardwood decline and mortality, (2) determine the number and volume of dead and declining trees, and (3) provide baseline data to be used to determine trends over time.

The survey utilized a two-stage sampling design. The first stage consisted of 170 photo blocks (sample points) established at a uniform interval over the entire State. The photo blocks were 360 acres in size. The secondary sampling units were established by dividing each photo block into 144, 2.5 acre cells. Seventy five

1314

cells were later selected for ground measurements.

Cooperators. This was a cooperative effort between the Vermont Department of Forests, Parks and Recreation; the USDA Forest Service, Forest Pest Management, Durham, New Hampshire field office; and the Methods Application Group, Fort Collins, Colorado.

Aerial photography. Color infrared aerial photography at a mean scale of 1:8,000 was acquired between late August and mid September 1985. The 170 photo points were on lines 7.4 miles apart, at 7.4 mile intervals along each line (Figure 1). The first flight line and the first photo point on each flight line was on a random start. Five consecutive 9"x 9" film transparencies with 70 percent forward overlap were taken at each point by the USDA Forest Service Beechcraft Queen Air photo aircraft, equipped with a Zeiss RMK 21/23 camera system. Kodak Aerochrome Color Infrared (CIR) film (Type 2443) was used in combination with a Wratten 12 (minus blue) and antivignetting filters. CIR film was chosen to provide haze penetration, easy separation of conifers from hardwoods, and to enhance tree mortality and foliage loss (decline classes).

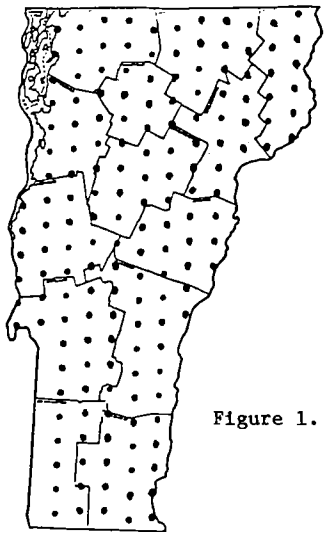


Figure 1. Sample point distribution in the Vermont Hardwood Tree Health Survey - 1986

Photo interpretation. The center photo from each sample point was selected for interpretation, using the two adjacent photos for stereo viewing. Clear plastic overlays consisting of 144 cells on a 12x12 grid were constructed for each 500 scale increment between 1:7,000 and 1:9,000. The overlay closest to the average scale for each center photo was used to establish a 360 acre block. Each 2.5 acre grid cell within the 144 cell grid was examined in stereo and classified in the following types and classes.

1. Vegetation Type - hardwood, inundated (possible high water damage), other (mixed wood, conifer, agriculture, etc.), and cloud cover.
2. Size Class - poletimber and sawtimber.
3. Mortality Class - light (less than 10 percent of hardwood component dead), moderate (10-30 percent), heavy (more than

30 percent), and snag (not considered since it is difficult to determine if conifer or hardwood).

Following photo interpretation, a sample of cells (2.5 acres) was selected for intensive ground examination.

Results. On the basis of photo interpretation, 2.5 million acres of hardwood type were estimated present in Vermont. Of this total acreage, 12,000 acres (0.5 percent) were estimated to have moderate to heavy mortality. Dominant/codominant hardwood trees average 77 percent healthy, 16 percent moderately declining (11 to 50 percent of crown dead), 5 percent severely declining (with more than 50 percent of crown dead), and 2 percent dead.

Wisconsin Survey

A survey was initiated in 1987 to evaluate the decline and mortality of sugar maple and other northern hardwoods in Northern Wisconsin. The photo interpretation and ground survey phases will be completed in 1988. Forest managers, maple syrup producers, and the public are increasingly concerned about the alleged effects of acid rain on the health of sugar maple. The Wisconsin Department of Natural Resources, Bureau of Air Management, has determined, through long term monitoring, the presence of an annual weighted mean pH gradient over the range of sugar maple in the State. The gradient consists of four pH zones, moving from west to east, across 19 northern counties (Figure 2). A survey was designed to evaluate the occurrence of sugar maple decline and mortality under different levels of precipitation pH (Mielke et al. 1987).

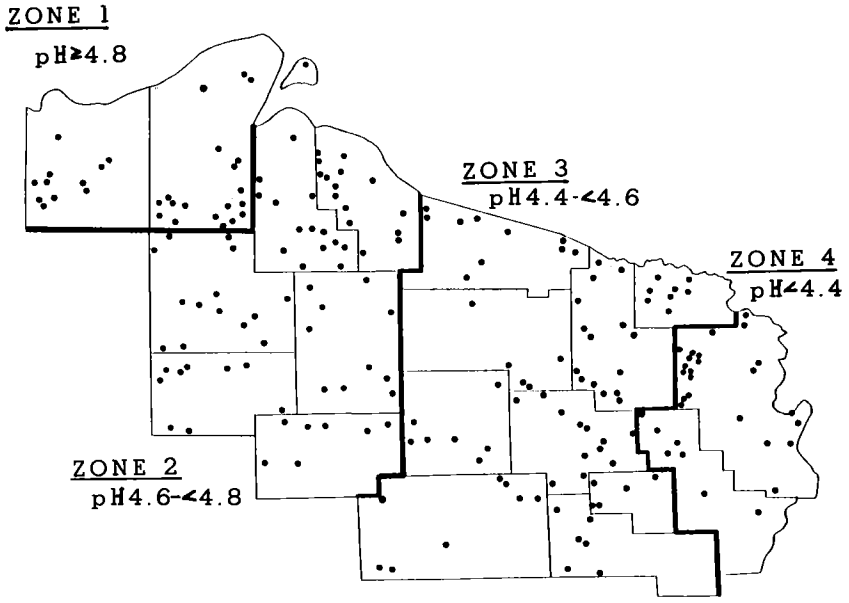


Figure 2. Sample point distribution and pH zones in the Wisconsin Hardwood Survey - 1987/1988

Survey objectives and design. The objectives of the survey are to determine: (1) the difference in the number, volume, and basal area per acre of healthy, dead, and declining sugar maple and associated hardwoods between pH zones and the totals in Northern Wisconsin, (2) the acres of sugar maple decline and mortality in four damage classes, and (3) the amount of decline and mortality associated with known insect and disease pests.

The major difference in the design of this survey from the Vermont survey is the distribution of sample plots. In Wisconsin, the 19 county area was stratified for maple type by selecting Forest Inventory and Analysis (FIA) plots where sugar maple was a component of the stand. Within each county, FIA plots were selected at random from a list of FIA plots with $\geq$ 30 percent of the total basal area in sugar maple (Figure 2). This was a two-stage sampling design similar to the Vermont survey. The first stage consisted of 210 photo blocks (sample points) that were 360 acres in size. The secondary sampling units were established by dividing each photo block into 144, 2.5 acre cells. A random selection of these cells in each pH zone will be ground surveyed in 1988.

Cooperators. This is a cooperative effort between the Wisconsin Department of Natural Resources, Bureau of Forestry and Bureau of Air Management, Madison, WI; USDA Forest Service, Forest Pest Managaement, St. Paul, MN; Methods Application Group, Fort Collins, CO; and Nationwide Forestry Applications Program, Salt Lake City, UT.

Aerial photography. A sample block containing the FIA plot was used as a target area (sample point) and located on 1:100,000 Wisconsin county series maps. A strip of five 9"x9" photos with 70 percent forward overlap was taken at a mean scale of 1:8,000 at the sample points. Kodak Aerochrome Infrared (Type 2443) was used in combination with a Wratten 12 (minus blue) filter and an antivignetting filter. Photos were acquired in August 1987 by the USDA Forest Service Beechcraft Queen Air equipped with a Zeiss RMK 21/23 camera system. Color infrared film was selected for the same reasons as in the Vermont survey.

Photo interpretation. Utilizing the same 12x12 cell grid as in the Vermont survey, a grid of the appropriate scale will be placed over the center photo. Each grid cell (2.5 acres) will be examined in stereo and initially classified according to vegetation type and damage class as follows.

Vegetation Type

1. Northern hardwood (sugar maple and associated northern hardwoods)
2. Other forested (conifer or other hardwoods)
3. Non-forested (agriculture, water, etc.)
4. Cloud cover or shadow

For a cell to qualify in a particular type, it must be occupied by more than 50 percent of that type. Cells identified as non-forested or cloud cover require no further classification.

Damage Class

1. Class 0 - No dead or declining hardwood
2. Class 1 - One dead or declining hardwood
3. Class 2 - Two to four dead or declining hardwoods
4. Class 3 - More than five dead or declining hardwoods.

Declining hardwoods are defined as trees with crowns more than 50 percent dead.

Detailed photo counts of dead and declining trees will be made on a selected number of sample grid cells in each type/damage class. The number of cells to be counted will depend on the distribution and abundance of cells within each vegetation type/damage class combination. The photo interpreter will tally the number of healthy, dead, and declining sugar maple in each selected sample cell.

Following the photo interpretation phase, a sample of the grid cells in each pH zone will be randomly selected for ground survey during the summer of 1988.

Prairie Dog Assessment

Black-tailed prairie dogs, Cynomys ludovicianus, occupy approximately 56,300 acres on 11 National Grasslands (administered by USDA Forest Service) in the West. If unchecked, overpopulated colonies can cause widespread deterioration of rangelands. Prairie dogs prefer sites with closely cropped vegetation to guard against predators; therefore, they establish themselves on grazed areas in competition with livestock for forage.

A two-phase survey was conducted in 1983 using aerial photography to inventory all prairie dog colonies in the Conata Basin of the Buffalo Gap National Grassland in South Dakota. The second phase was an intensive assessment of the effectiveness of a management program to control a large and rapidly expanding prairie dog population in the Conata Basin (Schenbeck and Myhre 1986).

This program involved the use of a rodenticide (zinc phosphide bait) treatment on many of the prairie dog colonies in 1978. The program also provided for numerous selected colonies to remain untreated and active to protect the social and environmental values associated with this species.

Survey objectives. The objectives of the survey/inventory were to: (1) determine the number of prairie dog colonies and total acres occupied by colonies on the National Grassland, (2) determine the effectiveness of the rodenticide treatment for controlling expansion of colonies, and (3) evaluate colony expansion if no treatment/control is initiated.

Aerial photography. In order to evaluate the effectiveness of the treatment program, two sets of photography were utilized - one set prior to treatment (1978) and one set five years after treatment (1983). The 1983 photography was also used to conduct the complete inventory of all prairie dog colonies in Conata Basin.

The pre-treatment photography was available at the Wildlife Research Center, USDI Fish & Wildlife Service, Denver, CO. The photography was acquired during 1978, just prior to the rodenticide treatments, at a photo scale of 1:16,000, using black and white Kodak Plus-X (Type 2402) film and a high contrast filter.

The post-treatment photography was acquired in August 1983 using the USDA Forest Service Beechcraft Queen Air equipped with a Zeiss RMK 21/23 mapping camera system. Kodak Aerochrome Infrared (Type 2443) film was used, with a Wratten 12 (minus blue) filter and an antivignetting filter. The photography was acquired at a photo scale of 1:16,000 to compare with the 1978 photography.

Photo interpretation. For the overall inventory (Objective 1), all prairie dog colony boundaries were delineated on transparent sleeves containing the 1983 CIR photos. Each polygon representing a colony was transferred to a 7-1/2 minute USGS topographic map. The polygons were then planimetered to determine the number of acres per colony.

The photo interpretation procedures for the evaluation of treatment/control effectiveness (Objectives 2 and 3) were more detailed. A sample of treated and untreated colonies was examined on both the 1978 and 1983 photography. Colony boundaries were delineated on both sets of photography and acreage estimates obtained. A technique was developed for estimating prairie dog mound density which shows up on aerial photos as a pattern of white spots. Prairie dog burrow mounds eventually revegetate following effective rodenticide treatments due to a reduction or absence of prairie dog activity. A 10x10 matrix grid with each cell representing one acre on the 1:16,000 scale photo was designed and photographed on clear transparent film. The grid was placed over a colony, and mounds were counted within a random sample of cells to determine mound density per acre.

Results. The inventory of all prairie dog colonies (treated and untreated) in Conata Basin, using post-treatment photography, showed a total of 224 individual colonies covering 23,914 acres. The smallest colony detected was 0.2 acres in size, and the largest colony covered 4,046 acres.

The evaluation of treatment results indicated that the rodenticide treatments were effective in preventing further expansion of the treated colonies. The untreated colonies increased on an average of 61 percent in area over a five year period. The treated colonies remained within an average of one percent of their original size during the same time period. A comparison of pre- and post-treatment photography showed that mound densities within treated colonies decreased, while mound densities in untreated colonies increased.

The application of aerial photography not only proved to be an operationally effective technique, but a cost effective technique. The total cost of the aerial technique was $0.05 per acre (including aircraft, pilot salary, crew per diem, film and processing, and photo interpretation). The best cost figures available for ground inventories indicate that the cost per acre varied inversely with the size of the prairie dog colony, ranging from $2.51/acre on a 556 acre colony to $9.23/acre on a 39 acre colony.

DISCUSSION

Aerial photography has been used as a tool by resource managers to detect, map, and evaluate existing and ongoing pest problems, as well as new and unusual pest problems as they arise.

In order that aerial photography can be a useful application to pest management problems, the following conditions must be addressed.

1. The pest problem must be defined in terms of its effects and relationships to the vegetation being effected.
2. The information needs of the resource manager have been defined.
3. The optimum photo parameters (film type, photo scale,

biological window of detection, etc.) have been determined.
4. The photo interpretation techniques can be developed to extract the information the resource manager needs.
5. The aerial photo techniques used can be more cost effective and can provide as good, if not better, data than other methods (such as ground surveys).

REFERENCES

Ciesla, W.M. 1983, The Multi-Faceted Control of Pests That Damage Our Forests: Using Our Natural Resources - Yearbook of Agriculture, USDA, Washington, D.C., pp. 196-203.

Kelley, R.S. and Eav, B.B. 1987, Vermont Hardwood Tree Health Survey - 1986, Vermont Department of Forests, Parks and Recreation, Waterburg, VT, 30 pp.

Mielke, M., Cummings, J., and Rezabek, C. 1987, Cooperative Survey of Decline and Mortality of Sugar Maple and Other Northern Hardwoods Across a PH Gradient in Wisconsin, unpublished work plan, USDA Forest Service, Forest Pest Management, St. Paul Field Office, St. Paul, MN, 12 pp.

Myhre, R.J. 1982, Photo Mission Logistics and Feasibility Testing: in proceedings of In-Place Resource Inventories: Principles and Practices, a national workshop, Orono, ME, August 1981, Society of American Foresters, Washington, D.C., pp. 255-265.

Myhre, R.J. 1984a, The Forest Pest Management Nationwide Aerial Photography Program - First Year Accomplishments, USDA Forest Service, Forest Pest Management, Methods Application Group, Fort Collins, CO, Rpt. No. 84-6, 11 pp.

Myhre, R.J. 1984b, An Aerial Photography Acquisition Program for Forest Pest Management: in proceedings of Technical Papers of 50th Annual Meeting of the American Society of Photogrammetry, Washington, D.C., March 1984, pp. 395-401.

Schenbeck, G.L. and Myhre, R.J. 1986, Aerial Photography for Assessment of Black-Tailed Prairie Dog Management on the Buffalo Gap National Grassland, South Dakota, USDA Forest Service, Forest Pest Management, Methods Application Group, Fort Collins, CO, Rpt. No. 86-7, 15 pp.

Weiss, M.J., McCreery, L.R., Millers, I. and Ciesla, W.M. 1985, Use of Color Infrared Aerial Photography for Assessing Red Spruce Mortality and Decline: in proceedings of Pecora 10, Remote Sensing in Forest and Range Resource Management, Fort Collins, CO, August 1985, pp. 241-250.

1317

REMOTE SENSING INVENTORY APPLICATIONS IN APPLIED VEGETATION INVENTORIES --THE ALASKA EXPERIENCE

Kenneth C. Winterberger and Vernon J. LaBau
USDA, Forest Service, Forestry Sciences Laboratory
201 East 9th Avenue, Suite 303
Anchorage, AK 99501

ABSTRACT

The USDA Forest Service Forest Inventory and Analysis research project in Anchorage, Alaska, has been field testing a four-phase sampling design for multiresource inventory for the last 4 years. The sample design uses three levels of remote sensing data: Landsat MSS data; high-altitude (1:60,000) color infrared photography, and low-altitude (1:5-7,000) color infrared photography; and a fourth level of ground-plots. This paper presents some of the successes and problems encountered during the testing of the four-phase sampling system, with emphasis on problems with Landsat MSS data analysis and their possible solutions.

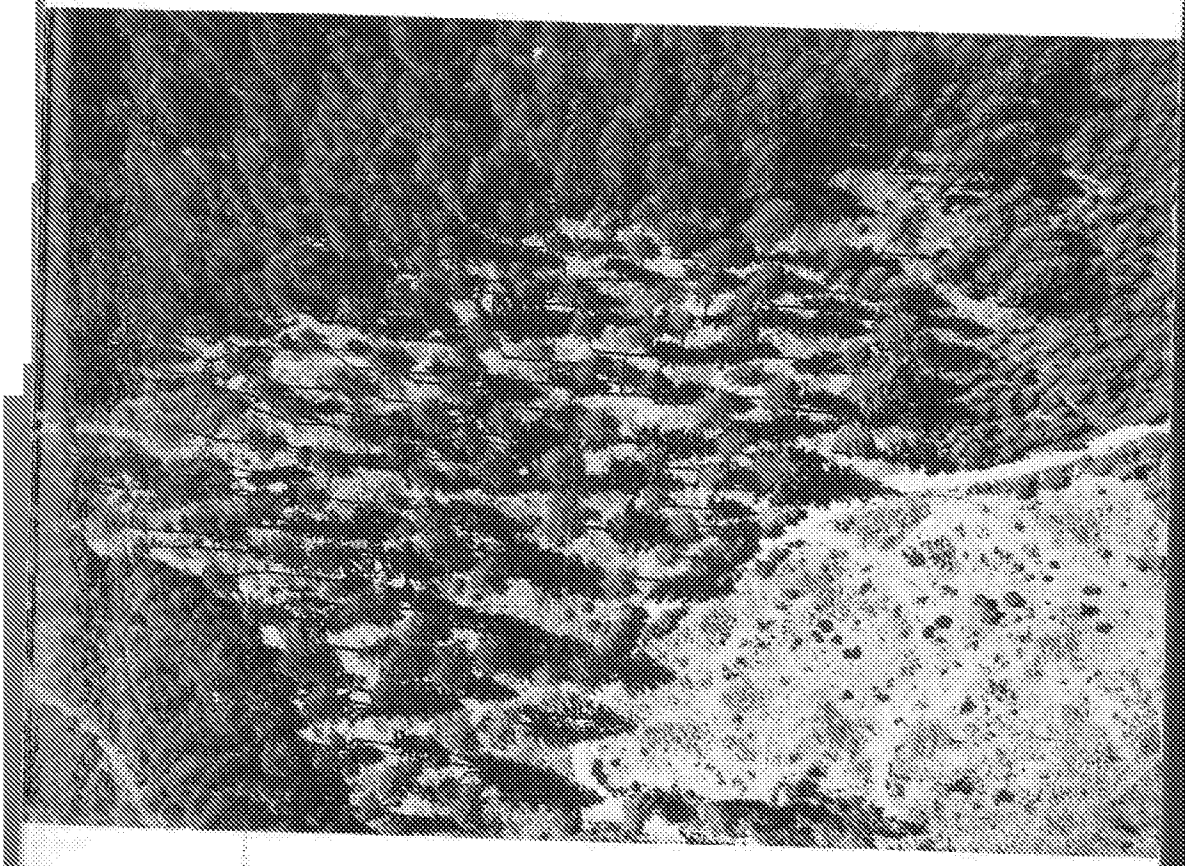
INTRODUCTION

Alaska has about 378 million acres of land and inland water. About 290 million acres (> 75%) are estimated to be forest and rangeland (USDA, 1990 RPA report, in preparation). The Forest Service and the Soil Conservation Service together share responsibilities for inventorying the renewable natural resources, primarily vegetation, associated with this very large area.

Much of the vegetated area of Alaska is inaccessible, precluding traditional ground-based inventories and making use of remote sensing an imperative. The Forest Service is responsible for inventorying the timber resource of Alaska, and the first timber inventory began in the early 1950's. The first statewide report of the timber resource was written by Hutchison (1967). In collecting data for this report a two-phase sampling design was used in coastal Alaska, and the use of a three-phase design was attempted in interior Alaska. Both programs used a layer of remote sensing (black-and-white aerial photos) as the primary basis for efficiently estimating the timber resource.

Although the two-phase design was very effective in coastal Alaska and was used until the early 1980's by the Forest Service, the three-phase design tried in interior Alaska was collapsed to a two-phase design because of the difficulty in designing three-phase sampling estimators; in fact, they were not developed until 1979 (Frayer, 1979). But, application of aerial stand volume estimates on large-scale (1:5,000) black-and-white infrared photos

REMOTE SENSING FOR RESOURCE INVENTORY, PLANNING, AND MONITORING



Proceedings of the Second Forest Service Remote Sensing Applications Conference — Slidell, Louisiana and NSTL, Mississippi

April 11-15, 1988

American Society for Photogrammetry and Remote Sensing

REMOTE SENSING FOR RESOURCE INVENTORY, PLANNING, AND MONITORING

The Second Forest Service Remote Sensing Applications Conference

Held at

The National Space Technology Laboratories, NSTL, Mississippi

and

The Holiday Inn

Slidell, Louisiana

April 11-15, 1988



Sponsored by:

United States Department of Agriculture, Forest Service

National Aeronautics and Space Administration,

National Space Technology Laboratories

The Institute for Technology Development Space Remote Sensing Center

Remote Sensing and Photogrammetry Working Group (A-2),

Society of American Foresters

AIRBORNE VIDEO TECHNOLOGY

Richard J. Myhre
Lee A. Graham
and
Carl W. Sumpter
USDA Forest Service
Forest Pest Management/Methods Application Group
3825 E. Mulberry St.
Fort Collins, CO 80524

ABSTRACT

Airborne videography is another potential remote sensing tool for resource managers. Airborne video technology is presently being evaluated and a total system is being developed for use by forest pest managers in the U.S. Forest Service. The package consists of two major components -- an airborne video image acquisition system and a video image analysis system. This package could have wider use in resource management disciplines other than forest pest management.

INTRODUCTION

Airborne video imagery is a potential tool for resource managers dealing with forest pest activities and problems. It provides a new mechanism for acquiring timely information to assess and evaluate the status of resources and for identifying and monitoring problem areas. This technology also shows promise for applications in other resource management domains. In forest pest management, airborne videography is not viewed as replacement for aerial photography, but can be substituted for photography where the needs do not demand the quality and cost of photography. There are many resource activities where remote sensing and aerial photography data are not being used. These gaps could be filled by initiating airborne videography techniques. This paper describes the airborne video data acquisition and analysis package currently being developed by the Methods Application Group, Forest Pest Management (FPM/MAG) of the USDA Forest Service.

The advantages of airborne video over conventional aerial photography/camera systems are:

(1) the immediate availability of imagery
(2) error-proofing, in that what is recorded can be viewed in flight on the video monitor
(3) provision for a straightforward pathway from tape to digital format for computerized image processing
(4) the lower cost of video cameras/videotape relative to that of cameras/film used in conventional photography
(5) improved success rate in acquiring the desired coverage at a given point in time (especially important where narrow biological windows are involved).

OPEK07503

Forest Pest Management in the U.S. Forest Service is evaluating imagery to supplement the current sketch mapping techniques used for forest pest surveys. Initial tests were conducted with a color infrared video camera over test areas containing mountain pine beetle mortality in Wyoming and forest tent caterpillar defoliation in Minnesota (Munson et al., 1988). Two general conclusions were apparent from the examination of the video imagery, sketch map data, and aerial photography. First, the degree of detail possible in mapping classes of defoliation from video is superior to that obtainable via the sketch mapping technique. Secondly, the positional accuracy of polygons (map locations) of insect damage appears to be greater when using video imagery. The discouraging part of the tests was the poor resolution of the color infrared tube camera.

An evaluation was recently conducted to determine the status of commercially available video equipment now on the market that could be adapted for airborne use. This evaluation produced the following information:

(1) new solid state (chip/CCD) cameras are superior to tube cameras for improving resolution
(2) shuttered video cameras are available that produce higher quality imagery plus reduce image motion/blue and vibration problems that may arise in airborne systems
(3) VHS recorders and tape will soon be supplemented by a new recording system called Super-VHS (S-VHS). S-VHS has several advantages over the present system, among them increased resolution, improved color quality and improved signal-to-noise ratio through increased band width.

Based on the findings of this evaluation, FPM/MAG personnel began development of an airborne video package suitable suitable for addressing forest pest management applications. Planned for delivery in Spring, 1991, this package consists of an airborne video acquisition module and a video image analysis module. Its components are described in the following sections.

AIRBORNE VIDEO IMAGE ACQUISITION SYSTEM

The airborne video data acquisition system assembled by FPM/MAG consists of the following components:

Video Camera
The major features of the camera are (a) S-VHS format, (b) three charge coupled device (CCD) sensors, and (c) high speed shutter system for reducing image motion and blurring, and (d) remote-controlled zoom lens.

Video Recorder
A portable S-VHS recorder unit is used for recording both audio and video data.

Video Monitor
A small monitor is used in-flight for both observing what is being recorded and to adjust the camera for image quality.
Auxilliary Equipment
This includes all cabling to link/connect all components and the power converters and inverters needed to match equipment power demands to power sources (both aircraft and portable power supplies).
Caption Generator
This unit provides a linkage between the video camera/recorder and an aircraft navigation system. Through this linkage, positional information (latitude, longitude, aircraft track or bearing) can be recorded on video frames and in microcomputer text files. Microcomputer software (IBM PC-based) controls the manner of recording these data on videotape.
Electronic Navigation Unit
A LORAN-C navigation system can provide positional data as well as time, date, and aircraft heading through an RS-232 interface to the caption generator.

Techniques are being developed to address video mission flight planning and airborne operation in order to facilitate the operational utilization of the airborne video system.

VIDEO IMAGE ANALYSIS SYSTEM

The product of a successful video mission is a videotape(s) containing the areal coverage needed for a resource management application. The first step in using these data is to review the entire tape, making note of the beginning and ending points of each flight line relative to the VCR's time or framecounting meters. Audio information recorded in-flight is particularly helpful for identifying these points as well as an indicating navigation errors and/or features to be noted.

Once the tape has been reviewed, the process of interpretation can begin. There are many ways in which video imagery can be used in management applications. The simplest approach is to view the videotape and sketch features of interest directly on to hardcopy maps or mylar overlays. The positional information recorded on the videoframes is used as an aid to locating a particular frame on the reference map (usually a topographic map). No special equipment beyond the S-VHS recorder and monitor from the data acquisition module is required, although photointerpretation aids can be used to expedite the interpretation process. Templates can be constructed that approximate the areal coverage of a videoframe of a particular swath width. This tool can help the interpreter in avoiding double interpretations and estimating the position of a feature seen on the monitor compared to the aligned template on a map. Scales for measuring the approximate size and areas of features for a particular swath width can also be used.

Microcomputers equipped with special image capture graphics boards and software provide a platform for interpreting information from video imagery in a format suitable for geographic information systems (GIS) applications. Since pest and resource inventory surveys tend to cover large geographic areas, numerous images must be captured from videotape into digital computer files. FPM/MAG's survey of available image processing software indicated that although there were many image processing packages on the market, none were capable of grabbing large numbers of frames with a uniform endlap between frames. However, most image capture board vendors supply software libraries for use in coding image capture programs. The AT&T Truevision libraries for the TARGA line of image capture boards were used to write a program called AUTOGRAB. AUTOGRAB can perform the following functions:

(1) capture images with a user-defined endlap a flight line at a time
(2) approximately georeference each image using positional information derived from a video mission-planning program (also produced by FPM/MAG) or LORAN-C coordinate information recorded during the mission
(3) reorient the images in an approximate North-South direction
(4) prepare the captured images for inclusion in a computerized indexing system called HyperIndex.

The captured images are stored in the TARGA file format, which can be easily integrated into a number of image analysis packages for subsequent processing.

As mentioned earlier, a video mission produces a large number of images that require interpretation to address the desired resource management problem. Since each captured video frame is stored in an individual computer file, a mechanism for indexing and retrieving the files in a efficient manner is desirable. For forest pest management use, some type of IBM PC/compatible platform was desired. The HyperIndex module of MIPS (Map and Image Processing System, MicroImages, Inc.) was positively evaluated by FPM/MAG as a low-cost and efficient means of indexing a wide range of geographic data, including scanned maps, photographs, and slides, vector data imported from different GIS formats or derived from interpretations, video and satellite imagery, and databases. HyperIndexed images and information are retrieved from an object hierarchy by selecting a feature of interest in the current display with a click of the computer mouse. In FPM pest survey applications, indexed video imagery is retrieved by clicking on a location within scanned topographic maps. Once an image has been retrieved, it is possible to scroll up, down, and across flight lines using the arrow keys on the keyboard.

HyperIndex can also be used to perform quick point location interpretations of pest damage from video imagery. A pilot project now underway in Texas will use the symbol overlay feature of HyperIndex to mark southern pine beetle spot locations using a 4 color symbol scheme (each color representing the severity of the outbreak in terms of number of trees infested). Each symbol is in turn linked to a record in a database, providing a mechanism for entering, retrieving, and updating management information related to that spot. The goal of the application is to provide fast-turnaround hardcopy prints of imagery and/or maps of pest locations for use by crews during ground surveys and control operations.

Other features of MIPS can be exploited to improve the quality and accuracy of geographic data interpreted from video imagery. For example, the AUTOGRAB program only approximately georeferences images at the time they are captured from videotape. Georeferencing of videoframes can be improved by adding control points to images or by using a process called vector warping. The later process involves plotting calibrated vector objects on top of video images, warping them to fit the image, then applying the resulting geometry to correct the image. The nature of video imagery does create problems in the application of these methods. Since video surveys are often flown so that an individual frame covers a very small piece of ground, identifying control points or features suitable for warping can be quite a challenge in heavily forested areas. FPM/MAG will continue to refine in-flight georeferencing techniques (by incorporating global positioning technology and/or corrections for tip and tilt of the aircraft in current LORAN-C methodologies) so that they can adequately substitute for control point and warping methods.

Finally, image processing software packages such as MIPS typically include methods for interpreting polygonal information, estimating the areas of features, and/or exporting and importing the resulting information into GIS databases. Interpretation methods may be as simple as drawing around a feature using a mouse. Alternatively, automated and semi-automated image classification techniques can be applied that use data on color signatures and feature size to interpret classes of information from imagery. It is worth noting that great caution must be taken when applying automated and semi-automated classification techniques to images derived from scanned photographs and videotape. The color signature of a a particular feature in the center of the image may be quite different than the same type feature found on the its edge. Typically, an interpretation tool which provides elements of automated image classification methods in a format permitting a high degree of interaction with the user (allowing subjective interpretations of how features are to added/deleted from a particular classification) is desirable for interpreting video imagery. The Feature Mapping process within

MIPS is a one example of an interpretation tool with these capabilities and was in fact designed specifically to address the challenges posed by video imagery.

As stated earlier, there are a number of hardware and software platforms available that capable of handling video imagery. The equipment and software described in this document were evaluated, developed, and selected with forest pest management applications in mind. FPM/MAG will continue to evaluate available technologies for acquiring and processing video imagery and adapt the modules of the video package as required.

SUMMARY

A need for alternative imagery sources for detecting and evaluating forest pest insect damage has been recognized by the U.S. Forest Service. FPM/MAG has responded by evaluating video technology and by developing an airborne video package that can be used by forest pest managers in the field. This package includes a data acquisition module (consisting of video camera, recorder and monitor, and a microcomputer-controlled caption generator and geographic positioning component) and a video image processing module (providing methods for manual and computer-assisted interpretation of forest resources and pest damage from video data). This package will be completed in Spring, 1991.

ACKNOWLEDGEMENTS

The authors wish to thank our cooperators (Don Hunter and Michael Scott) at the National Ecology Research Center, U.S. Fish and Wildlife Service, Fort Collins, CO, for assisting in the early development of the airborne video package.

REFERENCES

Munson, A.S. 1988. Assessment of a Color Infrared Aerial Video System for Forest Insect Detection and Evaluation. In Proceedings of Second Forest Service Remote Sensing Applications Conference, Slidell, LA and NSTL, MS, April 1988, pp. 242-252.

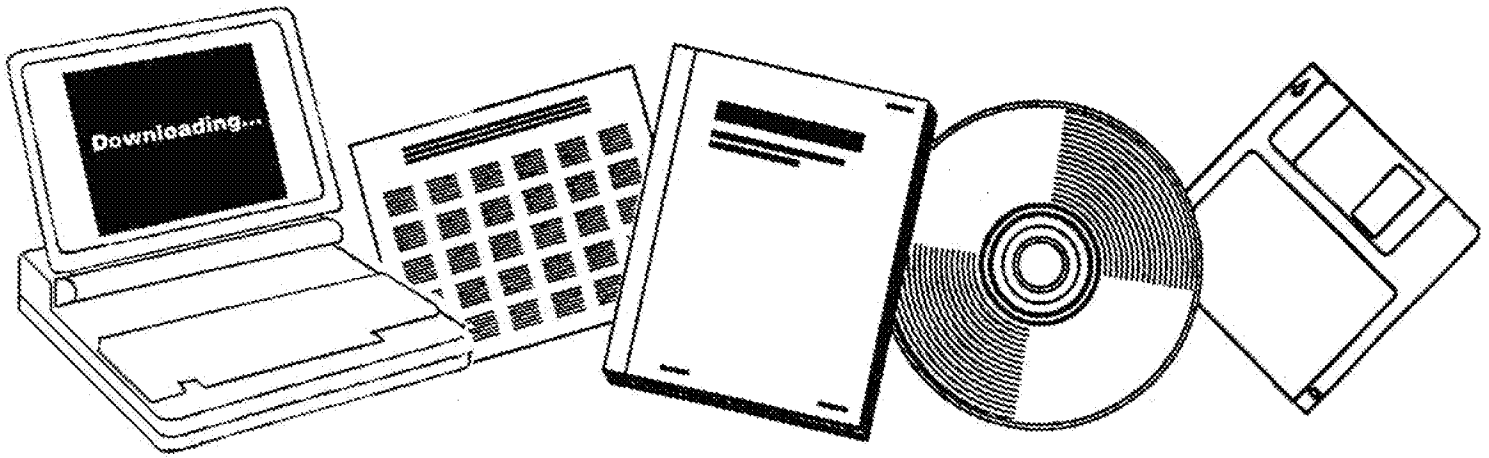
ADP002058

NTIS
One Source. One Search. One Solution.

SAMPLE SURVEYS FROM LIGHT AIRCRAFT COMBINING VISUAL OBSERVATION AND VERY LARGE SCALE COLOUR PHOTOGRAPHY

ARIZONA UNIV., TUCSON

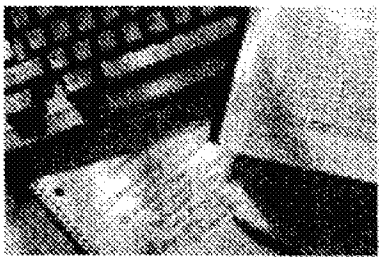
JUN 1982



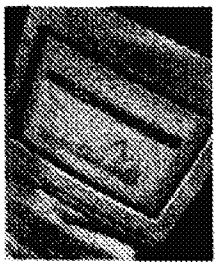
U.S. Department of Commerce
National Technical Information Service

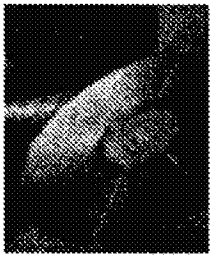
One Source. One Search. One Solution.

NTIS



Providing Permanent, Easy Access to U.S. Government Information





The National Technical Information Service is the Nation's largest repository and disseminator of government-initiated scientific, technical, engineering, and related business information. The NTIS collection includes almost 3 million information products in a variety of formats: electronic download, online access, DVD, CD-ROM, magnetic tape, diskette, multimedia, microfiche and paper.

Search the NTIS Database from 1990 forward

More than 600,000 government research information products have been added to the NTIS collection since 1990. All bibliographic entries for those products are searchable on the NTIS Web site at www.ntis.gov.

Download Publications (1997 - Present)

NTIS provides the full text of many reports received since 1997 as downloadable PDF files. When an agency stops maintaining a report on its Web site, NTIS still offers a downloadable version. There is a fee for each download of most publications.

For more information visit our website:

www.ntis.gov

U.S. DEPARTMENT OF COMMERCE
Technology Administration
National Technical Information Service
Springfield, VA 22161

AD P002058

SAMPLE SURVEYS FROM LIGHT AIRCRAFT COMBINING VISUAL OBSERVATION AND VERY LARGE SCALE COLOUR PHOTOGRAPHY

M. Norton-Griffiths and T. Hart

EcoSystems Ltd.
Nairobi, Kenya

M. Parton

Office of Arid Lands Studies
University of Arizona
Tucson, Arizona

ABSTRACT

The Systematic Reconnaissance Flight (SRF) is a sample survey technique utilising visual observation and small-format aerial photography taken from low-flying aircraft. The collection and assignment of data to a sampling grid allows for its compilation and integration with ancillary data, both point- and grid-referenced. New data variables, which can be derived from SRF and ancillary data, are compiled in a highly-structured database that provides a cost effective survey technique for developing countries.

1. TECHNICAL

The Systematic Reconnaissance Flight (SRF) is a sample survey technique for quantifying the spatial distribution of land use parameters through a combination of visual observations and vertical photography from low-flying, high-wing light aircraft. The aircraft flies parallel transects across a study area at a ground speed of around 160 kilometers per hour and at a height of some 122 metres above ground level. Visual observations are recorded continuously along the length of each transect, but are divided into successive subunits on the basis of elapsed time or distance. One or more vertical sample photographs are taken within each subunit, and all data recorded during the survey are cross referenced to an individual transect/subunit.

With the SRF method the aircraft is accurately located along the selected transects by using a navigation system that tunes into the worldwide network of OMEGA/VLF radio beacons. Each subunit along each transect, therefore, can be accurately located in space. The SRF thus yields a set of data points, each of which is accurately georeferenced.

An SRF survey is always carried out within the framework of a sampling grid, and each data point (subunit) is assigned to an individual grid cell. The Universal Transverse Mercator Grid (UTM) is widely used for such sampling frames since it is a worldwide standard grid system which is projected easily onto aerial photographs or other cartographic/thematic data sources.

1.1 VISUAL OBSERVATIONS

Visual observations supply most of the information on animal numbers and characteristics, both livestock and wildlife, as well as a set of general observations on the land use setting. To conduct systematic visual recording, observers sitting in the rear seats of the aircraft continuously scan a 150m-wide sampling strip that is demarcated by rods attached to the aircraft wing struts. The observers record all their observations onto tape for later transcription, along with time pulses to distinguish between successive subunits. Domestic stock and wildlife species are tallied by subunit; any large herd of animals is photographed (oblique photo through window) for accurate counting at a later date.

Experienced observers also can record a wide range of quantitative and qualitative information on land use characteristics, cultivation methods, settlement types, physiognomic and phenologic characteristics of the vegetation, and erosion phenomena.

1.2 VERTICAL 35MM AERIAL PHOTOGRAPHY

The vertical, 35mm colour diapositives taken along the length of each transect provide most of the data on land use. Typically, one sample photograph is taken in each subunit, although the frequency can be increased over areas of particular interest.

A vertically mounted Olympus OM-2 camera, fitted with an 18mm lens and loaded with high speed Ektachrome film, images approximately 4 hectares at a flying height of 122m above ground level for an image scale of approximately 1:6,700. The actual height above ground level of each photograph is recorded from a radar altimeter at the moment of exposure so that scale and area calculations can be controlled individually for each frame.

The colour diapositives are manually analysed after vertical projection at 10x enlargement onto a 36cm x 24cm dot grid for an interpretation scale of 1:670. Data are obtained from an 18cm x 12cm inner "interpretation area" comprised of 160 cells of 2cm x 2cm, each of which contains four randomly located dots. Each dot has an equivalent ground diameter of approximately 1m, while each grid cell has an equivalent ground area of 183 Km^2.

Three types of data variables are obtained from the 35mm colour diapositives: count, area, and class. Count data are simple enumerations of objects on the colour slides, such as house compounds, buildings with thatched and tin roofs, water tanks, cattle dips, stock compounds, individual trees by species (mango, baobab, coffee, banana), and erosion gullies with associated land use. Area data are estimates of the proportional area of different land use types on the photography. These data can be obtained for land under active cultivation or different crops and crop combinations; areas of fields of different sizes or different methods of cultivation; land taken up by roads, tracks, houses, contour strips and other kinds of on- and off-farm infrastructure; land under fallow or active forest management; canopy cover of woody vegetation; and area affected by gully or sheetwash erosion.

Class data are obtained by classifying the entire frame on some aspect of land use or the environment such as soil colour, method of cultivation (hoe, ox, mechanised), or soil conservation (terraces, contour ploughing, contour bands).

1.3 ANCILLARY DATA

Ancillary data can be integrated into the SRF data set from a variety of sources, including maps, ground survey, and additional orbital/suborbital imagery. Map data can include administrative units, local slope angles and/or landform, rainfall and climatic data, soil type, distances to nearest service/veterinary centre/health centre/market centre/major road, and vegetation zone. Ground survey data can include farming systems, population density and structure, crop yields, and measurements of erosion rates and intensities. Satellite/air photo data can include existing land uses, past land uses, and areas of changing land use intensity.

1.4 DATA COMPILATION AND INTEGRATION

Both original and ancillary data collected in the course of an SRF survey are in either "point" or "grid" form. Point data are individual samples or observations collected at precisely determined points in space, while grid data, which are much more coarse, are derived from the classification of individual UTM grid squares by particular attributes such as rainfall, mean slope angle, and elevation. Since every sample point is assigned to a particular grid cell containing a precisely-determined set of sample points, data are freely transferable between points and grids. Thus, a grid cell can be characterised on the basis of some attribute measured at all of the sample points falling within it, while the points assigned to a grid cell can be characterised by any attribute defined for the grid cell as a whole.

Although some data types do not fall naturally into the point/grid classification, they can still be accommodated in the data set. For example, each point can be classified according to an administrative division or Landsat image stratum into which it falls. Similarly, population census data can be accommodated by classifying the points by the census unit in which they appear, and by assigning to them the value provided from the census unit.

Once the data are compiled into point or grid form, new data variables can be created from any combination of original variables. For example, the effective density of livestock can be expressed as a density of livestock on land available for grazing, which is derived from land area less active cropland, forest land, and land taken up by infrastructure. Similarly, the efficiency of land management can be assessed by expressing the area of on- and off-farm infrastructure which is supporting each hectare of actively cultivated land. Finally, in those rare cases for which the relevant data are available, crop yields can be calculated from measured crop areas weighted by environmental and management factors.

2. APPLICATIONS

2.1 GENERAL

The lack of systematic land use data in a spatial context is a major constraint to efficient development planning. While orbital level remote sensing techniques are valuable for the compilation of small scale/coarse texture land cover information, the finer details of land husbandry and productivity are very expensive to acquire at a regional scale. The SRF provides a cost-effective solution to this problem through the compilation of a highly structured data base within which development projects can be designed, implemented and monitored, specifically in the context of smallholder rural agricultural systems in the developing countries.

2.2 SEASONAL PATTERNS OF MIGRATION

The seasonal patterns of resource abundance and utilisation can be determined by repeating SRF surveys at critical times of the year. In the

85,000 Km^2 impact area of the Jonglei Canal, Southern Sudan, three SRF surveys were conducted during the periods of peak and medium flooding at the height of the dry season. Seasonal movements of domestic stock, of the people associated with them and of wildlife were monitored and mapped on a grid of 10Km x 10Km, with other seasonal characteristics of land use and phenology of the vegetation (Figure 1). The results of the SRF surveys provided the main source of data for assessing the environmental impact of the canal, locating crossing points for domestic stock, and designing agricultural and livestock development programmes.

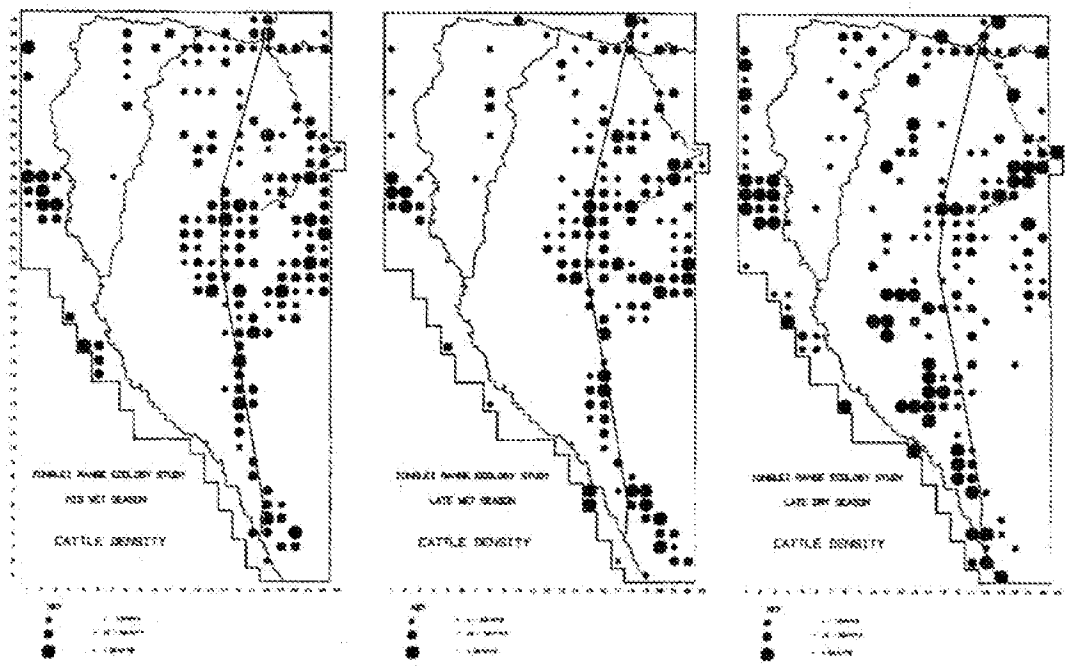


Figure 1. Jonglei Range Cattle Density for A) Mid Wet Season, B) Late Wet Season, and C) Late Dry Season

2.3 LAND USE INVENTORIES

An intensive SRF survey of Machakos District, Kenya, provided land use inventories within each division, location, and sublocation of the 14,000 Km^2 study area. Some 86 parameters of land use and erosion were quantified and mapped from the analysis of 6,500 35mm vertical sample photographs (Figure 2). In addition to land use inventories within each administrative unit, land use analyses were made for agro-climatic zones, major soil types, local slope angles and watersheds (Figure 3). A sediment budget was calculated for the entire district.

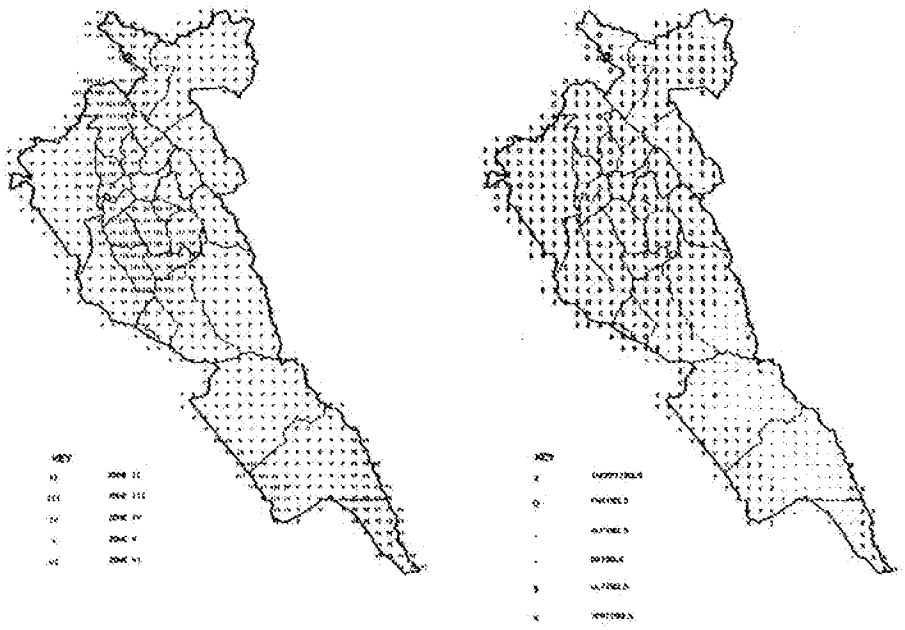


Figure 2. Machakos District Maps of A) Agro-Climatic Zones, B) Major Soil Types

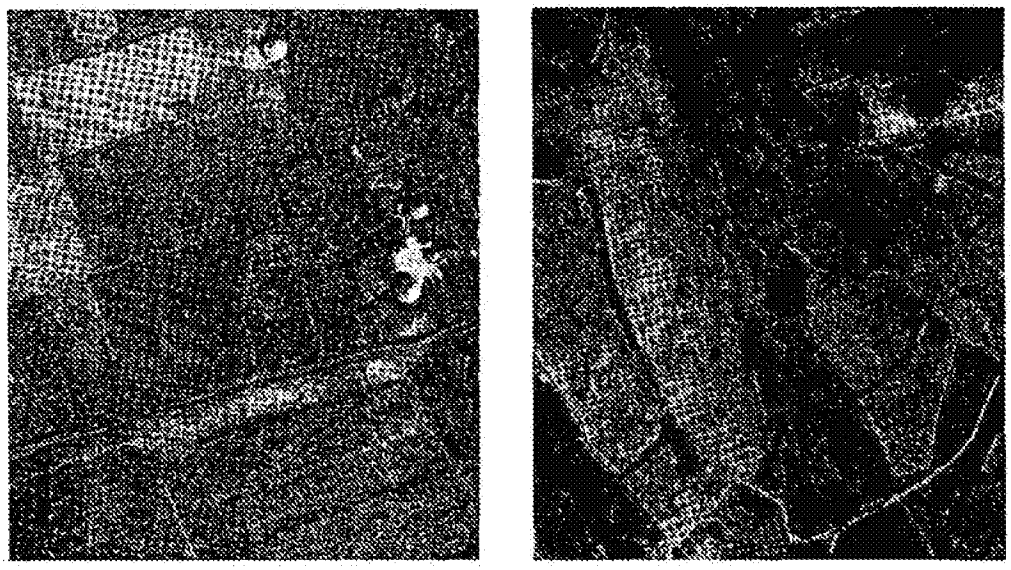


Figure 3. 35mm Aerial Photography, Machakos District

843

2.4 RURAL AGRICULTURAL LAND USE PATTERNS

The characteristics of land use within 2 Km on either side of 52 recently completed rural access roads (RAR) in Kenya were quantified by intensive SRF survey with flight lines spaced 1 Km apart and sample photographs spaced 500m apart. The sample of RARs, which covered the entire environmental spectrum of Kenya, ranged from arid, marginal agricultural land to areas of high agricultural potential. The gradient of land use from shifting agriculture to high intensity commercial farming is clearly demonstrated by ranking the road areas on the percentage of land under active cultivation (Table I).

Table I. Land Use Characteristics of Rural Access Roads

Number of RARs (50 Km^2)	10	11	14	9	8
Resources					
Cultivation/Km^2 (Ha)	6	16	26	36	49
Commercial cultivation %	21	24	32	43	52
Cultivation/Fallow	2	1	3	4	10
Livestock units/Km^2	40	91	101	87	65
Woody Cover/Km^2	37	19	17	11	10
Population/Settlement					
Population/Km^2	52	140	183	264	294
Buildings/Km^2	43	98	109	127	136
Buildings w/tin roof %	21	20	33	34	50
Land Management					
Overhead/Km^2 (Ha)	5.7	8.7	9.4	6.9	11.1
Cultivation/Overhead	1.1	1.8	2.8	5.2	4.4
Per Capita Resources					
Persons/Building	1.2	1.4	1.6	2.0	2.1
Persons/Ha Cultivation	9.0	8.6	7.0	7.3	5.9
Persons/Livestock Unit	1.3	1.5	1.8	4.0	3.3
Persons/Ha Woody Cover	1.3	7.4	10.9	24.2	30.5

Source: Data drawn from 52 rural access roads throughout the Republic of Kenya, each sample area approximately 50 Km^2. Rural Access Roads Impact Study funded by NORAD

2.5 LAND OVERHEAD

The proportion of land that must be set aside for on- and off-farm infrastructure and support can be a major constraint to the absolute level of production. In Machakos District, Kenya, land overhead rises steeply as a function of the area of cultivation per square kilometre. In this hilly and well-terraced area, land is effectively saturated for cultivation at a cultivation intensity of 60 percent. The SRF survey data show that less than 2 percent of the land is cultivated at an intensity greater than 50 percent (Figure 4).

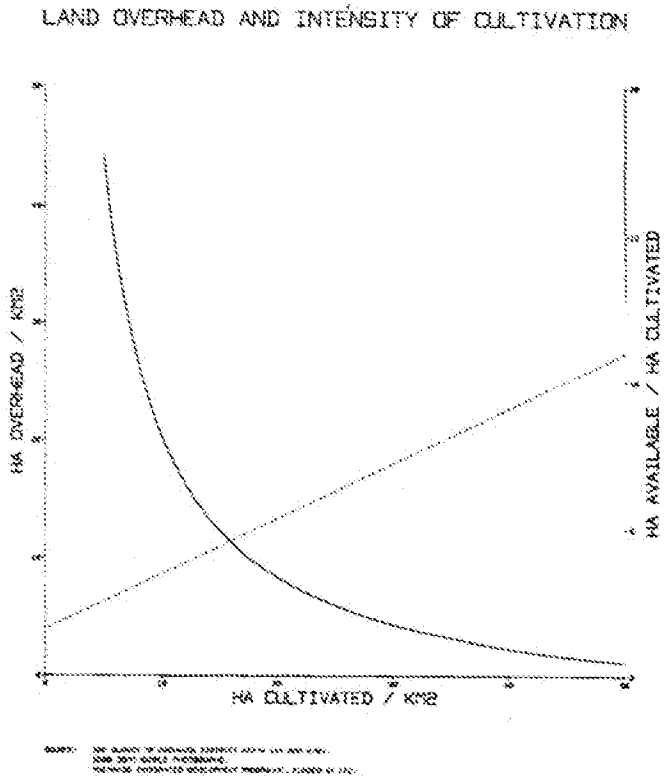


Figure 4. Land Overhead and Intensity of Cultivation

3. REFERENCES

Croze, H., and M.D. Gwynne. 1980. Rangeland Monitoring: Function, Form, and Results. The Global Environment Monitoring System, Selected Works on Ecological Monitoring of Arid Areas (United Nations Environment Programme, GEMS PAC Information Series No. 1, Document 3). vp.

Gwynne, M.D., and J.J. Croze. 1975. The Concept and Practice of Ecological Monitoring Over Large Areas of Land: The Systematic Reconnaissance Flight (SRF). Proceedings of the Ibadan/Garoua International Symposium on Wildlife Management in Savanna Woodland, University of Ibadan, Nigeria.

_____. 1981. Light Aircraft and Resource Monitoring. Low-Level Aerial Survey Techniques (International Workshop, November 1979, Nairobi, Kenya), International Livestock Centre for Africa Monograph 4. pp. 11-25.

Norton-Griffiths, M. 1975. The Numbers and Distribution of Large Mammals in Ruaha National Park, Tanzania. East African Wildlife Journal 13, pp. 121-140.

Norton-Griffiths, M. 1978. Counting animals. Nairobi: African Wildlife Federation, Handbook No. 1 (2nd ed.), P.O. Box 48177, Nairobi, Kenya.

Pennycuick, C.J., J.B. Sale, M. Price, and G.M. Jolly. 1977. Aerial Systematic Sampling Applied to Censuses of Large Mammal Populations in Kenya. East African Wildlife Journal 15, pp. 139-146.



ALL SALES ARE FINAL

NTIS strives to provide quality products, reliable service, and fast delivery. Please contact us for a replacement within 30 days if the item you receive is defective or if we have made an error in filling your order.

▲▲ E-mail: customerservice@ntis.gov
▲▲ Phone: 1-888-584-8332 or (703)605-6050

Reproduced by NTIS

National Technical Information Service
Springfield, VA 22161

This report was printed specifically for your order from nearly 3 million titles available in our collection.

For economy and efficiency, NTIS does not maintain stock of its vast collection of technical reports. Rather, most documents are custom reproduced for each order. Documents that are not in electronic format are reproduced from master archival copies and are the best possible reproductions available.

If you have questions concerning this document or any order you have placed with NTIS, please call our Customer Service Department at 1-888-584-8332 or (703) 605-6050.

About NTIS

NTIS collects scientific, technical, engineering, and related business information – then organizes, maintains, and disseminates that information in a variety of formats – including electronic download, online access, DVD, CD-ROM, magnetic tape, diskette, multimedia, microfiche and paper.

The NTIS collection of nearly 3 million titles includes reports describing research conducted or sponsored by federal agencies and their contractors; statistical and business information; U.S. military publications; multimedia training products; computer software and electronic databases developed by federal agencies; and technical reports prepared by research organizations worldwide.

For more information about NTIS, visit our Web site at http://www.ntis.gov.

NTIS

Ensuring Permanent, Easy Access to U.S. Government Information Assets



U.S. DEPARTMENT OF COMMERCE
National Technical Information Service
Alexandria, VA 22312 703-605-6000

Journal of Biogeography (1988) **15**, 149–156

Aerial point sampling for land use surveys

M. NORTON-GRIFFITHS EcoSystems Ltd, Nairobi, Kenya

ABSTRACT. Aerial point sampling (APS) is an aerial survey method for quantifying land use patterns specifically among African smallholders where the tiny size of the fields, the incidence of intercropping, and the highly varied cropping calendar, all reduce the effectiveness of more conventional survey methods. In an APS survey, vertical sample 35 mm colour diapositives are taken at intervals along flight lines at an image scale of 1:7000.

The colour slides are analysed by downward projection on to a desk-top dot grid at an interpretation scale of 1:700. Crop areas are given by the proportion of dots falling into a crop class, expressed as a per cent which is equivalent to hectares per square kilometre. Densities of objects such as houses are found by dividing the numbers counted by the area analysed on the photograph.

Ancillary data, such as climate, landform, soils or population density can be easily integrated into the data set since the position of each photograph is known with considerable accuracy.

Statistics are rapidly produced in sectorial or cross sectorial form for any set of reporting units.

Introduction

EcoSystems Ltd (ESL) has developed aerial point sampling (APS) as an aerial survey method for quantifying land use patterns within the context of regional planning. The specific motivation for developing APS was the African smallholder farming system where the tiny size of fields, the wide incidence of intercropping, and the highly varied cropping calendar, all reduce the effectiveness of more conventional survey methods.

Conventional large format photography suffers from two main drawbacks. Firstly, costs prohibit the use of scales large enough to resolve the intricate patterns of smallholder land use. Secondly, the climatic 'window' during which high altitude photography can be carried out, especially in East Africa, rarely coincides with the stage of maximum crop differentiation and usually coincides with the post-harvest period.

Satellite systems, which are often promoted as a useful tool for smallholder land use monitoring and mensuration, suffer the same drawbacks. Imaging conditions are often poorest at the times most suitable for surveys; while resolution, even of SPOT, is still inadequate to pick apart the intricacies of the landscape. For example, in Kenya the median field size for all cereal crops is 0.2 ha which requires a resolution approaching 2 m (Bowker, 1985; Park, 1981).

The APS method overcomes these problems in two ways. Firstly, by flying relatively low (between 400 and 1200 ft above ground level) weather conditions, even heavy rain, rarely interrupt the flying schedule. Secondly, the

method uses very large scale, sample colour photography.

The equipment requirements for an APS sample are modest compared to more conventional photography. Minimum requirements are for a light aircraft with a vertically mounted 35 mm camera with a bulk back and a radar altimeter for monitoring height above ground level (agl). Colour diapositive film is used which can be developed commercially virtually anywhere with a 24 h turn around. ESL uses a Cessna 206 with twin vertical bulk backed 35 mm Nikon F3 cameras, a radar altimeter, and an OMEGA/VLF navigation system.

Sampling

Aerial point sampling is a three-level system of flight lines (primary units), vertical point sample photographs taken at intervals along them (secondary units), and sample estimates of land cover taken off the photographs.

A typical APS survey will cover between 20,000 and 50,000 km². Although the primary sampling can be random or systematic, stratified or unstratified, ESL has found in surveys covering over 1.2 million square kilometres that unstratified, systematic sampling consistently provides the most useful data.

This is simply because in most regional development contexts all parts of a development area, and all aspects of land cover, are of equal interest and importance. Furthermore, the results from an APS survey will be required for Districts, Divisions and Locations (equivalent to County, District and Parish in the United Kingdom); and for catchments and sub-catchments; and for agro-climatic zones; and for strata of land potential. Therefore, since no single sampling frame will meet all these survey objectives efficiently, the practical advantages of frameless (systematic) sampling far outweigh the theoretical advantages of statified random sampling.

The primary sample intensity is therefore controlled by the median size of the smallest set of reporting units. In Kenya these are usually the Locations which average around 200–300 km². This requires a spacing of 2.5 km between flight lines with the point sample photographs every kilometre along each flight line. At our typical photo scale, this yields a primary sampling fraction of 10% with a secondary sampling fraction of 17%.

Vertical photography

The vertical point sample photographs are taken on high-speed colour diapositive film. Flying height and focal length of lens are selected to give a nominal image scale of 1:7000 (e.g. 50 mm lens at 1150 ft agl) and a ground coverage of 4.2 ha. However, the exact height of the aircraft is recorded each time a photograph is taken, so that the exact scale can be calculated later. At this nominal scale each photograph covers about 4.2 ha and on average there will be one sample photograph for every 2.5 km².

Georeferencing the sample photographs

Each photograph is now treated as a point sample, and fixing their exact location is essential to the whole APS method. Every time a photograph is taken, the distance along the flight line from the start point, and the distance left or right of track, is recorded from the OMEGA/VLF navigation system. From these two parameters it is possible to plot the locations of each sample photograph on a map overlay to within 200–300 m.

Typically a 1:250,000 scale map overlay is made showing the position of each of the sample photographs. This overlay is then used to assign each individual point sample to any stratum, such as a District, Division or Location; catchment or sub-catchment; soil type; climate zone; or UTM grid cell. This is done simply by placing the overlay on to the appropriate 1:250,000 scale base map of the stratum boundaries.

Once a sample point has been assigned to a stratum such as a Location or a soil type it can be associated with any characteristic of that stratum such as population density or inherent erodibility. The APS method thus provides a powerful tool for integrating a wide range of ancillary data into a land use survey.

All data associated with the sample points can now be used to create statistical estimates for the different strata, for example for each District, Division and Location within the survey area. Estimates can also be made for individual UTM grid cells which can then be mapped in a cell format.

Ground truth

Since the bulk of the land use data from an APS survey comes from the interpretation of the sample aerial photographs, ground truthing is of

obvious importance. The first stage is for the interpreters to fly on the surveys and make notes of the crops, intercrops, vegetation and other items of interest that they see, and in particular whenever they see something that they do not understand. Next, these areas are visited with the aircraft as soon as possible for a closer look, which often suffices to solve the problem.

All 'problem areas' are none the less noted on to a master map, and after the main survey is completed the aircraft visits each in turn making low passes so that the observers can clearly see the crops and intercrops. The problems are again discussed, and solutions and interpretations proposed. Finally, a helicopter is sent out to visit the few remaining problem areas about which the interpreters remained uncertain. Low hovers, and landings, are made until all conflicts are resolved.

Photo interpretation procedures

For interpretation, each colour diapositive is projected down on to a desktop dot grid at a ×10 enlargement to give an average interpretation scale of 1:700. The semi-random dot grids consists of an array of 18×12 cells of 2×2 cm in size, in each of which are randomly located two dots of approximately 1.5 mm diameter, equivalent to 1.05 m on the ground at the average interpretation scale. The photo interpretation is carried out only within an inner interpretation area of 16×10=160 cells containing 320 dots, thus overcoming interpretation problems associated with the edges of the field of view.

Count data are simple enumerations within the inner interpretation area of objects such as house compounds, buildings with iron sheet roofs, buildings with thatched roofs, or even the numbers of individual plants or trees. In general the 50% rule is followed, which specifies that 50% or more of the object being counted must lie within the inner interpretation area to be included into the tally.

Area data are measurements of the proportional area of different kinds of land cover, the proportions being expressed in terms of the number of dots falling within each land cover class. Area data are obtained for individual crops and crop combinations; for the canopy cover of the natural vegetation; for the land taken up by roads, tracks, houses and other kinds of overheads; and for fallow land. The 50% rule is again used to decide if a dot should be included into a particular area measurement.

Qualifiers are recorded on a presence/absence basis, and are used primarily to describe the status of land management, the methods of cultivation, and the occurrence of terracing or contouring.

The procedures followed during photo interpretation are designed to control the accuracy and consistency with which the interpretation is carried out. The procedures are iterative, and included the following stages: (i) Pre-reconnaissance survey to qualify the range of crop types and crop combinations, natural vegetation classes, etc., that might be used as individual photo interpretation classes. (ii) Initial selection of interpretation classes, examination of a range of colour diapositives to check feasibility. Classes are subsequently added/deleted, merged/split, and an initial key is formulated which defines the important visual, textural and other characteristics of each interpretation class. (iii) Testing the interpretation classes with a further selection of diapositives, cross checks and discussions between entire photo interpretation team. (iv) Final selection of the interpretation classes. (v) Ground truthing involves all interpreters flying in the survey aircraft, additional low flights over problem areas, and final checking by helicopter. (vi) The senior photo interpreter continuously monitors the performance of all the photo interpretation team, to achieve consistency of results.

Typically, some 100 non-overlapping photo interpretation classes will be selected. These will include perhaps 60 classes covering agricultural land use, 15 classes of infrastructure, 25 classes of natural vegetation, and always a miscellaneous (dustbin) class. Other classes might describe land management, erosion, and soil/water conservation activities.

The interpreters record data directly on to a data sheet which allows quick and efficient visual checking, and a skilled interpreter can process between 30 and 40 slides a day. The data are next transferred onto 8-bit microcomputers (such as Osbornes) using dBaseII, before transfer to Olivetti M24s and dBaseIII for processing.

The survey estimates

The survey estimates provide densities and total numbers within defined areas such as Districts

and Locations. Densities express the numbers per square kilometre of, for example, houses or woodlots, but when applied to crops they express hectares per square kilometre which is equivalent to percentage cover. Total numbers (or hectares) express the totals within the defined area.

The survey estimates are calculated using a derivation of the ratio method, which is designed for unequal sized sampling units and which eliminates the influence of sample unit size on the sample estimate and the sample variance. It is known as the ratio method because the estimates are derived from the ratio between the amount of material sampled and the area sampled, in other words the density (Jolly, 1969; Norton-Griffiths, 1978).

In this application of the ratio method, the individual flight lines are treated as the primary sampling units. The basic calculations are set out below. If we consider one crop at a time, then:

z=the area of each primary sample unit (flight line)

y=the number of crop hectares enumerated along the sample unit (calculated from the individual point samples)

R=total hectares counted/total area counted
=the average density
$=\Sigma y/\Sigma z$

The survey estimate is then found by:

$$Y=R\cdot Z$$

where Z is the total area under survey.

The precision of a survey estimate is calculated as follows. Let:

s_y^2=the variance between the numbers or hectares in all sample units

s_z^2=the variance between the areas of all sample units

s_{yz}=the covariance between numbers or hectares and the areas of the sample units

Then the variance of a survey estimate is:

$$\mathrm{Var}(Y)=N(N-n)/n\times(s_y^2-2\times R\times s_{yz}+R\times s_z^2)$$

(note the negative sign of the covariance term) with a standard error $\mathrm{SE}(Y)=\sqrt{\mathrm{Var}(Y)}$

y, z and R defined above; n is the number of sample units in the sample; and N is the total number of sample units from which the sample was drawn.

There is a second term to the variance of the survey estimate derived from the variance between point samples (i.e. photographs) within sample units (Norton-Griffiths, 1973). Fortunately this term is very small and contributes no more than 1.5% of the total variance. It can therefore be safely ignored.

The 95% confidence limits of a survey esti-

TABLE 1. Standard errors of survey estimates (expressed as per cent of the estimate)

Ha/km²	Area (km²)										%
	50	100	200	400	600	800	1000	2500	5000	>5000	
0.02	95	68	50	36	30	27	24	17	13	11	8
0.04	68	50	36	27	23	20	18	13	11	9	3
0.06	57	41	30	23	19	17	16	11	9	8	3
0.08	50	36	27	20	17	15	14	11	9	7	2
0.10	45	33	24	18	16	14	13	10	8	7	6
0.20	33	24	18	14	12	11	10	8	7	6	9
0.40	24	18	14	11	10	9	9	7	6	6	7
0.60	21	16	12	10	9	8	8	6	6	5	5
0.80	18	14	11	9	8	8	7	6	6	5	5
1.00	17	13	10	9	8	7	7	6	5	5	9
2.00	13	10	9	7	7	6	6	5	5	5	10
4.00	10	9	7	6	6	6	5	5	5	5	7
6.00	9	8	7	6	6	5	5	5	5	4	3
8.00	8	7	6	6	5	5	5	5	5	4	2
10.0	8	7	6	5	5	5	5	5	4	4	5
20.0	7	6	5	5	5	5	5	4	4	4	7
40.0	6	5	5	5	5	4	4	4	4	4	4
60.0	5	4	4	4	3	3	3	2	2	1	2
80.0	5	4	3	3	3	2	2	2	2	1	3
%	10	19	29	14	10	5	3	6	3	1	100

mate can be calculated by multiplying the standard error by the t value for $n-1$ degrees of freedom. These confidence limits can then be expressed as a percentage of the estimate itself.

The precision of any estimate from an APS survey is influenced by the absolute size of the sample and by the size of a stratum. A sample of 50 units will always be more precise than will be a sample of 25 units, whatever the sample fraction while, for a given sample fraction, an estimate from a large area will always be more precise than will be an estimate from a small area. The precision of an estimate is also influenced by the overall abundance of the attribute under survey. An estimate of a crop with 10% cover will always be more precise than will be an estimate of a crop with only 5% cover.

The influence of these factors at our typical sampling intensity is shown in Table 1 where the columns of the Table represent areas of different sizes (in square kilometres) such as Districts or Locations; the rows of the Table represent mean densities of attributes such as houses and crop areas; and each cell in the Table shows, for a given mean density and area, the standard error (expressed as a percentage of the mean) of 95% of all survey estimates. Table 1 thus provides a simple look-up table for assessing the precision of any survey estimate.

Data manipulation

One of the most important features of the APS method is the flexibility with which data can be integrated within a spatial context. As described above, this is achieved by fixing the spatial coordinates of each sample point to an accuracy of 250–300 m, the operational accuracy of the navigation system in the survey aircraft. Once the coordinates of each sample point are known, they can be assigned to any spatial domain imposed upon the data. It is also possible to calculate the distance between each sample point and any other defined point in the survey area, such as a crop store or a major road.

Recombinant data variables can be created from any existing variable in the database, either singly or in combination, and with or without ancillary data. A simple example is afforded by soil types, for once a sample point is assigned to a soil type it can be characterized on the wide range of soil attributes associated with that soil type. A second example is given by the 'Total Area Under Cultivation' which is found by summing all the individual crop and intercrop areas.

The control of bias

Errors and bias in aerial surveys are two very different things. Errors, by definition, are random and their cumulative effects cancel out. Errors affect the precision of a survey estimate, and are quantified by the standard error or confidence limits of a survey estimate. In constrast, a bias is an error in a consistent direction whose cumulative effect does not cancel out. Biases affect the accuracy of a survey estimate, and must be controlled if accuracy as well as precision is sought.

Biases can arise through the design of an aerial survey, from inaccurate maps, from the way in which an aircraft is flown, or from the analysis of the sample photography. There are three aspects to the control of biases. Firstly, design the survey operation to minimize biases; secondly, hold biases constant throughout the survey; and thirdly, identify the major sources of bias and, where practicable, correct them.

Systematic sampling is known to give unbiased estimates so long as simple precautions are taken when designing the orientation of the flight lines. It is, for example, conceivable that

TABLE 2. Comparison between GNS500A position fixes and map references

	Absolute error	East–West error	North–South error
No. of comparisons	300	300	300
Mean (m)	380	250	240
Standard deviation (m)	210	200	180
Standard error (m)	12	12	10
Nominal accuracy (m)	261	185	185

the flight line spacing might harmonize exactly with some feature of the landscape. This possibility is minimized by orientating the flight lines so that they cut across the dominant relief and drainage features in the surveyed area. However, the variances of the estimates from a systematic sample are always biased in an upward (positive) direction. Estimates from systematic samples are therefore always more precise than indicated by the calculated variances.

Bias can arise from the way in which the aircraft is flown, from inaccurate navigation, poor speed control and poor height control. However, the flight information collected during the survey is used to test whether such biases are present, to estimate their magnitude, and to correct them before the data are analysed.

The GNS500A navigation system virtually eliminates bias from gross errors in navigation. The accuracy of the GNS system has been tested by comparing the GNS lat/long readout recorded when the camera was fired against the lat/long derived from map sheets. The photographs were first plotted on to up-to-date 1:20,000 scale black-and-white aerial photographs before being transferred to 1:50,000 topographical maps. On a sample of 300 comparisons, the mean error in the GNS navigation system was found to be 380 m (Table 2), which is almost certainly an overestimate.

TABLE 3. Correction factors for mean slope angles

Slope angle (degrees)	f (%)	Per cent of photographs	Correction factor*
0	7	10	1.0000
1	21	22	1.0003
2	18	17	1.0011
3	14	14	1.0026
4	12	9	1.0046
5	7	7	1.0073
6	4	4	1.0105
7	3	3	1.0143
8	3	3	1.0188
9	2	2	1.0239
10	1	1	1.0297
11	1	1	1.0361
12	2	1	1.0433
13	1	1	1.0512
14	1	1	1.0599
15	1	1	1.0649
16	1	1	1.0798
17	1	1	1.0910

Source: Machakos Integrated Development Programme Survey of Agriculture and Land Use, February 1981, 4200 35 mm diapositives.

* At mean flying height of 418 ft agl.

The height above ground level of the aircraft is recorded every time a photograph is taken, so that the scale and area imaged can be calculated exactly. This removes any bias from inaccurate flying. However, if the aircraft is in a straight and level altitude but the ground beneath it is sloping, the area photographed will be larger than

TABLE 4. Recounts of houses and structures from 35 mm diapositives

No. of frames	Mean of first counts	Total houses on first count	Total houses on second count	Per cent difference	Mean of second counts	SE (%)
126	1	126	128	+1.6	1.02	9.6
63	2	126	136	+7.9	2.16	7.2
83	3	249	262	+5.2	3.16	6.3
32	4	128	135	+5.5	4.22	5.4
21	5	105	112	+6.7	5.33	6.8
26	6	156	163	+4.5	6.27	7.2
8	7	56	59	+5.4	7.38	6.4
18	8	144	151	+4.9	8.39	3.9
16	9	144	147	+2.1	9.19	3.4
8	10	80	80	0.0	10.00	3.2
8	11	88	90	+2.3	11.25	3.8
4	13	52	53	+1.9	13.25	3.5
4	14	56	56	0.0	14.00	3.6
4	15	60	62	+3.3	15.50	3.6
4	16	64	65	+1.6	16.25	3.2
4	19	76	76	0.0	19.00	3.8
4	27	108	111	+2.8	27.75	1.9
429	4.24	1818	1886	+3.7	4.40	2.5

Source: Machakos Integrated Development Programme Survey of Agriculture and Land Use, February 1981.

that calculated from the height above ground level. The slope of the ground relative to the altitude of the aircraft is therefore another potential source of bias.

Table 3 shows the slope angle of the ground under the aircraft for each of 4200 sample photographs. Also shown is the 'correction factor', namely the amount by which the area of each photograph calculated from the height above ground level must be multiplied to take the slope into account, assuming that the direction of any slope was parallel to the direction of flight. Over the whole set of photographs, the mean correction factor is only 1.0080, so the influence of this source of bias is negligible.

In general, bias from photo interpretation is minimized firstly by training the photo interpreters on the interpretation key being used, and secondly by carefully monitoring and checking their performances while the photographs are being analysed.

The presence of bias can be detected by carefully reanalysing a sub-sample of photographs, treating the recounts as giving the more accurate information. Table 4 shows the results of recounting the number of houses and other buildings on a sub-sample of 429 photographs. Over the whole sub-sample, the recount gave a figure of 1886 buildings compared to the original count of 1818 buildings, a difference of 3.7%.

The most important data derived from the 35 mm diapositives are the estimates of crop areas, cultivation and other aspects of land use. Table 5 presents an analysis of a recount of 116 'areas' measured off a sample of 35 mm diapositives. A total of 258 recounts were carried out, on areas ranging from less than 5% of the field of view to over 50% of the field of view. In no case are any of the recounts significantly different from the original counts.

TABLE 5. Recounts of crop areas from 35 mm diapositives

Crop cover	Original counts			Re-counts		
	n	Mean	SE (%)	*n*	Mean	SE (%)
0–5	16	3.2	6.6	37	3.2	4.5
5–10	23	7.3	3.9	51	7.3	2.7
10–15	12	12.6	3.7	29	12.7	2.2
15–20	8	16.3	1.7	19	16.3	1.4
20–30	26	22.9	2.3	57	23.3	2.5
30–40	14	37.2	2.2	30	36.9	1.5
40–50	7	46.7	2.4	13	46.1	2.0
>50	10	63.9	5.3	22	63.1	3.5

Whereas the data in Tables 4 and 5 test the consistency of the photo interpreters under operational conditions, a controlled experiment was set up to test if there was any bias in the estimation of sizes and shapes arising from the design of the dot grid itself. Seven areas were chosen (Table 6) ranging from 92 m^2 to 3670 m^2 at the average interpretation scale, the expected number of dots ranging from 1 to 40. Each area was counted in seven different shapes in which the ratio of length to breadth varied from 1:1 (Shape A) to 1:25 (Shape F). Shapes A–E simulate fields, while Shape F simulates long thin linear features such as roads and hedges.

Fifty dot counts were carried out on each combination of size and shape (Table 7). The first important result is that none of the estimates show any bias, and in no case is the mean estimate of a size/shape combination significantly different from the expected value. Furthermore, the standard errors of the estimates are all acceptably small. The dot grid is therefore providing acceptably precise and apparently unbiased estimates of areas of different shapes. Indeed, a two-way analysis of variance (Table 8) shows that the shape of the area is having no influence

TABLE 6. Shapes and sizes for testing dot grid bias

Expected dots:	1.0	3.5	8	13	20	29	40
Hectares:	0.01	0.03	0.07	0.12	0.18	0.27	0.37
Square metres:	92	321	734	1193	1835	2661	3670
Dimensions of shapes (m)							
A 1:1	10×10	18×18	27×27	35×35	43×43	52×52	61×61
B 1:1.5	8×12	15×23	22×23	28×42	35×53	42×63	49×74
C 1:2	7×14	13×26	19×38	24×48	30×60	38×76	43×86
D 1:4	5×20	9×36	14×56	17×68	21×84	26×104	30×120
E 1:11	3×33	6×66	8×88	10×110	13×143	16×176	18×198
F 1:25	2×50	3×107					

Note: Dimensions (m) of each shape A–F are approximate.

TABLE 7. Results of bias test on dot grid

Shape		Expected dots						
		1.00	3.50	8.00	13.00	20.00	29.00	40.00
A 1:1	$\bar{x}$	1.06	3.72	8.00	13.14	19.68	28.14	39.20
	SD	0.76	1.01	1.26	18.60	3.64	4.72	3.19
	SE	0.11	0.14	0.18	0.26	0.51	0.67	0.45
	SE (%)	11	4	2	2	3	2	1
B 1:1.5	$\bar{x}$	1.02	3.52	7.84	13.28	20.47	29.26	40.16
	SD	0.84	1.20	1.62	1.80	2.10	2.66	3.09
	SE	0.12	0.17	0.23	0.25	0.30	0.38	0.44
	SE (%)	12	5	3	2	1	1	1
C 1:2	$\bar{x}$	1.18	3.54	7.60	13.24	20.33	29.24	39.80
	SD	0.94	1.22	1.56	1.42	2.46	2.95	3.39
	SE	0.13	0.17	0.22	0.20	0.35	0.42	0.48
	SE (%)	11	5	3	1	2	1	1
D 1:4	$\bar{x}$	1.18	3.60	7.62	13.00	20.52	29.50	39.98
	SD	0.94	1.34	1.61	1.84	3.05	2.96	3.10
	SE	0.13	0.19	0.23	0.26	0.43	0.42	0.44
	SE (%)	11	5	3	2	2	1	1
E 1:11	$\bar{x}$	0.96	3.50	7.56	12.78	19.58	27.84	39.82
	SD	0.86	1.49	2.17	2.89	3.61	5.29	5.63
	SE	0.12	0.21	0.31	0.41	0.51	0.75	0.80
	SE (%)	13	6	4	3	3	3	2
F 1:25	$\bar{x}$	0.98	3.62					
	SD	0.91	1.82					
	SE	0.13	0.26					
	SE (%)	13	7					

TABLE 8. Two-way analysis of variance of sizes against shapes

Source	ss	df	ms	F
Size	6017.7	6	1003.0	10030
Shapes	1.5	5	0.3	3
Residual	2.6	30	0.1	
Total	6021.8	34		

Data from Table 7, seven sizes and five shapes (A–E only).

at all on the number of dots being counted; the only influence comes from the size of the area.

Conclusions, and costs

The APS method has evolved over the last 6 years in response to requirements from East Africa development planners for regional level data on land use and land cover. The method is now widely tested. It appears to be very robust and able to deliver usable data on a wide range of land covers within a wide range of reporting units. The ability to integrate ancillary data within the photo database is an additional advantage.

Costs are difficult to generalize upon since the costs of labour, aircraft and film varies widely between countries. But in Kenya a typical APS survey in 40,000 km^2, with a sample point density of 1 per 2.5 km^2, analysing some 200 land cover variables and fifty ancillary data variables, reporting on twelve major strata and producing some 100 coloured thematic grid cell maps, will cost in the order of US$6.00 per square kilometre. This cost can be as low as US$2.00 per square kilometre if very few variables are analysed and as high as US$10.00 per square kilometre if the survey results in a major database creation and installation.

References

Bowker, D.E. (1985) Priorities for worldwide remote sensing of agricultural crops. *Photogrammetric Engineering and Remote Sensing,* **51,** (10), 1625–1631.

Jolly, G.M. (1969) Sampling methods for aerial census of wildlife populations. *East Afr. Agric. For. J.* **34,** 46–49.

Norton-Griffiths, M. (1973) Counting the Serengeti migratory wildebeest using two-stage sampling. *East Afr. Wildl. J.* **11,** 35–49.

Norton-Griffiths, M. (1978) *Counting Animals,* 2nd edn. African Wildlife Leadership Foundation, Nairobi.

Park, A.B. (1981) Recent advances in remote sensing. Presented at the International Geoscience and Remote Sensing Symposium (IGARSS), p.17.

Review Article

Rectification of Digital Imagery

Kurt Novak
Department of Geodetic Science and Surveying, The Ohio State University, 1958 Neil Avenue, Columbus, OH 43210

ABSTRACT: Different methods can be applied to generate digital orthophotos. Three commonly used approaches are analyzed and compared in this paper. They can be applied to rectify both digitized aerial photographs and satellite scenes. These methods are polynomial, projective, and differential rectifications. The first two are defined by analytical transformations between image and orthophoto without considering the geometry and orientation of the camera. They are approximate solutions. The last one models the physical reality of the imaging process by means of the collinearity equations and corrects for relief displacements. For eliminating distortions of the camera system, additional parameters were included. This proves to be necessary when images are directly taken by video cameras. All three methods were implemented on a workstation and were tested with digitized aerial photographs and video images. By overlaying GIS data over the digital orthophoto, the quality of the rectification is checked. To determine the planimetric accuracy of the results, the coordinates of targets were measured in a digital orthophoto and compared to known map coordinates.

INTRODUCTION

THE COMBINATION OF REGULAR LINE MAPS with aerial photographs is desirable for many applications. While line maps usually consist of topographic elements such as roads, buildings, and rivers, many features important for disciplines like geology, archaeology, forestry, etc., are missing. However, they can be found in aerial or satellite images. In order to be able to exactly overlay images and maps, their geometry has to be the same: that is, an orthogonal projection of all points of the ground to a reference surface. This process is called *rectification*, and the resulting image-based map is the *orthophoto*.

Recently rectification methods have gained more significance due to the fact that digital maps (stored in a geographic information system, GIS) are to be combined with digital imagery. To make sure that they are overlaid at the correct locations, both have to be related to the same datum (map projection). Many image processing systems designed for digital mapping and remote sensing provide routines that perform this rectification procedure; it is sometimes called geo-referencing or geocoding. The mathematical models applied range from simple affine transformations, utilizing higher order polynomial and projective transformations, to differential rectification with relief displacement correction.

The last method is of particular importance if a surface model of the landscape has to be created. Because digital images and digital elevation data are both related to a planimetric grid, they are basically stored in the same way: as matrices of gray or elevation values. Digital rectification assigns a gray value to each grid-element of the digital elevation model (DEM), so that both elevation and density of the surface are stored at the same planimetric location.

This paper investigates different rectification methods, explains the modifications necessary to apply them to satellite imagery, and tries to point out the advantages and setbacks of each. Practical examples show how the planimetric positions of points vary in the different orthophotos. Differential rectification is enhanced by additional parameters in order to correct for lens and film distortions. This is important if video cameras are used for data collection, as well as with satellite imagery to model deviations of the orbit.

Only a few authors have covered digital rectification in recent years. The first system for digital orthophoto generation using scanning microdensitometers was presented by Keating and Boston (1979). This system replaces the optical projection of a small slit through zoom lenses and dove prisms (applied in analytical orthophoto projectors) by electronic sensors that digitize small parts of the image, a processor that positions the sensor, and a film writer that directly exposes each pixel on the film. The basics of digital rectification are explained by Konecny (1979), and are discussed in Baehr (1985). A very interesting method has been implemented by Jansa (1983). He uses linear prediction to recitfy Landsat MSS images in a dense network of control points. Digital rectification is an important module of digital stereo workstations (Mueller *et al.*, 1988; Hood *et al.*, 1989). Systems of that kind are mostly based on commercial image processing systems, and allow one to combine digital orthophotos with vector data of a GIS.

TRANSFORMATION OF DIGITAL IMAGES

To transform a digital image by an analytical function, one can pursue either a direct or an indirect approach. The *indirect method* takes each pixel location of the result (e.g., orthophoto), determines its position in the original image by the selected transformation f_x and f_y (Equation 1), and interpolates the gray value by a given resampling method (Figure 1a); that is,

$$\begin{aligned} x &= f_x(x', y') \\ y &= f_y(x', y') \end{aligned} \quad \text{indirect transformation of point } (x', y') \text{ from the result to the original image.} \tag{1}$$

where

x, y = pixel coordinates of the original image,
x', y' = pixel coordinates of the result, and
$f_x(\ ), f_y(\ )$ = transformation functions.

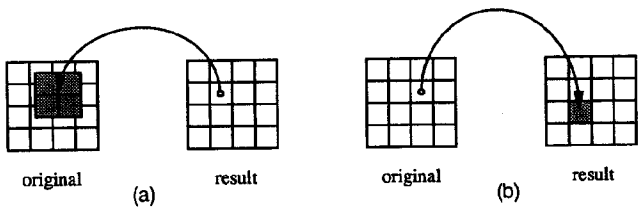


FIG. 1. Indirect (a) and direct (b) transformations of a pixel.

PHOTOGRAMMETRIC ENGINEERING & REMOTE SENSING,
Vol. 58, No. 3, March 1992, pp. 339–344.

0099-1112/92/5803-339$03.00/0
©1992 American Society for Photogrammetry
and Remote Sensing

©2008 INIST CNRS . Tous droits de propriété intellectuelle réservés. Reproduction, représentation et diffusion interdites. Loi du 01/07/92. Articles 5 ,6 et 7 des CGV

On the other hand, the *direct method* starts from the pixel location in the original image, transforms its coordinates into the result, and places the gray value to the nearest integer pixel (Figure 1b).

The direct method only assigns gray values that are given by the original image; therefore, the contrast and density are not changed by the transformation. However, it might happen that some pixels do not get any gray value, which means that they have to be filled after the transformation in a second pass through the resulting image. The indirect transform assigns a gray value to exactly one pixel in the result (an integer coordinate pair). It has to be computed by interpolation from the original gray values. This is necessary, as the location of the pixel which was transformed into the original does not correspond to an integer position. The process is called *resampling*. By using the indirect method, the gray values are altered in dependency of the resampling algorithm.

The resampling method is chosen with respect to the accuracy, contrast, and resolution required in the result. The ideal resampling function is the sinc-function $(\sin(x)/x)$. It cannot be applied practically, as an infinite number of pixels would have to be convolved with the original image to compute one gray value of the result. Therefore, it is approximated by simpler resampling functions. The most popular ones are listed in Table 1, which compares the size of the convolution window and the number of multiplications necessary for the interpolation of one pixel.

For most applications bilinear resampling yields sufficiently good results. The cubic convolution gives a better contrast than bilinear resampling, which smoothes the original gray values. Nearest neighbor resampling causes step patterns in almost horizontal or vertical lines; however, it is the least computationally intensive method.

THREE RECTIFICATION METHODS

Three methods were investigated for this paper. They are commonly used in image processing systems, and represent only part of the spectrum of approaches available.

Polynomial Rectification

The transformation between the original and the rectified images is done by polynomials (Equation 2). That is,

$$x = \mathbf{x}'^{\mathrm{T}}\,\mathbf{A}\,\mathbf{y}' = f_x(x', y') \qquad y = \mathbf{x}'^{\mathrm{T}}\,\mathbf{B}\,\mathbf{y}' = f_y(x', y') \tag{2}$$

where

x,y are coordinates of the original image,
x', y' are coordinates of the rectification, and
$\mathbf{A}$, $\mathbf{B}$ are coefficient matrices of the polynomials.

$$\mathbf{x}'^{\mathrm{T}} = (1, x', x'^2, x'^3, \ldots)$$

$$\mathbf{y}'^{\mathrm{T}} = (1, y', y'^2, y'^3, \ldots)$$

$$\mathbf{A} = \begin{pmatrix} a_{00} & a_{01} & a_{02} & \cdots \\ a_{10} & a_{11} & a_{12} & \cdots \\ a_{20} & a_{21} & a_{22} & \cdots \\ \cdots & \cdots & \cdots & \cdots \end{pmatrix} \qquad \mathbf{B} = \begin{pmatrix} b_{00} & b_{01} & b_{02} & \cdots \\ b_{10} & b_{11} & b_{12} & \cdots \\ b_{20} & b_{21} & b_{22} & \cdots \\ \cdots & \cdots & \cdots & \cdots \end{pmatrix}$$

TABLE 1. COMPARISON OF THREE DIFFERENT RESAMPLING METHODS.

Method	Window	Multiplications
Nearest Neighbor Resampling	(1 × 1 pixel)	0
Bilinear Resampling	(2 × 2 pixels)	4
Cubic Convolution	(4 × 4 pixels)	110

This method corrects for distortions of the image relative to a dense set of control points. The order of the polynomial depends on the number of control points available. The more control information one has, the more accurate the result of the rectification will be. This approach is completely independent of the geometry of the imaging sensor, so it can be used both for satellite images and aerial photographs. Due to the polynomial transform, the original image is shifted, rotated, scaled, and squeezed so that it fits best to the given reference points. This is the reason why the method is most often used for satellite images, whose geometry and distortions are sometimes difficult to model. Moreover, the relief displacement due to the topography of the Earth is relatively small compared to the flying height of the satellite and does not influence the result significantly.

Although polynomials are very easy to use for rectifications, they can cause problems and errors in the transformed image. They do not adequately correct relief displacements, nor do they consider the special geometry of the imaging system. For the inexperienced user a high-order polynomial may seem to provide a perfect fit at the reference points, as the residuals are small; however, due to undulations between the reference points, large errors could be created. The biggest advantage of the polynomial transform is the fact that all distortions of the image (due to sensor geometry, relief displacement, Earth curvature, etc.) are corrected simultaneously.

Projective Transformation

The projective transform describes the relationship between two planes (Figure 2). It is defined by eight parameters (Equation 3), which can be derived from four object points lying in a plane and their corresponding image coordinates. The elements of exterior and interior orientations are not needed, as they are implicit in these parameters. This method is typically used to rectify aerial photographs of flat terrain or images of facades of buildings.

$$x = \frac{a_1 x' + a_2 y' + a_3}{c_1 x' + c_2 y' + 1} = f_x(x', y') \qquad y = \frac{b_1 x' + b_2 y' + b_3}{c_1 x' + c_2 y' + 1} = f_x(x', y') \tag{3}$$

where $a_1, a_2, a_3, b_1, b_2, b_3, c_1, c_2$ are the projective parameters.

The projective transformation can be modified so that satellite imagery can be rectified. Satellite sensors, such as SPOT, only capture one line of the image at a time. Therefore, we get a

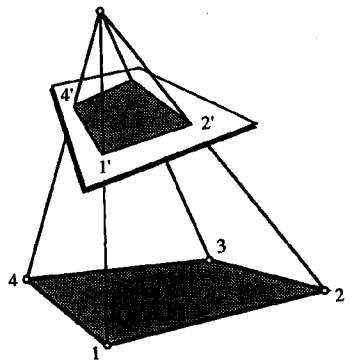


FIG. 2. The projective relationship between an object and the image is defined by eight parameters which can be determined from four control points.

©2008 INIST CNRS . Tous droits de propriété intellectuelle réservés. Reproduction, représentation et diffusion interdites. Loi du 01/07/92. Articles 5 ,6 et 7 des CGV

line-perspective relationship between the ground (plane) and the image (Figure 3). Each scan-line has a different perspective center, and one can assume that all are tied to a straight line approximating the orbit. If y is given in the flying direction and x represents the pixel in a scan line, the projective transform is modified to Equation 4. That is,

$$x = \frac{a_1 x' + a_2 y' + a_3}{c_1 x' + c_2 y' + 1}$$
$$y = b_1 x' + b_2 y' + b_3 \qquad (4)$$

Due to Earth curvature, one can hardly define a plane area on the ground which can be related to a satellite scene by Equation 4. Even for very flat terrain the Earth curvature cannot be neglected. Therefore, this method has little practical significance for satellite scenes, but could be applied for airborne line scanners.

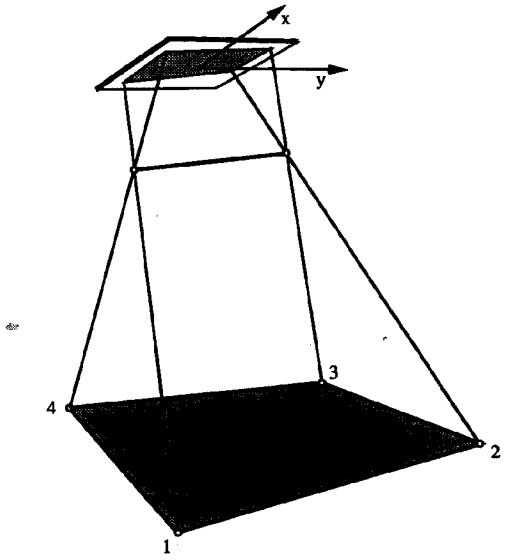


FIG. 3. Line-perspective relationship between an object plane and a satellite scene.

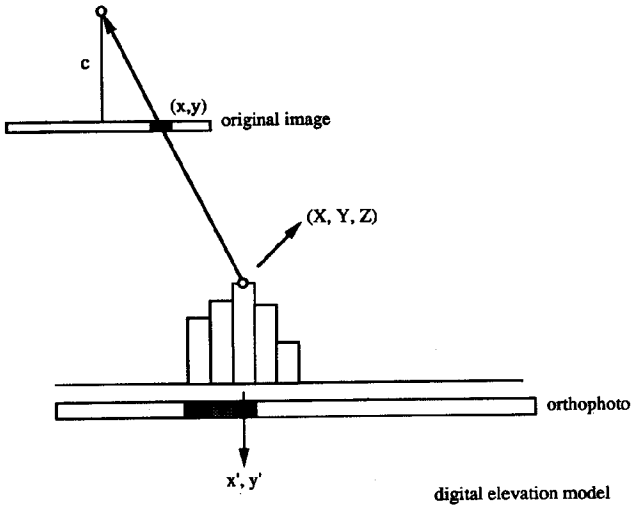


FIG. 4. Each three-dimensional surface point defined as a pixel of the DEM is transformed into the image to find the density from a digitized aerial photograph. This gray value is assigned to the orthophoto raster at the same pixel location as the DEM point.

DIFFERENTIAL RECTIFICATION

The term *differential rectification* has its origin in the approach of rectifying small parts as of a photograph at a time. Conventional analog or analytical orthoprojectors do this by optical image transfer. A tiny slit is moved over the orthophoto, while its corresponding part in the original image is found by shifts, rotations, and scaling. For digital differential rectification, each pixel is separately transferred form the original image to the resulting image using the indirect approach (Equation 1).

A digital elevation model (DEM) is needed to correct for relief displacements in the image. It is assumed that the DEM is stored in the same format as the digital image, i.e., as a raster of digital values, which in this case expresses elevations instead of densities and are 16 bits long (compared to 8 bits of gray value). The DEM has to be related to the map projection of the resulting orthophoto.

In the digital case, the objective of rectification is the assignment of gray values from the aerial photograph or satellite image to each pixel of the DEM. After the rectification, both elevation and density are stored at the same (x, y) location. This is basically similar to the concept of groundels which has been suggested by Helava in connection with the automatic derivation of DEMs (Helava, 1988).

To determine gray values, we follow this procedure: The three-dimensional coordinates (X, Y, Z) defined by a DEM pixel are transformed into the image by the collinearity equations (Equation 5). At the image position (x, y) the gray-value is interpolated by one of the resampling methods. The density is stored at the X, Y location of the digital orthophoto, which is equal to the position of the DEM point (Figure 4).

$$x = x_p - c\frac{r_{11}(X - X_0) + r_{21}(Y - Y_0) + r_{31}(Z - Z_0)}{r_{13}(X - X_0) + r_{23}(Y - Y_0) + r_{33}(Z - Z_0)} = f_x(x', y')$$
$$y = y_p - c\frac{r_{12}(X - X_0) + r_{22}(Y - Y_0) + r_{32}(Z - Z_0)}{r_{13}(X - X_0) + r_{23}(Y - Y_0) + r_{33}(Z - Z_0)} = f_y(x', y') \qquad (5)$$

where x', y' are equivalent to the map coordinates X, Y.

To perform this transformation, the following parameters have to be available:

- the interior orientation of the camera: x_p, y_p, c,
- the exterior orientation of the camera: X_o, Y_o, Z_o – perspective center, R a rotation matrix composed of ω, φ, κ-rotation angles,
- the pixel-spacing of the digital image in camera units: p_x, p_y (mm),
- the cell-size of the DEM pixels in ground units: g_x, g_y (m),
- the reference coordinates of one DEM pixel in the given map-projection (usually the left upper corner of the DEM file).

If SPOT images are to be used, the mathematical model has to be modified to line-perspective geometry (Equation 6). That is,

$$x_i = -c\frac{r'_{11}(X - X_{i0}) + r'_{21}(Y - Y_{i0}) + r'_{31}(Z - Z_{i0})}{r'_{13}(X - X_{i0}) + r'_{23}(Y - Y_{i0}) + r'_{33}(Z - Z_{i0})} = f_x(x', y')$$
$$0 = -c\frac{r'_{12}(X - X_{i0}) + r'_{22}(Y - Y_{i0}) + r'_{32}(Z - Z_{i0})}{r'_{13}(X - X_{i0}) + r'_{23}(Y - Y_{i0}) + r'_{33}(Z - Z_{i0})} = f_y(x', y') \qquad (6)$$

where x_i is the coordinate in scan-line i, orthogonal to the direction of travel, and x_p, $y_p = 0$.

Basically, the orientation parameters of each scan line are different. However, due to the smooth motion of the satellite along the orbit and the relatively short time it takes to capture a full scene, neighboring perspective centers are highly correlated. For most purposes the change of the exterior orientation

parameters can be approximated by linear functions (Equation 7). That is,

$$\begin{aligned} X_{oi} &= X_0 + k_X y_i \\ Y_{oi} &= Y_0 + k_Y y_i \\ Z_{oi} &= Z_0 + k_Z y_i \\ \omega_i &= \omega + k_\omega y_i \\ \varphi_i &= \varphi + k_\varphi y_i \\ \kappa_i &= \kappa + k_\kappa y_i \end{aligned} \tag{7}$$

where

X_{oi}–κ_i	exterior orientation parameters of line i,
X_0–κ	exterior orientation parameters of the center-line of the scene,
k_X–k_κ	linear coefficients of the exterior orientation, and
y_i	line number (coordinate component in the flying direction).

In this case, there are 12 parameters of exterior orientation for each image compared to six for regular aerial photos. Additionally, the Earth curvature has to be considered with satellite images and small scale aerial photographs. The reference of the orthophoto is a map projection related to the Earth ellipsoid (e.g., UTM, Lambert's Conformal). The coordinate triplet (X, Y, Z) of the collinearity equations, however, is related to a tangential plane touching the ellipsoid at the center of the image (Figure 5). Due to the large coverage of a satellite scene (60 by 60 km for SPOT), the differences of the map and plane coordinates cannot be neglected. The largest influence appears at the elevations (Z-component); at the edge of the satellite image the height-difference can be more than 70 m, as compared to a vertical accuracy of about 10 to 20 m. To transform a pixel location (x', y') of the orthophoto to the original image, one has to go from the map coordinates (X_M, Y_M, Z_M; with $X_M = x'$, $Y_M = y'$) to the tangential plane coordinates (X, Y, Z), and from there (X, Y, Z) to the satellite scene (x_i, y_i) utilizing Equations 6.

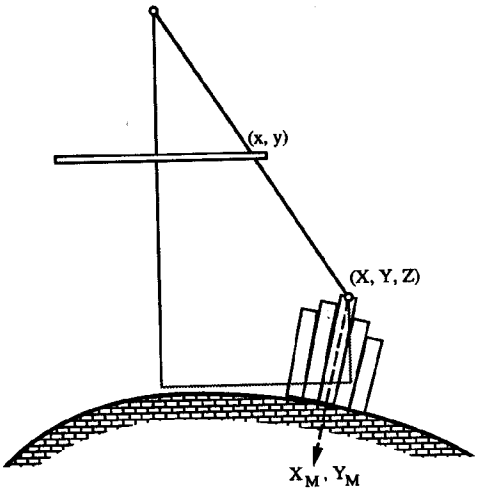


FIG. 5. Correction of the Earth curvature in satellite images and small scale aerial photographs. The map coordinates X_M, Y_M have to be transformed into a Cartesian system (X, Y, Z).

IMPLEMENTATION CONSIDERATIONS

As every pixel of the orthophoto has to be processed separately, computation time is a major concern. It can be largely reduced by optimizing the image transformation. Multiplications must be avoided and substituted by simple additions. This is done by taking advantage of the incrementation of pixel locations at the resulting image (orthophoto).

As an example, the projective transform (Equation 3) is used; practically, this technique can be applied to any transformation. With the indirect approach we take a pixel of the result, compute its corresponding position in the original image, and interpolate a gray value. Then we proceed to the next pixel by adding 1 to the x-coordinate. The left, upper corner of the orthophoto has pixel-coordinates $x' = y' = 0$; the transformed values are given by Equation 8; that is,

$$\begin{aligned} x_{0,0} &= a_3/1 \\ y_{0,0} &= b_3/1 \end{aligned} \tag{8}$$

Then the next pixel of the same line ($x' = 1$, $y' = 0$) is transformed by adding a_1, b_1 to the numerators and c_1 to the denominator of Equation 8; no multiplication is necessary (Equation 9). That is,

$$\begin{aligned} x_{1,0} &= \frac{a_1 + a_3}{c_1 + 1} \\ y_{1,0} &= \frac{b_1 + b_3}{c_1 + 1} \end{aligned} \tag{9}$$

For each following pixel of this line the same three additions are done to get the location in the original image. When we switch the line ($y' = 1$), we start by adding a_2, b_2 and c_2 to the numerators and denominators of $x_{0,0}$ and $y_{0,0}$, respectively. Thus, the transformation of all pixels of this orthophoto can be performed without a single multiplication; of course, the division of the projective transform is still necessary.

COMPARISON OF METHODS

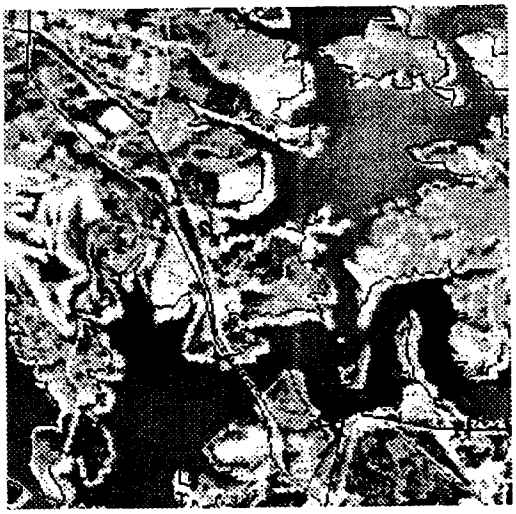
The three methods have been implemented on a workstation. The whole orthophoto production, consisting of the orientation of the images and the rectification, was done digitally. First, the image coordinates of control points were measured on a monitor employing a cursor and a mouse. The reference points on the ground were digitized from an existing map. The parameters of each transformation were computed from these measurements. The residuals of image coordinates after the adjustment were displayed as vectors on the screen to evaluate the quality of the points and to eliminate blunders. Afterwards, the transformation parameters were used in the rectification programs. For differential rectification a DEM was available with the same cell size as the orthophoto. It was captured from the original aerial photos on an analytical plotter.

Figure 6 shows different rectifications of a part of an aerial photograph, which was digitized with an EIKONIX camera at a format of 1024 by 1024 pixels. Image (a) was done by polynomial rectification, image (b) by projective transformation, and image (c) by differential rectification. The streets and lakeshores were digitized manually from an existing map and overlaid over the orthophotos. The polynomial approach shows the largest displacements, while both the projective transformation and differential rectification fit very well to the digital map. It seems that the ground plane of the projective transform is tied to the lakes, thus showing almost no deviations from differential rectification.

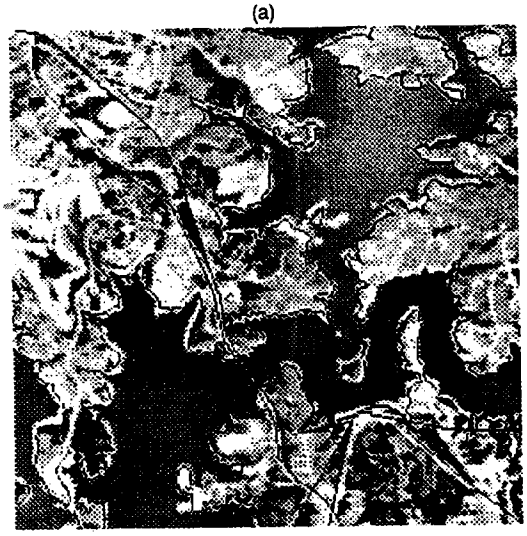
CORRECTION OF DISTORTIONS

The accuracy of differential rectification can be further improved by extending the analytical model. Parameters (Δx, Δy)

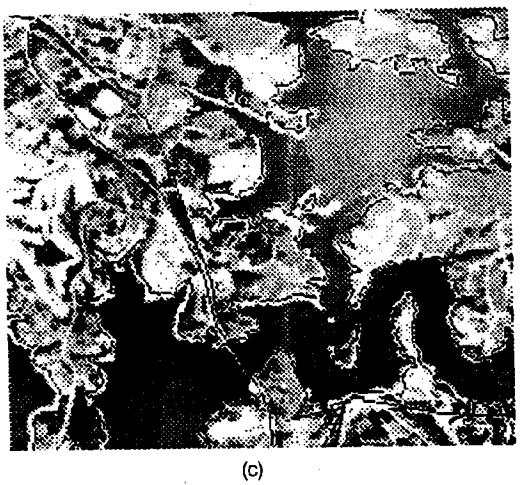
©2008 INIST CNRS . Tous droits de propriété intellectuelle réservés. Reproduction, représentation et diffusion interdites. Loi du 01/07/92. Articles 5 ,6 et 7 des CGV



(a)



(b)



(c)

FIG. 6. Comparison of different rectifications of the same area. The images have been overlaid by a digital map. While the polynomial transform (a) caused very large displacements, projective (b) and differential (c) rectifications are very similar, as the relief displacement has only a small influence due to the large flying height.

were added to the collinearity transformation to correct for all kinds of distortions of the digital image. This is especially important if CCD and video cameras are used for imaging, as their lenses are of lower quality than those of metric cameras and show considerable distortions. The coefficients implemented are correcting symmetric and asymmetric radial distortions, tangential distortions, as well as affinities (Equation 10) (Konecny, *et al.*, 1984). They can be added to the image coordinates of the projective transformation and the collinearity equations. They are obsolete for polynomial rectification, as most of the coefficients are correlated with the parameters of the polynomial.

$$\begin{aligned}\Delta x &= a_1 x (r-r_0) + a_2 x (r^3-r_0^3) + a_3 x (r^5-r_0^5) \\ &\quad + a_4 x (r^7-r_0^7) + a_5 x \cos 2\alpha + a_6 x \sin 2\alpha - a_7 y \cos 2\alpha \\ &\quad - a_8 y \sin 2\alpha - a_9 x \\ \Delta y &= a_1 y (r-r_0) + a_2 y (r^3-r_0^3) + a_3 y (r^5-r_0^5) + a_4 y (r^7-r_0^7) \\ &\quad + a_5 y \cos 2\alpha + a_6 y \sin 2\alpha + a_7 x \cos 2\alpha + a_8 x \sin 2\alpha \\ &\quad - a_9 y + a_{10} x\end{aligned} \tag{10}$$

where

$a_1 \ldots a_{10}$ are additional parameters computed by the bundle adjustment,
r, r_0 are the radial distances from the principal point, and
α is the angle between the x-axis (horizontal) and the direction to the image point.

To prove the effectiveness of these corrections, a video image of a two-dimensional test field was rectified with and without the added parameters (Figure 7). The target locations were measured by least-squares template matching in both rectifications and compared to the correct point coordinates. The results are show in Table 2. The mean accuracy of the points in the rectified images improved by a factor of three to about half a pixel in both directions.

CONCLUSIONS

Digital rectification methods are gaining importance due to the fact that images must be combined with digital maps in GISs. The higher the resolution of the images, the more sophisticated the rectification method should be. All possible distortions caused by the imaging sensor can be corrected during the rectification to obtain best results. The comparison of three different approaches commonly used in image processing systems proved that a differential rectification that corrects both for relief displacements and camera distortions yields the best results, and should be used both for aerial and satellite images.

This method not only generates orthophotos, but it actually finds the gray value of each DEM point and stores it at the same location. Thus, a digital surface model is created which contains elevation, density, and maybe other attributes (such as exposure, slope, temperature, etc.) at each position. These different layers of raster data are given in a geo-referenced, orthogonal projection, and can easily be overlaid by vector data stored in the GIS.

Moreover, both orthophoto and DEM can be created at the same time by digital image matching. During the matching procedure the gray value which has to be assigned to a given location is available twice (in the left and in the right image). Therefore, the mean value could be used. One might even develop more sophisticated methods that determine which of the gray values yields a better result, and thus solve the problem of occlusions.

REFERENCES

Baehr, H. P., 1985. *Digitale Bildverarbeitung - Anwendung in der Photogrammetrie*. Herbert Wichmann Verlag, Karlsruhe.

©2008 INIST CNRS . Tous droits de propriété intellectuelle réservés. Reproduction, représentation et diffusion interdites. Loi du 01/07/92. Articles 5 ,6 et 7 des CGV

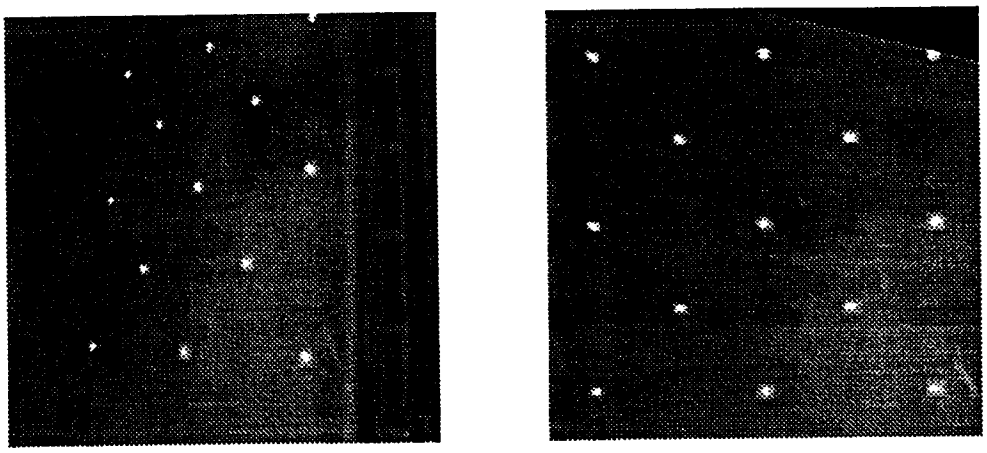


FIG. 7. The digital image of a testfield (left) has been rectified (right) with and without corrections for distortions. The improvement has been quantified by measuring the image coordinates of the two rectifications by least-squares matching.

TABLE 2. STANDARD DEVIATION OF POINT POSITIONS IN DIGITAL IMAGES RECTIFIED WITH AND WITHOUT APPLYING ADDITIONAL PARAMETERS

Additional Parameters	Standard Deviation (RMS Error)	
	x	y
Without	1.65	1.73 [pixels]
With	0.56	0.63 [pixels]

Helava, U. V., 1988. Object-Space Least-Squares Correlation. *Photogrammetric Engineering & Remote Sensing*, Vol. 54, No. 6, pp. 711–714.

Hood, J., L. Ladner, and R. Champion, 1989. Image Processing Techniques for Digital Orthophotoquad Production. *Photogrammetric Engineering & Remote Sensing*, Vol. 55, No. 9, pp. 1323–1329.

Jansa, J., 1983. Rektifizierung von Multispektral-Scanneraufnahmen. *Geowissenchaftliche Mitteilungen der TU Wien*, Heft 24.

Keating, T. J., and D. R. Boston, 1979. Digital Orthophoto Production Using Scanning Microdensitometers. *Photogrammetric Engineering & Remote Sensing*, Vol. 45, No. 6, pp. 735–740.

Konecny, G., and P. Lehmann, 1984. *Photogrammetrie*. Walter de Gruyter, Berlin, New York.

Konecny, G., 1979. Methods and Possibilities for Digital Differential Rectification. *Photogrammetric Engineering & Remote Sensing*, Vol. 45, No. 6, pp. 727–734.

Mueller, W., and H. Sauleda, 1988. Orthophoto Production in the new ContextMAPPER System. *International Archives of Photogrammetry and Remote Sensing.*, Vol. 27, B 9, p. II-224 - II-231.

(Received 8 February 1991; accepted 10 April 1991; revised 13 May 1991)

1st Australian Conference on Mapping & Charting
"Mapping for A Green Future"

Adelaide, South Australia
14-17 September 1992

The Australian Institute of Cartographers is hosting a conference focusing on the role of cartography in monitoring and managing the nation's resources. Conference themes include:

Remote Sensing & Geographic Data for Environmental Management • Mapping Management & Professional Practice • Future Directions in Education & Training • Development of Mapping & Charting • International Mapping Opportunities • Thematic Cartography • GIS/LIS Development

For further information, contact:

Conference Secretariat
1st Austrailian Conference on Mapping and Charting
GPP Box 1922, Adelaide
SOUTH AUSTRALIA

GAP Bulletin Number 5
June 1996

GAP ANALYSIS

Point Sampling Surveys with GPS-logged Aerial Videography

Obtaining sufficient geographically unbiased data for verification and validation of vegetation communities is one of the greatest challenges in developing vegetation base maps for the Gap Analysis Program. These independent data are essential for classifying the Landsat Thematic Mapper (TM) imagery used in all Gap Analysis projects and for assessing the accuracy of the vegetation maps. Low altitude aerial surveys, combined with video data systems that tag each video frame with geographic coordinates from a global positioning system (GPS), provide a cost- and time-effective method for obtaining high resolution data on vegetation communities over large geographic areas. The Gap Analysis Program in New England is using this technology in conjunction with the hyperclustered, multitemporal Landsat TM imagery distributed through the Multi-Resolution Land Characteristics Consortium (MRLC) to produce its vegetation map of southern New England (Slaymaker et al. In press).

Aerial point sampling was developed to characterize the land cover of a region by interpreting a distributed sample of large-scale aerial images (Norton-Griffiths et al. 1982, Dunford et al. 1983). The Arizona Gap Analysis Program used this approach first to interpret its statewide Landsat TM coverage (Graham 1993), using aerial videography in combination with GPS-logged time code. The Arizona project used a Super-VHS camera flown at 2,000 ft above ground that covered 0.5 km at wide angle and zoomed to 15x magnification once every 10 seconds to collect a point sample image 30 m wide. The New England Gap Analysis Project modified Arizona's pioneering system by using two Hi8 band video cameras attached to a portable mount that can be operated from any highwing Cessna. The mount is clamped to the open window frame, then cranked out and adjusted to vertical with a bubble level. The video cameras are mounted vertically beside each other. One is set at wide angle, the other at 12x zoom, providing a swath of 30 m wide large-scale imagery down the middle of 0.4 km wide-angle coverage when flying 600 m above ground level. This approach provides more flexibility than a single camera in both the selection and density of sample points. Geographic position data are recorded in-flight from a GPS unit to a laptop computer using Geolink software. Flight lines can also be entered into this system for navigational purposes and will appear in correct relationship to the plane's position on the computer screen during filming. Time code is "sipped" from the GPS data stream by a Horita GPS time code generator to provide a matching SMPTE time code for the video tape recorders. SMPTE time code is the standard audible timing signal recorded to the audio track of professional video. Horita's time code generator substitutes GPS code for the normal internally generated signal, allowing each frame to be matched to a geographic position. In our system, time code is recorded directly onto the video images as well as the audio track, simplifying the synchronization of the two tapes during playback. We flew 10 - 24 km spaced transects of all six New England states (3,000 km) in the spring and fall of 1994, so as to capture both phenologies of our deciduous forests.

The video tapes from these transects are used to select and label sample Landsat pixel data.

Two TV monitors, one each for the wide angle and zoom videos, are set up beside a computer monitor showing the corresponding portion of the Landsat image. The GPS flight data are overlaid on the Landsat image as vector points that can be queried for their time code, allowing the video frames to be matched to that image. As the video tape is interpreted and plant communities identified, specific pixels in the Landsat image are tagged with their forest type or vegetation class. These points are later extracted as a set of attributed coordinates and used as training sites in a supervised classification or, as in our case, systematically modeled for a set of inference rules to relabel the hyperclustered classification. Each selected pixel takes only seconds to tag, and we collect 18,000 or more points per image in a stratified sample by region and by topographic slope. One quarter of the sample points (stratified by vegetation type) are set aside and later used to access the accuracy of the final vegetation map. The remaining points represent only 0.06% of the total pixel population of a Landsat image, but this sample is sufficient for modeling of the probable vegetation types of each spectral class under different conditions of terrain and spectral mixtures.

The models for each vegetation type are developed with a set of Excel templates. The contingency tables sort the sample points by slope/aspect, frequency of appearance within a vegetation type, and the characteristics of their immediate neighborhood (25 pixel block) within those vegetation types. These data are then used in another set of Excel templates to construct inference rules that relabel each Landsat pixel to its most probable vegetation class for its location and spatial context. The templates are available on our World Wide Web (WWW) home page (see "New England GAP Analysis" at http://tove.fnr.umass.edu/gaphome.html, or ftp://tove.fnr.umass.edu/pub/gap), along with complete sets of our rules, a more detailed explanation of the process, and our initial accuracy assessments, which indicate a near 90% reliability for the seven forest types tested so far.

Technical assistance, including on-site workshops, acquisition of aerial video coverage, and assistance in setting up video interpretation stations, has been provided to a variety of Gap Analysis projects such as Colorado, Florida, Maine, Montana, Oregon, Tennessee, Vermont, West Virginia, and parts of California, as well as new applications of GAP methods in Madagascar, Mexico, and Portugal. Several GAP state projects now have aerial video camera systems and are using them cooperatively with other states. Contact Dana Slaymaker at the University of Massachusetts at (413) 545-4853 or dana@tove.fnr.umass.edu for additional information or technical assistance on aerial videography and interpretation of multiseasonal hyperclustered TM data.

Literature Cited

Dunford, C., D. Mouat, M. Norton-Griffiths, and D.M. Slaymaker. 1983. Remote sensing for rural development planning in Africa. The Journal for the International Institute for Aerial Survey and Earth Sciences 2:99-108.

Graham, L.A. 1993. Airborne video for near-real-time vegetation mapping. Journal of Forestry 8:28-32.

Norton-Griffiths, M., T. Hart, and M. Parton. 1982. Sample surveys from light aircraft combining visual observations and very large scale color photography. University of

Arizona Remote Sensing Newsletter 82-2:1-4.

Slaymaker, D.M., K.M.L. Jones, C.R. Griffin, and J.T. Finn. In press. Mapping deciduous forests in southern New England using aerial videography and hyperclustered multitemporal Landsat TM imagery.

Dana M. Slaymaker
New England Gap Analysis Project
University of Massachusetts, Amherst

GAP Homepage - Table of Contents

View precise geospatial data in 3D stereo from your desktop with SUMMIT EVOLUTION™ from DAT/EM Systems International
DAT/EM
www.datem.com

EOM Earth Observation Magazine
Geospatial Technologies In Your World

Table Of Contents
- CURRENT ISSUES
- ARCHIVES
- INDUSTRY NEWS
- MISSION STATEMENT
- MEDIA KIT
- EDITORIAL GUIDELINE
- ABOUT US
- CONTACT US
- SUBSCRIBE

From the Publisher
By Roland Mangold

Madagascar Protected Areas Mapped with GPS-logged Aerial Video and 35mm Air Photos

By Kevin P. Corbley, Lee Hannah and Dana Slaymaker



We are in the process of rebuilding the Earth Observation Magazine website!

Resource mapping projects in remote areas often face a difficult choice between spatial resolution and economics. Imaging satellites offer relatively low-cost coverage for large areas, but they have insufficient spatial resolution for many applications. On the other hand, traditional aerial photography techniques acquire much higher resolution images, but are extremely expensive.

An international conservation group, however, has teamed with a U.S. researcher to fine-tune a low-cost GPS-logged aerial photography technique for a forest monitoring project in Madagascar. The process uses a standard 35mm SLR camera, Hi8 video cameras, unmodified Cessna aircraft, and commercially available image processing software to create geo-referenced and rectified digital photo mosaics with 1.5-meter spatial resolution.

Mapping Challenges in Madagascar

In the past 50 years, rice farming on Madagascar has steadily crept up from the coastal lowlands into the dense tropical forests that lie on the escarpment of the island's central plateau. Because many of these forests are protected in reserves, the Madagascar government asked Conservation International (CI), a non-profit biodiversity conservation group in Washington, D.C., to assist in the conservation of these reserves in partnership with local communities. An important part of this program is their effort to map and monitor the encroachment of farming.

The CI program focuses on the Ankarafantsika and Zahamena protected areas in northern Madagascar, and is part of a national Environmental Action Plan intended to improve environmental quality, as well as protect the diverse ecosystem and endemic species of the island. In recent years, Zahamena and Ankarafantsika have been threatened by the slash-and-burn practices of local rice farmers. CI is working with farmers to get them to understand and respect reserve limits, while also seeking to find development alternatives to forest destruction.

Tree clearing is illegal in the reserves, and it requires a permit in most other forest areas. Farmers often enter reserve lands unknowingly or without realizing that they require permits for clearing elsewhere. Monitoring this situation has proved difficult for authorities because the clearings are usually quite small, often less than a hectare, and located many kilometers from the nearest road.

CI's role is to help monitor the rate of illegal clearing, and to work with farmers in nearby villages on soil preservation techniques, rice storage methods, and sustainable agricultural practices. But right from the start, ecologists participating in this project knew that they faced the challenge of mapping a large area at high resolution, all with a limited budget.

Project leaders at Conservation International contacted Dana Slaymaker, a researcher of renewable resources at the University

of Massachusetts. He has developed a low-cost digital photo mapping procedure for application in U.S. biodiversity inventory work and international resource management projects. Mr. Slaymaker was thereupon contracted to bring his portable mapping system to Madagascar.

A Low-cost Air Photo System

Prior to the first air photo mission over the 53,000 hectare Ankarafantsika Reserve, project participants compared the cost of the 35mm system to that of an Africa-based aerial survey firm that would employ a large-format camera and modified aircraft. The cost to acquire, process, print and scan the 35mm photos was calculated at US$6,850, while the commercial firm would have charged US$41,200 to photograph the same area.

Every element in the GPS-logged photographic mapping system is commercially available except for the camera mount, which is a custom-made brace capable of holding one 35mm and two video cameras. The mount attaches either to the window frame of a single-engine Cessna, or to the co-pilot seat rails once the seat and door have been removed.

Other key elements include two Canon Hi8 video recorders used simultaneously, and a pair of Nikon N-90 35mm cameras with quick releases and 18mm wide-angle lenses, employed one after the other as film rolls are used and reloaded. Kodak Royal Gold 100- or 400-speed color film is preferred, depending upon lighting conditions. Two standard laptop computers and an airborne GPS also play important roles while in the air.

Most system components are interchangeable with other similar commercial products, with the exception of the TNTmips image processing/GIS software from MicroImages of Lincoln, Neb., which was chosen for its unique mapping capabilities. Therefore, all rectification, geo-referencing and mosaicking of the 35mm images was accomplished in the field by using a Pentium desktop computer equipped with TNTmips.

Acquiring the Photos

Prior to takeoff, participants planned each mission to include 60 percent photo overlap within a flight line, and 30 percent sideways overlap between flight lines. Photos were taken about 20 seconds apart, with time enough to switch cameras as each roll of film ran out. In Madagascar, the researchers flew the still photography at an altitude of 3000 meters, dropping later to a lower altitude for the videography.

While the aircraft was in flight, the GPS was linked to two software packages, each one on a different laptop computer. Geolink software (GeoResearch Inc., Billings, Mont.) controlled navigation by graphically displaying the aircraft's location on a map of pre-planned flight lines. The pilot simply flew up and down the lines as shown on the screen. The second software program, a homemade package called "foto," triggered the 35mm camera's shutter at the programmed coordinate locations. Foto also recorded the time and exact coordinates of each acquisition.

Once these photos were collected, the pilot descended to 150 meters for video acquisition. Guided by the navigation software, the pilot then flew a second set of flight lines and acquired video footage that lay precisely in the middle of the sideways overlap zone. Both video cameras rolled simultaneously, with one of them set for wide-angle and the other set at 12X zoom. They were linked to a Horita GPS-3 time-code generator, a device that prints the GPS time and frame number on each video frame for accurate correlation to the GPS coordinate data, thus precisely locating each video frame.

In U.S. biodiversity inventory work, the aerial videography was included in this technique as a ground-feature sampling method for vegetative cover mapping. The wide angle covers an approximately 200-meter swath, collecting about a four percent

vegetation sampling rate of the project area at the spatial resolution of one-half meter per pixel. The 12X-zoom video records a narrow swath down the middle of the wide-angle coverage at a resolution of two centimeters per pixel, which is sharp enough to identify most individual plant species for biological inventory purposes.

In the Madagascar application, wide-angle video was primarily used to geo-reference and rectify the 35mm frames. The video served as an excellent and inexpensive geo-referencing data source, since the geographic center of every frame could be precisely located with time and coordinate data from the GPS. This allowed the researchers to extract control points from the video to rectify the still-photo frames.

Processing the Digital Photos

The ultimate goal of the Madagascar project was to develop accurate, up-to-date maps that would assist CI in its forest conservation efforts. Fully rectified digital photo mosaics of the Ankarafantsika and Zahamena Reserves were created from the video and 35mm images. The digital mosaics were loaded into a GIS so that researchers and local officials could identify deforested areas, thereby planning development programs for each appropriate village. Hard-copy image maps were also printed and taken into the field by researchers.

Creation of the photo mosaic was conducted on-site in Madagascar using the image processing software, TNTmips. This package was chosen specifically for its ability to display many types and combinations of raster, vector and GPS log files in its reference window during geo-rectification-a crucial capability for this procedure.

At the end of each day's flying in Madagascar, the film rolls were taken to a one-hour photo shop that produced 4x6-inch color prints. Back at camp, these were scanned at 2700 dots per inch using a Polaroid PrintScan 35 Plus to create 2500x3800 pixel images, which were then imported into the image processing system. An outdated paper map of the reserves had also been scanned into the system, a visual reference for the technicians to use during the registration and rectification process.

Several windows of data were open simultaneously in the image processing software: the scanned raster map with overlaid flight lines, 35mm raster photo frames, and video frames. The video frames were not imported into the image processing software itself, but instead were digitized with a video frame-grabbing package and then displayed with that software as an overlaid window.

Using the flight-line photo centers as a guide, the technician placed the first digitized 35mm photo image from a specific flight line into its approximate location on the base map. The GPS points representing each video frame were displayed in the reference window as a series of points labeled by their time code. The technician then viewed the video until he found a frame that had an identifiable feature at its center, such as a bush or a tree. Then he found the same corresponding object in that portion of the 35mm photo image.

By clicking on the object in both the 35mm image and the video frame, the technician created a control point, one with a known coordinate from the GPS file. With hundreds of video frames available for a single 35mm image, he then followed the video path up and down the 35mm image, repeating the feature-matching process and creating a rectangle of control points. This collection of some 15 points rectified that first 35mm image, with great accuracy, to precise GPS coordinates. The technician then added the rectified 35mm frame to the reference window so that the next frame down the line could be precisely matched within the mosaic.

The next frame down the flight line was then brought into the

geo-referencing window with its overlap area already trimmed and ready to be pieced into the mosaic. The technician proceeded by geo-referencing this, and subsequent 35mm frames, both to the video control points and to the rectified image above, thus creating a continuous image mosaic. This was yet another step where the capabilities of the image processing software proved crucial. The TNTmips offered the unique ability of allowing the technician to place the rectified frames into the reference window, so that all subsequent frames were rectified to them. This further allowed the mosaic to be built as the geo-referencing proceeded.

The technician continued down the flight line, geo-referencing and rectifying each photo image and then adding it to the mosaic. When the end of the flight line was reached, the process began again with the next flight line, but this time the sideways overlap area of the previously rectified line was used to further rectify the frames.

Studying Results and Mapping the Future

Working at a speed of about 25 photo frames per day, the researchers ultimately built a 450-frame mosaic of Ankarafantsika. Two such mosaics of the reserve were created during two separate acquisition projects in 1996, and 1997. The project staff processed these mosaics into their GIS in order to find new clearings and to begin developing a land cover/land use database of the reserve.

For Zahamena, individual photos and smaller mosaics were also generated for comparison to black-and-white air photos that had been acquired above the reserve in 1992. These older photos were scanned and displayed in TNTmips in juxtaposition to the 1996 mosaics. In areas where change was detected, technicians geo-referenced the old photos with the new images so that new clearings could be precisely located and mapped.

The image processing system digitally calculated forest area that had been lost over the four-year period. It revealed a one percent to two percent annual loss in forest cover, a much lower rate than when the CI project had begun. Areas with higher-than-average levels of new clearing were targeted as priority zones for future project action.

Conservation International has since assembled its own GPS-video logged system with Mr. Slaymaker's help. The process has been employed with several other CI projects in Mexico, Peru, Ecuador, Brazil, Botswana, and the Ivory Coast.

In 1999, the participants expect to reunite in Madagascar to study a modified version of the technique. The University of Massachusetts researcher has added a pulse laser that will collect terrain elevation information along with the still and video frames. If successful, the researchers hope to generate a three-dimensional view of an area in southern Madagascar.

About the Author:

Kevin Corbley *is a freelance writer and consultant who specializes in remote sensing, GIS and GPS. He lives in Denver, Colo.* ***Dana Slaymaker*** *is a researcher in the Department of Forestry and Conservation Management at the University of Massachusetts. He also works as a consultant, conducting resource evaluation projects around the world.* ***Lee Hannah*** *is the senior director of CI's Regional Support Office in Capetown, Republic of South Africa. His special interests include management of protected areas in partnership with local communities, and quantifying the global impact of human alteration of natural habitat.*

Back

Cost-effective Determination of Biomass from Aerial Images*

H. Schultz[1], D. Slaymaker[2], C. Holmes[1], F. Stolle[1], A. Hanson[1], E. Riseman[1], M. Delaney[3] and M. Powell[3]

[1] Computer Science Department, University of Massachusetts, Amherst, MA 01003
{hschultz, cholmes, stolle, hanson, riseman}@cs.umass.edu

[2] Forestry and Wildlife Management Department,
University of Massachusetts, Amherst, MA 01003
dana@fnr.umass.edu

[3] Winrock International, 38 Winrock Drive, Morrilton, AR 72110-9370
{mdelaney, mpowell}@winrock.org

Abstract

This paper describes an ongoing collaborative research program between the Computer Science and the Forestry and Wildlife Management Departments at the University of Massachusetts to develop cost-effective methodologies for monitoring biomass and other environmental parameters over large areas. The data acquisition system consists of a differential GPS system, a 3-axis solid state inertial reference system, a small format (70mm) aerial survey camera, two video cameras, a laser profiling altimeter, and a PC based data recording system. Two aerial survey techniques for determining biomass are discussed. One primarily based on video and the other relying additionally on the 3D terrain models generated from the aerial photographs. In the first technique, transects are flown at 1,000 feet with dual-camera wide angle and zoom video, and a profiling laser operating at 238 Hz. The video coverage is used to identify individual tree species, and the laser profiler is used to estimate tree heights. The second procedure builds on this approach by taking sequences of 70mm photographs with an 80% overlap along a second higher altitude flight line at 4,000 feet. Detailed 3D terrain models are then generated from successive pairs of images. Several state-of-the-are computer vision algorithms are discussed, including the ITL system, which is an interactive ground cover classification system that allows an operator to quickly classify the large areas in a real-time, and Terrest, which is a highly robust 3D terrain modeling system. The work described in this paper is in a preliminary phase and all of the constituent technologies have not been fully integrated, we nevertheless demonstrated the value and feasibility of using computer vision techniques to solve environmental monitoring problems on a large scale.

* Sponsored by Grants from the National Science Foundation (EIA-9726401) and the National Fish and Wildlife Foundation (98-089)

1 Introduction

The Computer Science (CS) and Forestry and Wildlife Management (FWM) Departments at the University of Massachusetts are engaged in a three-year NSF grant to develop cost-effective, automated techniques to monitor forests and other natural environments. Our long-term goal is to automate and improve environmental monitoring techniques currently employed by FWM through the use of a variety of computer vision techniques, including 3D terrain reconstruction, classification, and automatic video mosaicking techniques.

Biomass estimation is an important application domain for this work. The UN Convention on Climate Change held at Kyoto, Japan in 1997 established a framework for assigning economic value to carbon sequestered in biomass. The effective implementation of the treaty depends on developing cost-effective methods that accurately establish the biomass of tropical forests. Because of vast amount of forests that maybe affected by this treaty, current labor intensive in-situ methods that make extensive use of permanent plots for estimating biomass [1], [2] are not feasible.

To extend coverage and simplify data collection, a range of techniques are being evaluated that utilize the general approach of extrapolating information from small area point samples (e.g., permanent plots), to high-resolution transects observed from low-altitude aerial surveys, to low-resolution, large area analysis derived from satellite images. The focus of our current work is on studying the effectiveness of classifying vegetation using narrow strips of high-resolution video (0.1 m GSD), wide-angle video, laser altimeter profiles, and 3D terrain models generated from small format aerial photography (0.5 – 1.0 m GSD).

1.1 Historical Perspective

To fulfil the terms of the Kyoto treaty the U. S. Government asked for voluntary efforts on the part of American industries to comply with the goals set forth in Kyoto. As part of an effort to respond to this challenge, the American Electric Power (AEP), PacifiCorp and BP America in collaboration with The Nature Conservancy (TNC), Fundación Amigos de la Naturaleza (FAN), and the government of Bolivia, have established the Noel Kempff Mercado Climate Action Project. Approximately 630,000 hectares of forest have been withdrawn from logging or agricultural development and added to the Noel Kempff Mercado National Park in northeast Bolivia. To determine the standing forest biomass of this region, TNC contracted with the Winrock International Institute for Agricultural Development to develop a stratified sample of ground sites where individual trees could be measured over time. Staff from Winrock and the Noel Kempff Mercado Natural History Museum in Santa Cruz established 625 nested plot sites in five basic vegetation strata. Each site was divided into two concentric regions - an inner region with a 4-meter radius, and an outer region with a 14-meter radius. In the inner region all woody stems with a diameter at breast height (dbh) greater than 5 cm were measured; and in the outer region all stems with dbh greater than 20 cm were measured. These dbh values and tree counts were then extrapolated to a per hectare estimate of standing biomass for the region using standard allometric equations.

Setting up 625 plots in a tropical rainforest with few access roads was a major costly and time consuming undertaking. With the vast amounts of forest subject to carbon sequestering under the Global Warming Treaty, it became obvious that manual sampling techniques are not practical. To reduce the amount of labor and extend coverage, the Electric Power Research Institute (EPRI) contacted with the University of Massachusetts to develop low-cost, robust methodologies to measure biomass.

2 Approach to computing biomass

Our initial focus has been on evaluating two aerial survey techniques for determining biomass, one primarily based on video [10] and the other relying additionally on the 3D terrain models. For both setups a Trimble real-time differential GPS system was used to collect position information to approximately 1 meter in X,Y,Z, and a Watson Industries 3-axis solid state inertial reference system were used to collect orientation information to approximately 0.1 degrees in role and pitch and 0.5 degrees in azimuth. To enable temporal registration of the various data streams, time codes were added to the data during collection. A time code generator was used synchronize the video data, which was recorded on a VCR, and a time code stamp was added to all digital data during the recording process.

In the first technique, which we refer to as the 2D approach, transects are flown at 1,000 feet. The instrument package consisted of the GPS, inertial reference system, two down-looking video camera (one with a wide angle lens and one with a telephoto lens), and a profiling laser altimeter. Figure 1 shows an example of a video sequence, and Figure 2 shows an example of a geo-referenced laser altimeter profile. The wide-angle camera covered a swath approximately 320 meters wide, with 50 centimeter per pixel resolution. The other camera was set at 12X zoom, covering a 26 meter wide swath at 4 cm per pixel resolution, a sufficient scale to identify individual tree species.

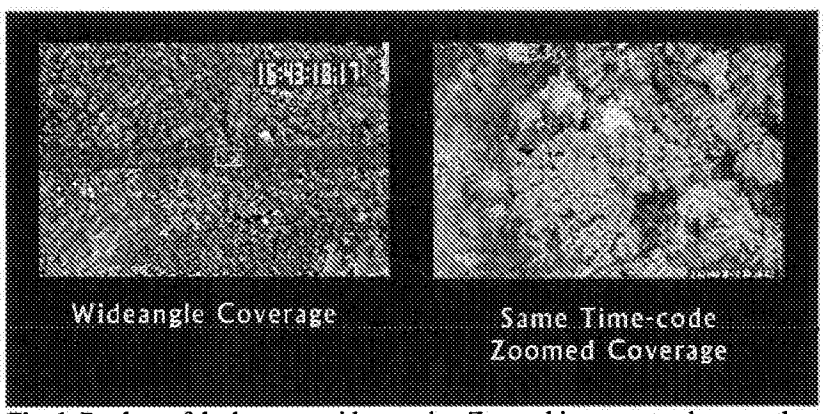


Fig. 1. Product of dual camera videography. Zoomed imagery tracks a swath down the center line of the wide angle coverage and can be matched by corresponding time codes.

The second sampling procedure builds on this approach by taking sequences of photographs with an 80% overlap along a second higher altitude flight line at 4,000 feet. The images were taken with a 70mm Hasselblad MWX photogrammetric camera. Detailed 3D terrain models were then generated from successive pairs of images. An Intergraph SSK workstation was used to build the stereo model and the UMass Terrain Reconstruction System (Terrest) was used for image matching and differential rectification. The excessive overlap was necessary to maintain radiometric consistency between frames.

Techniques were tested by processing a preliminary data set collected in September 1998 over a mixed hardwood/conifer forest area at an AEP test site in Crooksville, Ohio. Thirty-one plot sites were established along two transects and a per hectare biomass estimated for each. Half of the plot measurement sets are presently being used to calibrate the resulting video strips and 3D terrain models. These results will then be tested against the remaining sites to determine the relative success of each approach. A more extensive test over much larger area is planned in Bolivia this spring, to be conducted in the Noel Kempff Mercado National Park expansion zone in Bolivia. That survey should provide more accurate estimates of biomass at a considerably lower cost.

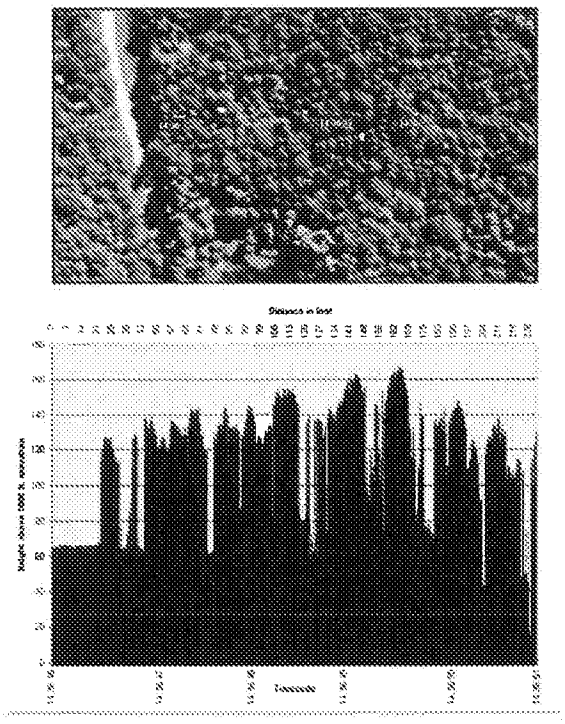


Fig. 2. An example of a laser altimeter profile

3 Three-dimensional Terrain Modeling using Terrest

The ability to generate accurate, high-resolution digital elevation maps (DEM) is essential to our environmental monitoring strategy. On a low-resolution scale (5-30m) DEMs provide important topographic information, such as elevation, slope and drainage patterns. On a finer scale (1 m or less) DEMs can be used to count individual trees, and/or determine 3D textural qualities of the surface.

The UMass Terrest system was designed to automatically generate high-resolution 3D terrain models from aerial images when the viewing angles become oblique (incidence angles greater than 45 degrees), and/or when the camera separation becomes large (base-to-height ratio exceeds 1.5). The system incorporated several specific features that increase the accuracy, robustness, and utility of the system [7], [8]. Figure 3 shows an example of a terrain model generated from a pair of images.

Figure 4 shows a 768 × 768 pixel section of the DEM and corresponding ortho-image taken from the center of the scene shown in Figure 3. To test the reliability of detecting trees in the 3D terrain model, two groups of four interpreters evaluated the DEM and ortho-image. The first group marked bumps in the DEM and looks for corresponding evidence of a tree in the ortho-image, while the second group identified trees in the ortho-image and looked for corresponding bumps in the DEM. Both groups found a reliability of at least 95%.

The Terrest system has recently been enhances to fuse information from multiple overlapping views (typically 3-6) [9]. When more than two images are available the system first produces separate DEMs from each ordered image pair. The system then fuses the individual DEMs using a robust method to produce an optimal terrain model consisting of a DEM, a geospatial uncertainty map, an ortho-image, and a set of 3D texture maps (see Terrain Classification below).

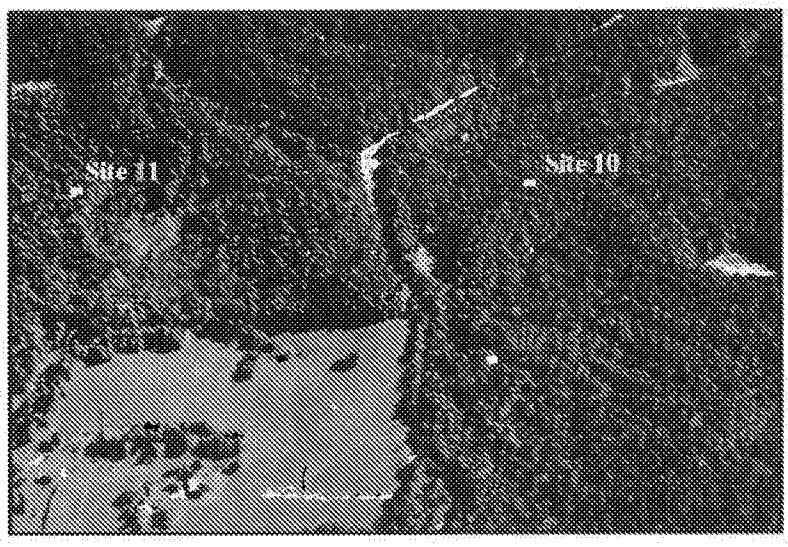


Fig. 3 A rendered view of the ortho-image draped over the DEM

The technique relies on two key factors for generating robust 3D terrain models, (1) the ability to detect unreliable elevations estimates, and (2) the ability to fuse the reliable elevations into a single optimal terrain model. The technique is based on the concept of using self-consistency measures, first introduced by Leclerc et al., [4], [5] to identify unreliable points in a distribution. The focus of their work was to obtain a quality measure for point correspondences. Their algorithm obtained a probability distribution by counting the number of corresponding image points for each object point that is consistent with the viewing geometry within a specified error limit. We extended the self-consistency concept to the problem of detecting unreliable elements in a DEM, generated from stereoscopic image pairs.

The geospatial uncertainty, occluded surface patches, and false matches are inferred by analyzing asymmetries in the elevation and confidence level estimates produced by reversing the roles of the left and right images during the image matching phase. If Z_{AB} is the DEM generated with image A as the left and B as the right, and Z_{BA} is the DEM generated by reversing the roles of A and B, then anomalies in Z_{AB} - Z_{BA} can be used to categories DEM errors. Unreliable elevation estimates, characterized by large values in Z_{AB} - Z_{BA}, may result from surface discontinuities, non-Lambertian surface patches, such as water, and occlusions. For regions where Z_{AB} and Z_{BA} agree within a predetermined range, the geospatial uncertainty can be inferred directly from the variance of (Z_{AB} - Z_{BA}). Consequently, an elevation estimate is said to be self-consistent when Z_{AB} - Z_{BA} is below a threshold. The self-consistency threshold is set as low-as possible to assure that all elevations arising from false image matches are rejected.

Figure 5 shows the results of a multi-image fusion. The processing started with 4 images, which resulted in 12 elevation estimates per pixel in the output grid. We then applied the self-consistency methodology and labeled each elevation estimate as reliable or unreliable. We then averaged all of the reliable estimates are each pixel to form an optimal DEM.

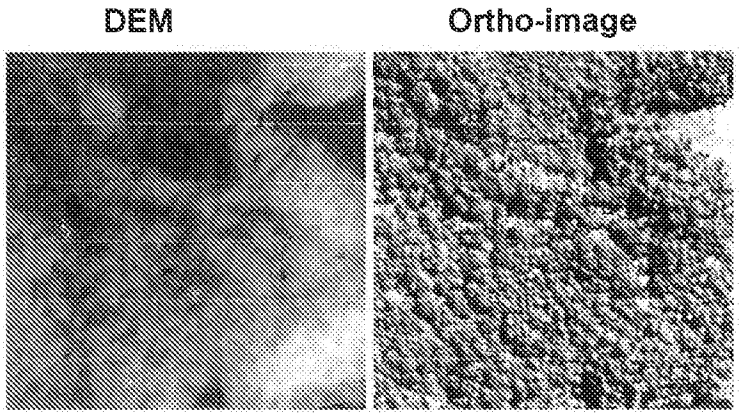


Fig. 4. The DEM and orhto-images used to test the reliability of detecting trees.

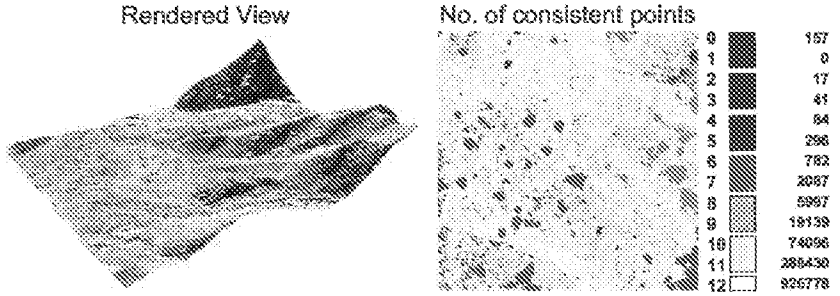


Fig. 5. A rendered view of the final 3D terrain model (left) and the number of self-consistent estimates used to compute each elevation

4 3D World Texture Measures

We have recently shown that classification performance can be significantly improved by adding to the usual 2D image texture measures [3] a set of new 3D texture measures [13]. Our concept is that 3D textures are a function of recurring patterns caused by physical coarseness, roughness, and other characteristics of 3D surface structure, and that certain intermediate results generated during the process of generating a 3D terrain model are related to the 3D textures. We derived four 3D texture measures and used them in the ground cover classification problem. We found that 3D textures significantly improved the performance of a standard classification system. The experiments in [13] showed that including 3D texture features improved classification skill from 72.5% to 83.4%. We believe the implications of these findings for terrain feature extraction are far reaching.

The 3D texture features are derived during the image matching phase in the 3D reconstruction process. During image matching left-right pixel correspondences are determined to a fraction of a pixel width. As a result, the statistical properties of the pixel correspondences are sensitive to the microstructure of the surface (3D structure at length scales approximately equal to the ground sampling distance). The four 3D texture features are: (i) The confidence level assigned to each correspondence; (ii) the variability of confidence levels within a 17×17 window surrounding each correspondence; (iii) the deceleration length for each correspondence; and (iv) the variability of deceleration length within a 17×17 window surrounding each correspondence.

5 Terrain Classification using ITL

Our classification system is based on the Interactive Teacher-Learner (ITL) paradigm [6], which employs a feedback mechanism between the operator (the Teacher) and a state-of-the-art real-time decision tree classifier (the Learner). The user receives feedback by interactively specifying training instances (using semi-automated graphical tools) and then seeing the effect that his/her actions had on the classifier. An efficient state-of-the-art decision tree classification algorithm, which is running in

the background, continuously updates its classification parameters, and displays its results in real-time.

It is important to contrast this approach with the standard methods of specifying training data. Typically, large numbers of pixels are laboriously hand-labeled to ensure a statistically valid sample. A large amount is selected because the user does not know what is a sufficient training size and which training instances are informative.

By overlaying the classification results on the scene in false color, the user can immediately see the impact that their selections on the classifier. This provides the human trainer with instant feedback as the classifier assimilates new training data. Rather than hand-labeling large numbers of pixels as input training data in off-line process, an operator trains the classifier by giving much more informed incremental training instances, e.g., correcting mistakes or defining new subclasses that are necessary for discrimination in the particular context. In this way natural user interaction leads to the judicious selection of a small amount of very important data in the training process.

Figure 6 shows a comparison between a scene classified using the ITL system and conventional batch processing, in which all the training data were selected in advance. The results of the comparison are shown in Table 1. The test was run using 17 features (12 standard 2D co-occurrence features, 4 3D texture features and the ortho-image). The percent correct were similar except that three orders of magnitude less training data were required with the ITL system.

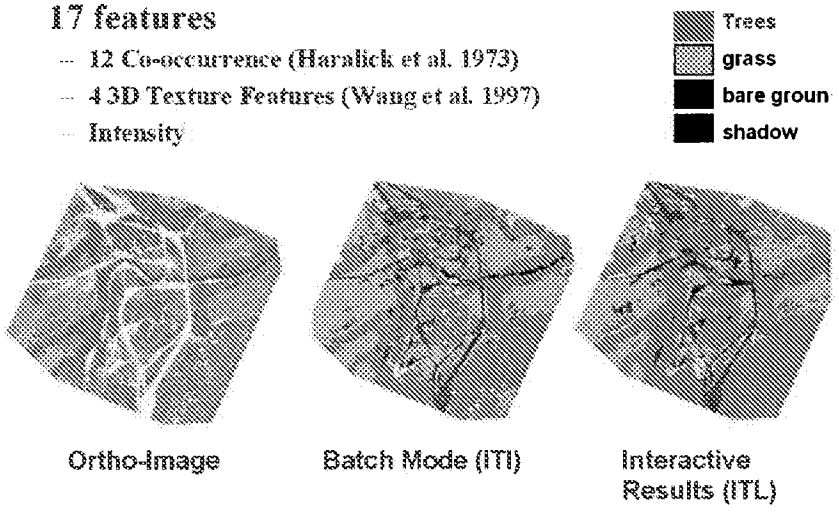


Fig 6. Comparison between ITL and batch mode processing

	ITL	Batch
Mouse Clicks	30	
Training Examples	270	16916
% Correct	85.1	86.4
Tree Nodes	25	71

Table 1. ITL vs. batch processing evaluation.

To make the feedback mechanism between the teacher (user) and learner (computer) practical, the ITL system requires a classification system that efficiently updates as the users selects new training instances. The Incremental Tree Inducer (ITI) decision tree developed at UMass [11], [12] was selected for this purpose. In addition to being one of the most accurate implementation of a decision tree, ITI is capable of updating an existing decision tree without rebuilding the tree structure. Thus, when the operator selects new training instances, ITI updates the existing tree instead of rebuilding the decision tree. In addition, ITI uses only those features that contribute to the decision making process. As a result, there is no need to guarantee in advance that any particular feature will be useful because the decision tree methodology will only select those features that improve the discrimination between the user-defined training classes. Thus, there is no need to validate a priori the utility of features.

Conclusions

Although this work is in a preliminary phase and all of the constituent technologies have not been fully integrated, we have nevertheless demonstrated the value and feasibility of using state-of-the-art computer vision techniques (Terrest and ITL) to solve environmental monitoring problems on a large scale. In the near future we plan to integrate terrain modeling and classification so that some skilled in Forestry but not necessarily photogrammetry or computer science will be able efficiently extract reliable environmental information from video and aerial photography.

References

[1] Brown, S., and A.J.R. Lugo: Biomass of tropical forests: a new stimate based on forest volumes. Science 223:1290-1293, 1984.

[2] Brown, S., A.J.R. Gillespie, and A.E. Lugo: Biomass of tropical forests of south and southeast Asia. Canadian Journal of Forest Research 21:111-117. Crow T.R. 1978. Common regressions to estimate tree biomass in tropical stands. Forest Science 24:110-114, 1991.

[3] Haralick, R., K. Shanmugam, and I. Dinstein: Textural Features for Image Classication," IEEE Trans.on Systems, Man, and Cybernetics, Vol. 3, No. 6, pp. 610-621, 1973.

[4] Leclerc, Y.G., Q.T. Luong, and P. Fua: A Framework for Detecting Changes in Terrain, *IEEE Trans. Pattern Analysis and Machine Intelligence*, vol. 20, no. 11, pp. 1143-1160, November 1998.

[5] Leclerc, Y.G., Q.T. Luong, et al.: Self-consistency: A novel approach to characterizing the accuracy and reliability of point correspondence algorithms, *DARPA Image Understanding Workshop*, Monterey, CA, 1998.

[6] Justus H. Piater, Edward M. Riseman and Paul E. Utgoff: Interactively Training Pixel Classifiers. International Journal of Pattern Recognition and Artificial Intelligence 13(2), pp. 171-194, 1999.

[7] Schultz, H.: Terrain Reconstruction from Oblique Views, Proc. DARPA Image Understanding Workshop, Monterey, CA, pp. 1001-1008, November 1994.

[8] Schultz, H.: Terrain Reconstruction from Widely Separated Images, Proc. SPIE, Volume 2486, pp. 113-123, Orlando, FL, April 1995.

[9] Schultz, H., Riseman, E., Stolle, F.: Error Detection and DEM Fusion Using Self-Consistency, Submitted to the 7th IEEE International Conference on Computer Vision, Kerkyra, Greece, September 1999.

[10] Slaymaker, D.M., K.M.L. Jones, C.R. Griffin and J.T. Finn: Mapping deciduous forests in Southern New England using aerial videography and hyperclustered multi-temporal Landsat TM imagery. Pages 87-101 in Gap Analysis: A Landscape Approach to Biodiversity Planning, J.M. Scott, T.H. Tear and F.W. Davis (eds). American Society of Photogrammetry and Remote Sensing, Bethesda, MD, USA, 1996.

[11] Utgoff, P. E.: An improved algorithm for incremental induction of decision trees, In Machine Learning: Proc. 11th Int. Conf, pp. 318--325, Morgan Kaufmann, 1994.

[12] Utgoff, P.E., N. C. Berkman, and J.A. Clouse: Decision tree induction based on efficient tree restructuring", Machine Learning 29(1), 5-44, 1997

[13] Wang, X., F. Stolle, H. Schultz, E. M. Riseman, and A. R. Hanson: Using three-dimensional features to improve terrain classification", In Proc. Computer Vision and Pattern Recognition, pp. 915-920, 1997.

A System for Real-time Generation of Geo-referenced Terrain Models

Howard Schultz[1], Allen R. Hanson[1], Edward M. Riseman[1], Frank Stolle[1], Zhigang Zhu[1]
Computer Science Department
University of Massachusetts, Amherst

Christopher D. Hayward[1], Dana Slaymaker[2]
Natural Resources Conservation Department
University of Massachusetts, Amherst

ABSTRACT

A growing number of law enforcement applications, especially in the areas of boarder security, drug enforcement and anti-terrorism require high-resolution wide area surveillance from unmanned air vehicles. At the University of Massachusetts we are developing an aerial reconnaissance system capable of generating high resolution, geographically registered terrain models (in the form of a seamless mosaic) in real-time from a single down-looking digital video camera. The efficiency of the processing algorithms, as well as the simplicity of the hardware, will provide the user with the ability to produce and roam through stereoscopic geo-referenced mosaic images in real-time, and to automatically generate highly accurate 3D terrain models offline in a fraction of the time currently required by softcopy conventional photogrammetry systems. The system is organized around a set of integrated sensor and software components. The instrumentation package is comprised of several inexpensive commercial-off-the-shelf components, including a digital video camera, a differential GPS, and a 3-axis heading and reference system. At the heart of the system is a set of software tools for image registration, mosaic generation, geo-location and aircraft state vector recovery. Each process is designed to efficiently handle the data collected by the instrument package. Particular attention is given to minimizing geospatial errors at each stage, as well as modeling propagation of errors through the system. Preliminary results for an urban and forested scene are discussed in detail.

Keywords: Terrain modeling, Three-dimensional reconstruction, stereo, mosaic generation, aerial image interpretation

1. INTRODUCTION

The long-term goal of the UMass aerial imaging research program is to provide sophisticated and practical means of creating high-resolution, content rich 3D terrain models from aerial images. An important component of this program is the construction of an instrument package and software system that generates stereoscopic geographically registered mosaic maps in real-time from a sequence of digital images. The successful implementation of this project will have far-reaching benefits for a diverse group of remote sensing applications ranging from basic research to law enforcement.

The rapid growth in digital imaging technology has led to a wide variety of commercial-off-the-shelf (COTS) high-resolution digital cameras. For the first time, it is possible to inexpensively generate sequences of closely spaced, spatially crisp, non-interlaced, radiometrically calibrated images. The noise, jitter and color inconsistency inherent in video are no longer a problem. These new generation of imaging systems will enable important applications that were not feasible a few years ago. In this paper, we develop the idea of producing geometrically accurate, geographically referenced, three-dimensional terrain models in the form of compact mosaics as a fundamental structure in processing large amounts of digital aerial images. We will describe our existing digital video based system [7][11], which has been operational for two years, and briefly outline our plans for a new fully digital, real-time system.

[1] Email: {schultz|hanson|chayward|riseman|stolle|zhu}@cs.umass.edu, telephone: (413) 545-2746
[2] Email: dana@fnr.umass.edu, telephone: (413) 545-2746

Paper: 4232A-08, SPIE Enabling Technologies for Law Enforcement Boston, MA, November 5-8, 2000

2. SYSTEM CONFIGURATION

A photograph of our current system is shown in Figure 1 and a schematic diagram of the setups is shown in Figure 2. The major system components are:

- A 12 channel real-time differential GPS (Trimble AGGPS receiver and an L-band Omnistar and GPS antenna) for collecting position information;
- A 3-axis attitude and heading reference system (Watson Industries AHRS-BA303) for collecting orientation information;
- A profiling laser altimeter PLA (Laser Atlanta), which gives instantaneous estimate at 238 Hz of the height of the airplane above the surface;
- Two Canon XL1 mini-DV camcorders. One camera is fitted with a Canon 5.8-88mm telephoto lens and the other with a Canon 3.4-10.2mm wide-angle lens. These camcorders use a 3-chip design (red, green, blue), which resulted in excellent color separation, and a progressive scan readout architecture, which eliminates even/odd field blurring.
- A time video time code generator (Horita) for synchronizing the video data;
- Two digital video recorder (Sony DV-G900);
- A data acquisition computer for collecting GPS, heading and reference, and laser data
- A navigation computer for helping the pilot stay of the predefined flight path.

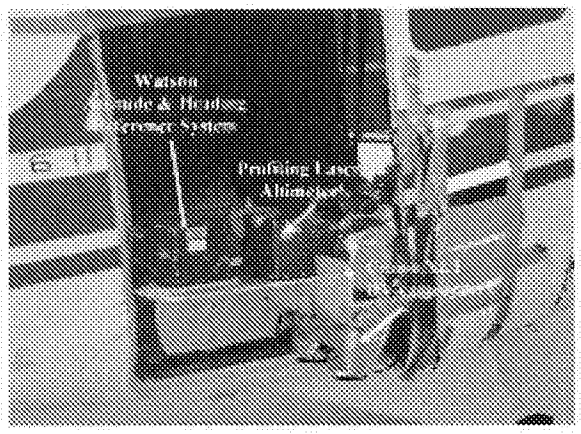


Fig. 1. A photograph of the UMass digital video acquisition system mounted on a lightweight aircraft.

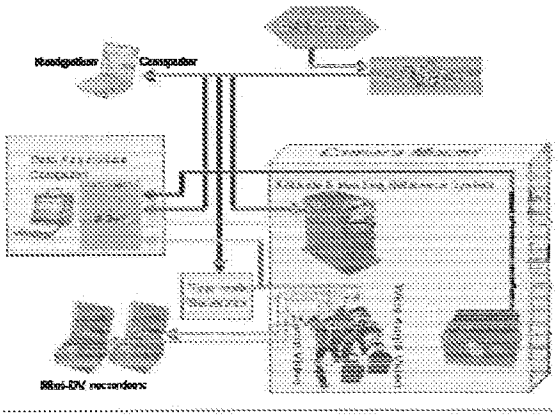


Fig. 2. A bock diagram of the UMass digital video acquisition system.

The telephoto camcorder provides information about the appearance of specific objects, while the wide-angle camcorder provides information for generating the terrain model. For typical applications, the telephoto lens is set to acquire images with 4-10cm pixels, and the wide-angle lens is set to acquire images with 0.5-2.0m pixels, which result in a 350-1500m swath width. The profiling laser altimeter (PLA) can be used to acquire detailed elevation profiles when the aircraft is flying at 1500 feet or less above the ground. The camcorders, PLA and AHRS are attached to a rigid mounting system, which was attached to the side of the airplane. This ensures that the angles measured by the AHRS gave the precise orientation of the cameras and PLA. To ensure accurate position measurements, the X,Y,Z-offsets between the GPS antenna and the cameras was measured after the antenna and cameras were installed in the aircraft.

The video cameras produced a continuous video stream, which was recorded inside the aircraft on the two Sony mini-DV recorders. The Horita GPS time code generator convert the GPS timing signal to a digital form that was compatible with the digital audio channel of camcorders. Thus, by feeding the digitally encode audio through the camcorders we were able to record GPS time information on the audio track. We also recorded the digital audio on the data acquisition computer. This gave us an independent machine-readable relationship between frame number and GPS time.

The GPS data provided several functions, including velocity compensation for the AHRS, synchronizing the video data by adding timing information to the audio track, and navigation. The GPS data were recorded directly on the data acquisition computer as well. As configured, the GPS had an absolute accuracy of approximately 1 meter horizontally and 2 meters

vertically. In addition, the AHRS provided us with precise orientation information to an accuracy of 0.1° about the two horizontal axes, and 0.5° about vertical axis (azimuth). The position and orientation information was used to initialize the bundle adjustment procedures for determining image orientation.

The data streams from the PLA, AHRS, GPS and time code generator were recorded through the serial ports on the data acquisition computer. Because each serial port received data at a different rate, the program that read the serial ports and write the data to disk adds a time stamp to each data record. To simplify data analyses, in a post-processing step, the raw data are interpolated so that the various data fields are coincident with the profiling laser altimeter data (the instrument with the fastest sampling rate).

3. DIGITAL MOSAICS AND TERRAIN MODELING

The key to the success of our system is a method for generating seamless geographically registered mosaics for a stream of digital images, and techniques for generating accurate 3D terrain models from mosaic images. A mosaic is constructed by sequentially pasting together a sequence of images to form a single large image that has all of the content of the original image sequence. For each new frame, as much as 99% of the image may overlap the mosaic. By discarding the redundant, overlapping image segments the mosaic forms a very compact representation of the raw image sequence. The amount of compression is a function of the overlap between frames, which in turn depends on several factors, including the frame rate, aircraft speed and altitude, and the field-of-view of the lens.

Mosaics are constructed by sequentially adding new image frames to a mosaic model [4]. This is done by first computing the geometric relationship between the new frame and the previous frame, which has already been registered to the mosaic model. Next, the registration parameters for the new frame are estimated by taking into account the incremental translation and rotation between the two frames. Once a new image is registered to the mosaic model, a strip from the new image is cut out and pasted on to the mosaic. The process then repeats for the next image in the sequence.

3.1. Geographic registered mosaics

Video mosaics are routinely produced on inexpensive PCs and commonly employed in aerial image applications. Current state-of-the-art techniques for producing video mosaics rely on image-to-image registration. If, in addition, a terrain model exists, these techniques have been extended to include mosaic to model registration [3]. We refer to these mosaic generation systems as "free mosaics" because at the time of mosaic generation they only satisfy optical matching and are not constrained by any geographic information.

Unconstrained (free mosaic) techniques incrementally build mosaics by registering each additional frame to the existing mosaic. Although these techniques are efficient, with the addition of each new frame they introduce small registration errors, which quickly accumulate over time. After a few seconds these errors will accumulate so the total registration error is on the order of several pixels.

Recently Zhu, et al. [16][17] developed a "georeferenced" mosaic technique that minimizes registration errors by constraining the placement of each new frame to be consistent with the known position and orientation information returned by navigation instruments. The technique uses orientation and position data from a GPS, AHRS and (if available) the laser altimeter to determine the proper placement of the image center of each new frame.

As part of NASA's Large Scale Biosphere-Atmosphere Experiment in Amazonia (LBA). The University of Massachusetts in collaboration with the University of California, Santa Barbara collected over 10 Terabytes of digital video sequences over the Amazon River Basin. Part of this coverage was over the Smithsonian's Biological Dynamics of Forest Fragmentation Project (BDFFP) study area. Our principle objective of our participation in this project was to produce high-resolution base maps of the Smithsonian study areas [14][15][16]. Because of perpetual cloud cover satellite and high-altitude aerial surveys were not capable of mapping the area, especially at spatial resolutions required to identify individual tree and small forest gaps associated with illegal logging. For the first time, we were able to produce a base map (shown in Figure 3.) with a 1.75m ground sampling resolution that covered an area of approximately 45km by 15km, with an absolute registration error less than 20m. In addition, for a selected number of sections stereoscopic mosaics were produced, which enabled researchers to estimate tree crown diameters for a biomass estimation study [12][13].

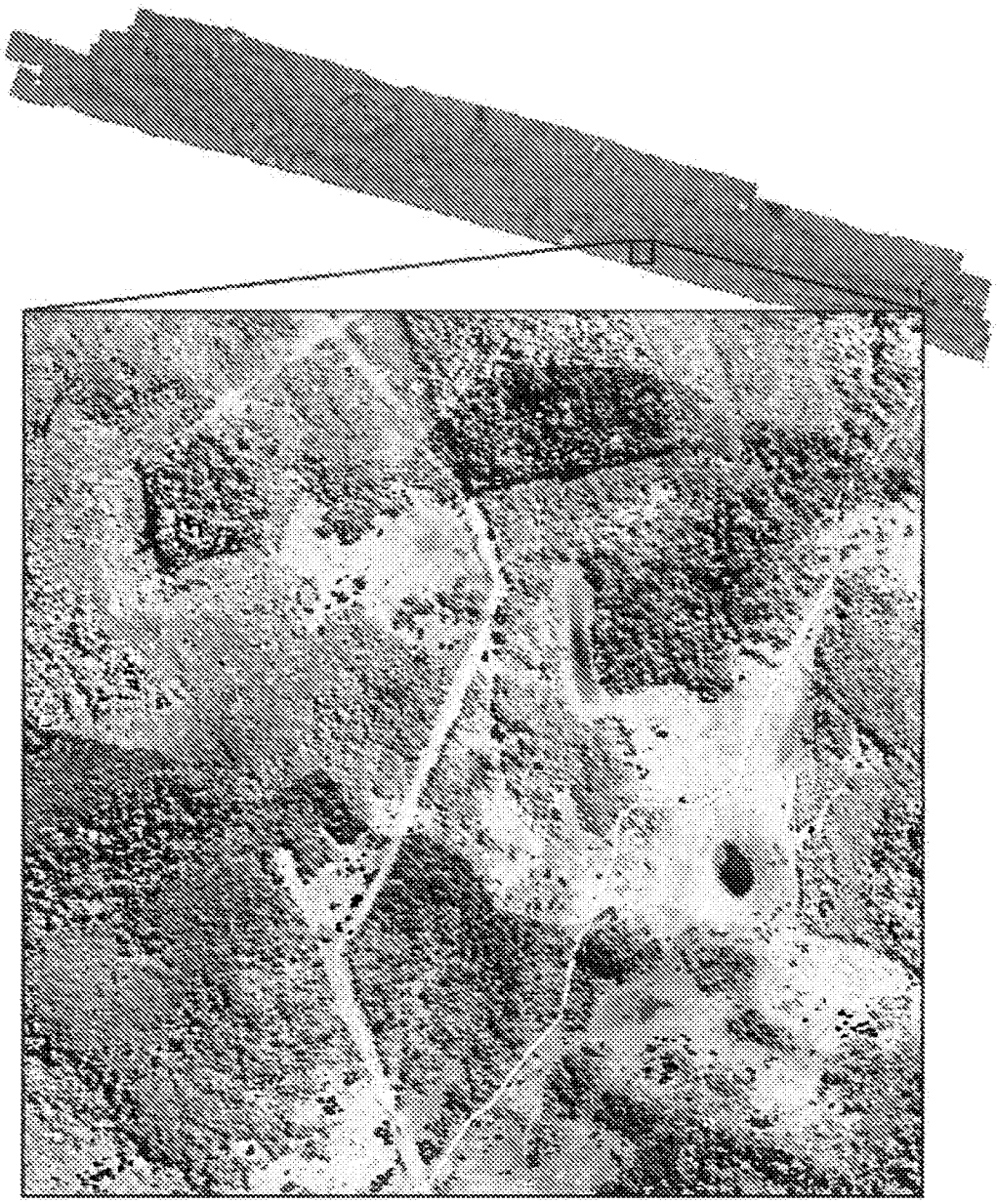


Fig. 3. An example of a high resolution (1.75 meter ground sampling distance) mosaic map built up from eight overlapping mosaic strips. The full mosaic map (at the top of the page) is 25,113 × 9,040 pixels, the insert is a small 761 × 749 section that shows three overlapping mosaic strips. The strips were deliberately not color balanced to show the alignment accuracy in the across track direction.

3.2. Stereoscopic Mosaics

A sequence of images taken by a moving camera captures the 3D structure of the underlying terrain. Objects closer to the camera will appear to move through the scene quicker than objects further away. Therefore, it is possible to recover the terrain topography by estimating the translation (motion parallax) of objects through two or more sequential images. These parallax shifts are lost in the mosaic process because only one view of any point on the surface is retained in the mosaic. However, by constructing two mosaics – one formed from the leading edge of each new frame and one formed from the trailing edge of each new frame – the parallax information can be retained [5]. Figure 4, shows a diagram of how stereoscopic mosaics are made. It is interesting to note that for this configuration, the stereoscopic effect is independent of the aircraft altitude. This happens because the stereo baseline is equal to the aircraft altitude times a constant that depends only on the field-of-view of the lens.

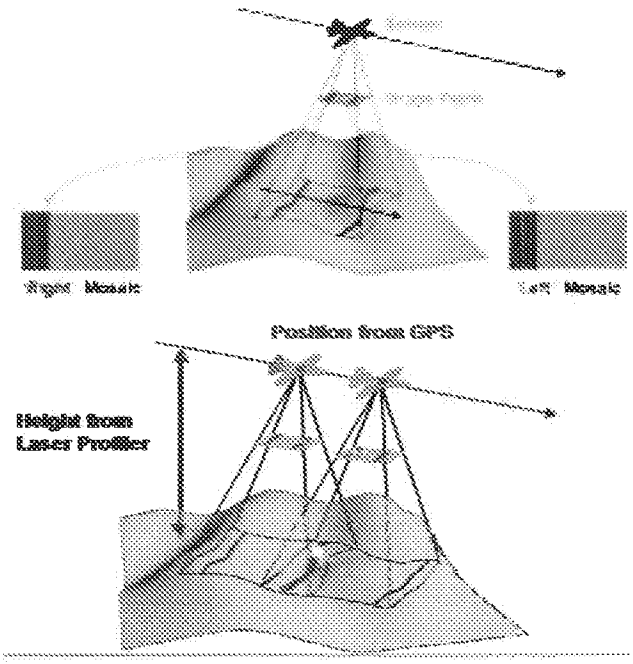


Fig. 4. (top) The **left** mosaic is assembled from the leading edge and the **right** mosaic from the trailing edge of each frame. (bottom) The position of a point on the ground is found by triangulating from its position in the left and right mosaic.

Once two images or two mosaics are generated from two viewpoints, a digital elevation map (DEM) can be recovered as well. We have implementing two methods for creating DEMs from a digital image sequence. The first recovers the topography directly from stereoscopic mosaics. While the second create a series of DEMs for sequential image pairs and then mosaic the individual DEMs. The principle advantage of the first method is that implementation of a real-time mosaic generation program would enable viewing the three-dimensional structure of the surface in real-time by simply looking at the left and right mosaics on a stereoscopic display. The principal disadvantage of this approach is the discontinuities in the mosaic that arise from discontinuities in elevation. An example of a stereoscopic mosaic pair is shown in Figure 5.

The second approach is conceptually equivalent to generating a long sequence of DEMs and ortho-images. Although this method will produce seamless mosaics without warping, it is computationally more expensive, and requires precise knowledge of the aircraft pose (location and orientation) for each frame.

3.3. Three-dimensional Terrain Modeling

In either case, the UMass Terrain Reconstruction System (Terrest) will be used to extract the terrain elevations. The Terrest system automatically generates high-resolution 3D terrain models from aerial images, even when viewing angles become oblique (incidence angles greater than 45 degrees), and when the camera separation becomes large [8][10]. Recently, we extended the capabilities of Terrest to include the ability to estimate geospatial uncertainty (i.e., elevation errors), detect occlusions and other anomalies, and fuse elevation estimates generated from multiple views into a highly accurate and robust digital elevation map [7][10]. The Terrest system has been proven to be highly robust in extensive testing and evaluation across many application domains, and has been selected by the National Imagery and Mapping Administration (NIMA) in their recent Pathfinder 2000 search for new image analysis tools in DoD application environments.

The ability of Terrest to produce robust elevation maps under difficult condition is illustrated in Figure 6 which shows a 768 × 768 pixel section of a DEM and corresponding ortho-image generated from an aerial view of a hardwood forest. To test the reliability of detecting trees in the terrain model, two groups of four interpreters evaluated the DEM and ortho-image. The first group marked bumps in the DEM and looks for corresponding evidence of a tree in the ortho-image, while the second group identified trees in the ortho-image and looked for corresponding bumps in the DEM. Both groups found a reliability of at least 95%.

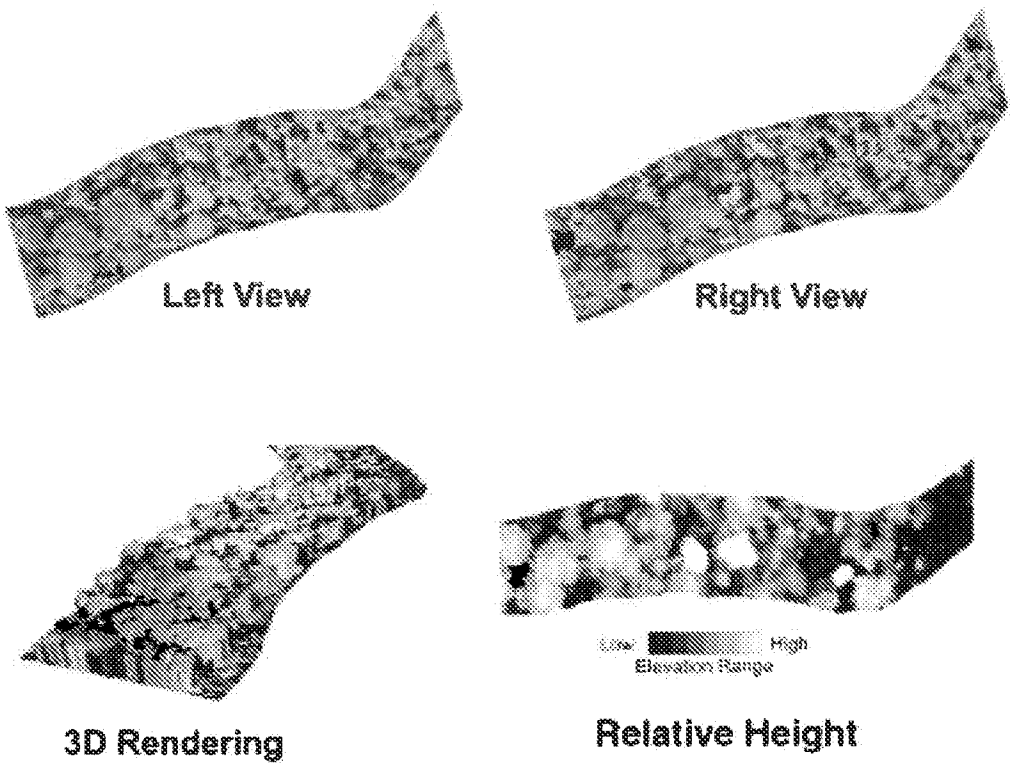


Fig. 5. An example of a left and right stereo mosaic generated from a digital video sequence taken over a Bolivian rainforest (top). A 3D rendering of the canopy (bottom-left) and a relative height map (bottom-right) were produced using the Terrest system.

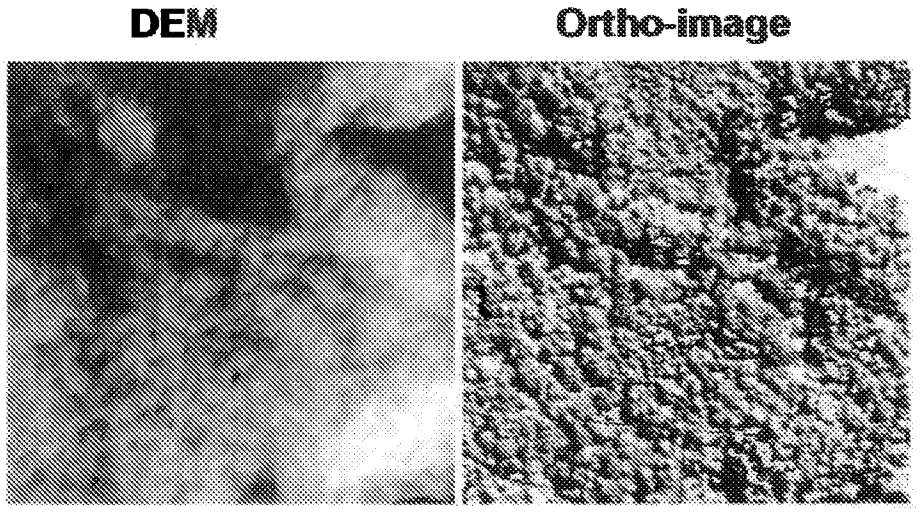


Fig. 6. A DEM (left) and ortho-image (right) of a hardwood forest. There is a 95% agreement between bumps in the DEM and trees in the ortho-image.

The Terrest system has recently been enhances to fuse information from multiple overlapping views (typically 3-6) [8]. When two ore more images are available the system first produces separate DEMs from each ordered image pair. The system then fuses the individual DEMs using a robust method to produce an optimal terrain model consisting of a DEM, an ortho-image, and a geospatial uncertainty map that gives error bounds for each elevation estimate. The technique is based on the concept of self-consistency measures, first introduced by Leclerc et al., (1998a,b) [1][2] to identify unreliable points in

a distribution. We extended the self-consistency concept to the problem of detecting unreliable elements in a DEM, and to estimating the mean and standard deviation of the elevation distribution. For example, if 4 overlapping images were available, 12 DEM could be generated by processing the ordered image pairs (1-2, 2-1, 1-3, 3-1, ···). This would result in 12 elevation estimates per pixel. The self-consistency methodology would determine if an elevation estimate were reliable or unreliable. The mean elevation and standard deviation would then be computed from all reliable estimates at each grid position.

4. FUTURE DIRECTIONS – TOWARDS A REAL-TIME DIGITAL SYSTEM

A successful and practical UAV imaging system must be capable of acquiring, and transmitting or storing images over a wide area. Conventional video and film aerial imaging systems are not well suited for UAV deployment because they generate tremendous amounts of data that are difficult to transmit, store and process into geographically registered terrain models. To meet these demands, we are building a real-time, fully digital system. We are enhancing our current design by improving both the system hardware and computational efficiency. Our new, real-time, system is based on a set of algorithms that create continuous stabilized mosaic images for a sequence of digital frames taken by a moving camera, and continuously updates the estimated aircraft state vector (location, orientation and velocity). When operational, the system will be capable of automatically producing high-quality, multi-spectral, 3D terrain model over large areas.

By far the greatest volume of data is attributed to the digital images. For example, a high-resolution (756 × 568 pixels) video camera generates three simultaneous frames (red, green and blue) at 30 frames per second. This results in approximately 37 Mbytes of data being generated every second. Because as much as 99% of sequential images overlap, a real-time mosaic generation system would result in a data compression of 100:1.

The key to building a real-time terrain modeling system is the ability to generate georeferenced mosaics in real-time. There is a considerable literature on real-time mosaic generation [4][5] and there are commercial systems capable of generating real-time mosaics (such as the Sarnoff Corporation PVT™ vision hardware and VideoBrush™ software systems). Although these systems operate in real-time, they produce unconstrained mosaics and are limited to standard video formats. Thus, the focus of our current effort centers on developing algorithms that predict the precise camera location and orientation in real-time. Our approach is the use of a real-time extended Kalman filtering (EKF) technique that assimilates the instantaneous aircraft orientation, position and velocity from the GPS and AHRS systems; and then to incorporate the real-time pose information into a real-time version of the UMass georeferenced mosaic generation software.

To further reduce the data rate and improve the spatial and spectral resolution of the system, the mini-DV camcorders will be replaced with digital cameras, which offer several advantages over digital camcorders, including:

- **Non-compressed, non-interlaced digital images.** Each frame is equivalent to a digitized image of the terrain. This format avoids motion blurring from the interlace read out architecture, and the color fidelity loss introduced by compression schemes associated with common video formats, such as NTSC, Hi-8, mpeg, jpeg and min-DV.

- **Externally triggered electronic shutter.** This enables the system to eliminate unnecessary processing and storage of images by controlling the time between frames. It also allows the system to synchronize instruments, generate the optimal amount of image overlap, and collect images over specific locations.

- **A beamsplitter design.** By placing a beamsplitter that separates the image into discrete spectral bands behind the lens, a single camera can collect a 3 or 4 band multi-spectral image in which the individual bands are perfectly registered.

When operational, the system will transmit stereoscopic, georeferenced mosaics directly to the ground receiving station, where the mosaics can be further processed by application specific algorithms, such as DEM and feature extraction. Our current plans call for an initial test flight of the real-time system in the spring of 2001.

ACKNOWLEDGMENTS

The research is sponsored by grants from the National Science Foundation (EIA-9726401, EIA9970046), The Defense Advanced Research Projects Agency, through the Army Topographic Engineering Center (DAAG55-97-1-0188), and the Army Research Office (DAAD19-99-1-0016)

REFERENCES

1. Leclerc, Y. G., Q. T. Luong and P. Fua, "A Framework for Detecting Changes in Terrain," *IEEE Trans. On Pattern Analyssi and Machine Intel.* Vol. 20., no. 11., pp 1143-1160, November 1998.
2. Leclerc, Y. G., Q. T. Luong and P. Fua, "Self-consistency: A Novel Approach to Characterizing the Accuracy and Reliability of Point, Correspondences Algorithms," DARPA Image Understanding Workshop, Monterey CA, pub by Morgan Kauffman, 1998
3. Kumar, Rakesh, Harpreet S. Sawhney, Jane C. Asmith, Art Pope, Steve Hsu, "Registration of video to geo-referenced imagery," *14th Inter Conf on Pattern Recog. (ICPR)*, pp 1393-1400, August 1998.
4. Kumar, Rakesh, P. Anadan, Michal Irani, James Bergen, Keith Hanna, "Representation of Scenes from Collections of Images," *IEEE Workshop on Representation of Visual Scenes*, Cambridge MA., May 1995.
5. Sawhney, H. Harpreet and Serge Ayer, "Compact Representation of Videos Through Dominant and Multiple Montion Estimation," *IEEE Trans on Pattern Analysis and Machine Intel.*, pp 814-830, Vol. 16, No. 8., August 1996.
6. Schultz, H., 1994. Terrain Reconstruction from Oblique Views, Proc. *DARPA Image Understanding Workshop*, Monterey, CA, pp. 1001-1008.
7. Schultz, H., Hanson, A., Holmes, C., Riseman, E., Slaymaker, D., Stolle, F., "Integrating Small Format Aerial Photography, Videography, and a Laser Profiler for Environmental Monitoring", *ISPRS WG III/1 Workshop on "Integrated Sensor Calibration and Orientation*, Portland, Maine, USA June 16-17, 1999.
8. Schultz, H., Riseman, E., Stolle, F., 1999. Error Detection and DEM Fusion Using Self-Consistency, Submitted to the *7th IEEE International Conference on Computer Vision*, Kerkyra, Greece.
9. Schultz, H., Schwickerath, A., Stolle, F., Hanson, A., Riseman, E., "Incremental Digital Elevation Map Generation From stereo Images," *ISPRS Workshop on Theoretical and Practical Aspects of Surface Reconstruction and 3D Object Extraction*, Haifa, Israel, September 9-11, 1997.
10. Schultz, H., "Terrain Reconstruction from Widely Separated Images", Proc. SPIE, Volume 2486, pp. 113-123, Orlando, FL, April, 1995.
11. Schultz, H., Slaymaker, D., Hanson, A., Riseman, E., Holmes, C., Powell, M., and Delaney, M., "Cost-effective Determination of Biomass from Aerial Images," *International Workshop on Integrated Spatial Data*, Portland, Maine, June 14-15, 1999.
12. Slaymaker, D., "Calculating Forest Biomass with Small Format Aerial Photography, Videography, and a Profiling Laser" The Proceedings of the *17th. Biennial workshop on Color Photography and Videography in Resource Assessment ASPRS*, Bethesda, Maryland, 1999.
13. Slaymaker, D., L. Hannah " Gps-logged Aerial Video as a Geo-referencing Tool For Digital Imagery in Remote Regions, a case study in Madagascar", *The Proceedings of the16th Biennial workshop on Color Photography and Videography in Resource Assessment*. ASPRS, Bethesda, Maryland, 1997.
14. Slaymaker, D., Schultz, H., Hanson, A., Riseman, E., Holmes, C., Powell, M., and Delaney "Calculating Forest Biomass With Small Format Aerial Photography, Videography And A Profiling Laser,", M., *Proc. of the 17th Biennial Workshop on Color Photography and Videography in Resource Assessment*, Reno, Nevada, May 1999.
15. Slaymaker, D.M., K. M. L. Jones, C. R. Griffin, and J. T. Finn 1996, "Mapping deciduous forests in southern New England using aerial videography and hyperclustered multi-temporal Landsat TM imagery," In *Gap Analysis, A Landscape Approach to Biodiversity Planning*, pp. 87--101 and 308--312, Bethesda, Maryland: American Society for Photogrammetry and Remote Sensing.
16. Zhu, Zhigang, Allen R. Hanson, Howard Schultz, Frank Stolle, Edward M. Riseman, "Stereo Mosaics from a Moving Video Camera for Environmental Monitoring," *International Workshop on Digital and Computational Video*, December 10, 1999, Tampa, Florida, USA
17. Zhu, Zhigang, Edward M. Riseman, Allen R. Hanson, Howard Schultz, "Automatic Geo-Correction of Video Mosaics for Environmental Monitoring", Report TR #99-28, Computer Science Department, University of Massachusetts at Amherst, April, 1999

Paper: 4232A-08, SPIE Enabling Technologies for Law Enforcement Boston, MA, November 5-8, 2000

INTEGRATING SMALL FORMAT AERIAL PHOTOGRAPHY, VIDEOGRAPHY, AND A LASER PROFILER FOR ENVIRONMENTAL MONITORING*

H. Schultz[1], D. Slaymaker[2], C. Holmes[1], F. Stolle[1], A. Hanson[1], E. Riseman[1]

[1] Computer Science Department, University of Massachusetts, Amherst, MA 01003
{hschultz, cholmes, stolle, hanson, riseman}@cs.umass.edu

[2] Forestry and Wildlife Management Department, University of Massachusetts, Amherst, MA 01003
dana@fnr.umass.edu

Commission III, Working Group I

KEY WORDS: Environmental Monitoring, Stereo, Terrain Modeling, Classification, Videography

ABSTRACT

This paper describes an ongoing collaborative research program between the Computer Science and the Forestry and Wildlife Management Departments at the University of Massachusetts to develop semi-automatic, cost-effective methodologies for monitoring environmental parameters over large areas. To meet these challenges we built a moderate cost system comprised of off-the-shelf instruments, including a differential GPS, a 3-axis solid state attitude and heading reference system, two mini-DV camcorders, a small format aerial survey camera, a profiling laser altimeter, and a PC based data acquisition system. The quality and format of the video and digitized photographic data were chosen to provide high quality input to several state-of-the-are computer vision algorithms for 3D terrain modeling, and ground cover classification. Although the work described in this paper is in a preliminary phase and all of the constituent technologies have not been fully integrated, we nevertheless demonstrated the value and feasibility of using the system to solve environmental monitoring problems on a large scale.

1 INTRODUCTION

The Computer Science (CS) and Forestry and Wildlife Management (FWM) Departments at the University of Massachusetts are engaged in a three-year NSF grant to develop cost-effective, automated techniques to monitor forests and other natural environments. An important long-term goal is to automate and improve environmental monitoring techniques currently employed by FWM through the use of a variety of computer vision techniques, including 3D terrain reconstruction, classification, and automatic video mosaicking techniques.

The specific application presented in this paper focuses on estimating biomass for aerial images. This work was motivated by the UN Convention on Climate Change held at Kyoto, Japan in 1997, which established a framework for assigning economic value to carbon sequestered in biomass. The effective implementation of the treaty depends on developing cost-effective methods that accurately establish the biomass of tropical forests. Because of vast amount of forests that maybe affected by this treaty, current labor intensive in-situ methods (Brown et al., 1984 and 1991) are not feasible.

To extend coverage and simplify data collection, a range of techniques are being evaluated that utilize the general approach of extrapolating information from small area point samples (e.g., permanent plots), to high-resolution transects observed from low-altitude aerial surveys, to low-resolution, large area analysis derived from satellite images. The focus of our current work is on studying the effectiveness using strips of high-resolution video, wide-angle video, laser altimeter profiles, and 3D terrain models generated from small format aerial photography for estimating the type, quantity, size and health of trees in a forest.

2 APPROACH TO INSTRUMENTATION

Our initial focus was on evaluating two aerial survey techniques for determining biomass, a low-altitude (<500 meters) system based primarily on video (Slaymaker et al., 1996), and the high-altitude (1000 – 3000 meters) system which relied additionally on stereo images to generate 3D terrain models. For both setups, a 12 channel real-time differential GPS (Trimble AGGPS receiver and an L-band Omnistar and GPS antenna) was used to collect position information and a 3-axis attitude and heading reference system (Watson Industries AHRS-BA303) was used to collect orientation information. In addition, the low-altitude setup contained a profiling laser altimeter (Laser Atlanta), which gave us the instantaneous height of the airplane above the canopy. To enable temporal registration of the various data streams, time codes were added to the data during collection. A time code generator (Horita) was used synchronize the video data, which were recorded on a mini digital video recorder (Sony DV-G900), and a time code stamp was added to all digital data during the recording process.

A photograph of the low-altitude setup is shown in Figure 1 and a schematic diagram of the low and high-altitude setups are shown in Figures 2 and 3. Both systems employ of a dual video system (wide-angle and zoom). The zoom camera provides information about the appearance of specific trees, while the wide-angle system provides information for determining the spatial distribution of tree species and size (a sample of

* Sponsored by Grants from the National Science Foundation (EIA-9726401) and the National Fish and Wildlife Foundation (98-089)

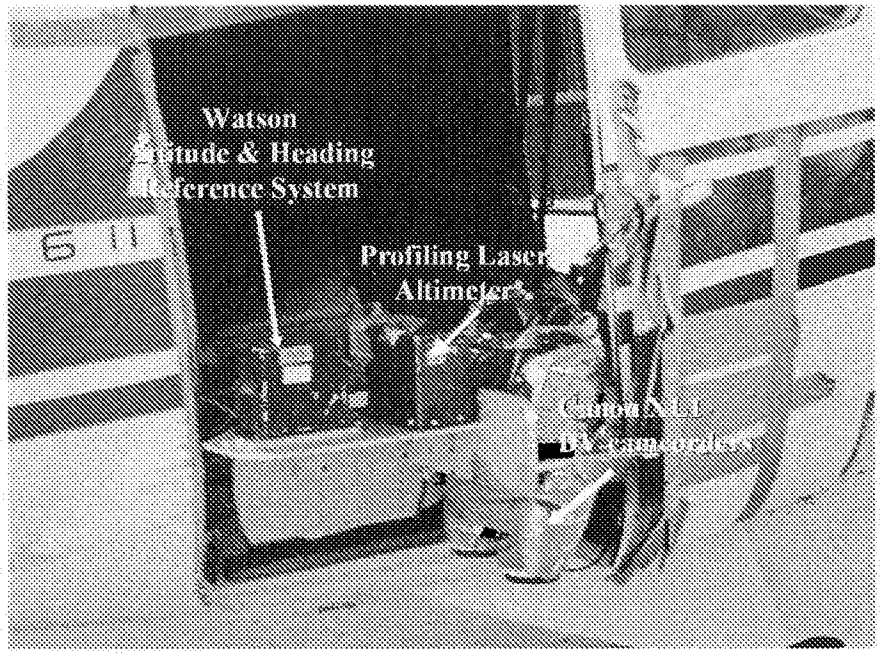


Figure 1. A photograph of the installed low-altitude configuration.

collocated wide-angle and zoom video are shown in Figure 4). The zoom video lens was set so that its swath width was 29 meters, which was equivalent to 4 cm pixels. The lens on the wide-angle camcorder was set so that it recorded a swath width of 320 meters, which was equivalent to 50 cm pixels. The profiling laser altimeter (PLA) was active for low-altitude flights. The fast sampling rate (238Hz) and narrow beam width (1 foot) of the PLA gave us the ability to resolve the shape in individual trees (see Figure 5). Because of range limitations we were not able to operate the PLA in the high-altitude configuration

In the high-altitude configuration the system was fitted with a Hasselblad MWK 70mm aerial survey camera, which gave us the ability to take stereoscopic images at a ground sampling distance of 0.5 meters or less.

The cameras, PLA and AHRS were attached to a rigid mounting system, which was attached to the side of the airplane. This assures that the angles measured by the AHRS gave the precise

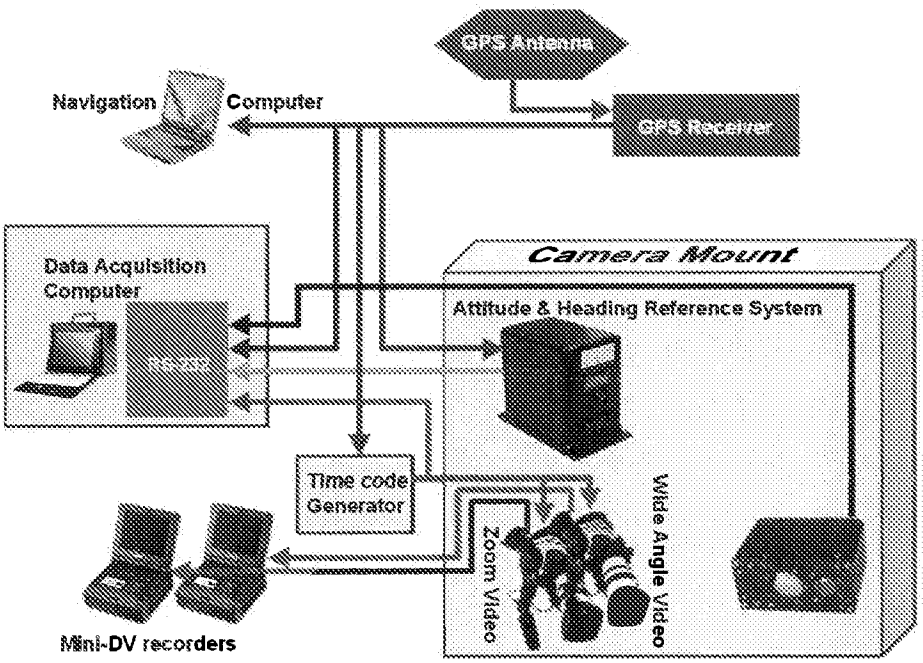


Figure 2. The low-altitude configuration.

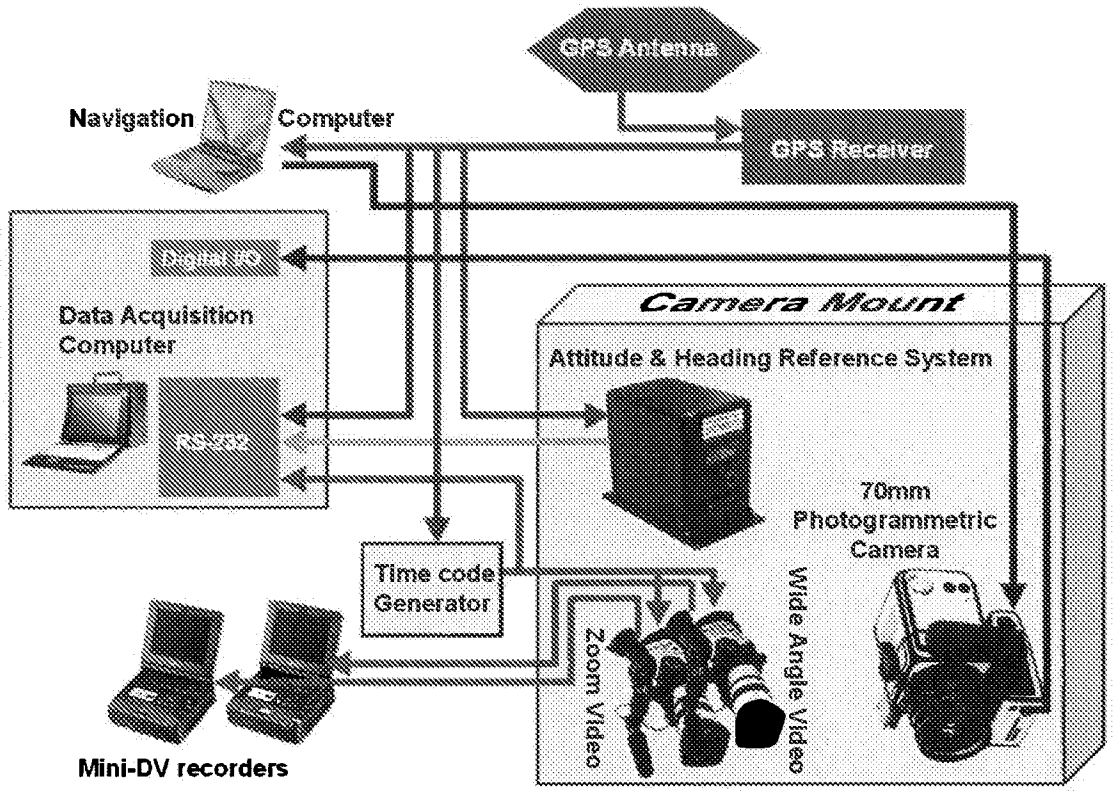


Figure 1. **The high-altitude configuration.**

orientation of the cameras and PLA. To assure accurate position measurements, the X,Y,Z-offsets between the GPS antenna and the cameras was measured after the antenna and cameras were installed in the aircraft.

The video system consists of two Canon XL1 mini-DV camcorders. One was fitted with a Canon 5.8-88mm telephoto lens and the other with a Canon 3.4-10.2mm wide-angle lens. These camcorders use a 3-chip design (red, green, blue), which resulted in excellent color separation, and a progressive scan readout architecture, which eliminates even/odd field blurring. The digital video recording systems were especially valuable because it enabled us to analyze and copy the digital video data without introducing a generation loss.

The video cameras produced a continuous video stream, which was recorded inside the aircraft on the two Sony mini-DV recorders. The Horita GPS time code generator convert the GPS timing signal to a digital form that was compatible with the digital audio channel of camcorders. Thus, by feeding the digitally encode audio through the camcorders we were able to record GPS time information on the audio track. We also recorded the digital audio on the data acquisition computer. This gave us an independent machine-readable relationship

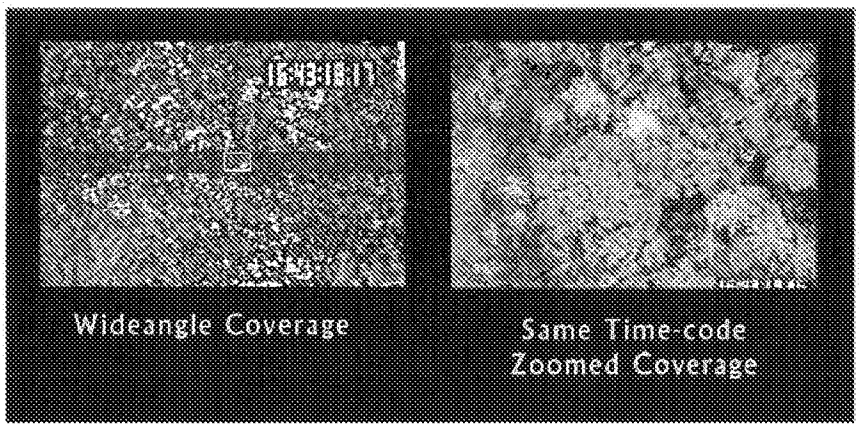


Figure 2 Product of dual camera videography. Zoomed imagery tracks a swath down the center line of the wide angle coverage and can be matched by corresponding time codes.

between frame number and GPS time.

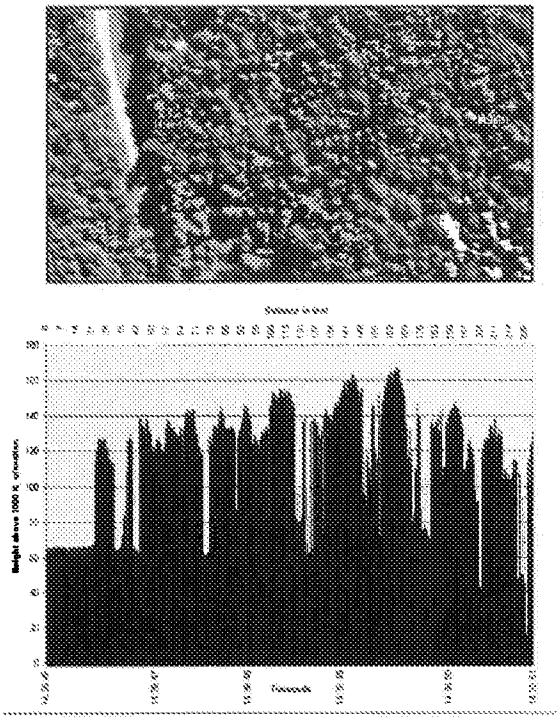


Figure 3. An example tree height profile generated from PLA data. The top panel shows the path across the tree canopy.

The GPS data provided several functions, including (i) velocity compensation for the AHRS, (ii) synchronizing the video data by adding timing information to the audio track, (iii) navigation, and (iv) triggering the aerial survey camera. The GPS data were recorded directly on the data acquisition computer as well. As configured, the GPS had an absolute accuracy of approximately 1 meter horizontally and 2 meters vertically. In addition, the AHRS provided us with precise orientation information to an accuracy of 0.1° about the two horizontal axes, and 0.5° about vertical axis (azimuth). The position and orientation information was used to initialize the bundle adjustment procedures for determining image orientation.

The data streams from the PLA, AHRS, GPS and time code generator were recorded through the serial ports on the data acquisition computer. Each instrument had a different sampling rate and baud rate, which are summarized in Table 1. The program that read the serial ports and wrote the data to disk added a time stamp, which was read from the system clock, to each record before it was written to disk. Because each port received data at a different rate, the various instrument records were not coincident in time. To simplify data analyses, in a post-processing step, the raw data were interpolated so that the various data fields were coincident with the PLA data (the instrument with the fastest sampling rate). The GPS time code was an exception. Because video frames cannot be interpolated, the GPS time codes were repeated between frames. Table 2 shows a few lines from the collated and interpolated data file. In addition to interpolated raw data, the file also contains a few computed data fields, including the aircraft height above the ground (gnd_alt), and the northing and easting of the point where the PLA beam intersected the surface (gnd_North, gnd_East).

GeoLink navigation software running on the navigation computer determined the camera trigger. At predetermined intervals, which resulted in approximately 80% overlap between frames, the navigation software sent a trigger to the Hasselblad camera. The precise exposure time was determined by recording the time when the camera flash relay closed.

An Intergraph SSK workstation was used to build the stereo models and the UMass Terrain Reconstruction System (Terrest) was used for image matching and building the 3D terrain models. The 80% overlap between frames was used to provide redundant elevation estimates (see Section 3) and to maintain radiometric consistency between frames.

Techniques were tested by processing a preliminary data set collected in September 1998 over a mixed hardwood/conifer forest area at an AEP test site in Crooksville, Ohio. Thirty-one plot sites were established along two transects and a per hectare biomass estimated for each. Half of the plot measurement sets are presently being used to calibrate the resulting video strips and 3D terrain models. These results will then be tested against the remaining sites to determine the relative success of each approach. A more extensive test over much larger area is planned in Bolivia this spring, to be conducted in the Noel Kempff Mercado National Park expansion zone in Bolivia. That survey should provide more accurate estimates of biomass at a considerably lower cost.

Table 1 Sampling and baud rate for the digital instruments

Instrument	Sampling rate (Hz)	BAUD rate
Profiling Laser Altimeter (PLA)	238	19.2K
Attitude and Heading Reference System (AHRS)	11.8	9600
Global Position System (GPS)	1	9600
GPS Video Time Code (Horita)	30	9600

3 THREE-DIMENSIONAL TERRAIN MODELING USING TERREST

The ability to generate accurate, high-resolution digital elevation maps (DEM) is essential to our environmental monitoring strategy. On a low-resolution scale (5-30m) DEMs provide important topographic information, such as elevation, slope and drainage patterns. On a finer scale (1 m or less) DEMs can be used to count individual trees, and/or determine 3D textural qualities of the surface.

The UMass Terrest system was designed to automatically generate high-resolution 3D terrain models from aerial images when the viewing angles become oblique (incidence angles greater than 45 degrees), and/or when the camera separation becomes large (base-to-height ratio exceeds 1.5). The system incorporated several specific features that increase the accuracy, robustness, and utility of the system (Schultz, 1994 and 1995).

ortho-image and looked for corresponding bumps in the DEM.

Table 2 Sample lines from a collated and interpolated data file. The fields are: *Labtime* the time stamp from cpu clock; *laser* the raw PLA range data in feet; *scat* a number proportional to the width of the PLA beam; *flg* a flag indicating if the AHRS data are reliable (I indicates reliable data); *tilt,tip,heading* the raw angle codes from the AHRS, *timecode* the GPS time (hour: minute: second: video frame); *alt* the GPS altitude meters; *a/c_North, a/c East* the aircraft GPS northing and easting in UTM coordinates; *gnd_alt* the computed vertical distance from the ground to the aircraft in meters; *gnd_North, gnd_East* the computed northing and easting where the PLA beam intersected the surface. An entry of 0 indicates missing data.

Labtime	laser	scat	flg	tilt	tip	Heading	Timecode	alt	a/c North	a/c East	Gnd alt	Gnd North	gnd East
3433121.4	0.0	0	I	6.1	0.3	111.3	16:03:07:01	571.5	8372950.6	632627.6	0.0	0.0	0.0
3433125.8	1020.6	35	I	6.1	0.3	111.3	16:03:07:01	571.5	8372950.6	632627.9	262.2	8372983.6	632629.5
3433130.2	1020.6	35	I	6.1	0.3	111.3	16:03:07:01	571.5	8372950.6	632628.1	262.2	8372983.6	632629.7
3433134.6	1021.8	42	I	6.1	0.3	111.3	16:03:07:01	571.5	8372950.6	632628.3	261.8	8372983.7	632630.0
3433139.0	1022.6	47	I	6.1	0.3	111.3	16:03:07:01	571.5	8372950.6	632628.5	261.5	8372983.7	632630.3
3433143.4	1023.8	46	I	6.1	0.3	111.3	16:03:07:01	571.5	8372950.6	632628.8	261.2	8372983.7	632630.6
3433144.0	0.0	0	I	6.1	0.3	111.3	16:03:07:02	571.5	8372950.6	632628.8	0.0	0.0	0.0
3433147.8	1023.6	38	I	6.1	0.3	111.3	16:03:07:02	571.5	8372950.6	632629.0	261.2	8372983.7	632630.8
3433152.2	1026.3	39	I	6.1	0.4	111.3	16:03:07:02	571.5	8372950.6	632629.2	260.4	8372983.8	632631.1
3433156.6	1025.8	36	I	6.1	0.4	111.3	16:03:07:02	571.5	8372950.6	632629.5	260.6	8372983.8	632631.4
3433161.0	1024.5	35	I	6.1	0.4	111.3	16:03:07:02	571.4	8372950.6	632629.7	261.0	8372983.8	632631.6
3433165.0	1026.0	35	I	6.1	0.4	111.3	16:03:07:02	571.4	8372950.6	632629.9	260.5	8372983.8	632631.9
3433169.0	1025.5	32	I	6.1	0.4	111.3	16:03:07:02	571.4	8372950.6	632630.1	260.6	8372983.8	632632.1
3433173.0	1026.0	35	I	6.1	0.4	111.3	16:03:07:02	571.4	8372950.6	632630.3	260.5	8372983.8	632632.4
3433177.0	1025.5	32	I	6.1	0.4	111.3	16:03:07:02	571.4	8372950.6	632630.5	260.6	8372983.8	632632.6
3433178.0	0.0	0	I	6.1	0.4	111.3	16:03:07:02	571.4	8372950.6	632630.6	0.0	0.0	0.0
3433179.0	0.0	0	I	6.1	0.4	111.3	16:03:07:03	571.4	8372950.6	632630.6	0.0	0.0	0.0
3433181.0	1026.0	37	I	6.1	0.4	111.3	16:03:07:03	571.4	8372950.6	632630.7	260.5	8372983.8	632632.8
3433354.0	0.0	0	I	5.9	0.5	111.2	16:03:07:08	571.3	8372950.6	632639.6	0.0	0.0	0.0
3433357.0	1033.1	30	I	5.9	0.5	111.2	16:03:07:08	571.3	8372950.6	632639.8	258.1	8372982.8	632642.6
3433361.0	1032.4	32	I	5.9	0.5	111.2	16:03:07:08	571.3	8372950.6	632640.0	258.3	8372982.8	632642.8
3433365.0	1031.9	28	I	5.9	0.5	111.2	16:03:07:08	571.3	8372950.6	632640.2	258.5	8372982.7	632643.1
3433369.0	1031.9	34	I	5.9	0.5	111.2	16:03:07:08	571.3	8372950.6	632640.4	258.5	8372982.7	632643.3

Figure 6 shows a 768 × 768 pixel section of a DEM and corresponding ortho-image taken from the center of one of the 3D terrain models. To test the reliability of detecting trees in the 3D terrain model, two groups of four interpreters evaluated the DEM and ortho-image. The first group marked bumps in the DEM and looks for corresponding evidence of a tree in the ortho-image, while the second group identified trees in the Both groups found a reliability of at least 95%.

The Terrest system has recently been enhances to fuse information from multiple overlapping views (typically 3-6) (Schultz, et al., 1999). When more than two images are available the system first produces separate DEMs from each ordered image pair. The system then fuses the individual DEMs

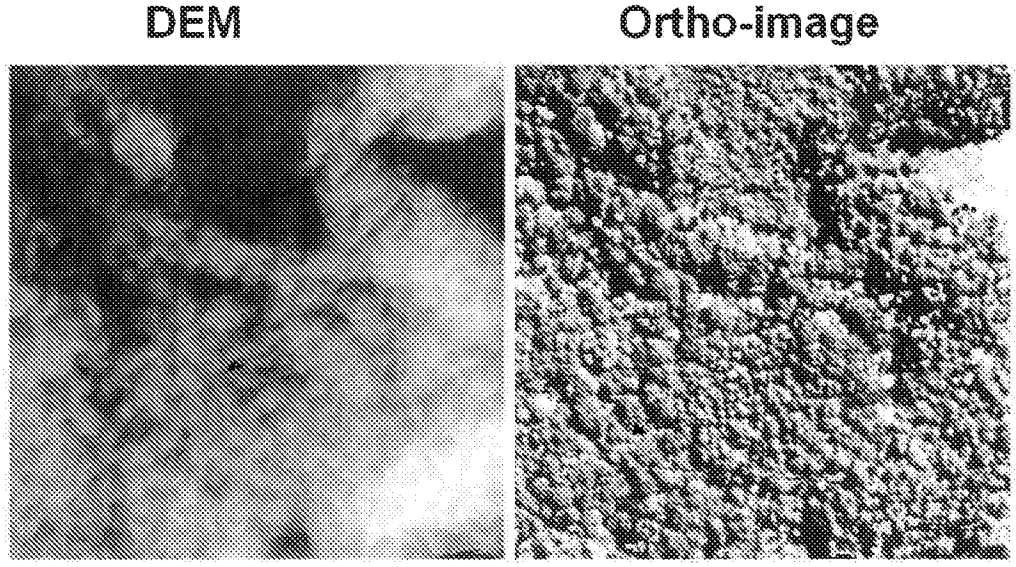


Figure 4 The DEM and orhto-images used to test the reliability of detecting trees

using a robust method to produce an optimal terrain model consisting of a DEM, a geospatial uncertainty map, an ortho-image, and a set of 3D texture maps (see Terrain Classification below).

The technique relies on two key factors for generating robust 3D terrain models, (1) the ability to detect unreliable elevations estimates, and (2) the ability to fuse the reliable elevations into a single optimal terrain model. The technique is based on the concept of using self-consistency measures, first introduced by Leclerc et al., (1998a,b) to identify unreliable points in a distribution. The focus of their work was to obtain a quality measure for point correspondences. Their algorithm obtained a probability distribution by counting the number of corresponding image points for each object point that is consistent with the viewing geometry within a specified error limit. We extended the self-consistency concept to the problem of detecting unreliable elements in a DEM, generated from stereoscopic image pairs.

Figure 7 shows the results of a multi-image fusion. The processing started with 4 images, which resulted in 12 elevation estimates per pixel in the output grid. We then applied the self-consistency methodology and labeled each elevation estimate as reliable or unreliable. We then averaged all of the reliable estimates are each pixel to form an optimal DEM.

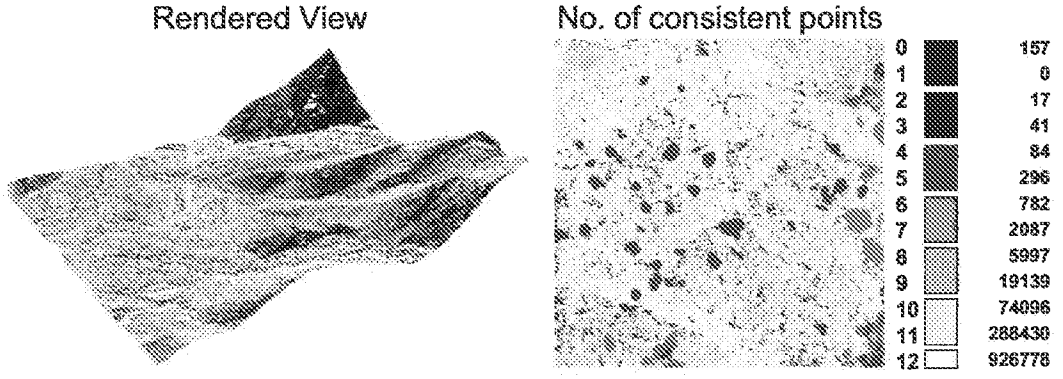


Figure 5. A rendered view of the final 3D terrain model (left) and the number of self-consistent estimates per pixel used to compute generate the model (right).

4 3D WORLD TEXTURE FEATURES

We have recently shown that classification performance can be significantly improved by adding to the usual 2D image texture measures (Haralick, et al. 1973) a set of new 3D texture measures (Wang et al.). Our concept is that 3D textures are a function of recurring patterns caused by physical coarseness, roughness, and other characteristics of 3D surface structure, and that certain intermediate results generated during the process of generating a 3D terrain model are related to the 3D textures. We derived four 3D texture measures and used them in the ground cover classification problem. We found that 3D textures significantly improved the performance of a standard classification system. The experiments in (Wang et al.) showed that including 3D texture features improved classification skill from 72.5% to 83.4%. We believe the implications of these findings for terrain feature extraction are far reaching.

The 3D texture features are derived during the image matching phase in the 3D reconstruction process. During image matching left-right pixel correspondences are determined to a fraction of a pixel width. As a result, the statistical properties of the pixel correspondences are sensitive to the microstructure of the surface (3D structure at length scales approximately equal to the ground sampling distance). The four 3D texture features are: (i) The confidence level assigned to each correspondence; (ii) the variability of confidence levels within a 17×17 window surrounding each correspondence; (iii) the deceleration length for each correspondence; and (iv) the variability of deceleration length within a 17×17 window surrounding each correspondence.

5 TERRAIN CLASSIFICATION USING ITL

Our classification system is based on the Interactive Teacher-Learner (ITL) paradigm (Piater et al. 1999), which employs a feedback mechanism between the operator (the Teacher) and a state-of-the-art real-time decision tree classifier (the Learner). The user receives feedback by interactively specifying training instances (using semi-automated graphical tools) and then seeing the effect that his/her actions had on the classifier. An efficient state-of-the-art decision tree classification algorithm, which is running in the background, continuously updates its classification parameters, and displays its results in real-time.

It is important to contrast this approach with the standard methods of specifying training data. Typically, large numbers of pixels are laboriously hand-labeled to ensure a statistically valid sample. A large amount is selected because the user does not know what is a sufficient training size and which training instances are informative.

By overlaying the classification results on the scene in false color, the user can immediately see the impact that their selections on the classifier. This provides the human trainer with instant feedback as the classifier assimilates new training data. Rather than hand-labeling large numbers of pixels as input training data in off-line process, an operator trains the classifier by giving much more informed incremental training instances, e.g., correcting mistakes or defining new subclasses that are necessary for discrimination in the particular context. In this way natural user interaction leads to the judicious selection of a small amount of very important data in the training process.

Table 3 shows a comparison between a scene classified using the ITL system and conventional batch processing, in which all the training data were selected in advance. The results of the comparison are shown in Table 1. The test was run using 17 features (12 standard 2D co-occurrence features, 4 3D texture features and the ortho-image). The percent correct were similar

except that three orders of magnitude less training data were required with the ITL system.

To make the feedback mechanism between the teacher (user) and learner (computer) practical, the ITL system requires a classification system that efficiently updates as the users selects new training instances. The Incremental Tree Inducer (ITI) decision tree developed at UMass (Utgoff 1994; Utgoff et al., 1997) was selected for this purpose. In addition to being one of the most accurate implementation of a decision tree, ITI is capable of updating an existing decision tree without rebuilding the tree structure. Thus, when the operator selects new training instances, ITI updates the existing tree instead of rebuilding the decision tree. In addition, ITI uses only those features that contribute to the decision making process. As a result, there is no need to guarantee in advance that any particular feature will be useful because the decision tree methodology will only select those features that improve the discrimination between the user-defined training classes. Thus, there is no need to validate a priori the utility of features.

When operational, the user will be able to visualize in a 3D fly-through graphical environment the 3D terrain models generated from the strips of stereoscopic aerial photography. The operator will also have access to collocated wide angel and telephoto video strips, which will help the operator to identify the appearance of specific tree species.

Table 3 Comparison between ITL and batch mode processing.

	ITL	Batch
Mouse Clicks	30	
Training Examples	270	16916
% Correct	85.1	86.4
Tree Nodes	25	71

6 CONCLUSIONS

Although this work is in a preliminary phase and all of the constituent technologies have not been fully integrated, we have nevertheless demonstrated the value and feasibility of using state-of-the-art computer vision techniques (Terrest and ITL) to solve environmental monitoring problems on a large scale. In the near future we plan to integrate terrain modeling and classification so that someone skilled in Forestry but not necessarily photogrammetry or computer science will be able efficiently extract reliable environmental information from video and aerial photography.

REFERENCES

Brown, S., and A.J.R. Lugo, 1984. Biomass of tropical forests: a new stimate based on forest volumes, Science 223:1290-1293.

Brown, S., A.J.R. Gillespie, and A.E. Lugo, 1991. Biomass of tropical forests of south and southeast Asia. Canadian Journal of Forest Research 21:111-117. Crow T.R. 1978. Common regressions to estimate tree biomass in tropical stands. Forest Science 24:110-114.

Haralick, R., K. Shanmugam, and I. Dinstein, 1973. Textural Features for Image Classication," IEEE Trans.on Systems, Man, and Cybernetics, Vol. 3, No. 6, pp. 610-621.

Leclerc, Y.G., Q.T. Luong, and P. Fua, 1998. A Framework for Detecting Changes in Terrain, *IEEE Trans. Pattern Analysis and Machine Intelligence*, vol. 20, no. 11, pp. 1143-1160.

Leclerc, Y,G., Q.T. Luong, et al., 1998. Self-consistency: A novel approach to characterizing the accuracy and reliability of point correspondence algorithms, *DARPA Image Understanding Workshop*, Monterey, CA.

Pister, Justus H., Riseman, Edward M. and Utgoff, Paul E., 1999. Interactively Training Pixel Classifiers. International Journal of Pattern Recognition and Artificial Intelligence 13(2), pp. 171-194.

Schultz, H., 1994. Terrain Reconstruction from Oblique Views, Proc. DARPA Image Understanding Workshop, Monterey, CA, pp. 1001-1008.

Schultz, H., 1995. Terrain Reconstruction from Widely Separated Images, Proc. SPIE, Volume 2486, pp. 113-123, Orlando, FL.

Schultz, H., Riseman, E., Stolle, F., 1999. Error Detection and DEM Fusion Using Self-Consistency, Submitted to the 7th IEEE International Conference on Computer Vision, Kerkyra, Greece.

Slaymaker, D.M., K.M.L. Jones, C.R. Griffin and J.T. Finn, 1009. Mapping deciduous forests in Southern New England using aerial videography and hyperclustered multi-temporal Landsat TM imagery. Pages 87-101 in Gap Analysis: A Landscape Approach to Biodiversity Planning, J.M. Scott, T.H. Tear and F.W. Davis (eds). American Society of Photogrammetry and Remote Sensing, Bethesda, MD.

Utgoff, P. E, 1994. An improved algorithm for incremental induction of decision trees, In Machine Learning: Proc. 11th Int. Conf, pp. 318--325, Morgan Kaufmann.

Utgoff, P.E., N. C. Berkman, and J.A. Clouse, 1997. Decision tree induction based on efficient tree restructuring", Machine Learning 29(1), 5-44.

Wang, X., F. Stolle, H. Schultz, E. M. Riseman, and A. R. Hanson, 1997. Using three-dimensional features to improve terrain classification", In Proc. Computer Vision and Pattern Recognition, pp. 915-920.

CALCULATING FOREST BIOMASS WITH SMALL FORMAT AERIAL PHOTOGRAPHY, VIDEOGRAPHY AND A PROFILING LASER

D. Slaymaker, Research Associate, dana@fnr.umass.edu
H. Schultz, Research Faculty, hschultz@cs.umass.edu
A. Hanson, Professor, hanson@cs.umass.edu
E. Riseman, Professor, riseman@cs.umass.edu
C. Holmes, Professional Staff, cholmes@periscope.cs.umass.edu
University of Massachusetts
Department of Forestry and Wildlife Management
& Department of Computer Science
Amherst, MA 01003-4610

Mark Powell, Program Officer, mhp@winrock.org
Matthew Delaney, Program Associate. md@winrock.org
Winrock International
38 Winrock Drive
Morrilton, AR 72110-9370

ABSTRACT

This paper reviews an aerial sampling technique that could reduce the cost of calculating standing forest biomass in remote regions by collecting a geographically distributed set of large scale transects that include a limited number of permanent plots. The biomass of these plots is calculated from allometric equations and extrapolated to the transects as a function of tree species, crown diameter and height.

Two kinds of aerial imagery sampling techniques were tested over a mixed hardwood /conifer forest in Crooksville, Ohio. Thirty-one 28-meter diameter plot sites were established along two transects within the test site and the dbh (diameter at breast height) of trees measured. Each transect was flown at 4,000 feet AGL with a small format photogrammetric camera, then at 1,000 feet AGL with global positioning system (GPS)-logged dual-camera video (wide-angle/zoom), and a profiling laser. The photogrammetric images were used to create 3D models of the terrain from which average tree heights and forest volumes could be calculated. The video / laser coverage was used to visually identify the species of individual trees, measure their crown diameters in a 2D geographic information system (GIS) and estimating their heights from the laser profile.

Due partly to an automatic georeference and mosaicking program developed for the video coverage during the project, it proved the more accurate / cost effective approach and this paper concentrates on its results. Average dbh values of one hectare transects calculated from the video are compared to those measured on site, showing a strong positive correlation given the small sample size. A much larger test of 635 plot sites has just been completed in Bolivia, which should allow us to refine the techniques.

INTRODUCTION

The 1997 UN Convention on Climate Change in Kyoto, Japan established a framework for assigning economic value to carbon sequestered in biomass. This could benefit efforts to preserve tropical forests in developing countries if their carbon content can be accurately measured and monitored. Field methods with extensive permanent plots can

estimate biomass in a forest to known levels of precision, but these plots are expensive to reach and maintain in isolated areas. The resulting costs that can vary from approximately $0.05 to $0.50 per ton depending on inventory frequency, accessibility, spatial variability of carbon pools, labor costs and scale, making the process least practical in some of the areas most worthy of preservation.

President Clinton has asked for voluntary efforts on the part of American industries to comply with the goals set forth in Kyoto. As part of an effort to respond to the President's request, the Electric Power Research Institute (EPRI), in collaboration with The Nature Conservancy (TNC), Fundacion Amigos de la Naturaleza (FAN), and the government of Bolivia, have established the Noel Kempff Mercado Climate Action Project. ??? hectares of forest have been withdrawn from logging or agricultural development and added to the Noel Kempff Mercado National Park in northeast Bolivia as an experiment in carbon sequestration as an economically viable, low-cost option for mitigating climate change. In order to determine and monitor the standing forest biomass of this region, TNC contracted with the Winrock International Institute for Agricultural Development to develop a stratified sample of ground sites where individual trees could be measured over time. Winrock established 635 nested plot sites in five basic vegetation strata, measuring the diameter of all woody stems 5 cm to 20 cm in an inner plot of 4 meters radius, and the diameter of all woody stems greater than 20 cm in a larger nested plot of 14 meters radius. These dbh values and tree counts were then extrapolated to a per hectare estimate of standing biomass for the region using standard allometric equations. Setting up 635 plots in a tropical rainforest with few access roads is a major undertaking in cost and mobilization of personnel. Winrock determined that it could reduce this time and cost in future projects of this type if it could establish fewer sites and use aerial sampling to capture the variability of the terrain. For this reason, they contacted the Department of Forestry and Wildlife Management (FWM), University of Massachusetts, where we have worked for several years in developing low cost methodologies to monitor natural resources with small format aerial surveys. We had previously developed a sampling method for classifying forest vegetation using Landsat satellite imagery and low level, GPS-logged, dual camera videography as part of the southern New England Gap Analysis Project (Slaymaker et al, 1996,). We have also worked for the last five years with Conservation International to adapt these techniques to monitoring tropical forests in Africa, Asia and South America (Slaymaker & Hannah, 1997). During these projects, we developed a combined package of videography and digital imagery that utilizes GPS-based mosaicking techniques to provide a more quantitative analysis of forest development and change detection.

FWM is presently engaged in a three-year NSF grant in conjunction with the Computer Vision Research Laboratory (CVRL) of the Department of Computer Science at the University of Massachusetts, a leading research facilities in machine vision and image classification techniques. The purpose of this project is to automate and improve our forest classification methodology through the use of terrain reconstruction and classification techniques that delineate the structure of forests as well as their vegetation communities. Mapping vegetation types in complex terrain has become more successful as computer processing power increases and large amounts of ground truth data can be obtained (either by large-scale video transects (Slaymaker et al., 1996) or by field sites (Schriever et al., 1995;)). However, the structure and age of a forest ecosystem is often more important for habitat, and resource assessment. Wildlife often respond more to the structural variables in a forest (stems/ha, basal area, height of the canopy, etc.) than to the species composition of the forest (Chadwick et al., 1986). Significant forest management practices, such as thinning, affect both the wildlife habitat value and quality and value of timber produced by a stand, but are often imperceptible to satellite and smaller scale aerial imagery after only a year or two. In addition to mapping vegetation types, wildlife biologists and foresters need to be able to map forest structure, stand age and biomass (Short and Hestbeck, 1995). Remote sensing techniques have successfully measured active biomass or chlorophyll activity using normalized vegetation or leaf area indexes (Spanner et al., 1990), but only limited success has been obtained mapping forest structure variables, or standing biomass. CVRL has been working on automatic georeferencing and pixel-specific digital elevation modeling techniques that may increase our ability to extract structural information from large scale sampling data. Given its large database of stratified ground sites, the Noel Kempff Mercado expansion zone was an excellent project to apply these techniques to a tropical forest. Given the size of the area however, we felt a smaller test of a temperate forest was warranted first. Therefore, with support from Winrock, NSF, and additional matching funds from The National Fish and Wildlife Foundation, we established a test site in Crooksville, Ohio to determine the relative accuracy and economics of using large scale aerial sampling of the forest canopy as an extension of Winrock's plot based strategy for estimating biomass.

METHODOLOGY

We set up aerial transects over a mixed hardwood/conifer forest managed by American Electric Power (AEP) in Ohio. AEP provided forestry support personnel to assist Winrock in measuring thirty-one plot sites along two aerial transects over the forest (Figure 1). The center of each plot was established within known tree stands that represented samples of mature and regenerating hardwoods, thinned hardwoods, and conifer plantations. Three criteria were used to select plot locations: 1) at least 100 m from roads, 2) along the target transects, and 3) in an area which was representative of the vegetation around it within a 100 m radius. Using a GPS receiver, the field crews navigated to each plot and marked the center with a four-foot metal stake. Estimates of understory vegetation, standing litter and soil biomass were collected from clip plots, but the vast majority of the standing biomass for each plot was estimated directly from the dbh values of measured trees, using species-specific allometric equations (Table 1). Equations of this kind are available for temperate tree species of the U.S. (Tritton and Hornbeck, 1982) and tropical tree species (Crow, 1978; Brown et al., 1984, 1989). Equations for temperate trees exist for individual species and for groups (e.g., all pines, all hardwoods) and have been generated over many different studies by measuring the trees, then actually cutting them down, drying and weighing them. Regression equations were developed to describe above ground biomass as a function of dbh alone or dbh and height. The differences in the equations reflect variations in wood density and tree allometry (relative mass in each component). The conifer/broadleaf distinction is usually the most important for both of these factors when grouping species, therefore the equations for tropical species are usually for all species in a single group. (In Bolivia only hardwoods and palm-trees are distinguished.)

Table 1. Biomass equations used for the Ohio test site.

Species	Equation	Source	dbh range and mass
Hardwoods	y = 0.5 + ((25,000*dbh^2.5)/(dbh^2.5+246,872))	Schroeder et al., 1995[1]	1-85 cm kilograms
Conifers	y = 0.5 + ((15,000*dbh^2.7)/(dbh^2.7+364,946))	Schroeder et al., 1995	3-71 cm kilograms
White Pine	y = 3.2031-(0.2337*dbh)+(0.006061*dbh^2)	Monteith 1979[2]	5-50 cm kilograms
Yellow/Tulip Poplar	y = (Exp(0.45689 + 2.6087 * (Log(dbh))))*0.454	Monteith 1979	5-50 cm kilograms
Elm	y =0.5 + ((25,000*dbh^2.5)/(dbh^2.5+246,872))	Schroeder et al., 1995	5-50 cm kilograms
Black Locust	y =0.5 + ((25,000*dbh^2.5)/(dbh^2.5+246,872))	Schroeder et al., 1995	5-50 cm kilograms
Red Pine	y =Exp(-2.3684 + 2.5303 * (Log(dbh)))	Monteith 1979	5-50 cm kilograms
Red Oak	y = (2.4601*(dbh^2.4572))*.454	Monteith 1979	5-50 cm kilograms
Black Cherry	y = (1.8082*(dbh^2.6174))*.454	Monteith 1979	5-50 cm kilograms

Where: y = biomass in kilograms, Exp = raised to the power of, dbh =diameter at breast height.

Dbh and species were the principal measures used by Winrock to calculate tree biomass in their plot sites.

[1] Schroeder, P., S. Brown, J. Mo, R. Birdsey and C. Cieszewski. 1997. Biomass estimation for temperate broadleaf forests of the United States using inventory data. Forest Science 43:424-434.

[2] Monteith, D.B. 1979. Whole-tree weight tables of New York. *In* Biomass Equations for Major Tree Species of the Northeast. Northeastern Forest Experiment Station. General Technical Report NE-69. L. M. Tritton and James W. Hornbeck. USDA, 46 pg.

Therefore, our goal in an aerial survey was to find if measurements of crown diameter made from the air could be sufficiently correlated to stem diameter to accurately calculate the dbh of trees visible in the canopy. The USDA Forest Service recently completed a forest health survey of the Northeast U.S. in which both dbh and crown diameter measurements were taken from over 7,500 different tree specimens. Two measurements were made from each crown, its largest diameter and a second value directly perpendicular to the first measurement. Dr. Barbara O'Connell of the USDA in Radnor, PA, provided us with records for 1997 and 1998. We correlated the data and developed regression equations between average crown diameter and dbh for each species found at the Ohio test site (Table 2).

Two approaches were taken to aerial coverage of the sites, essentially 3D and 2D. In the 3D approach, a small format photogrammetric camera was used to develop a bundle adjusted 3D model of each transect using a CVRL developed auto digital elevation modeling program called Terrest (paper reference?). This photographic coverage was flown at an altitude of 4,000 ft. above ground with a calibrated Hasselblad MKW camera. Images were exposed onto 70 mm film and digitally scanned at a resolution of 40 centimeters per pixel, with 80% overlap between frames. A Trimble real-time differential GPS (DGPS) was used for in-flight navigation and georeferencing data. An on-board computer recorded the GPS data and fired the camera at predetermined geographic locations. It also recorded the exact time of each exposure and the corresponding output from a Watson digital gyroscope, which was mounted on the same plane as the camera so that its precise orientation in space could be determined. The excessive overlap was necessary to maintain radiometric consistency in the 3D model generated from the coverage and was made practical by the use of a small format camera and automated digital image handling techniques. Working within this 3D space in a "fly-through" image-processing program, it was easy to identify and measure individual crowns, but very computer intensive and time consuming. However, CRVL is working on a program that may automate this procedure.

Table 2 Regression equations generated from USDA forest health survey data.

	Species	Regression	# of points
1	Hardwoods	$\hat{y} = 1.25310 + .03280\,x$	4452
3	White ash	$\hat{y} = 1.00709 + .03693\,x$	369
4	White pine	$\hat{y} = 2.08342 + .04305\,x$	626
5	Yellow/Tulip poplar	$\hat{y} = 1.31445 + .04100\,x$	448
6	Elm	$\hat{y} = 2.11935 + .02495\,x$	329
7	Black locust	$\hat{y} = 6.89910 + .01185\,x$	99
8	Red pine	$\hat{y} = 0.12001 + .05036\,x$	379
9	Red oak	$\hat{y} = 1.04406 + .03877\,x$	540
10	Black cherry	$\hat{y} = 1.70664 + .04169\,x$	219
		Total number of points	7461

The "2D" approach utilized video coverage of individual crowns at a much larger scale in conjunction with laser rangefinder data. Two Canon ES 500 Hi8 camcorders were then flown over each site at an altitude of 1,000 ft. above ground, providing of video coverage at two different scales. One camera was set at wide-angle coverage providing a swath approximately 320 meters wide, with 50 centimeter per pixel resolution. The other camera was set at 12X zoom, recording a 26 meter wide swath at 4 cm per pixel resolution, a sufficient scale to identify individual tree species (Figure 2). A Horita time code generator wrote the Trimble GPS time code and frame number to each video frame as a record of their geographic locations. It also logged the output from the Watson digital gyroscope and a pulse-modulated laser mounted in a vertical mode to provide a continuous profile of the canopy by sending a series of 248 pulses per second along the flight path. The laser beam was approximately one meter wide at the canopy surface and the instrument was set to record the last return on each pulse for maximum penetration to the ground. It was bore-sighted to the large scale zoomed video to identify sensor penetrations that clearly reached the forest floor and provided a measure of canopy height along each flight line (Figure 3).

This instrument package is a further modification of a system we have been developing over several years (Slaymaker et al., 1996, Slaymaker & Hannah, 1997), that can be attached to the window and door of any Cessna aircraft without additional modification (Figure 4). For the Bolivia coverage, we replaced the Hi8 cameras with a DV digital system and plan to replace that with higher resolution progressive scan cameras that will download directly to an on-board raid array.

ANALYSIS

At the inception of this project, we did not know how well the video / laser combination would work, as compared to a full 3D reconstruction from the calibrated camera. However, as the imagery was compiled and interpreted, it became obvious that the 2D approach was the most cost effective and accurate. The principal reason for this was that the identification of individual tree species and measurement of their crowns remained a manual photo-interpretation task. Work is being done at CVRL to automate these tasks within the 3D environment, but it has not yet matured to a useful stage. At present, the 3D reconstructions are computer intensive and time consuming to produce even with automatic, pixel specific, digital elevation models. Tree crown and heights can be easily identified and measured in a 3D "fly-through" image processing environment, but species identification is more problematic at the 40 centimeter per pixel resolution. Also, the manipulation of these models, even at that resolution, is frustratingly slow and difficult with the desktop computers presently available to most photo-interpreters.

However, other work within the NSF project had developed an automated geo-referencing and mosacking program that utilized the Watson gyroscope and laser data to rectify each video frame into an accurate strip of the ground (Zhu et al., in press). This made it practical to construct strip mosaics of the zoom video and delineate hectare size plots of 20 by 500 meters (Figure 5). At a pixel resolution of 4 centimeters, species could easily be identified and each crown fitted with a circle that averaged its diameter (Figure 6). Combined with the laser profile, this produced a simple model of the forest from which dbh values and heights, could be calculated (Figure 7).

For the purposes of this test then, we concentrated our analysis on manually measuring crowns within one-hectare linear strips from the zoomed video coverage, calculating the dbhs and percent canopy coverage for all visible trees within those strips. This was easily accomplished within a 2D GIS environment using the "object edit" program in TNTMIPS (Figure 6). Circles were fitted over each tree as CAD drawings, which preserved the center coordinates and diameter of each circle in the file database. After a first pass to draw the crown diameters, that file was edited for species type in conjunction with the laser data to attach a height value to each tree. Trees not directly measured by the laser were labeled with an average height for the stand, an average emergent height, or average understory height based on their size and shadow cast. The database for these drawings was then exported to Excel, where a dbh value for each tree was calculated from their crown diameters and the regression equations developed in Table 2. Because the circles in the CAD drawings tended to overlap, they were then converted to vector files with contiguous polygons that could be summarized to determine the percent coverage of canopy in each hectare plot.

Unfortunately, several of the plot sites in the Crooksville study were made within very localized stand conditions, which meant that the video strips had to hit them directly or pass within that stand in order to make a valid comparison. Inasmuch as the original GPS coordinates for the plots were not differentially corrected, this was as much a matter of luck as accurate aircraft aiming. The conifer stands were the most difficult, with only a half-hectare captured of one. We do not expect this to be a problem in Bolivia where the plots coordinates are differentially corrected and we will be using real time DGPS with an Ominstar satellite. We were able to analyze and compare 10 video strips, most of which spanned the distance between two sites in a homogeneous community, although the size of the strip had to be reduced in several cases to fit within the stand type. When a strip crossed a road or natural non-forest clearing, the plot was collapsed then reopened on the other side so that only normal or thinned breaks in canopy coverage were included. The average dbh for each strip was then compared to the average dbhs for their corresponding sites.

The results are summarized in Table 3. The video strips are divided by tree type, showing the plot size, number of trees counted and the percent canopy coverage. You will note that canopy cover ranges from a low of 65% in a mature thinned hardwood stand to a high of 92% in an eight year old stand of regenerating trees. This is as we would expect and we anticipate that one of the advantages of using this kind of linear swath through the landscape is that the sample will be a more accurate reflection of the natural and man-made breaks in the canopy than may be captured by a series of 28 meter plots. The number of trees per hectare predicted by these strips is calculated and compared to the number of trees per hectare calculated from the corresponding plot sites. Two sets of columns are presented for both the video strips and the corresponding plot sites. The first column for the video estimates the total number of trees per hectare based on the measured percentage of canopy coverage. The second column estimated that number of based on the assumption of 100% canopy coverage, as would often be the case if the estimate were extrapolated from a single plot site. The first column of plot calculations shows the range of tree estimates for the two plot sites covered by the hectare video strip. These estimates are achieved by multiplying the outer plot count by 16.25 and the inner plot by 201.2, essentially extrapolating the site counts to a hectare sized area. The second column averages those two values after removing the understory of trees less than 7 cm in diameter, which we don't appear to be measuring in the aerial count, but which contribute only a small fraction to the standing biomass. What is striking about these two column sets is the difference between the calculated number of tree between sites that are supposedly within a homogenous stand of vegetation. Given that range of variability it is difficult determine which estimate of tree numbers per hectare is the more accurate, although it appears obvious that the video is undercounting the smaller trees in the 40 year re-growth and the plot site calculations tend to over estimate the percent of canopy coverage.

However, we do have very good correlations between the averages of measured and calculated dbh's for each stand, measurements that are not dependent on the estimation of a larger population from small sites. The last column divides the average measured dbh of the combined ground plot sites by the average calculated dbh of their video strips. A perfect ratio match would be a value of 1, and the admittedly small population of mature hardwoods represented here has a Pearson's sample correlation coefficient of r =.8757, indicating a very strong positive match between the measured and calculated values. We would expect an overestimate the dbhs of trees in the regeneration stands as indicated by sites A11-12 and B27-28, since our equations were developed from a mature population. Given a larger sample base, we could probably develop a correction factor to better characterize that type of stand.

It is difficult to directly compare the plot site values to video strip values when we don't have precise locations for the plots, but a review of size distribution within the mature hardwoods for both video strips and sites, indicates that we appear to be missing the smallest trees and overestimating the sizes of the medium size trees, but that this is somewhat canceled out by a consistent underestimate of the largest trees. These are also adjustments that could be corrected for in a larger ground sample population. Flying over the Noel Kempff Mercado expansion zone was completed in April of 1999, using progressive scan DV digital video. We had precise differentially corrected locations for most of the 635 plot sites and are confident of hitting at least 400 sites with sufficient accuracy to image the plot in the zoom. Crown diameters were not measured in the original plots established by Winrock, but we expect to develop regression equations directly from our analysis of the site images by identifying the major trees, or correlating the total structure of the 28-meter diameter of the trees to the site biomass values.

Table 3 Summary of measurements and dbh calculations for plot sites and video strips.

Forest Stand type with video strips used for interpretation	Size of video strips in Hectares	Number of trees counted in strips	% canopy coverage of strip	Calculated # of trees per hectare from video adjusted to canopy coverage	Calculated # of trees per hectare from video asuming 100% canopy coverage	Range of Calculated # of trees from plots includes >7 cm. dbh trees	Calculated # of trees per hectare from plots with trees >7 cm. dbh removed	Ratio of dbhs averages, sites divided by strips *
White Pine								
site B18-19	0.599776	151	70%	252	360	260-524	398	1.034229
Regeneration Hardwoods								
site_A11_A12	0.29864	361	92%	1209	1314	398-1591	975	0.452874
site B27_B28	0.40029	453	74%	1132	1529	1283-2586	1755	0.633954
Natural Hardwoods								
site A3-A4	1.000024	475	80%	475	594	329-1652	584	0.94121
40 year planting of Hardwoods								
site B25_B26	1.00018	659	82%	659	804	1234-1981	1194	1.102431
site_A10_A9	1.001	323	85%	323	380	788-1137	840	1.04557
site B21_B22	1	403	79%	403	510	739-1202	952	0.998811
site_A8	0.7035	158	68%	225	330	443	438	0.974026
Thinned Hardwoods								
site_A7	0.4001	129	65%	322	496	426	422	1.098875
site_A1-A2	0.9479	453	72%	478	664	475-1104	480	1.021324
						Average ratio of Mature Hardwoods, Natural, planted and thinned =		1.026035286
						Average deviation from mean =		0.048
						Pearson's Sample Correlation Coefficent r =		0.8757

* In order to compare the different approaches to calculating DBH (Diameter at Breast Height), the DBH measurements for the plots associated with each strip were combined and averaged. Trees with less than 7 cm diameter were considered understory and not included in the average. That combined averag was divided by the average of the DBHs calculated from crown diameter regression equations for each video strip. A perfect ratio match would be a value c

CONCLUSIONS

This paper reviews the results of a feasibility study to determine the usefulness of GPS-logged aerial sampling in calculating standing biomass in forests. Although based on a small sample set, it demonstrates that a positive correlation can be drawn between crown diameters in a temperate forest and their corresponding dbh measurements, and that these crowns can be measured from large-scale video mosaics of the canopy. At present this is a manual process in a GIS system, but work is proceeding on a program that will automate the process in a 3D environment. We are also adapting the Terrest automated terrain reconstruction program to work with digital video data, which may prove to be the best adaptation of both techniques. Approximately 20 hours of digital video was recently collected over the Noel Kempff Mercado expansion zone in northeastern Bolivia. Over the next year, we will be comparing this data to the series of 635 site plots established by the Noel Kempff Mercado Climate Action Project, and will be able to make a more precise determination of the extent to which the standing biomass in tropical forests can be successfully predicted from large scale aerial video.

ACKNOWLEDGEMENTS

This work is partially supported by National Science Foundation (NSF) under grant number EIA-9726401, and the National Fish and Wildlife Foundation (NFWF) under Agreement #98089. The Winrock Corporation, under contract to The Nature Conservancy, also provided additional funding, and American Electric Power provided assistance and support personnel for the collection of plot data.

REFERENCES

Brown, S., and A.J.R. Lugo (1984) Biomass of tropical forests: a new estimate based on forest volumes. *Science* 223:1290-1293.

Brown, S., A.J.R. Gillespie, and A.E. Lugo. (1989) Biomass estimation methods for tropical forests with applications to forest inventory data. *Forest Science* 35(4):881-902,

Chadwick, N.L., D.R. Progulske and J.T. Finn. (1986.) Effect of fuelwood cutting on birds in Massachusetts hardwood forests. *Journal of Wildlife Management* **50**:398-405.

Crow T.R. (1978) Common regressions to estimate tree biomass in tropical stands. *Forest Science* 24:110-114.

Schriever, J.R. and R.G. Congalton. (1995) Evaluating seasonal variability as an aid to cover-type mapping from Landsat Thematic Mapper data in the Northeast. *Photogrammetric Engineering and Remote Sensing* 61(3):321-327.

Short, H.L. and Hestbeck, J.B. (1995) "National biotic resource inventories and gap analysis". *BioScience* 45 (8) : 535-539.

Slaymaker, D.M., K.M.L. Jones, C.R. Griffin and J.T. Finn. (1996) Mapping deciduous forests in Southern New England using aerial videography and hyperclustered multi-temporal Landsat TM imagery. Pages 87-101 in *Gap Analysis: A Landscape Approach to Biodiversity Pla*nning, J.M. Scott, T.H. Tear and F.W. Davis (eds). American Society of Photogrammetry and Remote Sensing, Bethesda, MD, USA.

Slaymaker, D.M. and Hannah L. (1997) GPS-logged Aerial Video as a Geo-referencing Tool For Digital Imagery in Remote Regions, a case study in Madagascar, *Proceedings of the 16th. Biennial workshop on Color Photography and Videography in Resource Assessment*,

Spanner, M.A., L.L. Pierce, D.L. Petersen, and S.W. Running. (1990) Remote sensing of temperate coniferous forest leaf area index: The influence of canopy closure, understory vegetation and background reflectance. *International Journal of Remote Sensing* 11(1):95-111.

Tritton, L.M. and Hornbeck, J.W (1982)., "Biomass equations for major tree species of the Northeast", *USDA Forest Service Gen. Tech. Report, NE-69*, p. 46,

Zhu Z., E. M. Riseman, A. R. Hanson, H. Schultz, D. Slaymaker (1999) Automatic Geo-Corrected Video Mosaics for Environmental Monitoring (reference?)

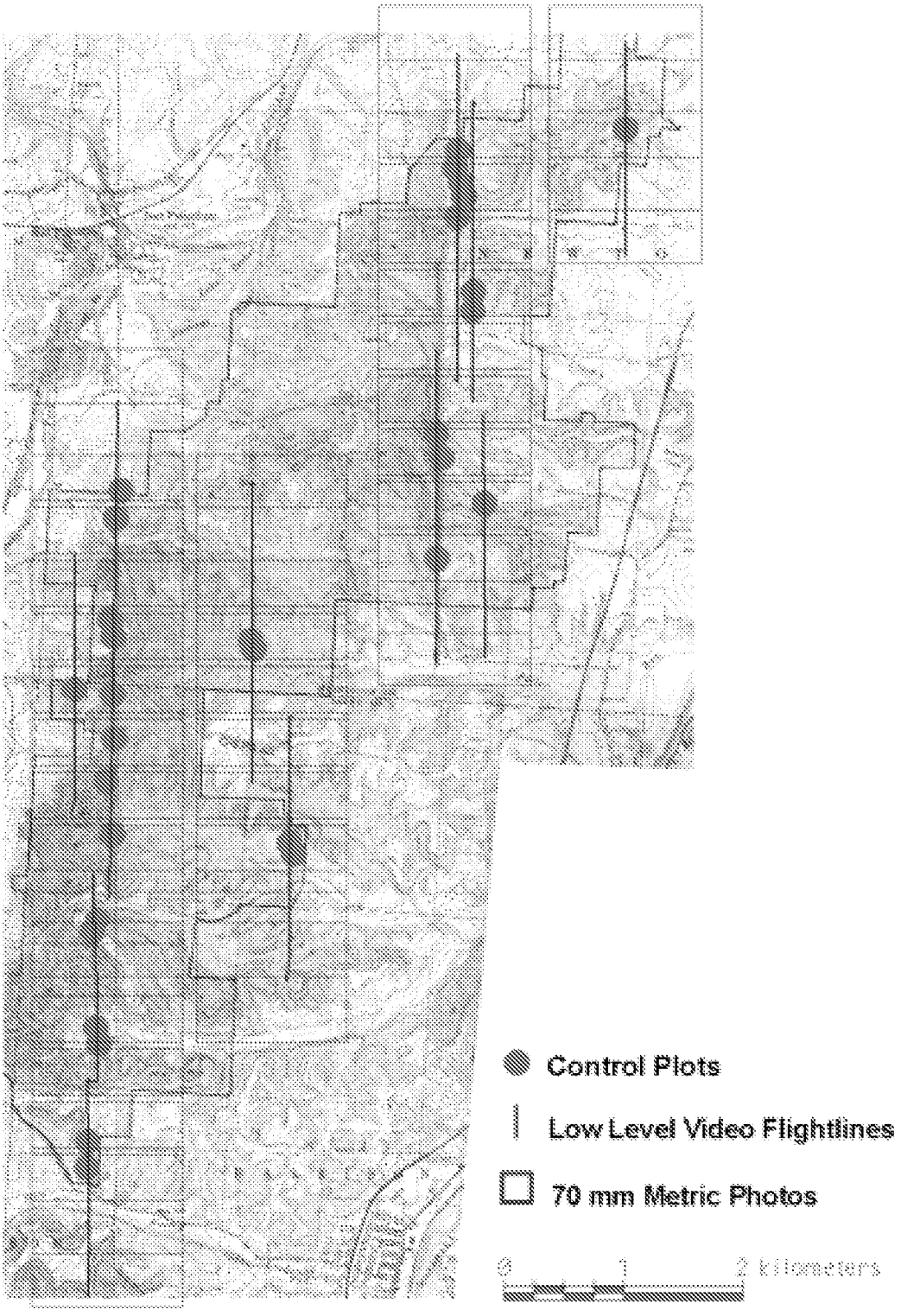


Figure 1 Plot sites and flight lines for Crooksville test.

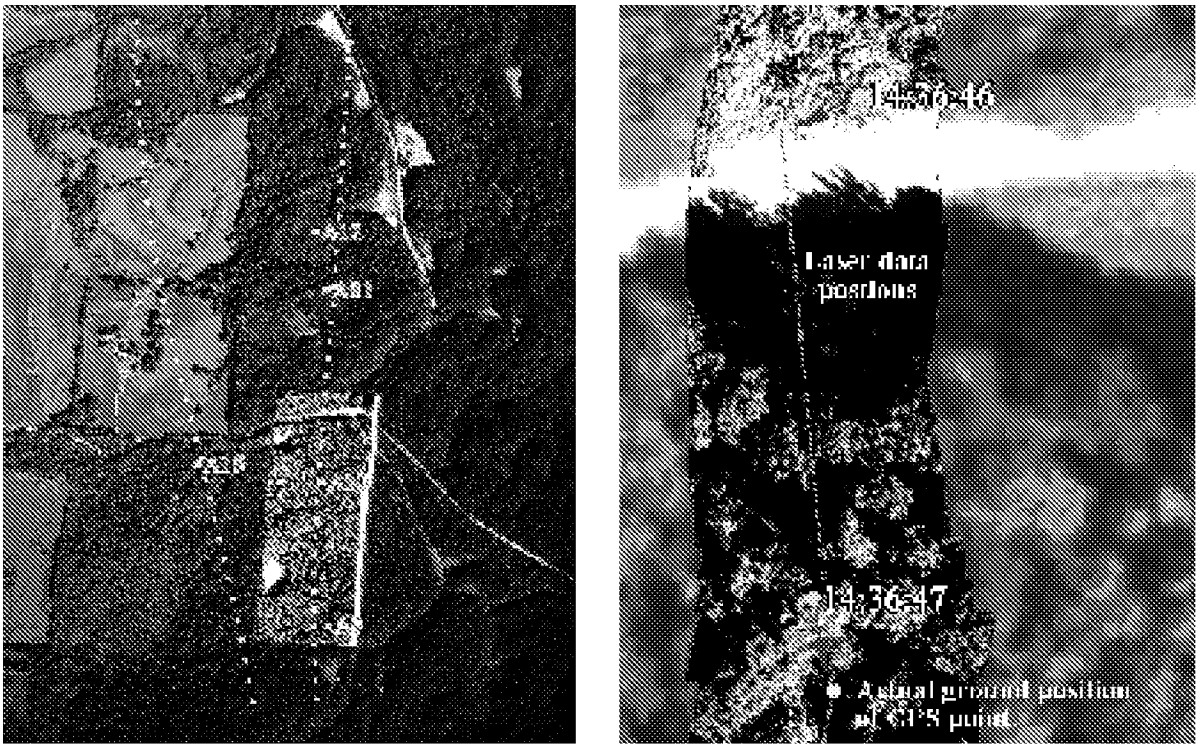


Figure 2. Wide-angle video mosaic superimposed on the 70 mm photographs, with detail showing the zoomed video mosaic. The ground coordinates of each GPS logged position are calculated from the orientation of the digital gyroscope.

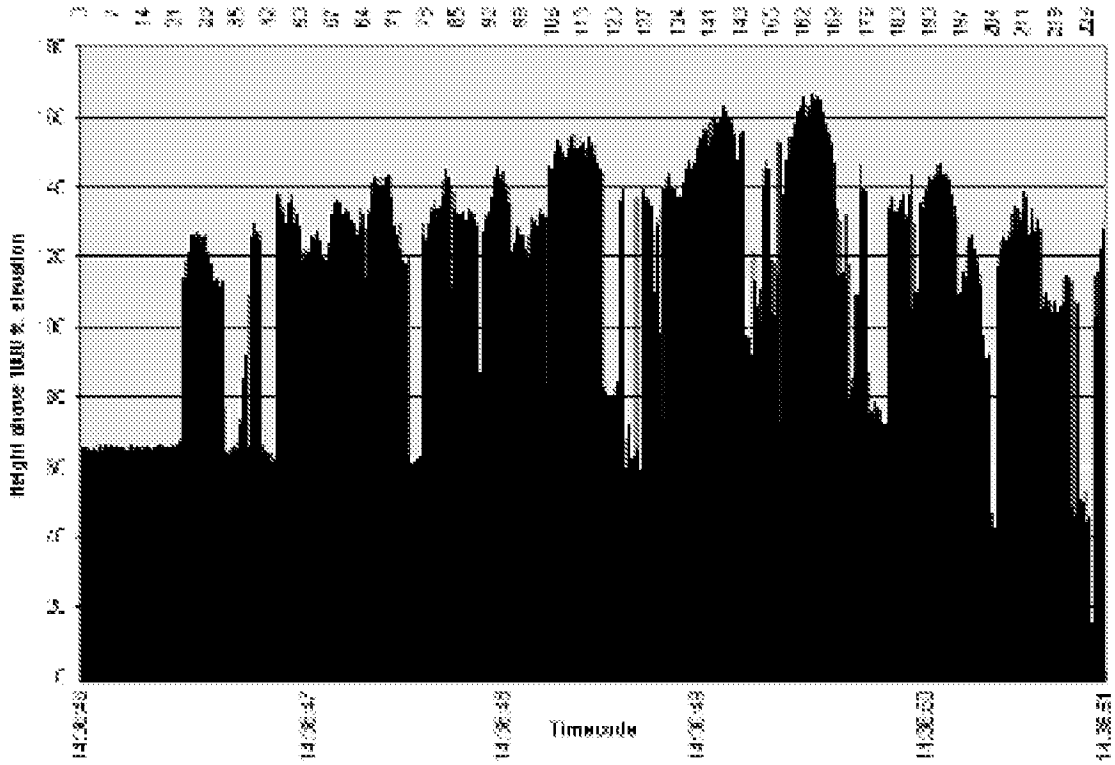


Figure 3. Laser profile of the video strip showing tree height in the stand.

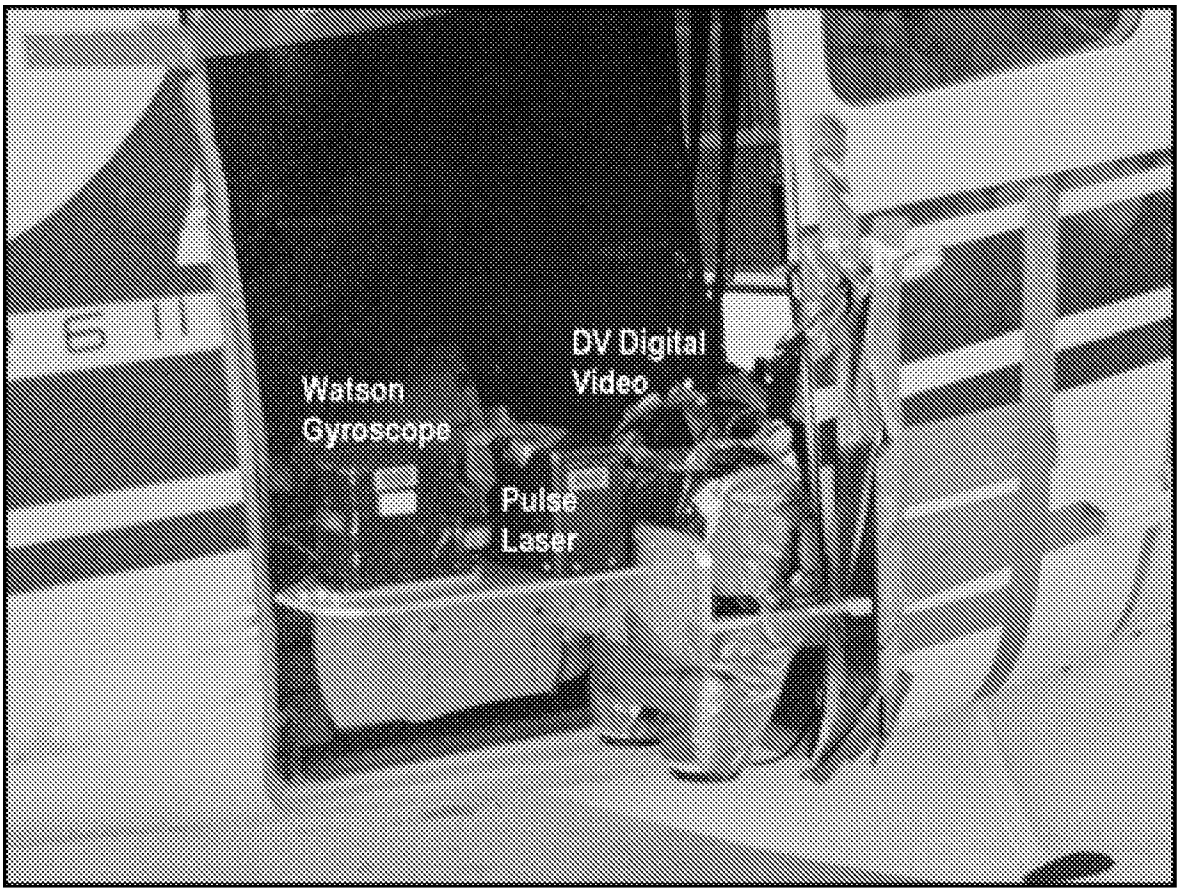


Figure 4 Camera system mounted out the side of a Cessna 206 in Bolivia. An airfoil has been attached to the forward door of the cargo bay to protect the cameras from the airstream.

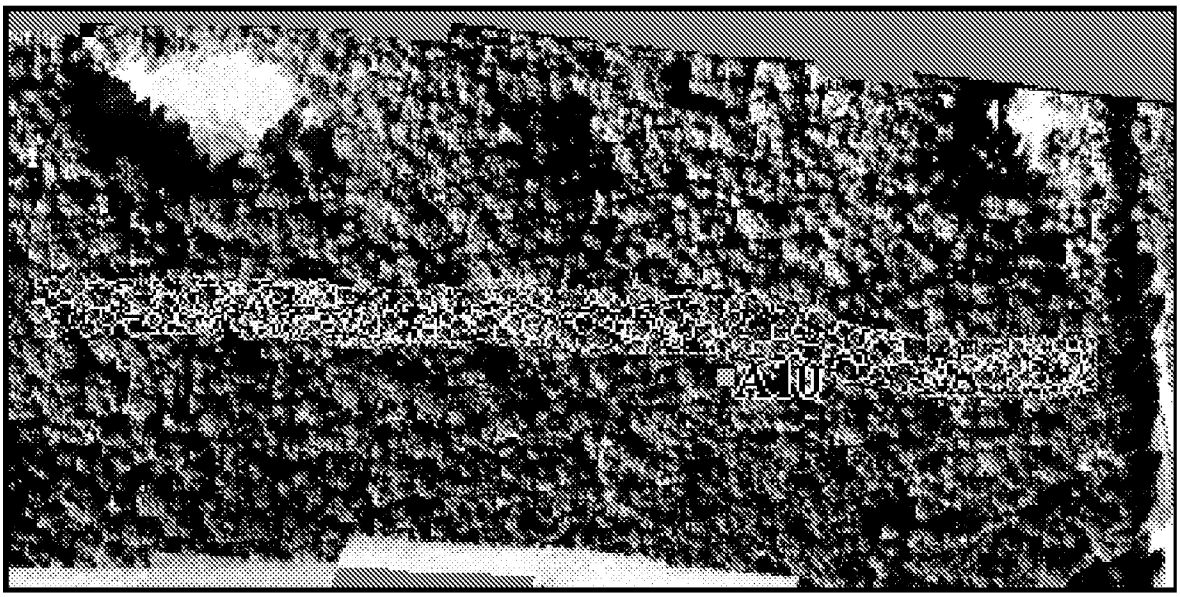


Figure 5. Zoomed video mosaic overlaid on wide angle mosaic with a one-hectare size strip plot. Crown diameters were measured by fitting circles over them in a GIS program.

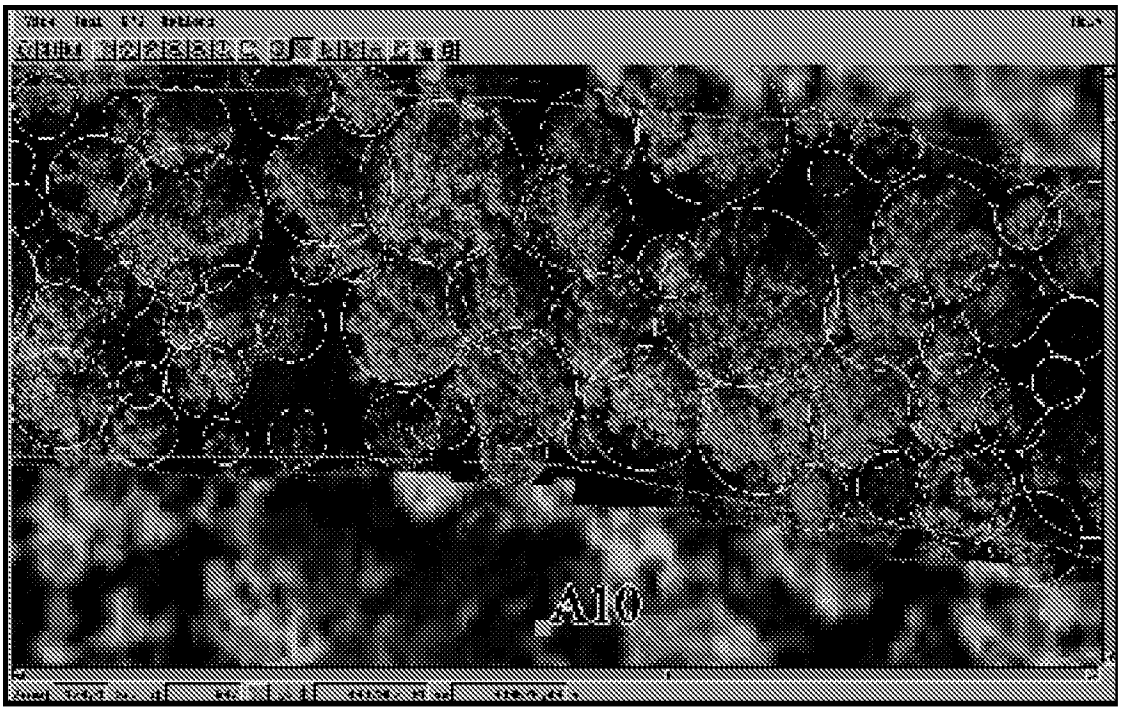


Figure 6. The detail and color discrimination of the zoomed video mosaics proved to be a greater advantage than the 3D modeling of a lower resolution surface. Draping the video strip over the terrain model combines the best features of both, but is a slow process most useful as a training tool.

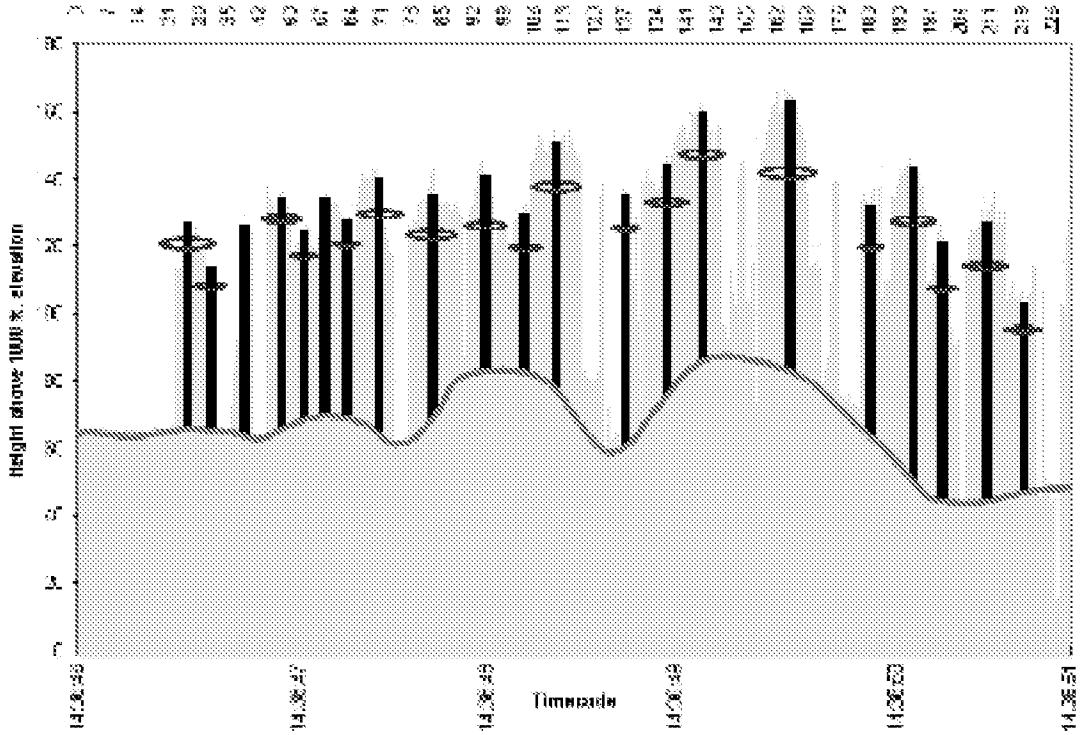
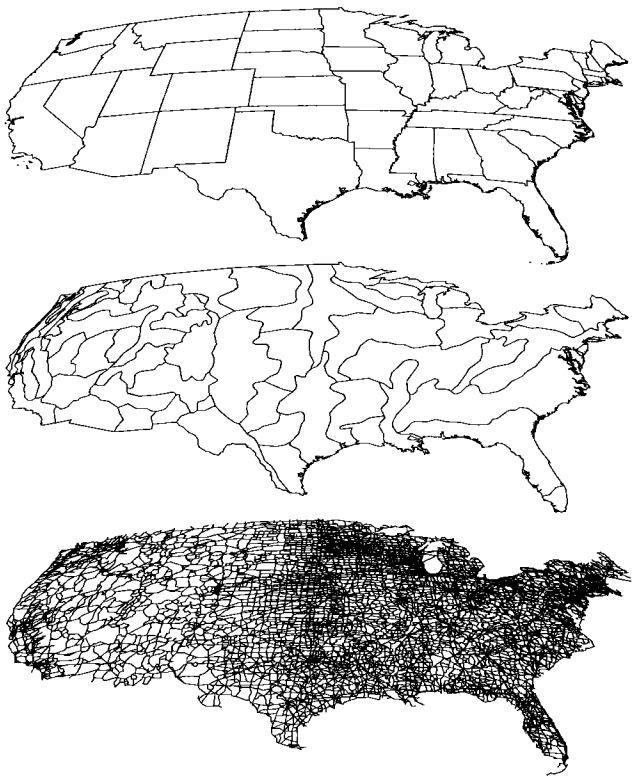


Figure 7. Combining these circles with the laser profiling data reduces the forest to a simple model of poles with height and diamete

Gap Analysis

A Landscape Approach to Biodiversity Planning



Edited by

J. Michael Scott
Timothy H. Tear
Frank W. Davis

Copyright © 1996 by the American Society for Photogrammetry and Remote Sensing. All rights reserved. Reproductions of this volume or any parts thereof (excluding short quotations for use in the preparation of reviews and technical and scientific papers) may be made only after obtaining the specific approval of the publishers. The publishers are not responsible for any opinions or statements made in the technical papers.

Permission to Photocopy: The copyright owners hereby give consent that copies of this book, or parts thereof, may be made for personal or internal use, or for the personal or internal use of specific clients. This consent is given on the condition, however, that the copier pay the stated copy fee of $2 for each copy, plus 10 cents per page copied (prices subject to change without notice), through the Copyright Clearance Center, Inc. 222 Rosewood Drive, Danvers, MA 01923, for copying beyond that permitted by Sections 107 or 108 of the U.S. Copyright Law. This consent does not extend to other kinds of copying, such as copying for general distribution, for advertising or promotional purposes, for creating new collective works, or for resale.

Then making reporting copies from this volume to the Copyright Clearance Center, Inc., please refer to the following code: **ISBN-1-57083-03603**.

Published by
American Society for Photogrammetry and Remote Sensing
5410 Grosvenor Lane, Suite 210
Bethesda, Maryland 20814-2160

Printed in the United States of America

MAPPING DECIDUOUS FORESTS IN SOUTHERN NEW ENGLAND USING AERIAL VIDEOGRAPHY AND HYPERCLUSTERED MULTI-TEMPORAL LANDSAT TM IMAGERY

Dana M. Slaymaker, Katharine M. L. Jones, Curtice R. Griffin and John T. Finn
Department of Forestry and Wildlife Management
University of Massachusetts
Amherst, MA 01003

Introduction

Obtaining sufficient geographically unbiased verification and validation data on vegetative communities is one of the greatest challenges in developing base land cover maps for Gap Analysis Projects. These data are essential for classifying the Landsat Thematic Mapper (TM) imagery used in all Gap Analysis Projects and for assessing the accuracy of vegetation maps developed. Airborne video data systems that tag each frame with geographic coordinates from a global positioning system (GPS), in combination with interpretation and ground-truthing procedures, provide a cost- and time-effective method for obtaining data on vegetative communities over large geographic areas (Graham 1993). The Gap Analysis Program in New England is using this video technology in conjunction with the hyperclustered, multi-temporal Landsat TM imagery distributed through the Multi-Resolution Land Characteristics (MRLC; Benjamin et al. this volume) program (http://geo.arc.nasa.gov/usgs/MRLCStart) to produce a vegetation map of southern New England. To test the feasibility of this approach, we conducted a pilot project on one Landsat image, mapping the vegetation type we had found most difficult to discriminate: deciduous forests. This paper discusses the results of that study and our development of an efficient mechanism for relabeling the spectral classes in the hyperclustered classification to successfully map deciduous forests at the Anderson III and IV levels (Anderson et al. 1976).

Mapping the forests of southern New England poses a variety of problems that make it an excellent test of the new multi-temporal hyperclustered imagery. The landscape is 50% to 95% forested with a wide variety of forest types occurring in relatively small stands interspersed throughout the region. Furthermore, this dispersion does not follow readily discernible rules. While most vegetation types in the United States have developed along natural limits and can often be modeled with respect to variations in elevation and terrain, the chief determiner of species distribution within the major forest regions of New England is historic human activity. Over 80% of Massachusetts was agriculture in the 1800's and has since been replanted or regrown to forest. The resulting landscape is an intricate mosaic of different forest communities arranged in a whimsical fashion. In addition, the initial unsupervised classifications we produced from traditional single season Landsat TM coverage showed poor discrimination of our forest types. Most forest types were composed of mixtures of spectral classes. Few spectral classes represented more than 15-30% of any one deciduous forest type and most deciduous forest types contained most spectral classes to some degree.

This spectral mixing is the essential problem of any Gap Project trying to regroup spectral classes into vegetation classes. They are fundamentally different kinds of categories, one based on the reflectance of energy and the other on human perceptions of what constitutes a community of plants. Therefore, the correspondence between them is rarely clear or straightforward, and must be modeled from a known sample set of both. The hyperclustered TM Landsat imagery represents a considerable improvement in the discrimination of spectral classes, with 240 categories generated by a robust algorithm (Kelly and White 1994). However, this large number of categories exacerbates their mixing and increases the complexity of regrouping them into information classes. We addressed this problem through the introduction of spatial context into the relabeling process, adjusting the informa-

tion class assignment of a particular pixel based on its terrain and neighborhood associations as well as its spectral class. We developed a systematic "cookbook" approach for identifying these associations and utilizing them in a set of hierarchical and sequential decision rules. While this pilot project was restricted to forest classes on one Landsat scene, the methodology will be used throughout New England and has wide application for other Gap Projects utilizing either the hyperclustered data or standard unsupervised classifications of satellite imagery. The process is driven by a large number of GPS referenced point samples that can be efficiently extracted from the video. The decision rules are computer intensive, but easily generated from USGS digital elevation models and pixel frequency tables produced on a spreadsheet. Furthermore, accuracy assessment is built into the approach with a stratified random subsample of the sample points excluded from use in the modeling and set aside for verification.

Methodology

Our study area is in southern New England, encompassing portions of three states (Massachusetts, Connecticut, and Rhode Island), and is characterized by several forest regions ranging from Northern Hardwoods-Spruce to Central Hardwoods (Color Figure #3).

Landsat TM scene 1331 delineates the study area and covers 31,000 km^2 (Color Figure #4). This scene was chosen because it was in the center of our region, and most New England forest types identified by the Society of American Foresters (SAF) (Eyre 1980) are represented within its coverage. The 12-band hyperclustered data combined spring (1992) and fall (1992) coverages and we assumed that the varying seasonal phenologies of the different tree species in the region would enhance identification of the forest types. It is well established that some native tree species can be more easily distinguished from each other in different seasons (Ahlgren 1957; Sayn-Wittgenstein 1978; Eder 1989), and this has been applied to interpreting satellite imagery (Beaubein 1979; Schriever and Congalton 1995). Multi-temporal classifications of Landsat data from different seasons have also improved the discrimination of forest classes (Wolter et al. 1995). Merging of the two seasons of imagery was done by the EROS Data Center as was the application of the hyperclustering algorithm. All reflective bands from both scenes were processed together to produce the 240 cluster classification.

Ground reference of vegetation cover was obtained from a grid of large scale GPS-logged videography flown over the study area to collect a distributed sample of the landscape (Color Figure #5). This type of aerial point sampling survey was originally developed by Norton-Griffiths et al. (1982) in East Africa. They logged geographic positions from an OMEGA/VLF navigation system onto large-scale vertical 35mm photography flown in a systematic grid. They then tabulated ground cover estimates from those images and entered those data into a GIS for analysis.

Dunford et al. (1983) applied Norton-Griffiths' approach to the interpretation of Landsat MSS (Multispectral Scanner) data, producing a vegetation map of the Arusha region in Tanzania. The Arizona Gap Analysis Project substituted a continuous swath of video for the 35 mm format (Graham 1993), flying a 30 km wide grid pattern of the state to interpret their Landsat TM coverage. Their Super-VHS camera covered 0.5 km at wide angle and zoomed once every 10 seconds to 15x magnification to collect a point sample image 30 m wide. GPS positioning data were collected during each flight and linked to corresponding Society for Motion Picture and Television Engineers (SMPTE) time code recorded on the audio track of the video tape. Our approach was based on the Arizona Gap Analysis Project, but differed from it in some aspects. Because of the greater complexity of our landscape, we flew much denser transects (15 km separation) in the spring and fall of 1994 to capture both phenologies. Approximately 1500 km of transects were flown for each season at an altitude of 600 m. Spring flight (late May) transects were flown along north-south lines; fall flight (October) transects along east-west lines (Color Figure #5). (Videography was also collected for the rest of New England in a 20 km grid pattern in spring and fall 1994.)

Modifying the system described by Graham (1993), our video data acquisition system consisted of a camera mount, two Hi8 band video cameras, two video recorders, a GPS unit, a laptop computer, a Horita time code generator with an additional time code reader, a video monitor, and associated software (Color Figure #6). Lacking access to a plane with a camera port, we developed a portable camera mount that could be operated from any highwing Cessna aircraft. The camera mount is kept inside the plane during take-offs and landings and extends out the window only when imagery is being collected. At the start of a flight line, the mount is clamped to the open window. Then the camera unit is cranked out and adjusted to vertical with a bubble level. Because the mount does not require modification of the aircraft and is not a permanent installation, we have not sought FAA approval. A Plexiglas airfoil is also attached to the leading edge of the aircraft window to reduce noise and wind in the cockpit and provide added protection for the camera unit. The video cameras are mounted beside each other. One is set at wide angle, the other at 12X zoom, providing a swath of 30 m wide large scale imagery down the middle of 0.4 km wide angle coverage when flying 600 m above ground level (Color Figure #7). This approach provided much more flexibility in both the selection and density of our sample points. Geographic position data were recorded from the GPS unit to the laptop computer using Geolink software. Time code was "sipped" from the GPS data stream by a Horita GPS time code generator to provide a matching SMPTE time code to the VCRs (R. Pargee, Horita, Inc., personal communication). SMPTE time code is the standard audible timing signal recorded to the audio track of video. Horita's time code generator substitutes GPS time for the normal internally generated signal, allowing each frame to be matched to a geographic position. We recorded the time code directly onto the video images, as well as the audio track, to simplify the synchronization of the two tapes during playback.

Data Analysis

Data analysis followed a three-tier point sampling methodology developed by Norton-Griffiths (1988):

1. Primary sample: the wide-angle video coverage (4.6% of the total study area covered by TM 1331).

2. Secondary sample: those frame sets within the wide angle video coverage that were located on the hyperclustered image and interpreted with the zoomed images to select sample point coordinates.

3. Tertiary sample: the attribute sets of specific pixel locations selected from the hyperclustered image; 1.6% of the pixels in the primary sample and 0.06% of the total pixel population of the image.

Organizing the samples in this manner delineates the data analysis at each level. The photo-interpretation of the secondary sample is a heuristic process. That is, it is based on expert knowledge which is acquired by interpreting the photographs and evaluating the results, but cannot be easily explained or transferred without reproducing the experience of the interpretation. By contrast, the tertiary attributes are correlated by a systematic series of sortings and cross-tabulations. It can be done in a "cookbook" fashion to generate sets of inference rules for the associations between spectral classes that are inherent in the data. However, the testing and refinement of those rules requires an active and repeated interaction with both the primary and secondary samples on the heuristic level of evaluating and testing results. Because the tertiary sample represents only a small subset of the other two, they remain additional sources of data for testing and interpretation.

Photo-Interpretation

Our overall strategy of interpretation also followed a methodology developed by Norton-Griffiths (1988), which was designed to obtain consistent and reliable results within a specific project by training photo-interpreters together with the data from their project. First, we de-

lineated our vegetation classes for deciduous forest types and selected frames from the video that were: 1) representative of each forest type, and 2) near a road or other landmark that would enable us to precisely locate the frame in the field. We then extracted the approximate coordinates of those frames from the GPS data, made prints of them using a video printer, and field checked them with the photo-interpreters. Using the results of those site visits, we created a visual key of forest types from the prints and trained on them until each photo-interpreter could consistently identify each type on the video. Although we used traditional source material on the recognition of tree species on aerial photographs (e.g., Sayn-Wittgenstein 1978), the core of the procedure is to achieve a consensus between the interpreters about the appearance of each tree species in the closed set of a specific season, scale and recording medium, and to verify the correctness and consistency of the classification through time and across different photo-interpreters.

We developed our forest type labels from the vegetation classification system defined for the region by the Society of American Foresters (SAF), because all habitat models being used in subsequent steps in our Southern New England Gap Analysis are linked to the SAF classification system via the wildlife habitat models of DeGraaf and Rudis (1986). We selected 104 training sites from the spring videography for field examination. Ninety percent of the sites were in the northwest quadrant of the Landsat scene. We anticipated the most variability in forest species in this quadrant because it encompasses the boundaries of all four regional vegetation types found in the study area: Northern Hardwoods-Spruce, Northern Hardwoods, Transitional Hardwoods-White Pine, Central Hardwoods-White Pine, and Hemlock (Color Figures 3 and 4). Given time and funding constraints, we expected to maximize our field efforts by choosing sites in this area. Eighty-seven sites were visited and, by the end of this ground truthing phase, we were confident in identifying the 17 SAF forest types present on the video coverage. During interpretation, however, we found that these forest types mixed into a variety of combinations across the landscape, forming vegetation communities at the alliance level (Anderson level IV), that were identifiable in the hyperclustered image. Therefore we developed additional forest classes with varying dominance and percentages of each member, and multiple member combinations to take full advantage of potential spectral distinctions. As the video interpretation progressed, we subtracted classes we could not find on the video, and added new ones we discovered. We also deleted or combined classes that still lacked spectral distinction in the hyperclustered data. At the completion of this stage, our classification consisted of seven major classes at Anderson level III, encompassing most of our SAF forest types, and 30 subclasses at Anderson level IV, mostly specific alliances among species or mixtures of level III classes (Table 1). It should be noted that these are specifically forest classes. The non-forest and wetland classes are included primarily to delineate those vegetation coverages from the forest types and reserve them for further discrimination. Therefore, they are somewhat arbitrary at this stage in our analysis.

Our video data interpretation system consisted of two Hi8 band video cassette recorders and two monitors with S-VHS cable inputs. A crosshair and frame were drawn on the center of the wide angle monitor, indicating the center point and corresponding field of view of the zoomed image. A second frame, the size of a 25-pixel block, was drawn around the first frame. We discovered that it was important that the photo-interpreter and the image classifying program work at the same scale. Because the inference rules drew spatial context data from a 5 x 5 neighborhood block to relabel the pixel values, this represented the minimum size block of a community we could sample from (about one third of the wide angle image). Correspondingly, we selected this block size as the best neighborhood context for our rules through our preliminary examination of forest type structure on the video. The two tapes were manually synchronized during interpretation. The video frames were matched to each other and their geographic positions using the time code imprinted on the video tape during flight. This process eliminated the need for the additional Horita time code generators used by Graham (1993).

Table 1. Classification system at Anderson levels III and IV used in the study area.

A. N. Hardwoods (Sugar Maple dominant)

Subclass 01 =	N. Hardwoods, Sugar maple dominant with Beech, Ash and/or Birch
Subclass 02 =	N. Hardwoods with up to 20% White Pine
Subclass 03 =	N. Hardwoods with up to 20% Red Oak
Subclass 04 =	N. Hardwoods Red Oak mixture with up to 20% White Pine

B. Red Maple, Red Maple dominant communities

Subclass 05 =	Hardwoods, Red Maple dominant
Subclass 06 =	Red Maple, with up to 20% Red Oak and/or Birch

C. Northern Red Oak, Oak dominant communities

Subclass 07 =	Red Oak dominant Oak mixture
Subclass 08 =	Oak dominant N. Hardwood and/or Red Maple mixture with Birch
Subclass 09 =	Oak dominant Birch mixture with N. Hardwood and/or Red Maple
Subclass 10 =	Oak dominant N. Hardwood and/or Red Maple mixture with Birch and up to 20% White Pine

D. Birch, Birch dominant communities

Subclass 11 =	Birch dominant with Red Oak and Maples
Subclass 12 =	Black Birch dominant birch mixtures
Subclass 13 =	Birch dominant Aspen mixture
Subclass 14 =	Birch dominant N. Hardwood and Red Oak mixture

E. Oak/Maple/Birch co-dominant communities

Subclass 15 =	N. Hardwoods 60%, Red Oax mixture 40%
Subclass 16 =	Red Oak, 60%, N. Hardwood and/or Red Maple mixture 40%
Subclass 17 =	Red Maples 60%, Red Oak, mixture 40%
Subclass 18 =	N. Hardwood and/or Red Maple, Red Oak, Biirch mixture
Subclass 19 =	N. Hardwood and/or Red Maple, Red Oak, mixture with up to 20% White Pine

F. Maple/Oak/Conifer co-dominant communities

Subclass 20 =	Red Oak 60%, White Pine mixture 40% with Maples
Subclass 21 =	White Pine 60%, Red Oak Mixture 40% with Maples
Subclass 22 =	N. Hardwoods 60%, White Pine 40% with Beech, Ash, and/or Birch
Subclass 23 =	Mix Conifers 60%, N. Hardwoods and/or Red Maple and/or Red Oak mixture 40%
Subclass 24 =	White Pine and/or Hemlock 60%, Maple mixture with Beech and/or Biirch 40%

G. Conifer

Subclass 25 =	White Pine stands
Subclass 26 =	Hemlock stands
Subclass 27 =	Mixed Conifer stands
Subclass 28 =	White Pine, 80%, N. Hardwood and/or Red Maple and/or Red Oak mixture 20%
Subclass 29 =	Hemlock 80%, N. Hardwood and/or Red Maple and/or Red Oak mixture 20%
Subclass 30 =	Mixed Conifer 80%, N. Hardwood, and/or Red Maple and/or Red Oax mixture 20%

H. Wetlands

Subclass 31 =	Marsh
Subclass 32 -=	Marsh with dead trees
Subclass 33 =	Scrub or shrub Marsh
Subclass 34 =	Mixed Deciduous/Conifer Marsh
Subclass 35 =	Forested Wetland - Conifer
Subclass 36 =	Forested Wetland - Deciduous

I. Nonforest

Subclass 37 =	Cleared land or industrial use, possibly in wetlands
Subclass 38 =	Pasture, sparce suburban lawns
Subclass 39 =	Suburban forest mixtures
Subclass 40 =	Golf courses or lush suburban lawns
Subclass 41 =	Cleared ground or old clear cut

Extracting and calculating the exact positions of specific video frames, as reported by Graham (1993), was unnecessary in our approach because we interpreted the video frames while using a third monitor to view their corresponding locations on the hyperclustered image. We had originally planned to follow Graham's (1993) approach of using the geographic positions tagged to each video frame as our sample point coordinates, playing the audio track back through the Horita time code generators and logging the selected sites using the Horita program PC-log. However, the GPS receiver records the plane's position in space rather than the projected image center on the ground, and any tip or tilt movement of the camera reduces the accuracy of the corresponding video frame's location. Before undertaking our survey, we conducted a test flight of video over identifiable targets, then walked to the indicated photocenters of selected frames and logged their GPS positions on the ground. When the aircraft and ground positions were differentially corrected and compared, it was apparent that variations in the plane and/or camera position could introduce positional errors of up to 70 m. Therefore, we would have had to assume a 5-pixel diameter of confusion on the hyperclustered image for the position of video frame photocenters in relation to the GPS points. This was too great an error for most of the forest mosaic structure in our region. We had also found location errors in the reprojection of selected PC-log points to a GIS vector layer, and once introduced in this fashion, these errors were difficult to detect.

Therefore, we avoided the potential error and inherent inaccuracy of time code logging, by simply setting our video monitors down beside our computer monitor and selecting sample points directly from the hyperclustered image. We converted our differentially corrected GPS data to ASCII files and overlaid all the one-second interval record points onto the hyperclustered image in the MIPSTNT (Microimages, Inc.) image processing program (Color Figure #8). This allowed us to match video frames to their corresponding positions on the Landsat screen by time code and directly query the spectral class values and geographic coordinates of individual pixels in the hyperclustered image. Using visual pattern recognition, we could orient ourselves between the wide angle video and the hyperclustered image, and accurately select sample points from identifiable communities. Also, because we were selecting sample positions directly from the hyperclustered image, we were able to document and monitor our point accuracy to within a nine-pixel block. In areas where we could not locate a video frame's position more accurately by pattern than by its corresponding GPS point, or identify specific pixels, we used the GPS-logged position, but restricted sampling to a surrounding community of at least a 10 x 10 pixel block, avoiding any error introduced by camera tip and tilt.

Two photo-interpreters examined 25 hours of video and collected 17,836 sample points, from approximately 2,300 locations, either as individual pixels or clusters of pixels. This process was most efficiently accomplished by adding the sample points directly to the GPS data file by editing it in the MIPSTNT "edit-vect" mode. Clicking on any GPS point displayed its date and time code, under "view-points", while clicking on a hyperclustered pixel under "add-points" displayed a set of data fields with the UTM coordinates of the pixel and an empty Z coordinate column space. The interpreted forest type was typed into the Z coordinate space and the new point set added to the database. This process took only seconds per point, and the sample point files were easily extracted from the data file after interpretation, because all the original GPS logged points have zero Z coordinate values in their internal table. Twenty-five percent of these points (4,459 samples) were set aside as a stratified random subsample for later accuracy assessment of our final map. This random subsample was selected using Microsoft Excel after the points had been sorted by forest type. Each point in a forest type set had a random number attached to it, which were then sorted in ascending order. The first quarter of the attached points are set aside. The remainder of the points for each forest type were exported as site files into the GIS program GRASS, a public domain GIS supported by the U.S. Army Construction Engineering Research Laboratories (USACERL) and used to formulate the rules. GRASS was used at this stage because of its excellent sample point analysis program (s.menu) and inference rules framework (r.infer).

The accuracy of this video analysis, and therefore the subsequent classification, is a function of the interpreter's ability to recognize individual tree species on the video frames and translate their distribution into a community class. Considering our wide angle coverage had an approximate resolution of one meter, it was adequate for only color and texture recognition. Our actual species identification was done on the strip of zoomed imagery through the center of the wide angle swath, which had a resolution of approximately 8 cm. Tree identifications were relatively simple at this scale and could be extrapolated to the surrounding patterns on the wide angle coverage to identify communities. Video frames that we verified in the field while the point sample collection was in process, yielded a high percentage of correct predictions by the photo-interpreters who were well into the learning curve. Therefore, we believe this method to have been adequate for our needs and resources.

Sample Analysis and Inference Rules

The essential problem in reassigning the pixels belonging to each spectral class in the hyperclustered image to a forest class, was designing a relabeling procedure that considered the mixture of spectral signatures associated with each forest type when it determines the most probable identity of each pixel. The need to model information classes as probabilistic mixtures of spectral classes is well established in the remote sensing literature (Jensen 1986), as are algorithms for exploiting these associations within a Gaussian model (Strahler 1980; Bouman and Shapiro 1992). Mapping deciduous forests in Wisconsin, Bolstad and Lillesand (1992) incorporated rule-based probabilities from ancillary soil and terrain data "along with knowledge of the relationships between tree species or species groups" into an unsupervised maximum likelihood classification of Landsat TM data. Their results showed a significant improvement over the same classification without pixel-specific prior probabilities. We did not wish to use soil data in our methodology because of its limited availability in a digitized format, but knowledge of the relationships between tree species and species groups is implicit in the photo-interpretation of forest types. Therefore, it can be incorporated into the relabeling of spectral classes if that knowledge can be expressed as a function of the immediate neighborhood of each pixel. However, in spite of the appearance of a multi-band image set in these hyperclusters, based on overall brightness assignments of the gray scale, the classes remain non-parametric, requiring a non-Gaussian analysis (Hutchinson 1982). Richards et al. (1982) presented a methodology for regrouping a non-Gaussian unsupervised classification to information classes by incorporating neighborhood values into a probabilistic label relaxation procedure. We followed their basic concept but implemented it through a set of hierarchical inference rules (Color Figure #9), similar to the approach reported by Stumpf and Koltun (1993).

We created several additional raster layers from the hyperclustered image in GRASS, using neighborhood functions that identified the most frequently occurring class value in a 5 x 5 pixel block around each pixel (majority), the maximum value found within that block (maxvalue), the minimum value found (minvalue), and the number of different values found (diversity). We then added the USGS digital elevation model of the region, because our photo-interpretation indicated that illumination differences on northwest and southeast slopes were affecting the correspondence between the vegetation and spectral classes. We also incorporated the forest regions map (Color Figure #3), specifically to help distinguish between dominant communities of Red Maple (*Acer rubrum*) and Sugar Maple (*Acer saccharum*), which are spectrally very similar, but occur as dominants in different regions. Values for each pixel location in our point sample data were extracted from these layers by the site file tabulation program in GRASS's "s.menu" and exported to Microsoft Excel for analysis in frequency tables.

In Excel, the sample point datasets were divided into three slope/aspect classes: northwest, southeast and flat. (We began the analysis with eight slope/aspect classes, but combined those that did not appear to have a distinctly separate effect on canopy reflectance.) Next, each forest type was ranked for ownership of each spectral class by the conditional probability of that spectral class being

that forest type on a given slope. Conversely, the spectral classes that appeared significant in each forest type were cross-tabulated to one another for their occurrence as most frequent neighbors in that forest type. From these comparisons, we developed a neighborhood set of spectral classes for each forest type that were consistent indicators of that forest type when in association with one another. These associations were distinct and non-linear as expected with non-Gaussian classes. Similar associations were developed for the minimum and maximum neighborhood values, though they were less distinct and more often used to restrict the application of rules in the presence or absence of indicator species. Therefore, in this model of the spectral mixtures within forest types, each region of pixels representing a polygon of a particular forest type consisted of: 1) a set of pixels whose spectral classes consistently represented that forest type in association with each other, and 2) a subset of the remaining pixels whose spectral classes were "outliers" with respect to that forest type. However, members of that "outlier" subset may be consistent indicators of other forest types when in association with other spectral values not in this particular group. The objective of our inference rules was to correctly identify and relabel the consistent spectral classes within each occurrence of a forest type community, then absorb the inconsistent spectral classes that were still part of each mixture.

To accomplish this, we applied three sets of sequential relabeling rules in the GRASS program "r.infer". They consisted of command variations on IFMAP, ANDIFMAP and THEN. Used iteratively in a hierarchical structure of conditional probabilities, this command sequence provided a sensitive and correctable mechanism for regrouping each occurrence of a spectral class into its best choice for a forest type. The first set of rules generated a preliminary map by assigning each pixel in the hyperclustered image to the most likely forest type for its spectral class on its slope/aspect, assuming its neighborhood values fit into the profile of associated neighborhood values for that forest type on that slope. Otherwise, the program continued to choose the next most likely forest type until it satisfied a set of conditions or assigned a value of zero to the pixel.

The second set of rules was applied to that preliminary map, selecting only those pixels whose new forest class value was different than the most frequently occurring neighbor within their immediate nine-pixel block. These class values were replaced by their majority neighbor's forest type if that forest type was one in which the original spectral class of the center pixel had logical standing. In other words, if the 3 x 3 pixel neighborhood of a reclassed pixel in the preliminary map had a different majority forest type that was a potential classification for that pixel farther down its hierarchy of probable identities, then the probability of the majority forest type being its correct label changed and the pixel was reassigned. However, if a pixel in the preliminary map was surrounded by a forest type that was not an available choice for its spectral value (e.g., a conifer-class pixel beside hardwoods at the corner of its stand), then it retained its first label.

The resulting map had a third set of rules applied to it that made similar assignments to any pixels that were labeled zero by the first set of rules (i.e., not significant for that particular community), but ended up after the application of the second set of rules with a most frequent set of neighbors belonging to a forest type to which they could have been assigned. This third step can be repeated several times. Finally, a "hole filling" equation is run in GRASS's "r.mapcalc", assigning the nine-pixel block majority to pixels whose spectral class belong to any forest type in the hyperclustered image, but remained labeled as zero after the application of all the rules (again not significant under the rules for that particular community). This equation produced our final re-classification at 30 m resolution (Color Figure #10).

An advantage to this approach is that these inference rules can be developed through repeated interaction with the video and hyperclustered imagery. We would complete a preliminary set of rules and process buffered corridors along the flight lines to reclass the primary sample (actually processing less than 10% of the full image but covering all our sample points.). This test labeling could be examined by querying the resulting class values of the sample points used in the model, overlaying

the resulting polygons on the hyperclustered image and comparing them to the forest communities we could identify in the video. Mistakes in logic, mislabeling, and erroneous associations or placement in the hierarchy of a particular class would become apparent and be corrected. In addition to modifying the rulesets, our forest classes were also altered, adding some, and combining others, to better reflect the aerial perspective and the reality of forest structure on the ground. The advantage of this approach is that both the rules and the conception of forest classifications can evolve as you train your results and are trained by them. In this context, neighborhood-based inference rules can be viewed as a way to bootstrap *a priori* probabilities to make the re-classification more Bayesian.

Results and Accuracy Analysis

The accuracy of our Anderson level III classification was determined by an error matrix of the stratified subset of points we extracted and set aside before the rest of the tertiary sample data was analyzed (Table 2). This subset was overlaid on the final classification map, and the forest classes assigned by photo-interpretation were compared with those generated from the rules. The error matrix was assessed by calculating producer's and user's accuracies for each class, percent correct, Kappa (Rosenfield and Fitzpatrick-Lins 1986), and Average Mutual Information Index (Finn 1993).

The chief difficulty in using sample points for accuracy analysis is separating out the errors caused by factors other than mislabeling by the rules. We had three other sources of error in the assignment of pixels to their interpreted forest type:

1. Random shifts in positional accuracy during the transformations of the point data. We monitored the spectral class identities of our sample points at each stage, including a subset of 75 points that had unique spectral values for each of their eight neighbors. The results indicated that some of these points could shift their raster cell association by one pixel in any direction through the transformation of geographic coordinates from raster to vector-based site files and back to raster. Therefore, the real location of all point data values was represented by their 3 x 3 pixel neighborhood and the positional accuracy of the final map was limited to 90 m.

2. Because of the complexity of the vegetation mosaic with subsequent small sized polygons in the final map, and the arbitrary nature of boundaries between clines, many of these sample points fell within the "error edge zone" defined by Burrough (1986).

3. Mis-assignment of sample sites in video interpretation had to be taken into account when using these points for verification. These mistakes tend to be filtered out of the modeling process as outliers, but we used the video to re-examine each point identified as mis-classified to assure the original reference was correct. As noted earlier, differences in the consideration of scale between the photo-interpreter and the neighborhood size that the inference rules were based upon can be a major source of error.

We had originally tried to correct for the first two sources of error by visually examining test sample points identified as errors and considering them to be correct if they fell within Burrough's "ambiguous" and "possibly out" zones of their correct class. However, we decided that this approach may have been a subjective source of bias towards accuracy, so we eliminated all edge zone samples by filtering the test points through an interspersion layer of the final classification map. Any pixels with less than 78% of their assigned forest type within a 5 x 5 pixel neighborhood were removed from consideration as sample points for verification. This reduced our original verification subsample of 4,459 points to 2,014 that were clearly within some forest type polygon. Both approaches produced overall accuracy levels within .05% of each other, which would indicate that most of the corrections we made by inspection in the first approach were illegitimate. However, the second approach reduces the number of points that have to be visually inspected in error checking, which is a time-consuming task with a large sample size.

Table 2. Error Matrix of the stratified subset of 2,014 points.
Reference pixel classes from videography interpretation

Classified Data	A	B	C	D	E	F	G	H	I	Row Totals	User's Accuracy
A	**269**	11	12		7	3		3		305	88%
B	2	**123**	18							143	86%
C	8	7	**284**	7	17	2		7	1	333	85%
D	7		25	**92**					1	125	74%
E	1		4		**309**	4	7	28		353	88%
F	6	1	12		1	**91**				111	82%
G					15		**198**			213	93%
H							1	**240**		241	100%
I	3					1			**186**	190	98%
Column Totals	296	142	355	99	349	101	206	278	188	**2014** Total Sample Points	89.7% Total
Producer's Accuracy	90.9%	86.6%	80.0%	92.9%	88.5%	90.1%	96.1%	86.3%	98.9%	**89.7%** Total	83.6% KAPPA

Average Mutual Information Index	H(classified Data)	= 3.0630 bits per pixel
	H(reference data)	= 3.0363 bits per pixel
	AMI	= 2.4065 bits per pixel
	% AMI	= 79.257
	% Correct	= 89.7

A. N. Hardwoods (Sugar Maple dominant)
B. Red Maple, Red Maple dominant communities
C. Northern Red Oak, Oak dominant communities
D. Birch/Birch dominant communities
E. Oak/Maple/Birch co-dominant communities
F. Maple/Oak/Conifer co-dominant communities
G. Conifers
H. Wetlands
I. Nonforest, pasture and suburban

As noted earlier, the classes in our error matrix (Table 2) focus specifically on forest types. The worst user's accuracy (74% for class D), is caused by misclassifying oak dominant communities (C) as oak/maple/birch co-dominant communities. The worst producer's accuracy (80% for class C) is from the same problem. Without this one error, the user's accuracy for D goes to 93% and the user's accuracy for C goes to 87%. The results also show that we have a specific problem distinguishing wetlands from mixed conifer/hardwoods communities, (viz., 10% of wetland samples were mislabeled as mixed conifer/hardwoods). However, we will be handling our wetlands separately, combining these classes with existing GIS data layers and the TM Landsat band number six (temperature). Our relabeling procedure had difficulties differentiating between species of conifers, and this may be a limitation of the multi-temporal hyperclustered classification when applied to species that do not demonstrate visible phenotypic change seasonally. We expect to improve these results during the next year by masking out the Conifer class and reclassifying it separately with the raw band data from a single date. However, the overall accuracy for all classes is 89.7 % (83.6% Kappa), which we

judge to be adequate for our Gap Analysis and considerably better than the 70% levels we achieved in previous analyses. The average mutual information index (AMI) indicates that of the 3.03 bits per pixel of information contained in the reference sample, the classified map explains 2.40 bits, or 79.2% (Finn 1993). These different measures indicate good accuracy and consistency at Anderson level III. As of yet, we do not have a sufficient number of points for a valid assessment of accuracy at the Anderson level IV (our subclasses), but this should be resolved as we extend the sampling to other scenes that contain the same forest types. We will also plan to apply information theory and similarity indices approaches to accuracy assessment (Finn 1993), combined with a stratified random resample of the primary sample level of video data, to evaluate the thirty-one subclasses that represent specific alliances among species.

It should be noted that accuracy assessment was done at the 30 m resolution of our raster image before the polygons were combined to form our minimum mapping unit (16 ha). Just as we consider it essential that the photo-interpreter and relabeling procedure operate at the same scale, we also strongly recommend that the resolution of the point data accuracy assessment match the resolution of interpretation (5 x 5 pixel blocks).

Conclusions

This work is part of a larger project to produce a vegetation map as an aid in mapping vertebrate distributions in New England. There are few ground truth or ancillary data layers available in the region. Therefore, this pilot study was designed to develop and test a methodology for reclassing a multi-temporal hyperclustered TM image using video point sampling and little additional data except USGS DEMs. For the purposes of this test, we concentrated on our most difficult type of land cover to discriminate -deciduous forests. However, we plan to expand the procedure to other types of land cover and TM images contiguous to Landsat scene 1331, which will provide us more information on the efficiency of the process. Inasmuch as we were unsure of the density and number of video transects required or how to proceed with the analysis, this pilot study was very labor intensive and time consuming for just relabeling part of one scene. However, based on the results of this work, we feel the sample point survey can be made more efficient by flying less dense coverage or just the fall season of videography, and we now have a systematic approach to the organization and analysis of those samples. These modifications would have reduced our analysis time to approximately 45 eight-hour person-days to complete the interpretation and rule generation for all major vegetation classes in the first Landsat scene of a project. This includes at least five days of ground truth field work for the crew and processing time. Within the work still to be done in our region, the process will continue to become more efficient as the same classes are extrapolated and new ones added over several scenes.

The real breakthrough in this approach is the development of the hyperclustered imagery and its distribution to all GAP Projects by the MRLC program. Given the apparent consistency of the hyperclustering algorithm, our relatively simple method of relabeling spectral classes in a systematic manner within a spatial context should be readily transferable to new scenes and scalable to much larger regions as long as they can be transected with an aerial point sampling survey. Obtaining videography is inexpensive compared to other aerial imagery or conducting ground visits. Transects for all of New England were flown in two weeks. Although phenology was not optimal for some areas, only a few areas in New England need to be reflown to obtain representative samples.

A measure of the methodology's usefulness will be its applicability to other GAP Projects using the hyperclustered imagery or their own unsupervised classifications to generate their vegetation maps. We have written a step-by-step cookbook for generating the rules in Excel, and will be publishing it on our internet home page, (http://tove.fnr.umass.edu/gaphome.html, or ftp://tove.fnr.umass.edu/pub/gap), along with all templates and necessary data structures. Maintaining a consensus of interpretation as more photo-interpreters become involved is a problem, but the visual keys will prove useful both for keeping photo-interpreters consistent

as they move from region to region, and for training new photo-interpreters. Further, efforts are being closely coordinated with GAP Projects in neighboring states to compare our visual indices and reach a general consensus on the appearance and structure of vegetation communities for our region. This should greatly facilitate edge matching between states and provide additional verification of our accuracy assessment.

Achievement of the high accuracy levels presented in Table 2 is attributable to the large number of sample points available for use in building and testing the classification rules. Information for this classification came from three sources: multi-date TM imagery, ancillary data (DEMs), and aerial videography. We feel that multi-date imagery is essential, as demonstrated by Schriever and Congalton (1995) achieving only 77% accuracy for their Anderson level IV forest classes in southern New Hampshire using multi-date imagery and field samples, but 86% accuracy when conifer classes are lumped as ours were. Their density of sampling (0.26 points per km^2) translates to more than four times the sample per km^2 that we used (0.06 points per km^2). The hyperclustered, two-date imagery is a good, inexpensive way to obtain an unsupervised classification, but we feel that any good clustering algorithm with multiple dates will produce adequate unsupervised classes. The ancillary data (DEMs) helped break apart forest types that were the same color because of variations in illumination caused by topographic relief (softwoods on southeast facing slopes can look like hardwoods on northwest facing slopes) and these are used in most classification projects of this type. The unique information sources for this study were the videography and the models for neighborhood associations between spectral classes. The large number of vegetation reference points interpreted from the video allowed us to model the spatial context in which spectral classes could represent different forest types. This produced a higher probability of success in the assignment of the pixels of a specific spectral class to their correct forest types, than by simply using the most consistent association of that spectral class to one forest type as the basis for relabeling. This, we feel, is the origin of the high accuracy levels. We are trying to quantify the contribution of multi-date over single-date imagery to the overall accuracy by classifying one of the spring hyperclustered images. As other Gap Analysis Projects use aerial videography in other ways (e.g., to label standard unsupervised cluster maps), it will become clearer whether the videography itself is what is important, or whether the combination of datasets and procedures used here is the key.

Future Improvements

Accuracy of our point source data was limited by our inability to document the tip and tilt of the video cameras at the moment of exposure. We tried incorporating a digital gyroscope that gave a continuous digital readout, but its response time, susceptibility to velocity changes, and large size limited its usefulness. Efforts are presently being made to incorporate a three-axis magnetic compass that will attach to the camera mount and log tip and tilt into the Horita time code generator with the GPS data.

We are also evaluating the incorporation of a neighborhood function that identifies the second most frequent neighbor as well as the first. This would be especially useful during the later stages in the sequence of rules, where it would help delineate the boundaries and increase the accuracy between land cover types. We are working on this function in "r.mapcalc" (GRASS) and receiving help from more experienced GRASS programmers. In reviewing the distribution of our sample points by their slope/aspect class, it was also clear that we should have stratified our collection of points to assure a sufficient representation of forest types in the less frequent slope/aspect classes. We are now displaying our slope/aspect classes over the hyperclustered image during point sampling and using them as a guide to increase the density of sampling on the steeper slopes.

While aerial videography served our purposes in this project, and was cost-effective, there are distinct limitations to the system:

- Although the resolution of the video imagery was sufficient for mapping, the inherent "jitters" in the images as

displayed on an interlaced TV monitor became very trying on the interpreters.

- The absence of stereo viewing was a major limitation to the interpretation of several types of plant communities. It could be achieved by printing overlapping frames in the video printer and viewing them with a pocket stereoscope, but this was too time-consuming for a technique whose success depends on spending less than a minute at each site.
- The tapes lose much of their color and resolution when reproduced, so most analysis has to be done from the originals. Unfortunately, they degenerate with use. This limits the extent to which the data can be freely shared. Further, video tape also degenerates from non-use over time, so the data are essentially temporary.
- Because video is an analog system recorded on tape, the image data is stored and displayed in the NTSC transmission format. This causes a loss of radiometric data that could be retained in an RGB or multi-band frame set.

We hope to improve this in the future with a completely digital system. Digital cameras are becoming available with resolutions of 2,000 to 4,000 lines which will download to a hard drive in the aircraft as RGB rasters with the GPS data written directly to the header. The images can be copied and permanently stored on recordable CD-ROM disks without any information loss and imported directly into a GIS program by anyone with a standard multi-media computer. Instead of a continuous recording, individual frames can be captured and stored at specific predetermined geographic positions along the flight path so as to maintain a 60% overlap between exposures for stereo viewing. Many modern image processing systems (e.g., ERDAS, ERmapper, Intergraph) are now providing the capacity to display this imagery in stereo, using a split window format or multi-image overlays with switching polarized glasses. This stereo-viewing capacity along with the higher resolution and greater stability of a non-interlaced computer display will greatly increase the interpretability of the data.

Acknowledgments

Dr. M. Norton-Griffiths is gratefully acknowledged for both his counsel and his pioneering work in aerial point sampling, as are C. Curtis, L. Graham and J. Walsh, from the School of Renewable Natural Resources of the University of Arizona, for their adaptation of video and GPS to the process. Our pilot, R. Kulis, assisted in the design of our camera mount and flew several hundred hours for us at cost, in his own aircraft. As a career forester with the Massachusetts Department of Environmental Management, his knowledge of New England forests from an aerial perspective proved invaluable. Several graduate students and staff at the University of Massachusetts participated in field checking, including: H. Lanza, D. Goodwin, M. Wiley, T. Rudnicky, M. Hale, C. O. Hale, and A. Trader. Resource Mapping / Land Information Systems at the Department of Forestry and Wildlife Management, University of Massachusetts, and the U.S. Fish and Wildlife Service, Connecticut River Fisheries Program, provided extensive computer support. We especially thank GIS managers D. Goodwin and H. Malcolm for generous access to their facilities. R. Shauffler of the Region 5 U.S. Fish and Wildlife Service GIS Lab was instrumental in coordinating our use of image processing software. J. Gasprich at the Center for Remote Sensing and Spatial Analysis, Dept. of Natural Resources, Rutgers University, compiled the GRASS 4.1 binaries for Solaris 2.4, which allowed us to use USFWS's computer, and R. Lozar@zorro.cecer.army.mil was also invaluable in his assistance and patience. Both these gentlemen are representative of the whole concept of GRASS, at USACERL and now at Rutgers.

The New England Gap Analysis Project is part of the national Gap Analysis Program of the national Biological Service. The New England Project is a joint effort of the Cooperative Fish and Wildlife Research Units in Massachusetts, Vermont and Maine. Several other cooperating agencies have also contributed to this effort, including: the Region 5 U.S. Fish and Wildlife Service office, state agencies, especially the state Heritage Programs, state universities, and the eastern regional office of The Nature Conservancy.

Literature Cited

Anderson, J. R., E. E. Hardy, J. T. Roach, and R. E. Witmer. 1976. A land use and land cover classification system for use with remote sensor data. *U.S. Geological Survey Professional Paper No. 964.* Government Printing Office, Washington, DC. 28 pp.

Ahlgren, C. 1957. Phenological observations of nineteen native tree species in northern Minnesota. *Ecology* 38(4):622-628.

Beaubein, J. 1979. Forest type mapping from Landsat digital data. *Photogrammetric Engineering and Remote Sensing* 45(8):1135-1144.

Bolstad, P. V., and T.M. Lillesand. 1992. Improved classification of forest vegetation in northern Wisconsin through a rule-based combination of soils, terrain, and Landsat Thematic Mapper data. *Forest Science* 38(1):5-20.

Bouman, C., and M. Shapiro. 1992. Multispectral image segmentation using a multiscale image model. Pages 565-568 in *Proceedings of IEEE International Conference on Acoustical, Speech and Signal Processing,* March 23-26 (extract under "i.smap" in "g.manual", GRASS). San Francisco, Ca.

Burrough, P.A. 1986. *Principles of geographical information systems for land resources assessment.* Oxford University Press, New York, Ny. XXX pp.

DeGraaf, R. M. and D. D. Rudis. 1986. New England wildlife, habitat, natural history and distribution. *General Technical Report NE-108.* U.S. Department of Agriculture, Forest Service, Northeastern Forest Experiment Station. Broomall, Pa. 491 pp.

DeGraaf, R. M., M. Yamasaki, W. B. Leak, and J. W. Lanier. 1992. New England wildlife: management of forested habitat. *General Technical Report NE-144.* U.S. Department of Agriculture, Forest Service, Northeastern Forest Experiment Station, Broomall, Pa. 271 pp.

Dunford, C., D. Mouat, M. Norton-Griffiths, and D.M. Slaymaker. 1983. Remote sensing for rural development planning in Africa. *The Journal for the International Institute for Aerial Survey and Earth Sciences* 2:99-108.

Eder, J. J. 1989. Don't shoot unless it's autumn. *Journal of Forestry* 6:50-51.

Eyre, F.H., editor. 1980. Forest cover types of the United States and Canada. *Society of American Foresters,* Washington, DC. 148 pp.

Finn, J. T. 1993. Use of the average mutual information index in evaluating classification error and consistency. *International Journal of Geographical Information Systems* 7(1):349-366.

Graham, L. A. 1993. Airborne video for near-real-time vegetation mapping. *Journal of Forestry* 8:28-32.

Hutchinson, C. F. 1982. Techniques for combining Landsat and ancillary data for digital classification improvement. *Photogrammetric Engineering and Remote Sensing* 48(1):123-130.

Jensen, J. R. 1986. *Introductory digital image processing, A remote sensing perspective.* Prentice-Hall, Englewood Cliffs, Nj. 379 pp.

Kelly, P. M., and J. M. White. 1994. *Preprocessing remotely-sensed data for efficient analysis and classification.* Computer Research Group, MS B-265. Los Alamos national Laboratory, Los Alamos, Nm.7 pp.

Norton-Griffiths, M., T. Hart and M. Parton. 1982. Sample surveys from light aircraft combining visual observations and very large scale color photography. *University of Arizona Remote Sensing Newsletter,* 82-2. Tucson, Az. 14 pp.

Norton-Griffiths, M. 1988. Aerial point sampling for land use surveys. *Journal of Biogeography* 15:149-156.

Richards, J. A., D. A. Landgrebe, and P. H. Swain. 1982. A means for utilizing ancillary information in multispectral classification. *Remote Sensing of Environment* 12:463-477.

Rosenfield, G. H., and K. Fitzpatrick-Lins. 1986. A coefficient of agreement as a measure of thematic classification accuracy. *Photogrammetric Engineering and Remote Sensing* 52(2):223-227.

Sayn-Wittgenstein, L. 1978. Recognition of tree species on aerial photographs. *Information Report FMR-X-118,* Forest Management Institute, Canadian Forestry Service, Ottawa, Ontario. 97 pp.

Schriever, J. R., and R. G. Congalton. 1995. Evaluating seasonal variability as an aid to cover-type mapping from Landsat Thematic Mapper data in the Northeast. *Photogrammetric Engineering and Remote Sensing* 61(3):321-327.

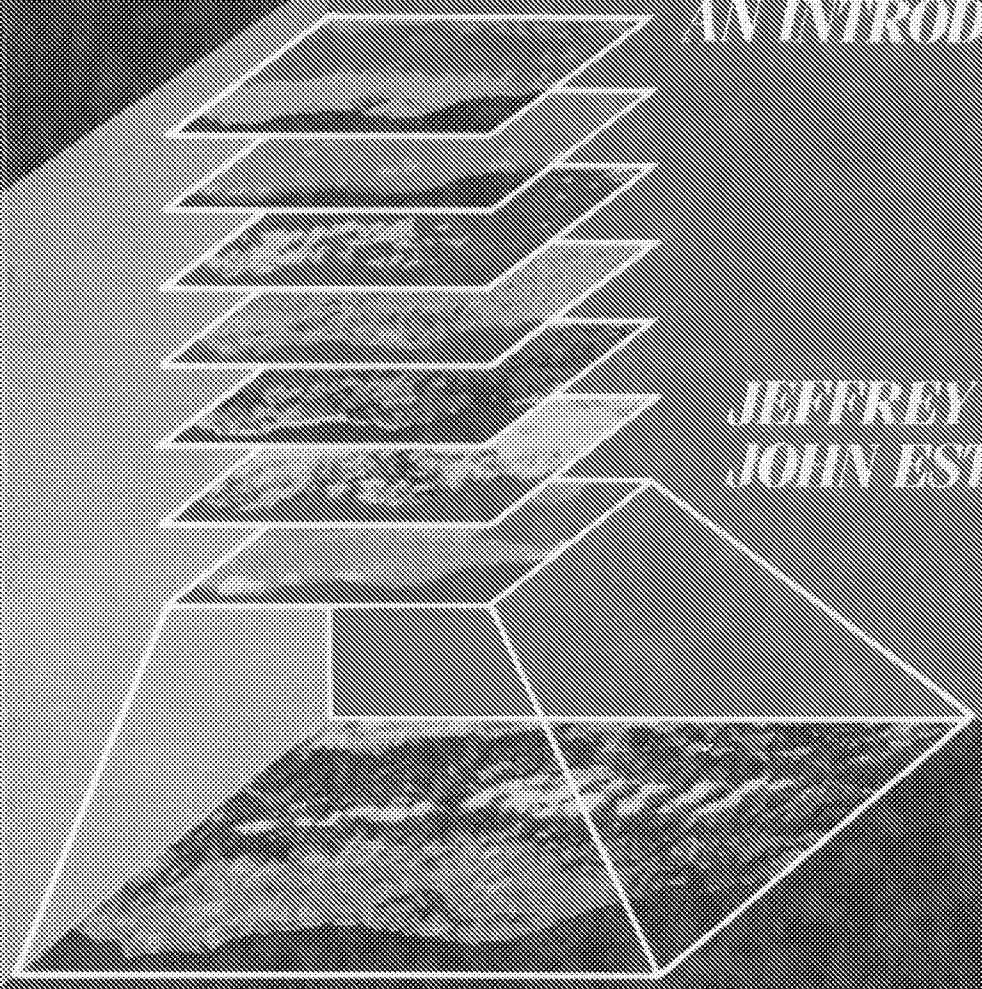
Strahler, A. H. 1980. The use of prior probabilities in maximum likelihood classification of remotely sensed data. *Remote Sensing of Environment* 10:135-163.

Stumpf, K. A., and J. M. Koltun. 1993. *Rule based aggregation of raster image classifications into vector GIS databases with five and forty acre minimum size mapping units.* ASPRS/ACSM Conference, Washington, DC.

Wolter, P. T., D. J. Mladenoff, G. E. Host, and T. R. Crow. 1995. Improved forest classification in the northern lake states using multi-temporal Landsat imagery. *Photogrammetric Engineering and Remote Sensing.* 61(9): 1129-1143.

Geographic Information Systems

AN INTRODUCTION



JEFFREY STAR
JOHN ESTES

GEOGRAPHIC INFORMATION SYSTEMS

An Introduction

JEFFREY STAR
JOHN ESTES

University of California, Santa Barbara



PRENTICE HALL, Englewood Cliffs, New Jersey 07632

Library of Congress Cataloging-in-Publication Data

Star, Jeffrey.
Geographic information systems : an introduction / Jeffrey Star, John Estes.
p. cm.
Bibliography: p.
Includes index.
ISBN 0-13-351123-5
1. Geography—Data processing. I. Estes, J. E. II. Title.
G70.2.S73 1990 89-31220
910'.285—dc20 CIP

Editorial/production supervision: Christina Ferrari
Cover design: Photo Plus Art
Manufacturing buyer: Paula Massenaro
Cover photograph: California Condor database. Photo by Jeffrey Star.
Color insert layout: Thomas Nery



© 1990 by Prentice-Hall, Inc.
A Division of Simon & Schuster
Englewood Cliffs, New Jersey 07632

All rights reserved. No part of this book may be reproduced, in any form or by any means, without permission in writing from the publisher.

Printed in the United States of America

10 9 8 7 6 5

ISBN 0-13-351123-5

Prentice-Hall International (UK) Limited, *London*
Prentice-Hall of Australia Pty. Limited, *Sydney*
Prentice-Hall Canada Inc., *Toronto*
Prentice-Hall Hispanoamericana, S.A., *Mexico*
Prentice-Hall of India Private Limited, *New Delhi*
Prentice-Hall of Japan, Inc., *Tokyo*
Simon & Schuster Asia Pte. Ltd., *Singapore*
Editora Prentice-Hall do Brasil, Ltda., *Rio de Janeiro*

To Toni and Claire

Brief Contents

1 Introduction 1

2 Background and History 14

3 The Essential Elements of a GIS: An Overview 24

4 Data Structures 32

5 Data Acquisition 61

6 Preprocessing 76

7 Data Management 126

8 Manipulation and Analysis 143

9 Product Generation 174

10 Remote Sensing and GIS 191

11 Practical Matters 220

12 Applications 230

13 Looking Toward the Future 245

Suggestions for Exercises 252
Glossary and Abbreviations 261
Bibliography 283
Index 297

Contents

Preface xi

1 Introduction 1

1.1 Geography 1
1.2 Information Systems 2
1.3 A Manual Geographic Information System 4
1.4 Applications 8
1.5 Geographical Concepts 9
1.6 The Four Ms 12

2 Background and History 14

2.1 The Cartographic Process 15
2.2 Early History 17
2.3 The Modern Era 19

3 The Essential Elements of a GIS: An Overview 24

3.1 Functional Elements 24
3.2 Data in a GIS 28

4 Data Structures 32

4.1 Raster Data Structures 33
4.2 Vector Data Structures 48
4.3 Comparisons between Data Structures 57

5 Data Acquisition 61

5.1 Introduction 61
5.2 Existing Datasets 64
5.3 Developing your own Data 70

6 Preprocessing 76

6.1 Format Conversion 77
6.2 Data Reduction and Generalization 91
6.3 Error Detection and Editing 93
6.4 Merging 95
6.5 Edge Matching 96
6.6 Rectification and Registration 97
6.7 Interpolation 114
6.8 Photointerpretation 118

7 Data Management 126

7.1 Basic Principles of Data Management 127
7.2 Efficiency 130
7.3 Conventional Database Management Systems 134
7.4 Spatial Database Management 139

8 Manipulation and Analysis 143

8.1 Reclassification and Aggregation 144
8.2 Geometric Operations on Spatial Data 154
8.3 Centroid Determination 156
8.4 Data Structure Conversion 157
8.5 Spatial Operations 157
8.6 Measurement 164
8.7 Statistical Analysis 167
8.8 Modeling 169

1418

9 Product Generation 174

9.1 Types of Output Products 174
9.2 Hardware Components 183

10 Remote Sensing and GIS 191

10.1 A Brief History 193
10.2 Remote Sensing Technology 195
10.3 Digital Processing of Remotely Sensed Data 209
10.4 Interfacing Remote Sensing and GIS's 213
10.5 Synergism 215

11 Practical Matters 220

11.1 A Case Study 220
11.2 Database Volume 223
11.3 Specifications 225
11.4 Project Management 228

12 Applications 230

12.1 Master Planning 230
12.2 Proposed Dam Site 232
12.3 Waste Site Selection 233
12.4 Irrigation and Water Resource Potential 234
12.5 Merging Raster and Vector Data for Map Update 235
12.6 Species Habitat Analysis 236
12.7 Municipal GIS 238
12.8 Agricultural Production Modeling 240
12.9 KBGIS: Artificial Intelligence and GIS 242

13 Looking Toward the Future 245

Suggestions for Exercises 252
Glossary and Abbreviations 261
Bibliography 283
Index 297

Preface

This book was written for several reasons. First, we hope it helps to fill a gap by providing an entry into the literature of geographic information systems. Up until very recently, most of the information about geographic information systems (GISs) has been in the fugitive, or *gray*, literature; the latter includes in-house technical reports, conference proceedings, non-refereed publications, and poorly distributed manuscripts describing efforts funded by federal and state agencies. Publications from professional conferences, such as Purdue University's "Machine Processing of Remotely Sensed Data" Symposia, the Harvard Computer Graphics Symposia, and the Urban and Regional Information Science Association meetings have been some of the best places to find current information about GISs, in terms of both the theoretical and the practical aspects of the field.

Special-purpose documents have also been useful sources, for those of us who know where to look. Briefing documents prepared by such agencies as the U.S. Forest Service and companies such as the Environmental Systems Research Institute, and surveys of the field by the American Farmland Trust, have been valuable resources in their respective narrow domains. Publications such as the American Society of Photogrammetry and Remote Sensing's *Photogrammetric Engineering and Remote Sensing* also have articles about GISs on a regular basis. Recently, journals have been started that emphasize spatial data processing. Two of these new journals are the *International Journal of Geographical Information Systems*, published quarterly by Taylor and Francis in the U.K., and *Aerial and Space Imaging, Remote Sensing and Integrated Geographical Systems*, published quarterly by Imaging Systems Publications in Sweden. Recent conferences have focused specifically on geographic information systems. In particular, the proceedings of GIS '87 (October, 1987; San Francisco) and IGIS '87 (November, 1987; Crystal City, Virginia) provide a summary of the state of the field, although primarily from an academician's point of view.

Information about geographic information systems may sometimes be found in one chapter of a book - see, for example, Short's *Landsat Tutorial Workbook* (1982), a classic volume which is unfortunately out of print, or the chapter edited by Marble in the second edition of the *Manual of Remote Sensing* (American Society of Photogrammetry and Remote Sensing, 1983). Recently, a monograph has been published that focuses completely on GIS's. Burrough's *Principles of Geographical Information Systems for Earth Resources Assessment* (1986) is an excellent resource in this rapidly emerging field. For information on a variety of aspects of GIS, see Marble, Calkins, and Peuquet (1984) - a self-published three ring binder of readings on GIS that has also become a well-known standard reference.

A second important function for this text is to serve as an introduction to the field, but at the upper-division undergraduate or beginning graduate level. Much of the material that follows has been used in short courses we have presented under the auspices of George Washington University and elsewhere. We hope it serves as a text for a one-semester course focusing on geographic information systems and their applications, as well as a resource for individual study. A student with some background in computer graphics, cartography, and geographic theory should find this text accessible.

A final reason for this book's existence is to raise the banner of *data integration* as a philosophical basis for modern GIS's. From one perspective, the essence of a geographic information system is its integration of the many different kinds of information we may be able to obtain about the spatial objects in an area. In other words, a user of a GIS should be able to work with many different types of data, bringing *all* the information relevant to a problem together in a consistent form, and should be able to bring to bear on the problem all the power of all the sophisticated analysis tools available. By the same token, we believe a geographic information system is the correct tool for integrating the different technologies that are used in gathering, analyzing, and assessing spatial data.

We begin with a chapter that introduces some of the jargon of geographic information systems. It does so by presenting a completely non-digital land-use planning problem: the design of a golf course. This is followed by a chapter on the history of geographic information systems, and by another that introduces the essential components of a GIS. Chapter 4 discusses data structures: how a GIS actually stores the kinds of data and information that are commonly used in systems.

In the next five chapters we explore the five essential parts of a GIS: data acquisition, preprocessing, database management, analysis and manipulation, and producing the final output. In these chapters we attempt to show the practical use of the different tools and techniques.

Chapter 10 examines the relationship between the technology of remote sensing and the philosophy of geographic information systems. From a theoretical point of view, the image processing systems used when working with remotely sensed data are geographic information systems, although with strengths in certain kinds of numerical operations and presentation functions. Based on our experience, we believe that remotely sensed data and GIS's are natural allies. In this chapter we have tried to highlight the interdependencies of these two areas, and indicate the potential each has for the other.

Chapter 11 briefly discusses some practical matters. Bringing a digital geographic information system into an organization requires changing the way the organization conducts its day-to-day operations. This affects an organization's management in several ways, including short-term disruptions and costs during the transition to a digital system, as well as changes to the long-term planning process. A GIS makes new demands on staff and staff development, and affects funding requirements in both the short and long term. Some of these are the same as the impacts of any other digital information system, and thus, there are some relevant guidelines and case studies. Problems specific to a GIS, in terms of estimating database volume, developing specifications, and managing the overall project, are discussed briefly.

In Chapter 12 we present a potpourri of applications, drawn from friends and colleagues who were able to contribute material to us. These applications cover a wide range, from the design and management of large facilities to long-range research on the global carbon cycle. The applications also touch on the wide range of hardware and capabilities now used to solve spatial data processing problems.

Finally, in the last chapter we gather our thoughts about the future. Shakespeare's Macbeth had perfect counsel about future events from three witches. We claim no such accuracy, and hope our prophecies are less disastrous. However, there are visible trends in the GIS industry, as well as interesting new developments coming out of the research laboratories. New data acquisition technologies are being developed and data continues to be less expensive to process and store, while our appetite for processing continues to grow. We report on some of these developments, both to describe the

1420